

BULETINUL INSTITUTULUI POLITEHNIC DIN IAȘI

**Publicat de
UNIVERSITATEA TEHNICĂ "GH.ASACHI", IAȘI**

Tomul LI (LV)

Fasc. 2

Secția

**ȘTIINȚA ȘI INGINERIA
MATERIALELOR**

2005

President of the Editorial Board of Bulletin of the Polytechnic Institute

Prof. univ. dr. eng Nicolae Badea, Technical University “Gh. Asachi” Iași, Romania
Rector of Technical University “Gh. Asachi” of Iasi

Editor-in-Chief of Bulletin of the Polytechnic Institute

Prof. univ. dr. eng Ion Giurma, Technical University “Gh. Asachi” Iași, Romania
Vice-Rector of Technical University “Gh. Asachi” of Iasi

Managing Editor of Bulletin of the Polytechnic Institute

Prof. univ. dr. eng. Dan Gălușcă, Technical University “Gh. Asachi” Iași, Romania
Dean of the Faculty of Materials Science and Engineering

Managing Editor of the *MATERIALS SCIENCE AND ENGINEERING*

Assoc. prof. dr. eng. Iulian Ioniță, Technical University “Gh. Asachi” Iași, Romania
Scientific secretary of the Faculty of Materials Science and Engineering

Editorial Board of the Section *MATERIALS SCIENCE AND ENGINEERING*

Prof.univ.dr.eng. Yuri A. Burennikov, Vinnitsia State Technical University, Ukraine

**Prof.univ.dr.eng. Borivoje Miškovič, Yugoslav Association of Metallurgical Engineers,
Belgrad, Serbia-Montenegro**

Prof.univ.dr.eng. Paolo Nanni, Universita degli Studi da Genova, Italy

Prof.univ.dr.eng. Strul Moisa, Ben-Gurion University of the Negev, Beer-Sheva, Israel

**Prof.univ.dr.eng. Corneliu Munteanu, Technical University “Gh. Asachi” Iași,
Romania**

**Prof.univ.dr.eng. Vasile Cojocaru-Filipiuc, Technical University “Gh. Asachi” Iași,
Romania**

Prof.univ.dr.eng. Constantin Baci, Technical University “Gh. Asachi” Iași, Romania

Prof.univ.dr.eng. Luchian Zaharia, Technical University “Gh. Asachi” Iași, Romania

Prof.univ.dr.eng. Ioan Carcea, Technical University “Gh. Asachi” Iași, Romania

Prof.univ.dr.eng. Adrian Dima, Technical University “Gh. Asachi” Iași, Romania

Prof.univ.dr.eng. Ioan Alexandru, Technical University “Gh. Asachi” Iași, Romania

**Assoc.prof.dr.eng. Leandru Gheorghe Bujoreanu, Technical University “Gh. Asachi”
Iași, Romania**

Assoc. prof.dr. eng. Ioan Rusu, Technical University “Gh. Asachi” Iași, Romania

**Assoc. prof.dr. eng. Gheorghe Bădărău, Technical University “Gh. Asachi” Iași,
Romania**

**Assoc. prof.dr. eng. Petrică Vizureanu, Technical University “Gh. Asachi” Iași,
Romania**

Editorial Secretary of the *MATERIALS SCIENCE AND ENGINEERING*

**Assoc.prof.dr.eng. Gheorghe Bădărău, Technical University “Gh. Asachi” Iași,
Romania**

MATERIALS SCIENCE AND ENGINEERING

CONTENTS	
DIMA, A., IONITA, I., BADARAU, GH. - AURELIAN I.SIMIONESCU (1923-2004)	1
GALUSCA, D.G., IONITA, I., BADARAU, GH. - CONSTANTIN C. CIOCHINA (1923-2004)	3
SEGAL, L., CIOBĂNAȘU, G. - RAPID PROTOTYPING: AN EFFECTIVE TOOL OF THE ENGINEERING DESIGN PROCESS	7
PALHOVICI, V., GOANTA, V., GRIMBERG, R., SAVIN, A., STEIGMANN, R., ANDREESCU, A. - PROBABILISTIC MODEL FOR FATIGUE ACCUMULATION IN SUPERCONDUCTOR MAGNETS FROM ITER REACTOR	15
GHIMBĂȘEANU, I., PAȚACHIA, S. - PROGRAMME OF DATA ACQUISITION FOR DETERMINING THE VARIATION OF THE ELECTRICAL RESISTANCE OF A SEMICONDUCTOR MATERIAL, WITH THE TEMPERATURE	23
TÂRCOLEA, M., CIUCĂ, S., VLĂȘCEANU, D. - AN ANALYTICAL MODEL FOR HOLLOW TUBE DRAWING	29
ALEXANDRU, A., IACOB STRUGARU, S., ALEXANDRU, I., CIOBANU, L., TANASUCA, S. - COMPUTERIZED QUANTITATIVE MICROGRAPHICAL ANALYZE OF DEPOSED LAYERS BY ELECTRICAL DISCHARGE IN IMPULSE ON AN HIGH ALLOYED TOOLS STEEL	35
ANGHEL, A., BUJOREANU, C. - CONTRIBUTIONS CONCERNING VIRTUAL INSTRUMENTATION IN DATA AQUISITION AND ANALYSIS	41
DĂNILĂ, R., CALANCIA, O., FLORESCU, A., VIZUREANU, P., GOANȚĂ, V. - HIGH SPEED DETERMINATION OF THE SPECIFIC ISOTHERMS OF THE THERMIC FIELDS CREATED IN THE PROCESS OF CASTING ALLOYS IN METALLIC MOULDS HELPED BY COMPUTER	45
CALANCIA, O., DANILĂ, R., MOLDOVEANU, V., FLORESCU, A., DRĂGOI, L. - HIGH SPEED DETERMINATION USING THE COMPUTER FOR THE THERMAL TENSIONS FROM METALLIC MOULDS AT ALLOYS CASTING	53
CANANAU, N., GURAU, GH., HANGANU, D. - SEMI-PLANETARY ROLLING PROCESS AND EXPERIMENTAL SIMULATION	59
CĂNĂNĂU, N., HANGANU, D., GURAU, GH. - THEORETICAL SOLUTION OF FORGE CUTTING PROCESS	67
BUJOREANU, C., ANGHEL, A. - VIRTUAL INSTRUMENTATION FOR SCUFFING DIAGNOSE OF BALL BEARINGS	75
BUJOREANU, C., CRETU, S. - CONSIDERATIONS REGARDING THE SCUFFING FAILURE OF BALL BEARINGS	81

CHIRILĂ, E., CĂRĂUȘU, C. - ANALYTICAL STUDY ABOUT THE TRANSITORY WORKING CONDITIONS BEHAVIOUR OF THE ELECTRIC RESISTANCE FURNACE	89
CHIRILĂ, E., CĂRĂUȘU, C. - THE CONCEIVING OF THE AUTOMATIC MEASURING AND ADJUSTMENT BLOCK, ASSISTED BY THE COMPUTER, FOR THE VAT TEMPERATURE OF THE ELECTRIC RESISTANCE FURNACE	95
DUMITRACHE, C., COMANDAR, C., SABĂU, A., AMARIEI, N. - NUMERICAL MODEL TO COMPUTE THERMAL STRESS-RELIEF PROCESSES AT CARBON STEEL	99
ALBU-IACOB, C. - EXPERIMENTAL RESULTS REGARDING THE PRECISION AND THE UNIFORMITY OF THE TEMPERATURE IN AN ELECTRICAL FURNACE FOR HEAT TREATMENT USING AN AUTOADAPTIVE CONTROL SYSTEM	103
ALBU-IACOB, C. - PROGRAMME CARRIED OUT FOR AUTOADAPTIVE CONTROL OF AN ELECTRIC FURNACE OF HEAT TREATING USING A COMPUTER	109
COMANEI, R., VITALARIU, V., ZAHARIA, L., CHELARIU, R. - STUDY OF MECHANICAL BEHAVIOR OF DENTAL RESTORATIONS BY USING DATA ACQUISITION SYSTEMS	117
DROESCU, R. - MUFFLER DESIGN USING FINITE ELEMENT MODELING AND SIMULATION	123
MIRON, V., GHERGHISOR, G., PAUNESCU, R. - THE CONTRIBUTION OF THE MATHEMATICAL MODELLING OF HOT AND COLD ROLLING AND OF COOLING REGIME TO THE IMPROVEMENT OF THE PLASTICITY CHARACTERISTICS OF LOW-CARBON STEEL SHEETS	131
MIHAI, D., ȘTEFAN, M., BADARAU, GH. - THE COMPUTER ASSISTED ESTABLISHING OF CREEP BEHAVIOUR AT 500 °C FOR THE STEEL 33MoCr11	137
COMAN, GH. - THE MYTHOLOGY OF METALS IN MIRCEA ELIADE'S WORK	151
SANDU, I., GĂLUSCĂ, D.G., CARCEA, I., ȘTEFAN, M., SANDU, A.V. - AUTHENTICATION OF ANCIENT BRONZE COINS I. ASPECTS CONCERNING THE COMPOSITION OF THE PATINA	157
SANDU, I.G., SANDU, I.C.A., DIMA, A., SANDU, I., NEACȘU, I., - AUTHENTICATION OF ANCIENT BRONZE COINS II. MICROCHEMICAL, IR AND XRD ANALYSES	167
SANDU, I.G., STOLERIU, Ș., SANDU, I., DIMA, A., SANDU, I.C.A., NEACȘU, I. - AUTHENTICATION OF ANCIENT BRONZE COINS III. COLORIMETRIC AND THERMOGRAVIMETRIC ANALYSES	177
SANDU, I.G., DIMA, A., SANDU, I., DIACONESCU, F., SANDU, A.V. - THE CONSERVATION LEVELS OF METALLIC ARTEFACTS. I. ANCIENT COINS AND OTHER METALLIC NUMISMATIC PIECES	189
SANDU, I.G., DIMA, A., SANDU, I., SULIȚANU, N., STOLERIU, Ș., DIACONESCU, F. - STUDY OF THE ARTIFICIAL PATINA OF THE RESTORED ANCIENT BRONZE ARTIFACTS	197
CRISTEA, L., ZSIGMOND, M., APOSTOLESCU, I. - THE ENVIRONMENT TECHNOLOGY APPLIED TO THE PURIFYNG STATION "SLOBOZIA"	205
COCEA, M., MARCUS, L. - THE FOOTWEAR DESIGNING SESSIONS USING CRISPIN DYNAMICS ENGINEER	211

COCEA, M., MARCUS, L. - A STUDY FOR THE MATHEMATIC MODELING OF 2D IRREGULAR SHAPES FOR FOOTWEAR CAD SYSTEM	219
HARNAGEA, F., MIHAI, A. - SELF AND THERMO ADHESIVE TEXTILE MATERIALS USED IN FOOTWEAR MANUFACTURING	227
HARNAGEA, F., MIHAI, A. - ASPECTS REGARDING THE USE OF ADHESIVE DISPERSIONS IN FOOTWEAR INDUSTRY	233
VIZUREANU, P. - THE COMBUSTION FURNACES OPTIMISATION ASSISTED BY COMPUTER	239
VIZUREANU, P. - INDUSTRIAL INCINERATION SYSTEMS	243
MOLDOVAN, P., FIRESUCU, L., APOSTOLESCU, I., POPESCU, G., BUTU, M. - THE HETEROGENEOUS NUCLEATION AND HYDROGEN ROLE ON THE PRIMARY MICROPOROSITY IN ALUMINUM ALLOYS	249
CIOBANASU, G., LUCA, D. - PARAMETRIC MODELING OF ELECTROMAGNETIC SHEET METAL FORMING DEVICES	257
CIOBANU, O., POP, GH., CANTEMIR, D. - HIGH RESIDUAL STRESS MEASUREMENTS	265
BADARAU, GH., STEFAN, M., IONITA, I. - STRATEGIES FOR REASONING CONTROL IN EXPERT SYSTEMS BASED ON PRODUCTION RULES	273
IONITA, I., STEFAN, M., BADARAU, GH. - INTERIOR POINT METHODS OF IN THE CONVEX OPTIMISATION OF THE PREHENSION FORCE OF A ROBOT USED IN THE TECHNOLOGICAL PROCESS OF CASTING	279
STEFAN, M., IONITA, I., BADARAU, GH. - METHODS OF INTERIOR POINT FOR THE CONVEX OPTIMIZATION OF THE LINEAR REGULATORS FOR THE PREDICTIVE CONDUCTION OF THE HEAT TREATING FURNACE, THE LABORATORY TYPE	283
STEFAN, M., BADARAU, GH., IONITA, I. - OPTIMIZATION AND COMPUTATIONAL METHODS IN MATERIAL SCIENCE AND ENGINEERING	289
STEFAN, M., IONITA, I., BADARAU, GH. - MATHEMATICAL MODELING AND OPTIMISATION IN MATERIALS SCIENCE AND ENGINEERING	293
ISARIE, C., MARIN, A. - HARDWARE AND SOFTWARE FOR ULTRASONIC FLOW METER TRANSDUCERS	297

ȘTIINȚA ȘI INGINERIA MATERIALELOR

CUPRINS	
DIMA, A., IONITA, I., BADARAU, GH. - AURELIAN I.SIMIONESCU (1923-2004)	1
GALUSCA, D.G., IONITA, I., BADARAU, GH. - CONSTANTIN C. CIOCHINA (1923-2004)	3
SEGAL, L., CIOBĂNAȘU, G. - PROTOTIPAREA RAPIDĂ: O UNEALTĂ EFICIENTĂ A PROCESULUI DE PROIECTARE INGINEREASCĂ	7
PALIHOVICI, V., GOANTA, V., GRIMBERG, R., SAVIN, A., STEIGMANN, R., ANDREESCU, A. - MODEL PROBABILISTIC PENTRU ACUMULAREA OBOSELII IN MAGNETII SUPRACONDUCTORI DIN REACTORUL ITER	15
GHIMBĂȘEANU, I., PAȚACHIA, S. - PROGRAM DE ACHIZIȚIE DE DATE PENTRU DETERMINAREA VARIAȚIEI REZISTENȚEI UNUI MATERIAL SEMICONDUCTOR	23
TÂRCOLEA, M., CIUCĂ, S., VLĂȘCEANU, D. - UN MODEL ANALITIC PENTRU PRELUCRAREA PRIN TRAGERE A ȚEVILOR	29
ALEXANDRU, A., IACOB STRUGARU, S., ALEXANDRU, I., CIOBANU, L., TANASUCA, S. - ANALIZA MICROGRAFICĂ CANTITATIVĂ COMPUTERIZATĂ A STRATURILOR DEPUSE PRIN DESCĂRCĂRI ELECTRICE ÎN IMPULS PE UN OȚEL BOGAT ALIAT DE SCULE	35
ANGHEL, A., BUJOREANU, C. - CONTRIBUȚII ASUPRA INSTRUMENTAȚIEI VIRTUALE ÎN ACHIZIȚIA ȘI ANALIZA DE DATE	41
DĂNILĂ, R., CALANCIA, O., FLORESCU, A., VIZUREANU, P., GOANȚĂ, V. - DETERMINAREA RAPIDĂ CU AJUTORUL CALCULATORULUI A IZOTERMELOR SPECIFICE CÂMPURILOR TERMICE LA TURNAREA ALIAJELOR ÎN FORME METALICE	45
CALANCIA, O., DANILĂ, R., MOLDOVEANU, V., FLORESCU, A., DRĂGOI, L. - DETERMINAREA RAPIDĂ CU AJUTORUL CALCULATORULUI A TENSIUNILOR TERMICE DIN FORMELE METALICE LA TURNAREA ALIAJELOR	53
CANANAU, N., GURAU, GH., HANGANU, D. - SIMULAREA EXPERIMENTALĂ A PROCESULUI DE RULARE	59
CĂNĂNĂU, N., HANGANU, D., GURAU, GH. - SOLUȚIE TEORETICĂ PENTRU PROCESUL DE DEBITARE PRIN FORJARE	67

BUJOREANU, C., ANGHEL, A. - INSTRUMENT VIRTUAL PENTRU DIAGNOSTICAREA GRIPARII IN RULMENTII CU BILE	75
BUJOREANU, C., CRETU, S. - CONSIDERATII PRIVIND DETERIORAREA PRIN GRIPARE IN RULMENTII CU BILE	81
CHIRILĂ, E., CĂRĂUȘU, C. – STUDIU ANALITIC ASUPRA CONDIȚIILOR DE LUCRU TRANZITORII ALE CUPTORULUI ELECTRIC CU REZISTORI	89
CHIRILĂ, E., CĂRĂUȘU, C. – CONCEPEREA UNUI BLOC DE MĂSURARE ȘI REGLARE ASISTAT DE CALCULATOR PENTRU TEMPERATURA VAT A CUPTORULUI ELECTRIC CU REZISTORI	95
DUMITRACHE, C., COMANDAR, C., SABAU, A., AMARIEI, N. - METODA NUMERICA DE REZOLVARE A ECUATIEI DIFERENTIALE A PROCESULUI DE DETENSIONARE TERMICA PENTRU UN OTEL OLC45	99
ALBU-IACOB, C. - REZULTATE EXPERIMENTALE PRIVIND PRECIZIA SI UNIFORMITATEA TEMPERATURII IN CUPTOARELE ELECTRICE	103
ALBU-IACOB, C. - CONTROLUL AUTOADAPTIV AL UNUI CUPTOR ELECTRIC	109
COMANECI, R., VITALARIU, V., ZAHARIA, L., CHELARIU, R. - ACHIZITIA DE DATE IN STUDIUL COMPORTARII MECANICE A RESTAURARILOR DENTARE	117
DROSESCU, R. - MODELARE CU ELEMENT FINIT ȘI SIMULARE	123
MIRON, V., GHERGHISOR, G., PAUNESCU, R. - ASPECTE PRIVIND CONTRIBUȚIA MODELĂRII MATEMATICE ASUPRA REGIMULUI DE LAMINARE LA CALD ȘI LA RECE ȘI ASUPRA CONDIȚIILOR DE RĂCIRE ÎN VEDEREA ÎMBUNĂȚĂȚIRII CARACTERISTICILOR DE PLASTICITATE ALE BENZILOR DIN OȚELURI CU CONȚINUT SCĂZUT DE CARBON	131
MIHAI, D., STEFAN, M., BADARAU, GH. - COMPORTAREA LA FLUAJ LA 500 °C A OTELULUI 33MoCr11	137
COMAN, GH. - MITOLOGIA METALELOR ÎN OPERA LUI MIRCEA ELIADE	151
SANDU, I., GĂLUSCĂ, D.G., CARCEA, I., ȘTEFAN, M., SANDU, A.V. - AUTENTIFICAREA MONEDELOR VECHI DIN BRONZ I. ASPECTE PRIVIND COMPOZIȚIA PATINEI	157
SANDU, I.G., SANDU, I.C.A., DIMA, A., SANDU, I., NEACȘU, I. - AUTENTIFICAREA MONEDELOR VECHI DE BRONZ II. ANALIZA MICROCHIMICĂ, IR ȘI XRD	167
SANDU, I.G., STOLERIU, Ș., SANDU, I., DIMA, A., SANDU, I.C.A., NEACȘU, I. - AUTENTIFICAREA MONEDELOR ANTICE DIN BRONZ III. ANALIZA COLORIMETRICĂ ȘI TERMOGRAVIMETRICĂ	177
SANDU, I.G., DIMA, A., SANDU, I., DIACONESCU, F., SANDU, A.V. - NIVELE DE CONSERVARE A ARTIFACTELOR METALICE. I. MONEDE ANTICE ȘI ALTE PIESE NUMISMATICE METALICE	189
SANDU, I.G., DIMA, A., SANDU, I., SULIȚANU, N., STOLERIU, Ș., DIACONESCU, F. - STUDIUL PATINEI ARTIFICIALE OBȚINUTE PE ZONELE RESTAURATE A PIESELOR VECHI DIN BRONZ	197
CRISTEA, L., ZSIGMOND, M., APOSTOLESCU, I. – THENOLOGIE DE MEDIU APLICATĂ STAȚIEI DE EPURARE "SLOBOZIA"	205
COCEA, M., MARCUS, L. - SESIUNI DE PROIECTARE A INCALTAMINTEI UTILIZIND SISTEMUL CRISPIN DYNAMICS ENGINEER	211

COCEA, M., MARCUS, L. – STUDIUL PENTRU MODELAREA MATEMATICĂ 2D PRIN SISTEMUL CAD	219
HARNAGEA, F., MIHAI, A. - MATERIALE TEXTILE AUTO SI TERMOADEZIVE FOLOSITE LA CONFECTIONAREA ÎNCĂLĂMINTEI	227
HARNAGEA, F., MIHAI, A. - ASPECTE CU PRIVIRE LA UTILIZAREA DISPERSIILOR ADEZIVE ÎN INDUSTRIA DE ÎNCĂLĂMINTE	233
VIZUREANU, P. - OPTIMIZAREA CUPTOARELOR CU COMBUSTIE CU AJUTORUL COMPUTERULUI	239
VIZUREANU, P. - SISTEME INDUSTRIALE DE INCINERARE	243
MOLDOVAN, P., FIRESCU, L., APOSTOLESCU, I., POPESCU, G., BUTU, M. - NUCLEAREA HETEROGENA SI ROLUL HIDROGENULUI ASUPRA POROZITĂȚII PRIMARE ÎN ALIAJELE DE ALUMINIU	249
CIOBANASU, G., LUCA, D. - MODELAREA PARAMETRIZATĂ A DISPOZITIVELOR DE DEFORMARE ELECTROMAGNETICĂ A TABLELOR	257
CIOBANU, O., POP, GH., CANTEMIR, D. - MĂSURAREA TENSIUNILOR REMANENTE MARI	265
BADARAU, GH., STEFAN, M., IONITA, I. - STRATEGII DE CONTROL A RATIONAMENTELOR ÎN SISTEME EXPERT BAZATE PE REGULI DE PRODUCTIE	273
IONITA, I., STEFAN, M., BADARAU, GH. - METODE DE PUNCT INTERIOR ÎN OPTIMIZAREA CONVEXĂ A FORȚEI DE PREHENSIUNE A UNUI ROBOT UTILIZAT ÎN PROCESUL TEHNOLOGIC DE TURNARE	279
STEFAN, M., IONITA, I., BADARAU, GH. - METODE DE PUNCT INTERIOR ÎN OPTIMIZAREA CONVEXĂ A REGULATOARELOR LINIARE PENTRU CONDUCEREA PREDICTIVĂ A CUPTOARELOR DE TRATAMENT TERMIC TIP LABORATOR	283
STEFAN, M., BADARAU, GH., IONITA, I. - OPTIMIZARE SI METODE COMPUTATIONALE ÎN ȘTIINȚA MATERIALELOR	289
STEFAN, M., IONITA, I., BADARAU, GH. - MODELARE MATEMATICĂ SI OPTIMIZARE ÎN ȘTIINȚA SI ÎNGINERIA MATERIALELOR	293
ISARIE, C., MARIN, A. - HARDWARE ȘI SOFTWARE PENTRU TRADUCTOARE DE DEBIT ULTRASONICE	297

AURELIAN I.SIMIONESCU
(1923-2004)

by

ADRIAN DIMA, IULIAN IONITA AND GHEORGHE BADARAU

Abstract: This paper aims to bring into the attention of a larger public some things about the activity of one of the most important personalities who worked at the Faculty of Materials Science and Engineering from the Technical University of Iasi; it is intended to be a small recognition of the efforts and success of a great scientists and professor who lived among us.



It is hard to resume just in an article's space the professional activity of a so dedicated person like Aurelian I. Simionescu, but this is what the authors intend to do when they started to think of writing these lines. Actually, the difficulty lies in the fact that we all regret of not doing such an attempt when the professor could still judge it. But the past is past and life does go on.

It all started in a day of August 1923 in Suceava, when in the family of Ioan Simionescu, the Appeal Court councillor and Felicia Simionescu the piano player lady a little boy was born.

When the time came, he went to school in Lespezi (1930-1935), at the High Scholl, "Stefan cel Mare" in Suceava (1935-1938) and "Eudoxiu Hurmuzachi" in Radauti (1938-1943).

All these years he was raised and taught in great respect for the Romanian traditions and in patriotism, in the northern region of Romania, Bucovina. In 1943 he was admitted at the Faculty of Electromechanics at the Technical University of Iasi, the former Politechnical Institute of Iasi, and he graduated in 1948 becoming an engineer. His diploma was sustained with a work entitled "The electronic conductivity of non-metallic materials (semiconductors)" for what he received the greatest mention "Magna cum laude".

After graduation, at the proposal of professor dr. T. Câmpan he was named teaching assistant at the Thermotechnics Chair of the Faculty of Mechanics, of the Technical University of Iasi in 1949, becoming a lecturer and working in that position between 1950-1959.

After that, it was pushed away from teaching, for socio-political reasons (like he would say), in fact, for never giving up being a patriot.

He never stopped teaching even if he had to work in other places. He was in time a principal designer engineer at the Regional Designing Institute IPROCHIM Iasi (1959-1964) and principal scientific researcher at the Technical and Physical Research Centre

of Iasi of the Romanian Academy (1964-1966). He held the positions of head of the sector between (1966-1974) then he was named Chief of Laboratory (1974-1981).

During this time he sustained his doctoral thesis in the speciality Thermotechnics and Thermal Machines with the work entitled "The parameters of brown coal burning and elements of calculus for the steam boilers using these combustibles" in 1974. He also followed stages of specialisation at the Politechnical Institute of Sankt Petersburg, the Russian Federation (1969) and at the Technical University from Dresda, Germany (1973).

He regained his position at the Politechnical Institute of Iasi and he worked as a lecturer between (1981-1990), then he became professor (1990-1993) and advising professor (1993-2004).

In 1992 he became advisor for doctoral programs in the speciality of Thermal and Thermochemical Equipment and Installations and at the speciality of Materials Science and Engineering.

He published books, courses for students and over 140 scientific articles both in Romania and abroad. He obtained also 4 patents.

His research activity was wide but some directions were clear: heat recovery systems, heat pipes, improving the methods of determination of the thermal conductivity of materials, heat exchangers with intensified thermal flow rate.

In the field of heat pipes he was the one who conducted the team who achieved the first heat pipe and elaborated the first scientific article comprising testing and results in Romania. The heat pipes school in Iasi developed under his supervision a very long time and with significant results.

He conducted the teams who achieved 135 designs for the great industrial enterprises from Borzesti, Hunedoara, Galati, the Enterprise of Antibiotics of Iasi, the Enterprise of Plastic Materials from Iasi. He executed the design named "The reconstruction of the city of Iasi" stage 1962-1965, at the problem "Thermal District".

At the 31st of March 1975, the Romanian Academy awarded him with the price "Dragomir Hurmuzescu" for the group of works concerning the "Heat exchange in industrial installations". At the Inventions Saloon in Iasi, 1979 he was awarded with the Second Prize and the Third Prize.

He was very proud of being a Commandeer (r) from the Romanian Navy Forces and also for being awarded with the medal "Crucea Comemorativa de Razboi" 1941-1945 and the Medal "A XXV Aniversare a Eliberării Patriei".

He was a Member of the Romanian Academy of Scientists since 1987 and Scientific Secretary of the Branch of Iasi of this institution from 1995. He was an Honorary Member of the Ecological Academy since 1999 and his biography was published in the Romania, USA, and England. He was a member of the Society for Romanian Culture and Literature from Bucovina.

In November 2003 the Senate of the Technical University "Gh.Asachi" Iasi awarded him with the "Excellency Diploma" and the Medal "Gh. Asachi".

He was an honest and fair man, an example to follow. He supported the young researchers and his students really appreciated him as a professional and as a person.

He past through the other world on the 3rd of May 2004 after suffering for a long time and he was buried with military honours in the Cemetery Eternitatea from Iasi, near his beloved wife and daughter.

**CONSTANTIN C. CIOCHINA
(1923-2004)**

by

DAN GELU GALUSCA, IULIAN IONITA AND GHEORGHE BADARAU

Abstract: This paper aims to bring into the attention of a larger public some things about the activity of one of the most important personalities who worked at the Faculty of Materials Science and Engineering from the Technical University of Iasi; it is intended to be a small recognition of the efforts and success of a great professor who worked and lived among us.



Great personality with a high intellectual and moral identity the professor doctor engineer Constantin C. Ciochină served with real devotion the technical superior teaching more than 45 years.

He was born in 11th July 1923 in the commune Cristuru Secuiesc, county of Harghita.

He first go to school in Cristuru Secuiesc, then the first two classes of the high school at the Normal School in the same place 1934-1936. He continued studying at the High School „St. O. Iosif” from Odorhei 1936-1939. From the fall of 1940, following the giving up of the Northern Ardeal, he becomes a refugee with his parents in Sighisoara where he learn at the High School „Principele Nicolae” the last two classes the 7th and the 8th 1939-1942, at the scientific section.

After graduating he was admitted at the Politechnical Institute “Gh. Asachi” of Cernauti (later, Iasi and now the Technical University), at the Faculty of Electromechanics (1942-1948). He obtained the diploma of engineer with the mention „Magna cum Laude” in 1948.

At the beginning of 1949 he was hired in the university teaching at the Politechnical Institute Iasi, the Faculty of Mechanics, the Chair of Metals Technology where he worked all his life.

He obtained the scientific title of doctor in engineering in 1969 with the thesis „Contributions at the study of carburizing in solid media of some standardised carbon and alloyed steels”.

In 1968 the Ministry of Teaching, in Hungary, sent him at a specialisation by

documentation at the Technical University in Budapest in the field of heat and thermochemical treatments.

He went up the entire teaching career: teaching assistant (1949–1951), lecturer (1951–1970), assistant professor (1970–1981), and professor (-1981–1993).

He was doctoral programs adviser in the speciality Materials Technology starting from 1990 leading the way for a large number of doctors in technical sciences, became in time themselves, professors or assistant professors, and he also participated in many occasions at commissions of validation of doctoral thesis at the Technical University “Gh. Asachi” Iasi and in other universities like Bucuresti, Brasov, Cluj-Napoca, Galati.

He activated like a consultant professor between (1993-2004) and he participated in an active and constructive way at the scientific life of the university and more.

He was Head of the Chair of Machine Building and Machines for Agriculture between (1973-1974) and he was an important member in the Faculty Boards at the faculties of Textiles, Mechanics, and materials Science and engineering.

In parallel with the activity at the University he worked also at the Technical and Physical Research Centre, at the Sector of Physics of Metals, as an honorific scientists between (1967 – 1974).

From 1976, together with the creation of the Branch in Iasi of I.C.P.T.S.C. București he was named, on the behalf of the leadership of the I.C.P.T.S.C. București, to do the scientific guidance, and organisation of the research, designing and technical assistance activities of the Branch.

He was a Member of the Scientists Academy from Romania (AOS).

During his long activity he taught courses at the disciplines: Materials Technology, Study of Metals, Equipment and technology of heat treatments, Theoretical Bases of Casting and is one of the founders of the metallurgical teaching in Iasi.

In the didactic activity he was remarked through a high moral and intellectual and professional behaviour.

He published a rich and valuable material supporting the students and over 100 scientific works in Romania and abroad.

The scientific activity of professor Constantin Ciochina developed also in the frame of 25 research contracts between the Politechnical Institute of Iasi and various enterprises like: Fabrica de Rulmenți Bârlad, Combinatul Siderurgic Galați, Centrul de Cercetări Fizice și Tehnice Iași, EVLATEX Târgu Mureș, Fabrica de Industrie locală Bârlad, CIEET București, Universitatea Galați, IUPS Botoșani, ICPUC Brăila, CUG Iași, IM Nicolina Iași

The research fields that made him known were heat and thermochemical treatments, plastically processing of materials, machining, welding technology, corrosion and elaboration of new alloys.

He was awarded with two prizes of the Ministry of teaching for scientific research in 1953 – 1957, evidenced professor in 1986 and with the Medal of the technical University “ Gh. Asachi” Iasi 1996.

In the 45 years of work in the university teaching by his prodigious activity he contributed at the formation of over 40 generation, more than 5000 engineers.

He was a member of the research Board of Advisors of the American Biographical Institute and his biography is included in some prestigious speciality

publications from U.S.A., England and Romania.

He loved chess and he performed for a long time at high level of performance in this noble game.

He dedicated his entire life to the family and to the school honouring them with great devotion.

He past in the other world in the 7th November 2004 and he was buried in Iasi at the Saints Peter and Paul Cemetery.

RAPID PROTOTYPING: AN EFFECTIVE TOOL OF THE ENGINEERING DESIGN PROCESS

BY

LIVIU SEGAL and GEORGETA CIOBĂNAȘU

Abstract: Today it is very important to guide a new product from concept to market quickly and inexpensively. Rapid prototyping technology aids this process, allowing engineers to evaluate their designs through a physical model and facilitating the elimination of design errors early in the product development stage and before any significant investment is made. The purpose of this paper is to provide technical specialists with an overview of rapid prototyping in achieving of the design-to-manufacture process.

Keywords: rapid prototyping, solid modeling, design process

1. Introduction

The conventional mechanical design process requires construction of physical prototypes for testing and evaluation. The rapid progress of CAD technology replaces the need for physical prototypes and these computer-generated models are much less expensive and more flexible than physical models. But no matter how accurate is a CAD model, it will never be exactly the same as the manufactured part.

Nowadays, the information in the 3D solid modeling database has affected the role of the physical prototype in two ways: it has made it possible to simulate a prototype from a 3D model, and it has made it faster and cheaper to create a physical prototype than other methods. Because the volumes contained in a design are fully defined in a solid modeling CAD system, physical models can be created by non-traditional technologies that translate the data into a physical entity.

Rapid prototyping (RP) is the name given to a multitude of related technologies that are used to fabricate physical objects directly from a CAD model. These methods are unique in that they add and bond materials in layers to form objects. Such systems, are also known by the general names freeform fabrication (FFF), solid freeform fabrication (SFF) and layered manufacturing. The resulting prototype provides a "conceptual model" for design visualization and review by the entire design team. It may be used by engineers to check form and fit and perform limited functional tests. It can also be utilized for soft tooling for prototypes and as a pattern for hard tooling. Though there are no restrictions concerning complexity and geometrical features, the physical objects are limited in their size. Another advantage is the fact that the same CAD data used for the prototype creation can be used to go directly from prototype to production, eliminating further sources of human errors.

To reduce the lead-time and costs for the development of new industrial products, "rapid prototyping" has been recognized as a unique, layered manufacturing technique for making prototypes.

2. Rapid Prototyping Process

Regardless of existing rapid prototyping techniques, the methodology of creating a 3D prototype employ the same basic five-step process [1] (fig. 1).

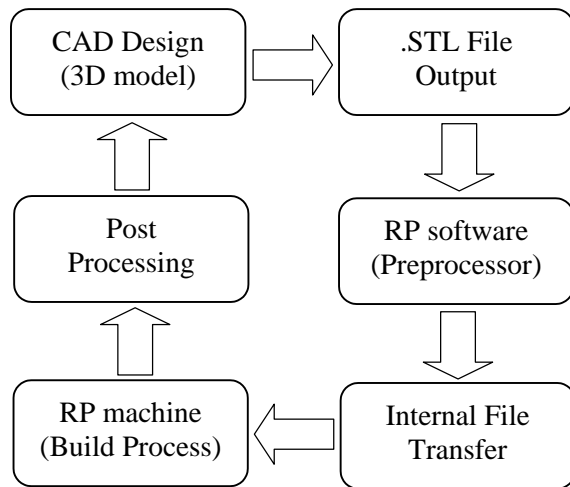


Fig.1 General Rapid Prototyping process

representing the outer skin of an object. Each facet is defined in terms of its vertices and a unit surface normal vector directed away from the interior of the part. The vertices of triangular facets are also ordered to indicate (using the right hand rule) which side of the triangle contains the part mass. As the STL file is a facet model derived from a precise CAD model, it is an approximation of the model. The size and number of these facets that are used in the representation of the model, determine how accurately the STL file matches the original object. For example, the fig. 2 shows the various settings present in the dialog box used to export a 3D model as STL file using SolidWorks system.

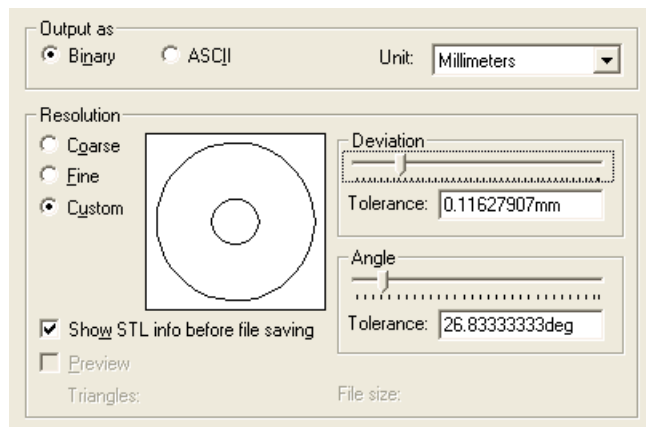


Fig.2 The STL output dialog box in SolidWorks

In the next step, the STL file must be prepared for various types of RP systems. Several programs are available, and most allow the user to adjust the size, location and orientation of the model for optimum part building. The pre-processing software slices the STL model into a number of layers from 0,01 to 0,07 mm thick, depending on the build technique and may also generate an auxiliary structure to support the model during the build. Pre-processing is usually done at a computer separate from the RP system, using a software that is usually part of the RP machine manufacturer. The output consists in a new slice file format, which is transferred to the RP device.

The fourth step is the actual construction of the part. Using different manufacturing techniques, most RP systems build parts within a few hours from polymers, paper or powdered metal. The final step is post-processing and this includes removing the prototype from the machine, as well as any necessary sanding or

finishing which will improve its appearance and durability. If the finished part meets the customer requirements, the cycle is complete.

3. Rapid Prototyping Technologies

In the last decade, a number of RP techniques have been developed. These techniques use different approaches or materials in producing prototypes and they give varying shrinkage, surface finish and accuracy. The most successfully developed techniques are presented bellow [1], [6]:

Stereolithography is the most widely used rapid prototyping technology, patented in 1986. The SLA process is based on photo-polymerization of liquid monomers using ultraviolet (UV) radiation (fig. 3a). A UV laser is scanned over a layer of the liquid monomer to cure the monomer in selected areas as dictated by the part geometry (or the computer generated tool paths). After completion of one layer, another layer of resin is coated on top of the cured layer, and the process is repeated until the part is completed.

Stereolithography generally is considered to provide the greatest accuracy and best surface finish of any rapid prototyping technology. Over the years, a wide range of materials with properties mimicking those of several engineering thermoplastics has been developed. Limited selectively color-changing materials for biomedical and other applications are available, and ceramic materials are currently being developed.

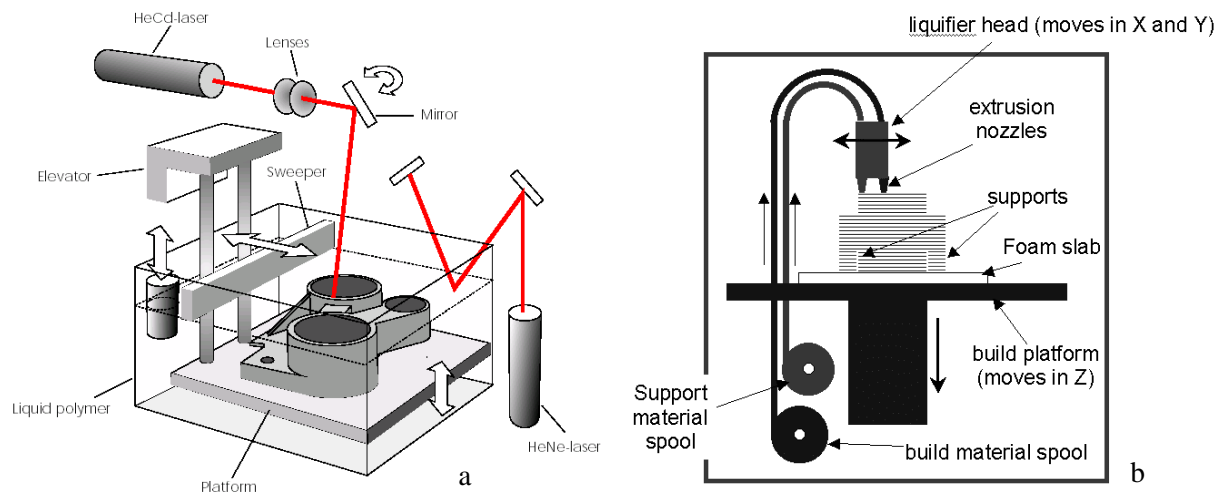


Fig.3 Schematic representation of SLA (a) and FDM (b) processes

Fused deposition modeling (FDM) is the second most widely used RP technology after SLA, developed by Stratasys, Inc. in the early 1990s. A plastic filament is unwound from a coil and supplies material to an extrusion nozzle. The nozzle is heated to melt the plastic and has a mechanism which allows the flow of the melted plastic to be turned on and off. The nozzle is mounted to a mechanical stage, which can be moved in both horizontal and vertical directions (fig.3b).

As the nozzle is moved over the table in the required geometry, it deposits a thin bead of extruded plastic to form each layer. The plastic hardens immediately after being squirted from the nozzle and bonds to the layer below. The entire system is contained within a chamber that is held at a temperature just below the melting point

of the plastic. Several materials are available for the process including ABS and investment casting wax.

Selective laser sintering (SLS), like SLA, is one of the pioneering RP techniques. It was commercialised around 1987 by DTM Corporation (Austin, Texas) who purchased the patents and licenses from University of Texas at Austin. The actual process could be thought of as a hybrid of 3D printing and SLA, in the sense that it involves deposition of a layer of dry powder, which is then sintered using a laser (fig.4a). In SLS, a thin layer (approx. 100-200 μm) of powder is spread on a surface using a cylindrical roller. A laser is then scanned over the powder bed, which heats the powder locally and sinter-bonds the adjacent particles to form one layer of the part.

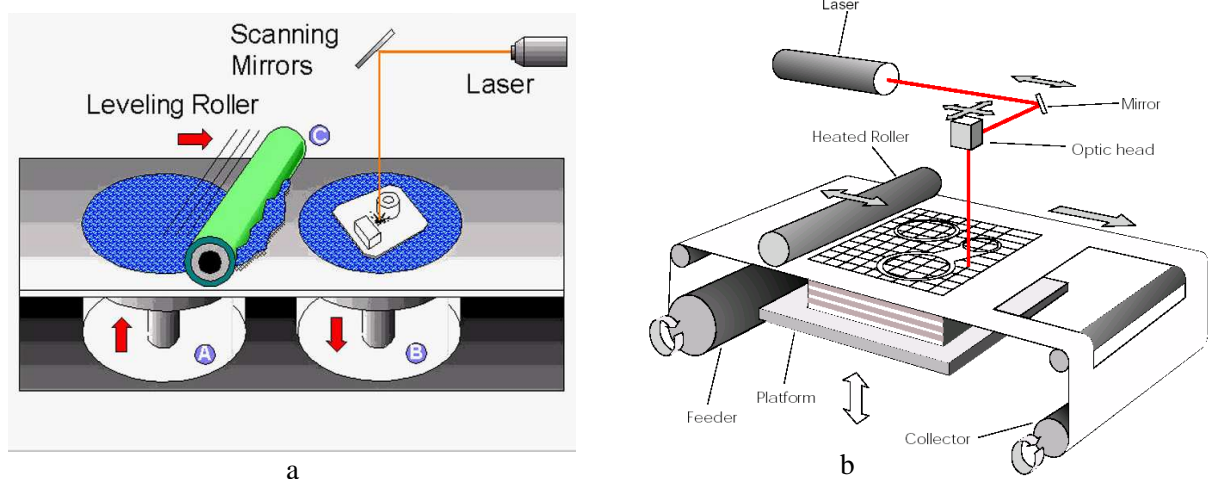


Fig.4 Schematic representation of SLS (a) and LOM (b) processes

Laminated object manufacturing (LOM), produces solid parts from sheet of material, such as paper or vinyl. LOM systems can be used to create larger prototype parts, as shown in fig. 4b. Like all rapid prototyping processes, software first generates cross-sectional slices through the model. Instead of fusing the layer, however, a computer-controlled laser cuts it from the first sheet of material. Then a heated roller bonds the next sheet to the previous layer, and the next cross section is cut from this sheet. The material that will later be removed is cut into crosshatched shapes to make removal easier.

3D Printing (3DP) was invented at the MIT in 1988. It's often used as a direct manufacturing process as well as for rapid prototyping. The process starts by depositing a layer of powder object material at the top of a fabrication chamber (fig. 5). To accomplish this, a measured quantity of powder is first dispensed from a similar supply chamber by moving a piston upward incrementally. The roller then distributes and compresses the powder at the top of the fabrication chamber. The multi-channel jetting head subsequently deposits a liquid adhesive in a two dimensional pattern onto the layer of the powder which becomes bonded in the areas where the adhesive is deposited, to form a layer of the object. Once a layer is completed, the fabrication piston moves down by

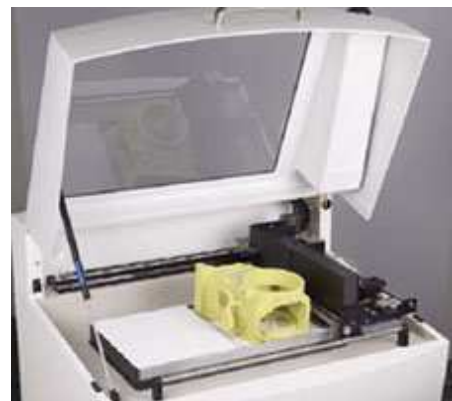
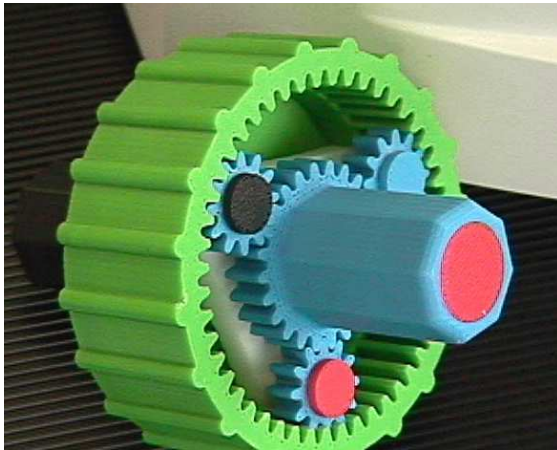


Fig.5 A 3DP printing system

the thickness of a layer, and the process is repeated until the entire object is formed within the powder bed. After completion, the object is elevated and the extra powder brushed away leaving a "green" object. No external supports are required during fabrication since the powder bed supports overhangs.

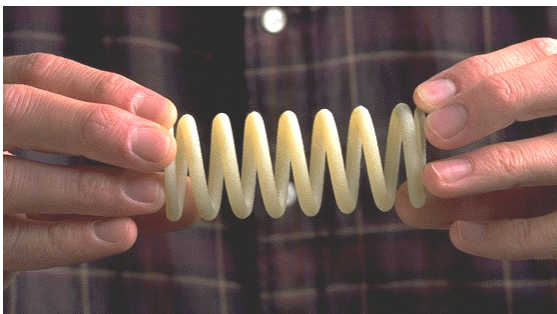
Three-dimensional printing offers the advantages of speedy fabrication and low materials cost. In fact, it's probably the fastest of all RP methods. Recently color output and new materials have also become available. However, there are limitations on resolution, surface finish, part fragility and available materials.



A full color functional assemble



The mold to produce a cast metal part



A part with elastomeric properties

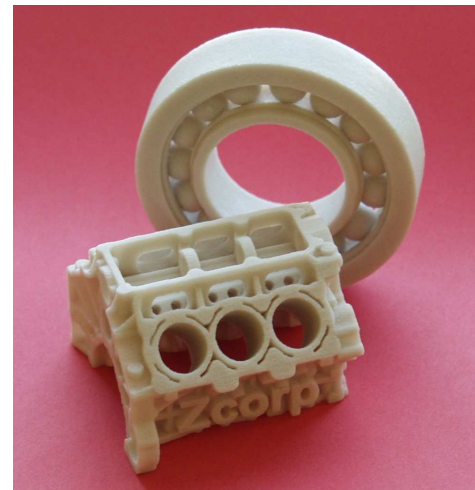


Fig.6 Some prototypes models produced by Z Corp.3D printers [8]

Z Corporation is one of the important vendors that radically streamline the process of building three-dimensional models from CAD files and other 3D data, which incorporates the 3DP process in its RP machines. Z Corp. offers a variety of 3D monochrome and color printers and two basic materials. The printers are fast, versatile and simple, allowing engineers to produce a range of concept models and functional test parts quickly and inexpensively.

The latest Z Corp. innovation, the ZCast Direct Metal Casting process, provides the ability to produce cast metal parts from a CAD file faster and less expensively than traditional prototype casting methods. The process involves printing molds and cores on a 3D Printer directly from digital data, eliminating the pattern and core box production step in the traditional sand casting process. Metal is then poured into the 3D printed molds. Some of prototype models produced by Z Corp. are shown in fig. 6.

4. Case study

The objective of this study was to evaluate the project of a piston, from an engine assembly, defined by the solid model data before final machining process. First, the object to be built is modeled using a CAD software package. Because solid modeling, the current state of the art in CAD, is the most sophisticated method of representing an object, providing more information than other modeling schemes, the part was modeled using the Autodesk Inventor modeler. The model creation start with the primary shape of the model. This base feature is created from the 2D sketch profile shown in fig. 7a, revolved about a centerline (fig. 7b). Then, different sketched and applied features are added to the base part so that, the finished 3D model of the piston with all needed features is shown in fig. 7c.

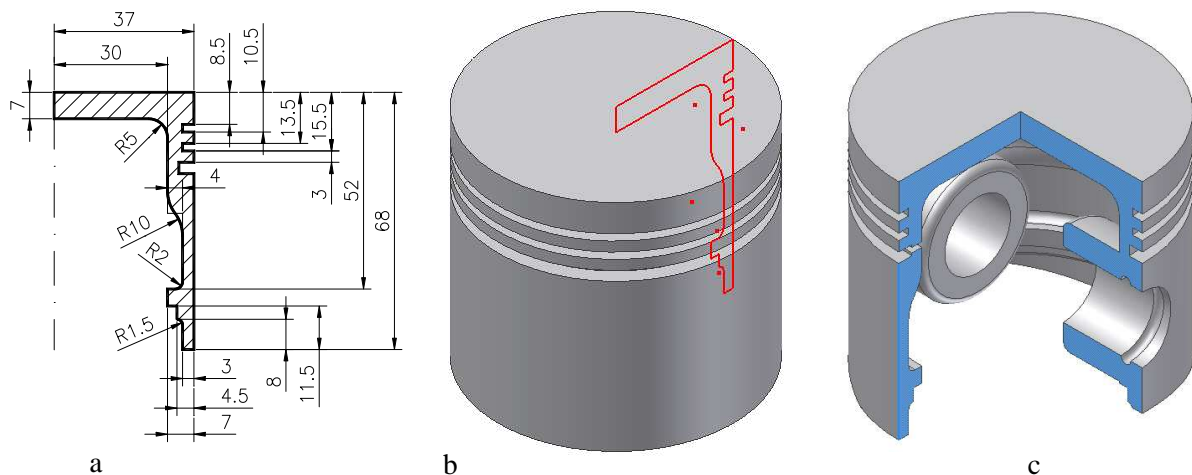


Fig.7 The parametric modeling procedure of the piston

Once the design is finished, the CAD model data must be exported to rapid prototyping system, using the STL standardized format file. STL files used in RP systems must be valid to avoid failure during manufacturing. However, because many commercial tessellation algorithms used by CAD vendors are not robust enough, the current STL file, can be verify using a STL viewer such as DeskArtes View Expert (fig. 8). The program is enable to display, smooth render, rotate, zoom, pan and print STL model data. More, the software identifies costly errors in the file and locates them so that the user can correct the problems in the CAD software. The STL file is then imported to any one of a variety of prototyping machines. For this case study, the rapid prototyping machine is a Z406 3D printing system made by Z Corp., USA.

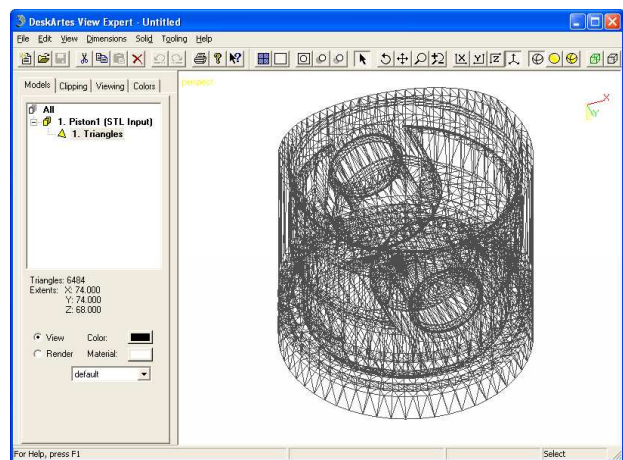


Fig.8 Analysis the STL file using DeskArtes viewer

The Z406 machine starts with STL file which is imported into Z Corp software where is automatically sliced and can be saved as a BLD file. After preprocessing, a "3D Print" command is issued and the part

file is sent to the machine to build. During the build the machine spreads a layer of powder from the feed box to cover the surface of the build piston.

The Z406 system then prints binder solution onto the loose powder, forming the first cross-section. Where the binder is printed, the powder is glued together. The remaining powder remains loose and supports the layers that will be printed above. When the cross-section is complete, the build piston is lowered slightly, a new layer of powder is spread over its surface, and the process is repeated. Finally, the build piston is raised and the loose powder is vacuumed away, revealing the complete part.

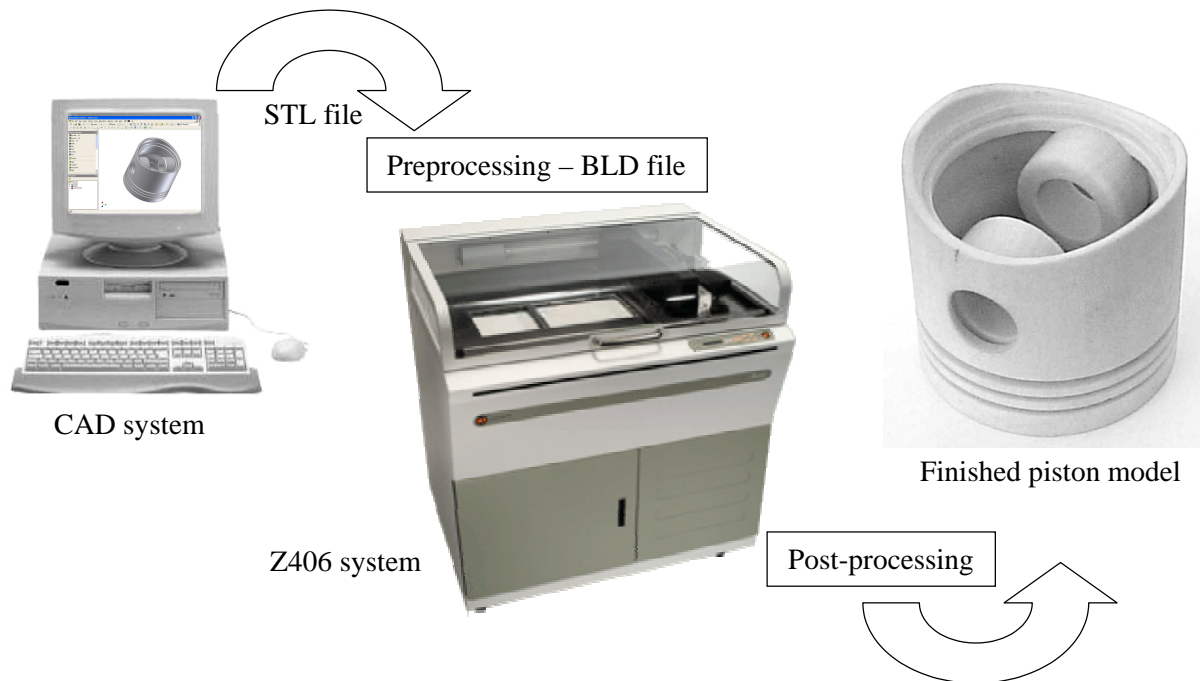


Fig.9 The RP process of engine piston fabrication

Once removed, the piston can be finished in a variety of ways to suit the customer needs. For a quick design review, the piston can be left raw or "green". To produce a more robust model that can be sanded, finished and painted, the part must be infiltrated with wax. The actual post-processing time will depend on the complexity of the part, the skill of the user, and the infiltrate used. The fig. 9 summarized the RP building process of the engine piston using 3D printing method, step by step.

5. Conclusions

Rapid prototyping is relatively a new technology that revolutionizing the manufacturing process, widely used in the automotive, aerospace, medical and consumer products industries. Within a rapid prototyping process, the object is firstly designed on a computer screen and then created based on the computer data. This eliminates inevitable errors that usually appear when a manufacturer interprets a set of drawings.

With such a 3D prototype, engineer designers dispose of an important aid wherewith can visualize potential problems and solutions, refining the product as early as possible in the design processes for low cost and high quality products to speed up the product development cycle.

Acknowledgements

The authors wish to express their thanks to *Z Corporation* for their support in building the physical model of engine piston and all additional materials.

Received April 25, 2005

The "Gh.Asachi" Technical University Iași

REFERENCES

1. Cooper K. G. – **Rapid Prototyping Technology**, Marcel Dekker, Inc., New York, 2001, ISBN 0-8247-0261-1.
2. Kai C. C., Fai K. L. – **Rapid Prototyping: Principles and Applications in Manufacturing**, John Wiley, 1997.
3. Drăgoi G., Guran M. – **Sisteme integrate de producție asistate de calculator**, Ed. Tehnică, București, 1997, ISBN 973-31-1124-4.
4. Lockhart D. S., Johnson M. C. – **Engineering Design Communication**, Prentice Hall, New Jersey, 2000, ISBN 0-201-33151-9.
5. www.stereolithography.com/rapidprototyping.php
6. <http://bmx.ab.ca/rapid-prototyping/rapid-prototyping-home-page.html>
7. www.directindustry.com
8. www.zcorp.com

PROTOTIPAREA RAPIDĂ: O UNEALTĂ EFICIENTĂ A PROCESULUI DE PROIECTARE INGINEREASCĂ

Rezumat: Astăzi este important ca apariția unui nou produs, pornind de la concepție și pînă la lansarea acestuia pe piață, să se facă într-un timp relativ scurt și la costuri cît mai mici. Prototiparea rapidă (RP) oferă un mare potențial pentru îndeplinirea acestui deziderat, oferind proiectanților posibilitatea evaluării și revizuirii produselor prin intermediul unor modele 3D vizuale (prototipuri funcționale). Scopul acestei lucrări este de a oferi specialiștilor o privire generală asupra importanței acestei tehnologii în dezvoltarea produselor.

PROBABILISTIC MODEL FOR FATIGUE ACCUMULATION IN SUPERCONDUCTOR MAGNETS FROM ITER REACTOR

BY

V.PALIOVICI*, V.GOANTA*
R.GRIMBERG**, ADRIANA SAVIN**, ROZINA STEIGMANN**, A.ANDREESCU**,

Abstract: The design and realization of International Thermonuclear Experiment Reactor (ITER) represents one of most ambitious research projects, launched by international scientific community. The reliability limit of the reactor working imposed by the design to 95% imposes that the confidence limit for the superconductor magnet shall be higher than 99.95%. The superconductor magnet works at 4K, the current intensity being 1.8×10^9 A. The jacket material is AISI 316L with external diameter 40.6mm and 2mm wall thickness. The jacket is weld on generatrix, the weld bead having 1mm. The jacket is control by eddy current using a transducer with orthogonal coils. The distribution rule of discontinuities with dimensions smaller than detection threshold through eddy current is considered as Marshall type. The numerical simulations were making with Monte Carlo method. To assure the lifetime imposed by ITER designers, the detection limit of evaluation method shall be 0.78mm length, 0.39mm high at 99.95% POD. In these conditions, the average lifetime will be 2×10^6 cycles. The experimental tests have shown that the mentioned above defect could be detect and thus the prescribed lifetime can be reach.

Keywords: International Thermonuclear Experiment Reactor, Probabilistic model, fatigue accumulation, cracks.

1. Introduction

One of most ambitious research project, launched by world research community is represented by the design and realization of „International Thermonuclear Experimental Reactor” - ITER. The thermonuclear fusion is made in this reactor confining high temperature plasma using very high power superconducting magnets. In these conditions, the temperature of plasma reaches at millions Kelvin degree, but due to confinement, the plasma doesn't enter in contact with the inner wall of reactor, thus, for relative short periods the reactor shall realize fusion of deuterium nucleus that shall give helium nucleus with high quantity of energy release.

The principle scheme of the reactor is presented in Figure 1.

The consortium that design the reactor has identified 100 important components of whom design was made on the basis of fundamental principles of fracture mechanics. It was established that the reliability limit of the reactor shall be 95%, that imposes as confidence limit for each component must be higher than 99.95%, thus, the probability of failure must be better than 1/2000.

Due to the functioning of superconducting magnets at 4K temperature, as well as to the important electromotive forces, because through superconductor cables circulates a current continuum with intensity over $1,8 \times 10^6$ A and of the fact that will

exists periodical outage of installation, the critical components will be submitted to thermal and mechanical fatigue.

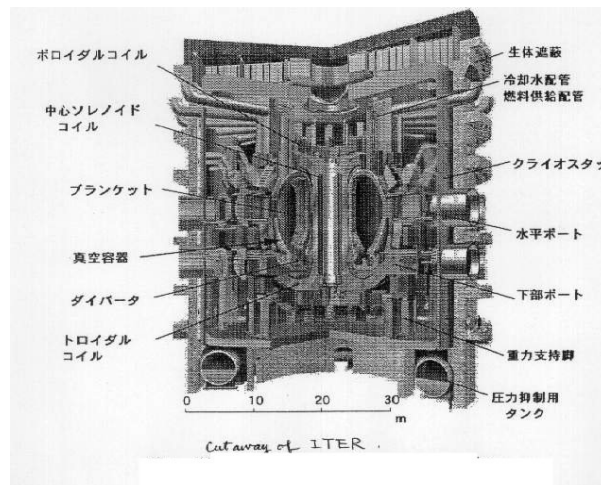


Figura 1. ITER

2. The problem

A very special problem is put in the case of the envelope of the superconductor cables. The material of cable's jacket is AISI 316L, austenitic steel used in nuclear energetic.

Japan Society of Applied Mechanics and Electromagnetics–JSAEM, together with Nondestructive Control Department had have the task to elaborate a method of nondestructive control that shall allows the detection and evaluation of cracks that can appear and grow in the jacket of superconductor cable from which the ITER's superconducting magnets are made.

The superconductor cables submitted to control have the jacket welded on generatrix. Inside, the cable superconductor is inserted. In figure 2 is presented one of the samples that have been controlled.



Fig.2. Super conductor cable from ITER

Through central inlet as well as through the space between superconductor and envelope, liquid Helium circulates. The dimensions of tubes that made the envelope are: inner diameter 38.6mm, wall thickness 2mm, the weld has 1mm inner accretion.

The accretion serves as guide for the superconductor cable. After the inserting of cable in envelope, the assembly is modeled to form a turn of superconductor magnet.

The sheet from which the envelope of SC is made, is tested nondestructive using ultrasound method with Lamb waves, eddy current methods and penetrant liquid method. In these conditions, the body of envelope can be considered without defects. But, the weld on generatrix can presents the typical defects of a weld and discontinuities in thermal affected zone are possible to appear. The weld is made with laser beam.

The design criteria, as well as the database referring to the construction of ITER's superconductor magnets are given in *Design Criteria and Data Base, N 11 RI 01 94-06-30 W0, ITER EDA, Superconducting Coils and Structures Division, Naka-Co-Center, June, 1995*. The study of materials from which the jacket and conductors will follow to be constructed is synthesized in the publication of Naka Company - Memo on Jacket Materials.

According to designers, the lifetime should be at least 45000 fatigue cycles, realized in the following conditions:

Table 1

Case	First Peak	Second Peak
1	340Mpa, R=0, x1	526Mpa, R=0.54, x20
2	200Mpa, R=0, x1	412Mpa, R=0.19, x20

The evaluation of fatigue state was made through a numerical code developed by MIT – Plasma Science and Fusion Center, Massachusetts Institute of Technology USA, in the following conditions:

- The fracture mechanics are applied in linear elastic range, using Paris equation to estimate lifetime.
- In the moment of failure due stress intensity factor, the breaking tenacity increases
- The average stress is introduced with Walker exponent.
- The model of cracks growth supposes a elliptical crack having long axis a and short axis b; thus exist 2 growing speed, after long axis and after short axis, respective.

3. Basis equations.

The growth speed of cracks at constant loading, is expressed in the conditions of linear elastic range of fracture mechanics by Paris law

$$\frac{da}{dN} = c(\Delta K)^n \quad (1)$$

where $\Delta K = K_{\max} - K_{\min}$, c and n are Paris parameters, a – half of the crack's length and N fatigue cycle.

The increase of average stress $(\sigma_{\max} + \sigma_{\min})/2$ for an applied stress, generally shorten the lifetime. The effect of average stress is expressed by stress intensity factor given by

$$\Delta K_{eff} = K_{max} (1-R)^m = \Delta K (1-R)^m \quad (2)$$

Where R is the ratio between $(\sigma_{min} / \sigma_{max})$ and m is Walker exponent.

From the two equations results

$$\frac{da}{dN} = c (K_{max})^n (1-R)^{mn} \quad (3)$$

where $K_{max} = Y \sigma_{max} \sqrt{\pi a}$.

Integration of eq. (3) gives the lifetime (the number of cycles until failure).

$$N_f = \sigma_{max}^{-n} (1-R)^{-mn} \xi \quad (4)$$

where $\xi = \frac{1}{c} \int_{a_i}^{a_f} \frac{da}{Y^n (\pi a)^{n/2}}$

The expression of ξ can be obtained function of crack depth b, instead of semi length of crack, on the basis of knew ratio b/a. the expression for Y must be modified thus

$$\xi = \frac{1}{c} \int_{b_i}^{b_f} \frac{db}{Y^n (\pi b)^{n/2}}$$

where b_i and b_f are initial and final depth, respective. s

4. Development of probabilistic model for accumulative fatigue in the presence of material inhomogeneities and micro cracks.

Starting by the situation of testing the jacket of superconductor cable necessary to realize the superconducting magnets, it has came to the idea that the cracks in welding joint can not be nondestructive detected than if the dimensions of discontinuities exceed a certain value named detection threshold.

In these conditions, we are obliged to consider that in the weld joint exists the possibility of the presence of discontinuities smaller than detection threshold but due to the mechanical and thermal cycles stress they are growing contributing effectively to the nonlinear accumulation of fatigue.

We haven't apriori information about the discontinuities with dimensions smaller that detection threshold, thus we are obliged to suppose that this distribution is purely random. The field of probability doesn't form a Markov chain and in the same time didn't present memory.

The distribution law of discontinuities with dimensions smaller than detection threshold is a Marshall distribution [1]

$$p(b) = \frac{1}{\mu} \exp\left(-\frac{b}{\mu}\right) \quad (5)$$

where b is crack's depth and μ is average depth.

Because the dimensions of cracks are randomly, a probabilistic model can be elaborated, the numerical simulation being made with Monte Carlo method.

In Figure 3 is presented the histogram of cracks dimensions for 10000cracks possible to appear in weld joint of the superconductor jacket

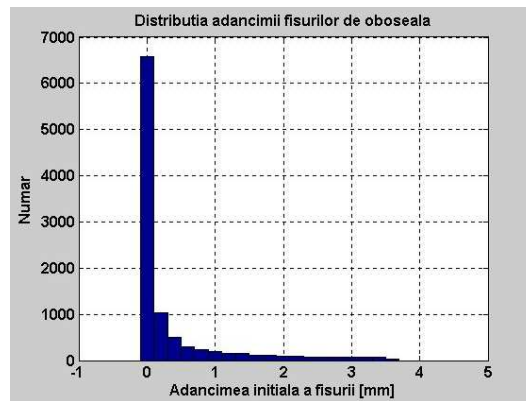


Fig 3. The distribution of fatigue cracks depths

The numerical code was developed in Matlab 6.5, using the own randomly numbers generator, uniform distributed. To determine in probabilistic sense the average depth of crack, the probability of the existence from the star of a crack with depth equal with the width of weld joint was imposed to be 10^{-4} . Using eq. (5), the average depth of crack is the solution of a transcendent equation that was graphically solved, the mean value being the abscissa of A point – the intersection of both curves presented in Figure 4.

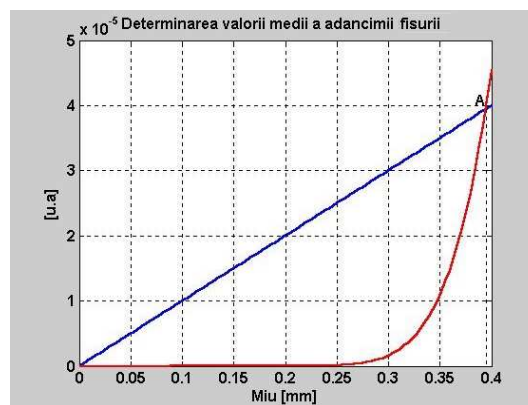


Fig. 4. The determination of man depth crack

Due to the fact that the number of simulated cracks is big, it can be considered that the probability of ratio $r=b/a$ distribution is given by a normal distribution law, having the expression

$$p(r = b/a) = \frac{1}{\sigma\sqrt{2\pi}} \exp\left(-\frac{(r-\bar{r})^2}{2\sigma^2}\right) \quad (6)$$

where \bar{r} is the mean value of ratio b/a and σ is the standard deviation.

It is logic to suppose that, in the case in which the cracks can appear in weld joint have a relative small length, the mean of ratio b/a is 0.5. If we consider a standard deviation of 0.16, the Monte Carlo simulation leads to a distribution of the crack's spectrum as those presented in Figure 5.

The mean value 0.39 of crack depth (abscissa of point A in figure 4) shows that the most probable, the length of crack shall be double, i.e. 0.78mm.

To ensure the life time required by ITER's designers, it was obtained that, through nondestructive control methods which are used to testing the coil of

superconducting magnet, the minimum discontinuity that can be emphasized shall have 0.39mm depth and 0.78mm length.

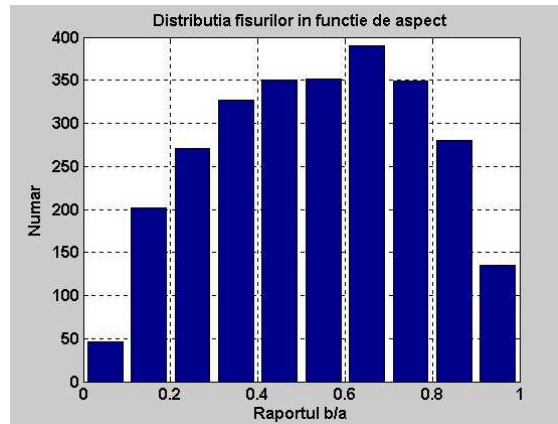


Fig5. Distribution of cracks function of aspect

5. Experimental results about fatigue of AISI 316L at 4 K

The fatigue testing as well as the growth of cracks measurements were independently performed by National Bureau of Standards (NBS)[2] and Naka Company Japan [3] as superconductor's producer. The mean value of results are presented in table 2.

Table 2. Lifetime at 4K

Nr	$c(m/cycli) \times 10^{-12}$	n	ref	N (cycles)	$\ell \ln(N)$
1	12.3	2.5	10	525805	13.17269
2	0.756	3.26	10	998129	13.81364
3	20	2.35	11	503182	13.12871
4	0.617	3.44	11	749958	13.52777
5	13.2	2.56	11	411264	12.92699
6	13.2	2.56	11	411264	12.92699
7	0.21	3.8	12	844495	13.64649
8	0.789	3.26	12	956387	13.77092
9	0.12	3.96	12	971946	13.78706
10	0.012	4.55	12	2142467	14.57747
11	0.09	3.96	12	1295603	14.07449
12	0.35	3.69	12	677595	13.4263
13	0.25	3.65	12	1054813	13.86887
14	0.5	3.57	12	652790	13.38901
15	0.14	3.81	12	1233796	14.02561
16	0.26	3.75	12	778260	13.56482
17	4.81	2.91	13	414414	12.93462

Case 1 - stress: 340 MPa x 1, R=0; 526 MPa x 20, R=0.54

Initial depth = 0.4 mm

Ratio b/a = 0.5

Critic factor of stress intensity = 128 MPa*m^{1/2}

Exponent Walker = 0.67

These data were supplied by NBS –USA, to participants at ITER Project.

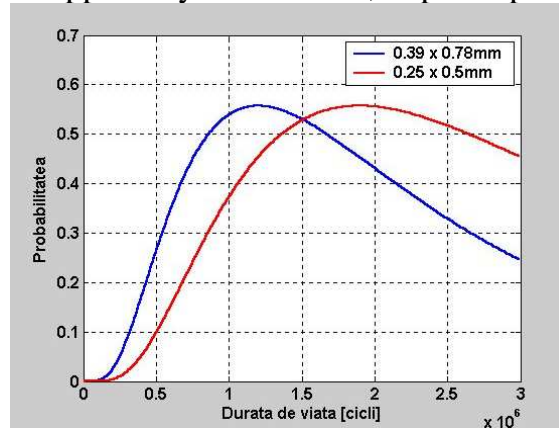


Fig 6. Distribution of lifetime for case 1

Naka Company has used other conditions to determine the fatigue strength. The results are presented in table 3.

Table 3. Lifetime at 4K

Nr	c (m/cycles) $\times 10^{-12}$	n	ref	N (cycles)	$\ell \ln(N)$
1	12.3	2.5	10	404197	12.90966
2	0.756	3.26	10	685842	13.4384
3	20	2.35	11	396364	12.89009
4	0.617	3.44	11	502763	13.12787
5	13.2	2.56	11	313157	12.65446
6	13.2	2.56	11	313157	12.65446
7	0.21	3.8	12	539571	13.19853
8	0.789	3.26	12	657103	13.3956
9	0.12	3.96	12	608114	13.31812
10	0.012	4.55	12	1241174	14.03157
11	0.09	3.96	12	810885	13.60588
12	0.35	3.69	12	439236	12.99279
13	0.25	3.65	12	687425	13.44071
14	0.5	3.57	12	430006	12.97155
15	0.14	3.81	12	787311	13.57638
16	0.26	3.75	12	500500	13.12336
17	4.81	2.91	13	299279	12.60913

Case 2 - stress: 200 MPa x 1, R=0; 412 MPa x 20, R=0.19

Initial depth = 0.4 mm

Ratio b/a = 0.5

Critic factor of stress intensity = $128 \text{ MPa} \cdot \text{m}^{1/2}$

Exponent Walker = 0.67

Conclusions

The method used for nondestructive examination of superconductor's jacket was the eddy current method. This method presents the advantage that has good sensitivity and allows the emphasizing surface breaking defects as well as subsurface defects. To control the superconductor jacket, the eddy current transducer with orthogonal coils [4].

If the minimum detecting crack shall have 0.39mm depth and 0.78mm length, then to the maximum probability shall correspond a 1.2×10^6 cycles lifetime, in the condition of case 1.

If the minimum detecting crack shall have 0.25mm depth and 0.50mm length, then to the maximum probability shall correspond a 1.72×10^6 cycles lifetime.

This lifetime assures 99,95% confidence limit imposed by designers

Acknowledgements

This paper was partially support by Romanian Ministry of Education and Research, under CNCSIS Grant No. 817/2003.

Received 1st May, 2005

*Faculty of Mechanical Engineering,
Technical University Gh.Asachi,

**Nondestructive Testing Department,
National Institute of Research and Development for Technical Physics

REFERENCES

1. W. Marshall, "An Assessment of the Integrity of PWR Pressure Vessels," Report by a study group, available from H.M. Stationary Office, London, United Kingdom, 1976.
2. N.J. Simon and R.P. Reed, Structural Materials for Superconducting Magnets, I.AISI 316 Stainless Steel, National Bureau of Standards, Boulder Co 80303, June, 1982.
3. **Design Criteria and Data Base**, N 11 RI 01 94-06-30 W0, ITER EDA, Superconducting Coils and Structures Division, Naka-Co-Center, June, 1995.
4. **R.Grimberg, R.Plavanescu, A.Andreescu, A.Savin**, Transducer for eddy current surface control, Romanian Patent no. 9960/1989
5. R. Grimberg & col., Modern Methods of Non Destructive Testing – ARoENd Simposium , second edition, 184-192, (1994)
6. C.E.Coleman, S Sagat, GK Shek – Int. J. Pressure Vessel Pipes, 43, 187-204, (1990)

MODEL PROBABILISTIC PENTRU ACUMULAREA OBOSELII IN MAGNETII SUPRACONDUCTORI DIN REACTORUL ITER

Rezumat: Proiectarea si realizarea a "International Thermonuclear Experiment Reactor" (ITER) reprezinta unul din cele mai ambitioase proiecte de cercetare lansate de comunitatea stiintifica internationala. Limita de incredere a functionarii reactorului impusa de proiect, la 95% impune o limita de confidenta de 99,95%. Magnetii supraconductori functioneaza la 4K, intensitatea curentului fiind de 1,8 milioane A. Materialul mantalei conductorului este AISI 316L, cu diametru exterior de 40,6mm si grosime de perete de 2mm. Mantaua este sudata pe generatoare, suprainaltarea fiind de 1mm. Se considera ca legea de distributie a discontinuitatilor cu dimensiuni mai mici pragului de detectie prin curenti turbionari est eo lege de tip Marshall. Similarile numerice s-au facut cu ajutorul metodei Monte Carlo. Pentru a asigura timpul de viata impus de proiect, trebuie ca limita de detectie a metodei de evaluare trebuie sa fie adancime de 0.39mm si lungime de 0.78mm la o probabilitate de detectie de 99.95%. In aceste conditii, timpul de viata mediu va fi 2×10^6 cycles. Testele experimentale au aratat ca defectele precizate au putut fi detectate si astfel timpul de viata prescris poate fi atins.

PROGRAMME OF DATA ACQUISITION FOR DETERMINING THE VARIATION OF THE ELECTRICAL RESISTANCE OF A SEMICONDUCTOR MATERIAL, WITH THE TEMPERATURE

I.GHIMBĂȘEANU, S.PAȚACHIA

***Abstract:** The semi-conductor material we analysed in this paper has a sensibly thermo resistance. The semi-conductor material is made up of syntherized mixtures of metal oxides, such as manganese, iron, cobalt, nickel, copper. The method we used in order to determine the resistance of the semi-conductor material is a modern method of data acquiring designed within the LabVIEW programme that uses LabJack U12 acquisition plate.*

***Keywords:** data acquiring, semiconductor, syntherized mixture.*

1. INTRODUCTION

LabVIEW is a program development application, much like various commercial C or BASIC development systems, or National Instruments LabWindows. However, LabVIEW is different from those applications in one important respect. Other programming systems use text-based languages to create lines of code, while LabVIEW uses a graphical programming language, G, to create programs in block diagram form. LabVIEW uses terminology, icons, and ideas familiar to scientists and engineers and relies on graphical symbols rather than textual language to describe programming actions. LabVIEW has extensive libraries of functions and subroutines for most programming tasks. For Windows, Macintosh, and Sun, LabVIEW contains application specific libraries for data acquisition and VI instrument control. LabVIEW also contains application-specific libraries for GPIB and serial instrument control, data analysis, data presentation, and data storage.

LabVIEW includes conventional program development tools, so it can set breakpoints, animate program execution to see how data passes through the program and single-step through the program to make debugging and program development easier.

Labview includes libraries of functions and development tools designed specifically for instrument control. For Windows, Macintosh, and Sun, LabVIEW also contains libraries of functions and development tools for data acquisition. LabVIEW programs are called virtual instruments (VIs) because their appearance and operation imitate actual instruments. However, they are analogous to functions from conventional language programs. VIs have both an interactive user interface and a source code equivalent, and accept parameters from higher-level VIs. LabVIEW programs are called virtual instruments(VIs). VIs have three main parts: the front panel, the block diagram, and the icon/connector. The front panel contains several numeric controls, boolean switches, slide controls, knob controls, charts, graph, and a thermometer indicator. The front panel contains a toolbar of command buttons and status indicators uses for

running and debugging VIs. Each front panel has an accompanying block diagram, which is the VI equivalent of a program. On create the block diagram using the graphical language G.

The block diagram contains source code. The components of the block diagram represent program nodes such as For Loops, Case structures, and multiplications functions. The components are wired together to show the flow of data within the block diagram.

The icon/connector pane is using to turn a VI into an object that can be uses in the block diagrams of other VIs as a subroutine or function.

The icon and connector are located in the upper right corner of the VI front panel. The connector terminals determine where must wire the inputs and outputs on the icon. The terminals are analogous to parameters of a subroutine or function.

The following are descriptions of these three VI features.

- VIs contain an interactive user interface, which is called the front panel, because it simulates the panel of a physical instrument. The front panel can contain knobs, push buttons, graphs, and other controls and indicators. The input data use a keyboard and mouse, and then the results appeared on the computer screen.
- VIs instructions were received from a block diagram, which was constructed in G. The block diagram supplies a pictorial solution to a programming problem. The block diagram contains the source code for the VI.
- VIs use a hierarchical and modular structure.

With these features, LabVIEW promotes and adheres to the concept of modular programming.

2. EXPERIMENTAL RESEARCH

In order to have an experimental measurement of the resistance-temperature characteristic, a programme in LabVIEW graphic language for data acquisition using a LabJack U12 acquisition plate is designed.

The LabJack U12 is a measurement and automation peripheral that enables the connection of a PC to the real world. The LabJack U12 requires a PC running Windows 98SE, ME, 2000, or XP.

The external features of the LabJack U12 are: USB connector, DB25 digital I/O connector, 30 screw terminals. The USB connection provides power and communication. No external supply is needed.

Each individual screw terminal has a label, AI0 through STB. The LabJack U12 has 8 screw terminals for analog input signals. These can be configured individually and on-the-fly as single-ended channels, 4 differential channels, or combination in between. Each input has a 12-bit resolution and an input bias current of $\pm 90\mu\text{A}$.

The input range for a single ended measurement is ± 10 volts. In differential mode, the voltage of each AI with respect to ground must be between ± 10 volts, but the range of voltage difference between the 2 AI is a function of gain. The LabJack U12 has 2 screw terminals for analog output voltages. Each analog output can be set to a voltage between 0 and the supply voltage (5 volts nominal) with 10-bits of resolution. Connections to 4 of the LabJack's 20 digital I/O are made at the screw terminals, and are referred to as IO0-IO3. These 4 channels include a 1.5 k Ω series resistor that provides overvoltage/short-circuit protection. Connections to 16 of the LabJack's 20 digital I/O are made at the DB25 connector, and are referred to as D0-D15. These 16 lines have no overvoltage/short-circuit protection, and can sink or source up to 25 mA.

There are 37 functions exported by the LabJack dll, and matching functions in the LabVIEW VIs. The analogic entries are used for data acquisition. The resistance values are acquired on the first analogic channel and the temperature values are acquired on the second analogic channel. A potentiometric assembly is used for obtaining the resistance values, and a LM335z temperature sensor is used for obtaining the temperature values. The assembly we used is shown in figure 1.

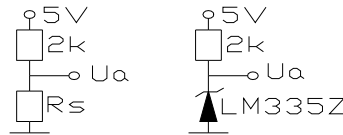


Fig.1 Assembly scheme

The data acquisition was done within a sampling period of 5 seconds. The results we obtained are shown in table 1, and the LabVIEW programme [1,2,3] is shown in figure 2 and 3.

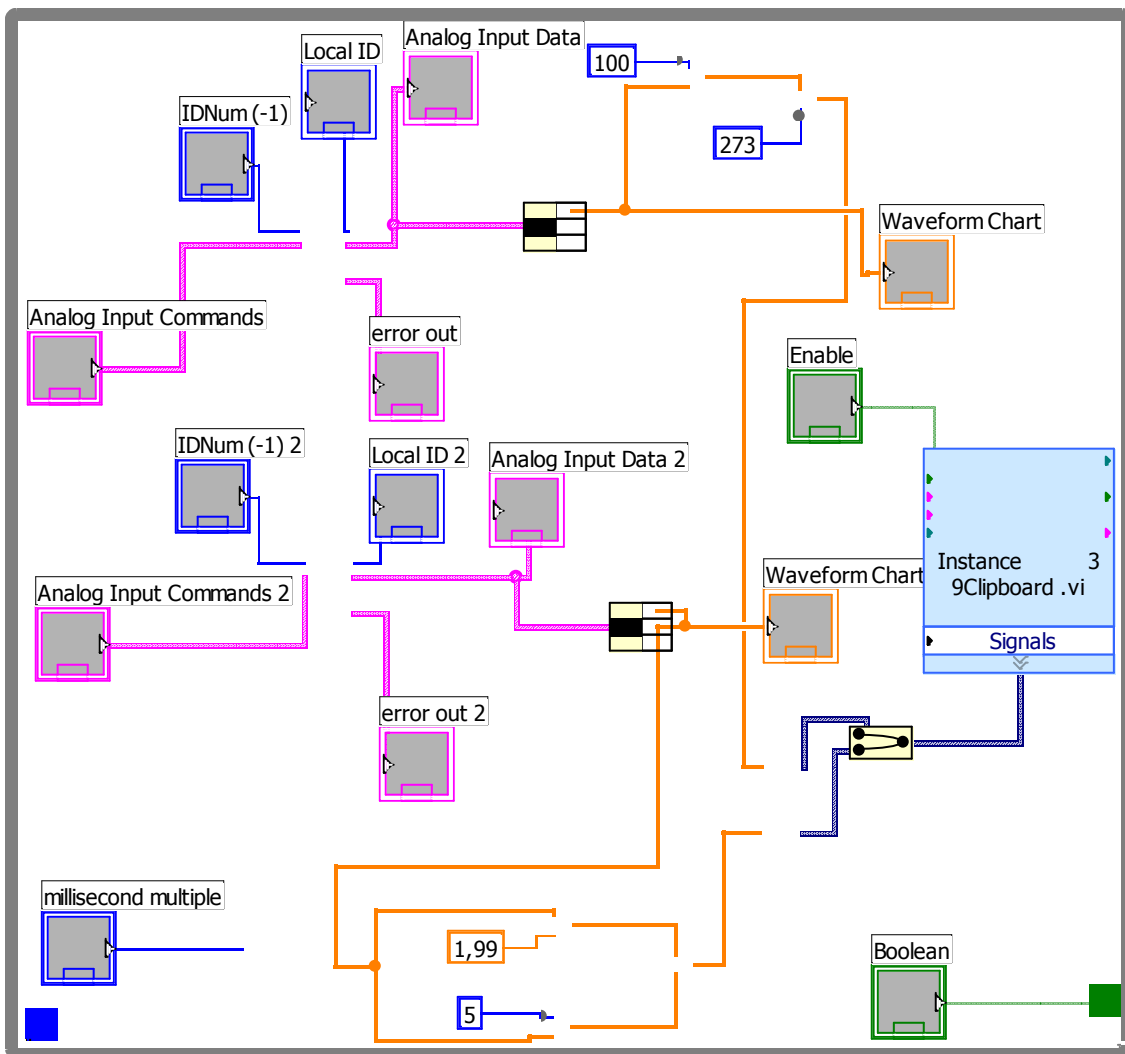


Fig.2. Aquisition block diagramme

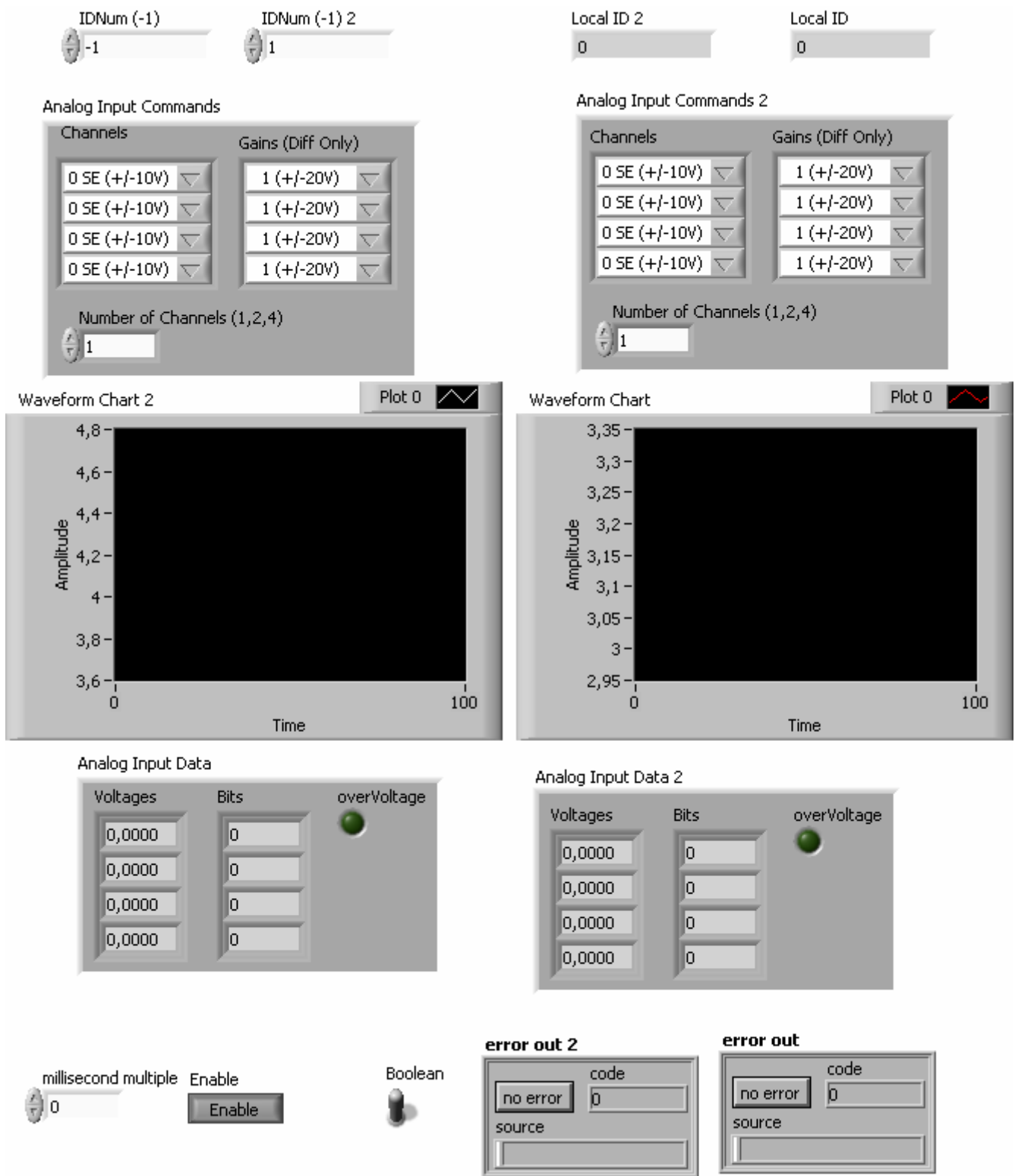


Fig. 3 Aquisition front panel

Table 1. Acquisition data

T[°C]	R[kΩ]	T[°C]	R[kΩ]
22.898437	24.135128	34.128906	15.279153
23.386719	24.474416	34.128906	15.426752
23.386719	23.804430	34.617187	14.991333
23.875000	24.135128	35.105469	14.712951
24.363281	23.804430	35.593750	14.577154
24.363281	23.482000	36.082031	14.312080
24.363281	23.167531	36.082031	14.312080
24.851562	23.804430	36.082031	14.055354
24.851562	22.860732	37.058594	13.806589
24.851562	22.860732	37.546875	13.447576
24.851562	22.561325	38.035156	13.331504
25.339844	23.167531	38.035156	13.331504
25.339844	22.561325	38.035156	12.884161
25.339844	22.269048	38.523437	12.565429
25.339844	21.983647	39.011719	12.260070
25.339844	22.561325	39.500000	12.063517
25.339844	21.983647	40.476562	11.778649
25.828125	21.704884	40.964844	11.595067
25.828125	21.432529	41.453125	11.328693
26.316406	21.983647	41.941406	11.156839
26.316406	21.166364	42.429687	11.072564
26.316406	21.166364	42.917969	10.746000
26.316406	21.166364	43.894531	10.588765
26.316406	20.906180	43.894531	10.285663
26.804687	20.906180	44.382812	10.139524
27.292969	20.906180	44.871094	9.926725
27.781250	20.651778	45.359375	9.721264
27.781250	20.159565	45.847656	9.588182
27.781250	19.921398	45.847656	9.394134
28.269531	20.402967	46.335937	9.330889
28.269531	19.688298	46.335937	9.024919
28.269531	19.460105	47.312500	8.907112
28.757812	19.688298	47.312500	8.678901
29.246094	19.236667	48.289062	8.568342
29.246094	19.017835	48.777344	8.406735
29.734375	19.017835	49.265625	8.198800
30.222656	19.017835	49.753906	7.999020
30.222656	18.387600	50.242187	7.713619
30.222656	18.185842	50.242187	7.854251
30.710937	17.988039	50.730469	7.532243
30.710937	18.185842	51.707031	7.400599
31.199219	17.988039	52.195312	7.189099
31.199219	17.794078	52.683594	7.066711
31.687500	17.234151	53.171875	6.869826
32.175781	17.054486	53.660156	6.681319
32.175781	16.705046	54.148437	6.536192
32.175781	16.878148	54.148437	6.45436
32.664062	16.368198	55.125000	6.361475
33.152344	16.535091	55.613281	6.226774
33.640625	16.204286	56.101562	6.032677

T[°C]	R[kΩ]	T[°C]	R[kΩ]
56.589844	5.939027	58.054687	5.447080
57.078125	5.817510	58.542969	5.474322
57.566406	5.642060	59.031250	5.529410
58.054687	5.529410		

The resistance(kΩ)-temperature(°C) dependence is shown in figure 3.

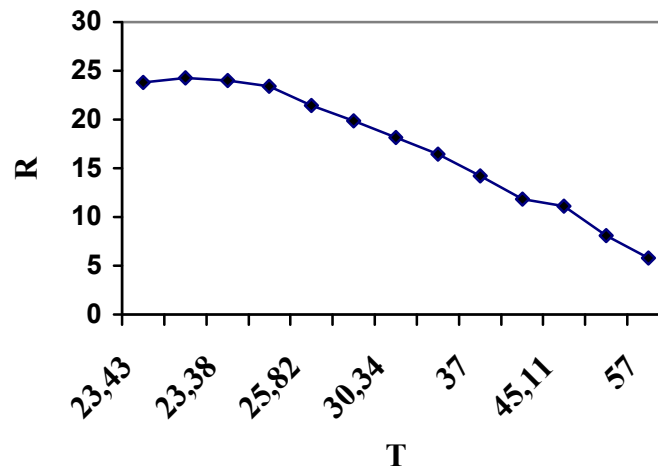


Fig. 3 Rezistence-temperature dependence

3) CONCLUSION

Analyzing the experimental results of the resistance-temperature variation, it could be observed a strong variation of this dependence on temperature.

This property defines the basic function of the material to change its electric resistance according to the variation of the temperature. Unlike metals, those electric resistance increases with the increasing of temperature, for the semi-conductors, the electric resistance decreases as the temperature increases.

4) REFERENCES

- [1] D. Ursuțiu, Initiation in LabVIEW, Lux Libris Publishing House, Brașov, 2001.
- [2] LabVIEW User Manual, National Instrument, January 1998.
- [3] LabVIEW Function and VI Reference Manual, National Instruments, January 1998.

Received March 12, 2005

University "TRANSILVANIA" of Brașov

PROGRAM DE ACHIZIȚIE DE DATE PENTRU DETERMINAREA VARIAȚIEI REZISTENȚEI UNUI MATERIAL SEMICONDUCTOR

Materialul semiconductor analizat are o rezistență sensibilă termic și este realizat din amestecuri sinterizate de dioxid de mangan, oxid de cobalt, oxid de nichel, carbonat de cupru, caolin. Metoda folosită pentru determinarea rezistenței materialului semiconductor este o metodă modernă de achiziție de date creată în programul LabVIEW care folosește o placă de achiziție LabJack U12.

Pentru determinarea experimentală a caracteristicii rezistență-temperatură se întocmește un program în limbajul grafic LabVIEW pentru achiziția datelor. Achiziția datelor se face pe intrările analogice. La primul canal analogic se achiziționează valorile rezistenței iar pe canalul analogic 2 se achiziționează valorile de temperatură. Pentru achiziția rezistenței se folosește un montaj potențiomtric iar pentru achiziția valorilor temperaturii se folosește un senzor de temperatură LM335z.

AN ANALYTICAL MODEL FOR HOLLOW TUBE DRAWING

by

Mihai TÂRCOLEA, Sorin CIUCĂ, Daniel VLĂȘCEANU

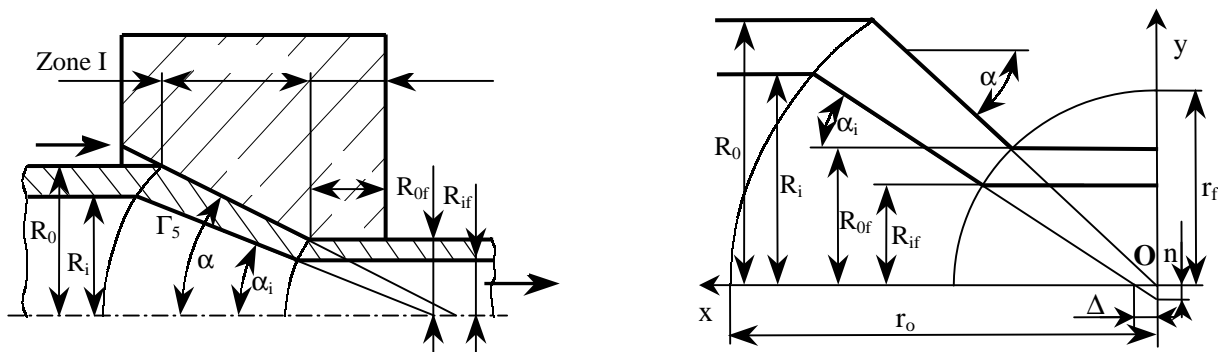
Abstract

The paper presents an analytical solution able to correlate almost all parameters of the drawing process, i.e. strain, stress, and power ones. Starting from Avitzur's distinct models for strain and respectively stress, is presented a new combined geometry of the deformation zone, able to determine simultaneously the draw force and the wall thickness, taking into account the evolution of material strength due to cold-work hardening. The aim of this solution is the definition of an "inner" hemi-angle, which determines the evolution of the inner surface of the tube in the deformation zone. The model permits also to determine the optimal angle of the die, correlated with the material characteristics, the geometry of the hollow billet and of the pipe.

Keywords: hollow tube drawing, mathematical model

Introduction

Computer simulation of real processes is an advantageous solution for technological design. The model for cold tube drawing is not clearly established yet. B. Avitzur presents two different models [1], one to determine the drawing force and another one to determine tube geometry. The present analytical solution [6] starts also from Avitzur's one, with some changes in the deformation zone geometry: we introduce here an "inner" hemi-angle that determine the evolution of inner surface of the tube; this angle α_i depends on all the geometric and energetic parameters of the process, including the stress hardening of the material. The geometry of the deformation zone is defined by the limiting surfaces $\Gamma_1, \Gamma_2, \Gamma_3, \Gamma_4$.



Zone II is limited by two spherical surfaces (Γ_1 with radius r_f and Γ_2 with radius r_o), and two conical surfaces (Γ_3 generated by the die angle α , and Γ_5 generated by the inner angle α_i , which determines the evolution of the inner diameter of the tube). The relative draw stress will be calculated with:

$$\frac{\sigma_{xf}}{\sigma_c} = \frac{F_{rod} - F_{core}}{\pi \cdot \sigma_c (R_{of}^2 - R_{if}^2)} = \frac{\sigma_{xf}/\sigma_c|_{rod} - (R_{if}/R_{of})^2 \cdot \sigma_{xf}/\sigma_c|_{core}}{1 - (R_{if}/R_{of})^2} \quad (1)$$

The friction can be considered considering the friction factor m or the friction coefficient f . Depending on this, the final form of the relative draw stress will be:

$$\begin{aligned} \frac{\sigma_{xf}}{\sigma_c} = & \frac{1}{1 - \left(\frac{R_{if}}{R_{of}}\right)^2} \left\{ 2f(\alpha) \ln \frac{R_o}{R_f} + \frac{2}{\sqrt{3}} \left(\frac{\alpha}{\sin^2 \alpha} - \text{ctg} \alpha \right) + \frac{2}{\sqrt{3}} m \left(\text{ctg} \alpha \ln \frac{R_o}{R_{of}} + \frac{L}{R_{of}} \right) \right\} \\ & - \left(\frac{R_{if}}{R_{of}} \right)^2 \left[2f(\alpha_i) \ln \left(\frac{R_i}{R_o} \frac{R_o}{R_{of}} / \frac{R_{if}}{R_{of}} \right) + \frac{2}{\sqrt{3}} \left(\frac{\alpha_i}{\sin^2 \alpha_i} - \text{ctg} \alpha_i \right) \right] - \frac{\sigma_{xb}}{\sigma_c} \left(\frac{R_o}{R_{of}} \right)^2 \left[1 - \left(\frac{R_i}{R_o} \right)^2 \right] \end{aligned} \quad (2,a)$$

or:

$$\begin{aligned} \frac{\sigma_{xf}}{\sigma_c} = & \frac{1}{1 - \left(\frac{R_{if}}{R_{of}}\right)^2} \left\{ \left[2f(\alpha) \ln \frac{R_o}{R_f} + \frac{2}{\sqrt{3}} \left(\frac{\alpha}{\sin^2 \alpha} - \text{ctg} \alpha \right) + \frac{2}{\sqrt{3}} f \left[\text{ctg} \alpha \left(1 - \frac{\sigma_{xb}}{\sigma_c} - \ln \frac{R_o}{R_{of}} \right) + \frac{L}{R_{of}} \right] + \frac{\sigma_{xb}}{\sigma_c} \right] \frac{1}{1 + 2f \frac{L}{R_{of}}} \right. \\ & \left. - \left(\frac{R_{if}}{R_{of}} \right)^2 \left[2f(\alpha_i) \ln \left(\frac{R_i}{R_o} \frac{R_o}{R_{of}} / \frac{R_{if}}{R_{of}} \right) + \frac{2}{\sqrt{3}} \left(\frac{\alpha_i}{\sin^2 \alpha_i} - \text{ctg} \alpha_i \right) \right] - \frac{\sigma_{xb}}{\sigma_c} \left(\frac{R_o}{R_{of}} \right)^2 \left[1 - \left(\frac{R_i}{R_o} \right)^2 \right] \right\} \end{aligned} \quad (2,b)$$

where:

$$f(\alpha) = \frac{1}{\sin^2 \alpha} \left[1 - \cos \alpha \sqrt{1 - \frac{11}{12} \sin^2 \alpha} + \frac{1}{\sqrt{11/12}} \ln \frac{1 + \sqrt{\frac{11}{12}}}{\sqrt{\frac{11}{12}} \cos \alpha + \sqrt{1 - \frac{11}{12} \sin^2 \alpha}} \right] \quad (3)$$

From the geometrical reasons of figure 2 we can determine all dependencies of the shape factors, considering first the equations:

$$\begin{cases} x^2 + y^2 = r_f^2 \\ y = m \cdot x + n \end{cases} \quad (4)$$

Taking into account that:

$$m = \text{tg} \alpha_i = \frac{n}{\Delta} \quad (5)$$

$$r_o = \frac{R_o}{\sin \alpha} \quad (6)$$

$$r_f = \frac{R_{of}}{\sin \alpha} \quad (7)$$

$$\sin \beta = \frac{R_i}{r_o} = \frac{R_i}{R_o} \sin \alpha \quad (8)$$

$$\Delta = R_o \frac{\cos \beta}{\sin \alpha} - \frac{R_i}{\operatorname{tg} \alpha_i} \quad (9)$$

$$n = \Delta \cdot \operatorname{tg} \alpha_i = R_o \frac{\cos \beta}{\sin \alpha} \operatorname{tg} \alpha_i - R_i \quad (10)$$

and the relative variable $Y = y/R_{of} = R_{if}/R_{of}$, we obtain the equation:

$$Y^2(1 + \operatorname{tg}^2 \alpha_i) + 2Y \frac{R_o}{R_{of}} \left(\frac{\cos \beta}{\sin \alpha} \operatorname{tg} \alpha_i - \frac{R_i}{R_o} \right) + \left(\frac{R_o}{R_{of}} \right)^2 \left(\frac{\cos \beta}{\sin \alpha} \operatorname{tg} \alpha_i - \frac{R_i}{R_o} \right)^2 - \left(\frac{R_{of}}{\sin \alpha} \right)^2 \frac{\operatorname{tg}^2 \alpha_i}{R_{of}^2} = 0 \quad (11)$$

Its only positive solution is:

$$\frac{R_{if}}{R_{of}} = A + \operatorname{tg} \alpha_i \sqrt{\frac{\cos^2 \alpha_i}{\sin^2 \alpha} - A^2} \quad (12)$$

with:

$$A = \frac{R_o}{R_{of}} \left(\frac{R_i}{R_o} - \frac{\cos \beta}{\sin \alpha} \operatorname{tg} \alpha_i \right) \cos^2 \alpha_i \quad (13)$$

$$\beta = \arcsin \left(\frac{R_i}{R_o} \sin \alpha \right) \quad (14)$$

Considerations about the inner angle α_i

The relative draw stress σ_{xf}/σ_c has a minimum \hat{n} in terms of inner angle α_i ; this minimum depends on almost all process factors, and the stress hardening of the material. The range of α_i values corresponding to the minimum of relative draw stress σ_{xf}/σ_c is relatively narrow, in the range of about $0.5 \cdot \alpha$ to, at most, $(1.8 \dots 2) \cdot \alpha$.

Mathematically, the problem is solved if there is determined the solution of equation:

$$\frac{\partial(\sigma_{xf}/\sigma_c)}{\partial \alpha_i} = 0 \quad (15)$$

The technological restrictions of the process do not allow to use a common numerical method to solve the above equation; that is because there is also possible to reach imaginary solutions; there was establish an original algorithm able to solve such an equation that can have only a narrow range of real values.

Influences of main processes parameters

Computer simulations were done using original programs developed under Matlab $\text{\textcircled{R}}$, using both models: **m** and **f**, named upon the friction law considered.

Firstly, there were studied the influences on the relative draw stress of reduction of the relative outer diameter R_o/R_{of} , and of the initial relative wall thickness R_i/R_o for constant die angle α (figure 3, table 1 and 2). For constant R_o/R_{of} , with the increasing R_i/R_o (i.e. with decreasing thickness) the value α_i corresponding to the minimum of draw stress decreases, at constant α . With the increase of R_o/R_{of} , the real solutions of the above equation (15) correspond to increasing values of R_i/R_o ; that means intense reduction of outer diameter can be applied only to thin wall tubes.

Another important factor is the die angle α (figure 4 and 5). With the increase of the die angle α , the corresponding values of the inner angle α_i for the minimum of σ_{xf}/σ_c are increasing; i.e. there is a tendency of more and more thickening of the final tube wall.

For tubes with thick initial walls ($R_i/R_o = 0.75$), no matter the value of outer diameter reduction R_o/R_{of} , the die angle α did not have a pregnant influence on the relative reduction of the cross-section δ . For tubes with thin initial walls ($R_i/R_o = 0.90$), the relative reduction of the cross-section δ decreases with the increase of α for low reductions of outer diameter and increases with the increase of α for high reductions of

Table 1. Calculus results for: $fm = 0.005$, $\alpha = 12^\circ$

No	R_o/R_{of}	R_i/R_o	σ_{xf}/σ_c	g_f/g_o	δ , [%]	R_{if}/R_{of}	α_i , [°]
1	1.3	0.75	0.2841	1.1593	17.28	0.6332	14.04
2	1.3	0.80	0.2870	1.1976	13.58	0.6886	14.04
3	1.3	0.85	0.2992	1.1882	12.64	0.7683	13.46
4	1.3	0.90	0.3353	1.1708	12.41	0.8478	12.89
5	1.3	0.95	0.4649	1.1215	14.75	0.9271	12.32
6	1.5	0.75	0.3837	1.1025	33.36	0.5866	12.89
7	1.5	0.80	0.3863	1.1663	28.72	0.6501	13.18
8	1.5	0.85	0.3978	1.2195	24.17	0.7256	13.18
9	1.5	0.90	0.4340	1.2472	20.66	0.8129	12.89
10	1.5	0.95	0.5773	1.3332	13.40	0.9000	12.61
11	1.7	0.85	0.4797	1.2062	35.09	0.6924	12.89
12	1.7	0.90	0.5142	1.3060	28.11	0.7780	12.89
13	1.7	0.95	0.6528	1.4120	19.92	0.8800	12.61

Table 2. Calculus results for: $f = 0.10$, $\alpha = 12^\circ$

No	R_o/R_{of}	R_i/R_o	σ_{xf}/σ_c	g_f/g_o	δ , [%]	R_{if}/R_{of}	α_i , [°]
1	1.3	0.75	0.3776	1.1593	17.28	0.6332	14.04
2	1.3	0.80	0.4014	1.1694	15.22	0.6958	13.75
3	1.3	0.85	0.4489	1.1882	12.64	0.7683	13.46
4	1.3	0.90	0.5542	1.1708	12.41	0.8478	12.89
5	1.3	0.95	0.8870	1.1215	14.75	0.9271	12.32
6	1.5	0.75	0.4609	1.1346	31.94	0.5745	13.18
7	1.5	0.80	0.4780	1.2063	26.81	0.6381	13.46
8	1.5	0.85	0.5151	1.2195	24.17	0.7256	13.18
9	1.5	0.90	0.6042	1.2472	20.66	0.8129	12.89
10	1.5	0.95	0.9102	1.1756	23.16	0.9118	12.32
11	1.7	0.85	0.5544	1.2720	32.23	0.6756	13.18
12	1.7	0.90	0.6188	1.3060	28.11	0.7780	12.89
13	1.7	0.95	0.8523	1.4120	19.92	0.8800	12.61

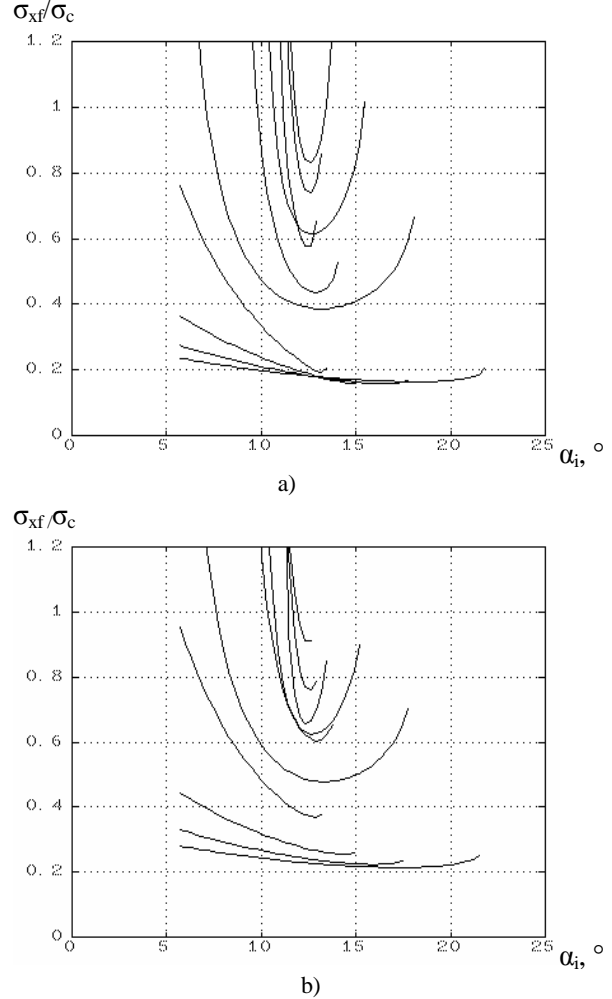


Figure 3. Influence of R_o/R_{of} and R_i/R_o on the value and position of the minimum of $\sigma_{xf}/\sigma_c = F(\alpha_i)$, for model **m** (a) and model **f** (b)

outer diameter. This confirm the hypothesis of an interaction between the geometrical parameters of the tube and is also determined by the evolution of the strain hardening of the tube material.

The friction conditions influence was also studied (figure 6). This must be correlated with all the geometrical conditions of the drawing. The evolutions of the results are similar for both mathematical models, even if they cannot be related because of the different friction laws considered. The models can be used independently in an experimental technique which allows us to evaluate the either the friction factor m or the friction coefficient f , if we can measure the draw force with strain gauges. This can be done by numerical solving of one of the following equations:

$$\frac{\sigma_{xf}(m)}{\sigma_c} - \left(\frac{\sigma_{xf}}{\sigma_c} \right)_{exp} = 0 \quad (16)$$

or:

$$\frac{\sigma_{xf}}{\sigma_c}(f) - \left(\frac{\sigma_{xf}}{\sigma_c} \right)_{exp} = 0 \tag{17}$$

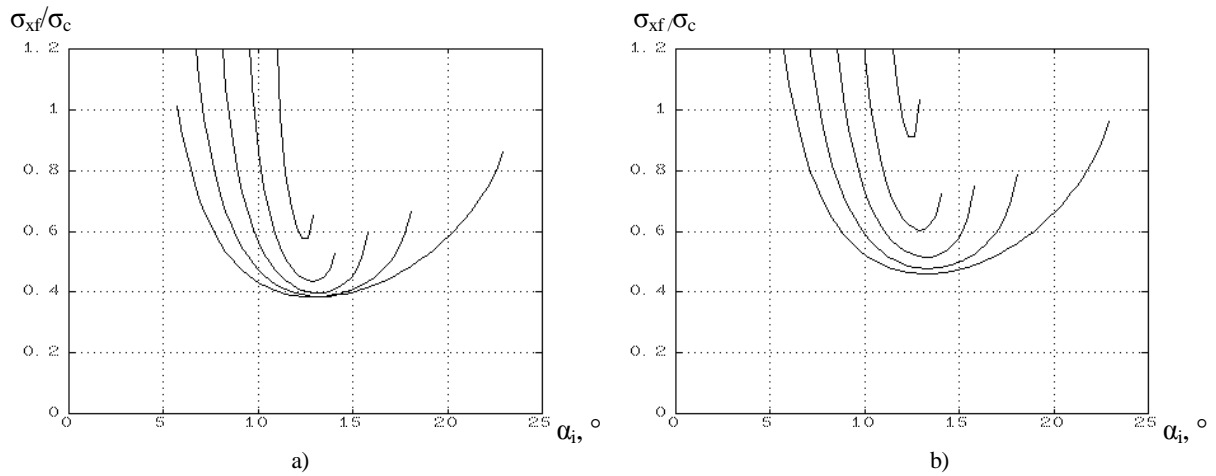


Figure 4. Dependence of the value and position of the minimum of relative draw stress σ_{xf}/σ_c on the inner angle α_i , and wall thickness R_i/R_0 , if relative reduction is $R_0/R_{of} = 1.5$, for model **m** (a) and model **f** (b).

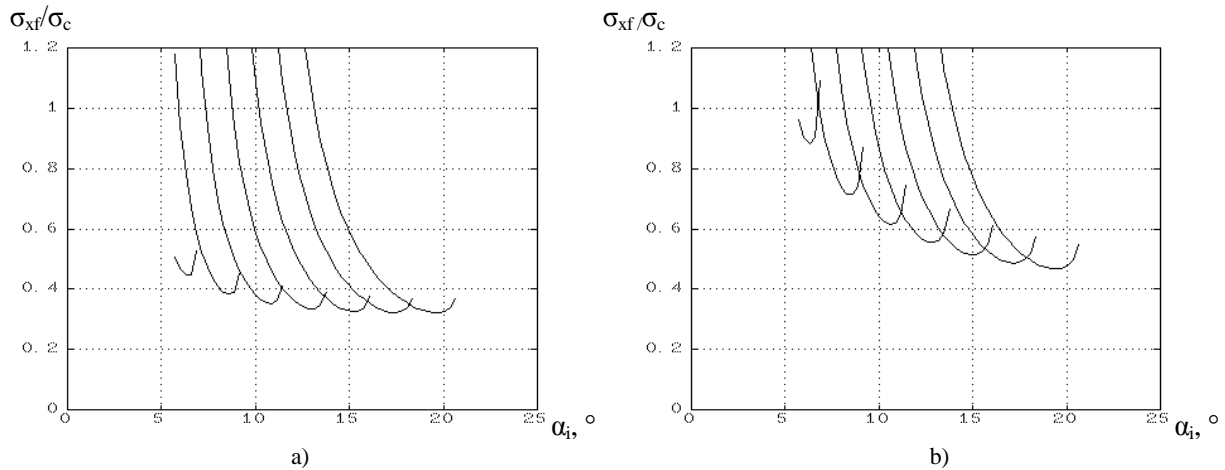


Figure 5. Influence of die angle α on the value and position of relative draw stress σ_{xf}/σ_c in regard to the inner angle α_i , with $R_0/R_{of} = 1.3$ and $R_i/R_0 = 0.90$, for model **m** (a) and model **f** (b).

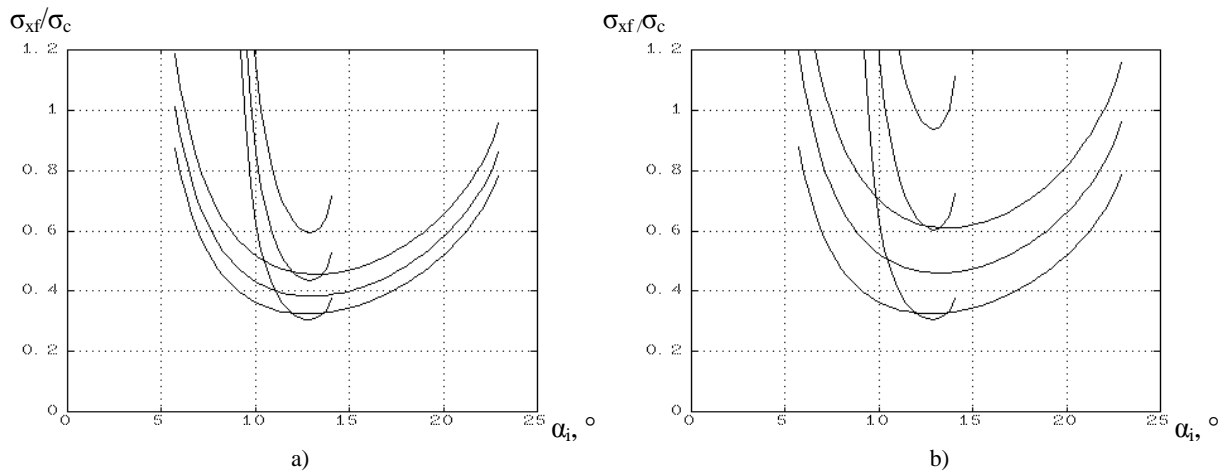


Figure 6. Influence of the value of friction factor m on the value and position of relative draw stress σ_{xf}/σ_c in regard to inner angle α_i , when $R_0/R_{of} = 1.5$ and $R_i/R_0 = 0.75$ (a), respectively 0.90 (b).

CONCLUSIONS

The paper is proposing an analytical solution to evaluate draw stress for hollow tube drawing in the same time with the complete determination of the geometrical factors resulting for a specific material and die; there is also possible to estimate correctly the final wall thickness of the tube after drawing. This model can be also used to determine the optimal die angle for a specific technology applied to a specific material and a specific initial geometry.

The main idea for this model is the use of an inner angle that determines the inner diameter of the tube, which value depends on all the process parameters, and is determined by the minimum drawing stress in a specific frame of work (geometrical context of the tube/die, back-tension applied, material involved and friction conditions).

The model is presented in two distinct forms, one for friction factor m and another one for friction coefficient f . The hypothesis of friction factor m is more and more considered because it determined simpler mathematical models for plastic forming processes and creates a clearer context for analysis: no friction means $m = 0$ and the adherence means $m = 1$.

There were also made experimental measurements that revealed a good concordance with computed values for relative draw stress as well as for geometrical parameters of the drawn tube.

Received May 2, 2005

“Politehnica” University Bucharest

References

1. Avitzur, B. - Metal Forming: Processes and Analysis, New York, Mc.Graw-Hill Book Co., 1968.
2. Cazimirovici, E., Târcolea, M. - Cercetări privind tragerea țevilor capilare pe dom deformabil, Metalurgia, vol.39, nr.6, 1987.
3. Cazimirovici, E., Târcolea, M. - Contribuții privind stabilirea comportării la deformarea prin tragere a oțelului inoxidabil pentru țevi capilare, Metalurgia, vol.40, nr.1, 1988.
4. Cazimirovici, E., Negulescu, I., Târcolea, M., Răducanu, Doina - Teoria și tehnologia deformării prin tragere, București, Editura Tehnică, 1990.
5. Cazimirovici, E., Târcolea, M. - Stabilirea parametrilor de tragere a țevilor capilare din oțel inoxidabil, Contract de Cercetare Nr. 45-5-11/1985-86 între Institutul Politehnic București și C.C.P.T.T. - București.
6. Târcolea, M. - "Studii și cercetări privind modelarea procesului de deformare plastică prin tragere fără ghidaj interior a țevilor" – TEZĂ DE DOCTORAT, UPB, 1994.

UN MODEL ANALITIC PENTRU PRELUCRAREA PRIN TRAGERE A ȚEVILOR

Rezumat

Lucrarea prezintă o soluție analitică capabilă să coreleze toți parametrii procesului de tragere, de exemplu, tensiuni, puteri specifice etc.

COMPUTERIZATED QUANTITATIVE MICROGRAPHICAL ANALYZE OF DEPOSED LAYERS BY ELECTRICAL DISCHARGE IN IMPULSE ON AN HIGH ALLOYED TOOLS STEEL

by

ADRIAN ALEXANDRU, SORIN IACOB STRUGARU, IOAN ALEXANDRU,
LAURENTIU CIOBANU, SORIN TANASUCA

Abstract: This paper work presents the experimental results of optical quantitative computerised analyze concerning the characterisation of the deposited layers by electrical discharge in impulse on a 155MoVCr115 steel.

Keywords: electric impulse, electric discharge, quantitative analyze

1. Introduction

The superficial thermic treatments technologies or deposition of thin layers, have each some disadvantages, so, today we trying to combine two or more technologies in order to increase the performances of the machine parts or tools.

The obtaining of thin layers by electrical discharge in impulse has some advantages as: verry good adherence of the coverings the possibility of deposition of all kind of materials with electric conductivity, the simplicity of the devices and technologies, but also presents some disadvantages: large roughness and residual stress in the deposited layer.

We can say that joining alloying and deposition by electric impulse with a superficial thermic treatment, many of those disadvantages will disapear.

Deposition and alloying by discharge in electric impulse uses inverse electroerosion, which means that the parts is the cathode and the tool electrode is the anode.

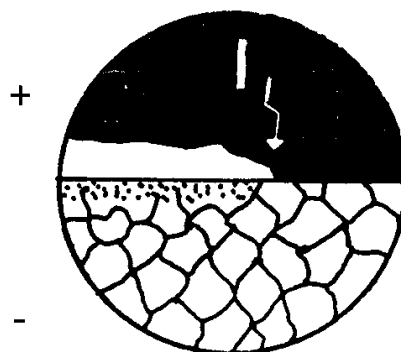


Fig.1 The process of superficial hardening by discharge in electric impulse

The experimental computerized quantitative optical research has as scope a complete characterisation of the deposited layers on studied samples and carbide characterisation.

Also was chasing the influence of deposition of these layers above the initial structure of superficial layer of the material and the influence of some treatments after deposition above the deposited layers.

2. Experimental procedure

The samples by which were made the deposition are from high alloyed tool steel 155MoVCr115 with electrode from Ti15Co6, WCo8, and W.

The chemical composition of the 155MoVCr115 steel is presented in table 1.

Table 1.

Sample	Steel	Chemical composition											Obs.
		C	Mn	Si	P	S	Cr	Mo	Ni	V	Al	Cu	
1	155MoV Cr115	1.5	0.18	0.1	≤0.03	≤0.03	11÷ 12	≤0.6	≤0.35	0.9	-	≤0.30	STAS 3611-88
		+	+	÷				+					
		1.6	0.45	0.4	0.8	1.1							
		1.38	0.41	0.22	0.021	0.025	11.7	0.72	0.16	1.05	0.03	0.23	

The mechanical properties and thermic treatments parameters for this type of steel are presented in table 2.

Table 2

Steel	Mechanical properties			Thermic treatment parameters							
				Annealing		Annealing		Quenching		Tempering	
	R _{p0.2} , N/mm ²	KCU ₂ , J/cm ²	HB daN/mm ²	T, °C	Mediu	T, °C	Mediu	T, °C	Mediu	T, °C	Mediu
155MoV Cr115	-	-	255	880	c	-	-	1020- 1030	U, a	160-200	a

The processing by electrical discharge in impulse were made by hand on plane surface without oxides and impurityties, using electrodes from Ti15Co6, with cilindrical sections (ϕ 2 mm) and length 25 mm.

The samples from 155MoVCr115 steel, before deposition of layers by electrical discharge in impulse were superficial thermic treated. The superficial thermic treatments parameters applied before deposition by electrical discharge in impulse are presented in table 3, and in table 4 and Fig. 2 are presented the experimental duplex variats of thermic treatments.

Table 3

Thermic treatment variant	Steel	Thermic treatment parameters
High frequency current hardening	155MoVCr115	1 000 ⁰ C/sintetic medium
Volume hardening + tempering	155MoVCr115	1 030 ⁰ C/oil + 180 ⁰ C/air

Table 4

Variant	Etapes
A	Volume hardening + tempering + deposition by electrical discharge in impulse
B	high frequency currents hardening + deposition by electrical discharge in impulse

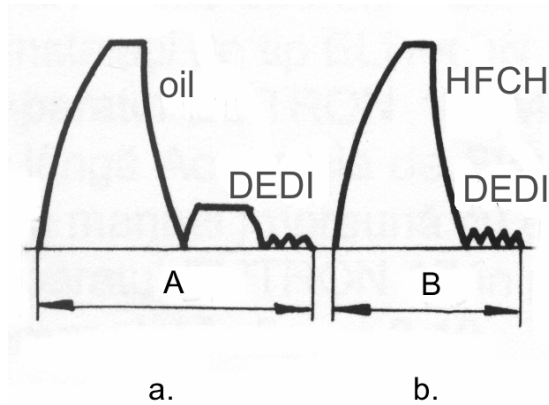


Fig. 2. The duplex variants of thermic treatments

The experimental researches of computerised quantitative analysis were made for a complete characterization of the deposited layers on studied samples and carbides characterization.

The computerised line of image analysis is composed from: optical microscope (REICHERT UNIVAR, video camera with adapter, computer, printer).

The main software component of image analysis line is a complex program – IMAGE PROPLUS, produced by MEDIA CYBERNETICS Company USA. This program is composed from a main general image analysis component and a component for quantitative metallographic determination – MATERIALS PROANALYZER.

The image processing takes place in this step:

- quantitative analyze of different images which have interest field as: grain limits, phases, particles etc;
- image processing, by hand or automatically when exists a controller for auto movement of the microscope table;
- quantitative measurement of interesting characteristics by using the A.S.T.M. agreed methods;
- determination of grain dimension;
- determination of dimension scale distribution of grains;
- determination of number and quantity of phases in poliphasic materials;
- quantitative determination of some particles by area, diameter, shape coefficients, perimeter etc;
- dimensional determination of the interdendritic spaces;
- thickness determination of singular or multiple layers.

On this computerized line for analyze were characterised the carbides and the thickness the deposited layers with diverse electrodes on 155MoVCr115.

In Fig. 3 are presented the white layer parameters of the 155MoVCr115 steel quenched in volume and processed by electrical discharge in impulse with Ti15Co6 electrode, and in Fig.4 are presented the parameters of white layer from 155MoVCr115 quenched in high frequency current and after processed by electrical discharge in impulse with WCo8 electrode.

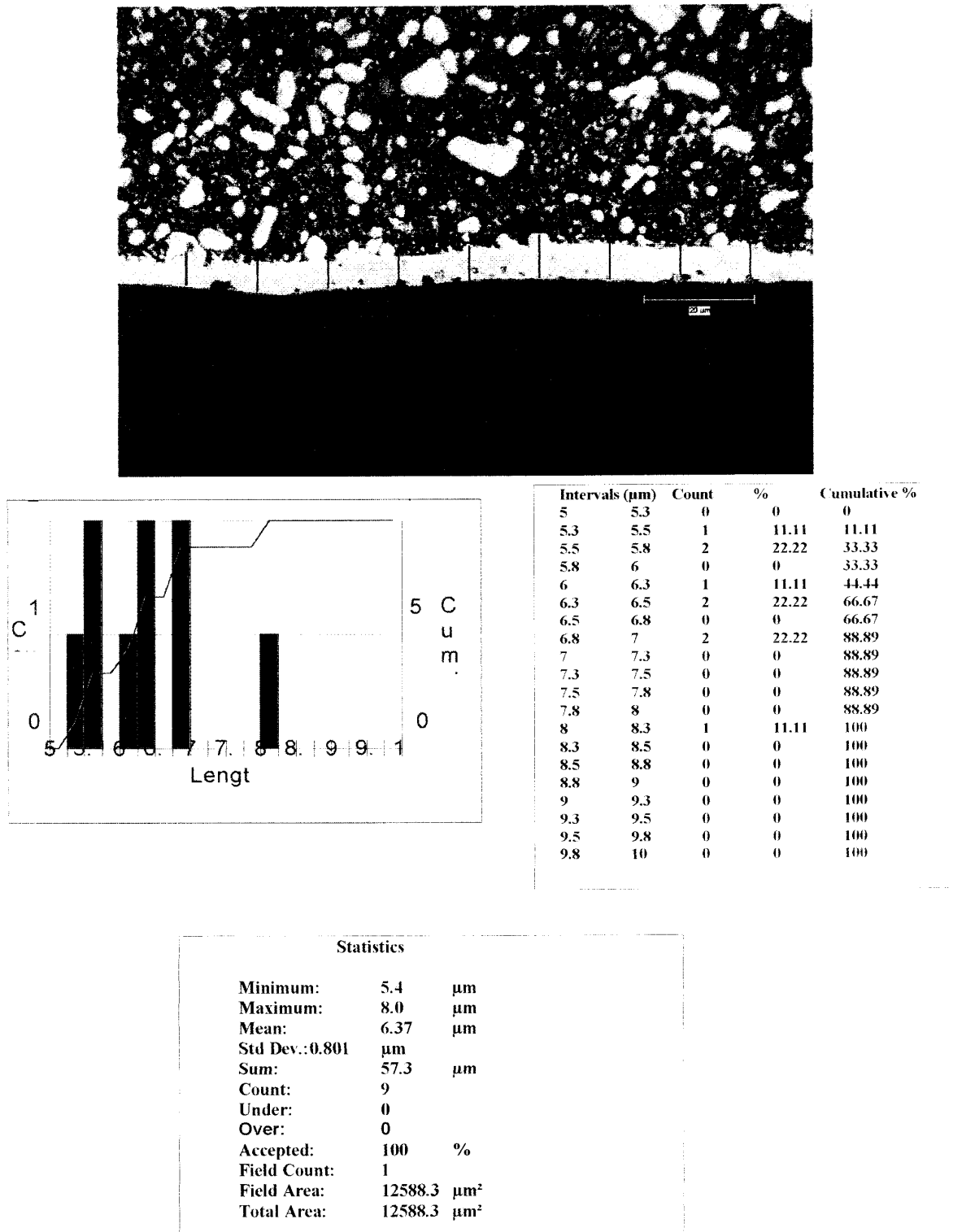
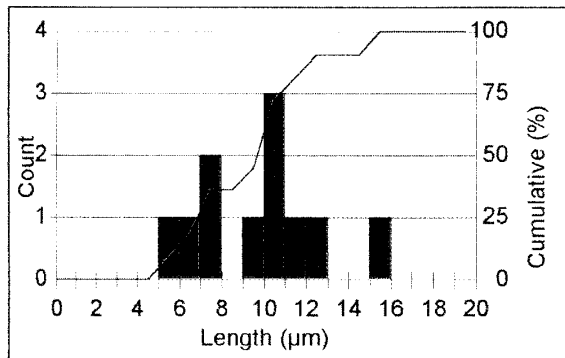
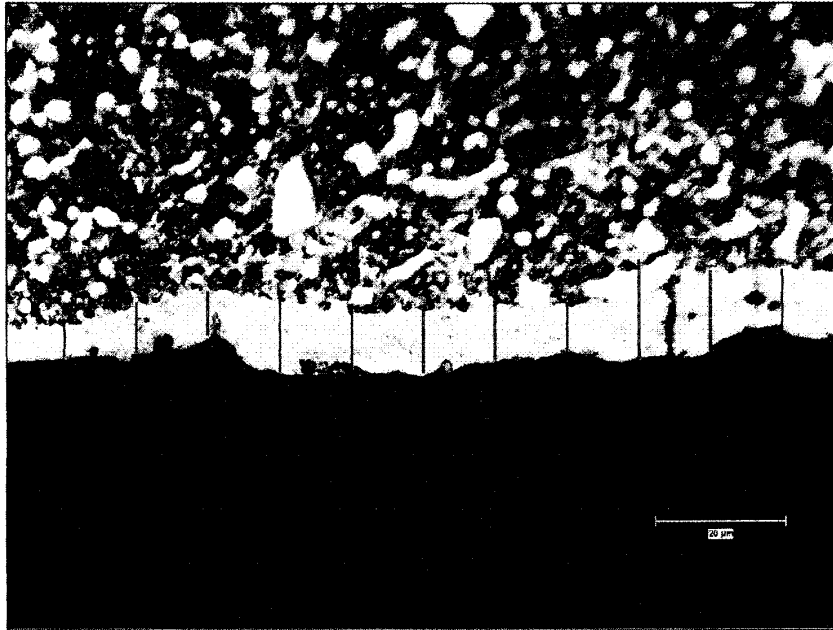


Fig. 3. White layer parameters of 155MoVCr115 steel quenched in volume and processed by electrical discharge in impulse with Ti15Co6 electrode



Intervals (μm)	Count	%	Cumulative
0	1	0	0
1	2	0	0
2	3	0	0
3	4	0	0
4	5	0	0
5	6	1	9.09
6	7	1	18.18
7	8	2	36.36
8	9	0	36.36
9	10	1	45.45
10	11	3	72.73
11	12	1	81.82
12	13	1	90.91
13	14	0	90.91
14	15	0	90.91
15	16	1	100
16	17	0	100
17	18	0	100
18	19	0	100
19	20	0	100

Statistics		
Minimum:	5.3	μm
Maximum:	15.5	μm
Mean:	9.82	μm
Std Dev.:2.81		μm
Sum:	108.0	μm
Count:	11	
Under:	0	
Over:	0	
Accepted:	100	%
Field Count:	1	
Field Area:	12588.3	μm ²
Total Area:	12588.3	μm ²

Fig.4. White layer parameters of 155MoVCr115 steel quenched in high frequency current and processed by electrical discharge in impulse with WCo8 electrode

3. Conclusions

- i. The obtained layers by thermic treatments variants at which the last process is the electrical discharge in impulse are more large;

- ii. The adherence and the compactity of the white layers with the transition sublayers is good;
- iii. The results obtained by quantitative computerized analyze are the same with those obtained by direct measurements with the PMT 3 device.

Received March 3, 2005

The "Gh.Asachi" Technical University Iași

REFERENCES

1. Alexandru, A. **Doctorate Thesis**, January 2002.
2. Alexandru, A., Pop, F. **Metallic materials with hardened deposit created by electric arc with vibrating electrode**. Proceedings EUROMAT-JUNIOR, Lausanne, 1994.
3. Pop, D., Pop, F., Alexandru, A. **Hardened deposition with tungsten carbides on steel specimens**. Proceeding, vol. II, EUROMAT, Lisabona, 1998.

ANALIZA MICROGRAFICĂ CANTITATIVĂ COMPUTERIZATĂ A STRATURILOR DEPUSE PRIN DESCĂRCĂRI ELECTRICE ÎN IMPULS PE UN OȚEL BOGAT ALIAT DE SCULE

Rezumat: Lucrarea prezintă rezultate experimentale de microscopie optică cantitativă computerizată privind caracterizarea straturilor depuse prin descărcări electrice în impuls pe un oțel bogat aliat de scule 155MoVCr115.

CONTRIBUTIONS CONCERNING VIRTUAL INSTRUMENTATION IN DATA AQUISITION AND ANALYSIS

BY

ALINA ANGHEL and CARMEN BUJOREANU

Abstract: The monitoring method that uses the vibrations as information carrying is one of the most widely used technique in the extraction of information from measured signal patterns and extracts the useful information from the signal by processing it. This paper presents a series of virtual instruments that save the vibration signal captured by the sensor and analyze it in time, amplitude and frequency domains.

Keywords: Digital Signal Processing, Virtual Instruments

1. General considerations

The monitoring methods for tool-wear deal with the extraction of information from signal patterns and this paper describes some aspects which are relevant in this field.

Powerful instrumentation systems, incorporating sophisticated analyzing and processing techniques are now available to the practitioner, but basic understanding and the capability to choose and evaluate these techniques often suffer because of the misleading ease of applying these.

The main reason to consider vibration signals for wear monitoring lies in their capability of responding to excitations occurring at practically inaccessible sources.

The ease of incorporating sensor in machine tool structure, its low price and the unsatisfactory performance of other known methods recommend the method as viable, in spite of the inherent difficulties.

2. The general processing scheme

The monitoring systems that use the vibrations as information-carrying operate using the following general scheme: the complex signal generated in the machining process is captured by a sensor, transformed into electrical signal and sent to a preprocessing block (containing hardware and software elements) that increases the ratio between the useful signal and noise, and makes data reduction.

The next block extracts the features and makes, after an analog-digital conversion, the signal analysis in time, amplitude and/or frequency domain. Through the comparison between the reference signal and the analyzed signal you can obtain information concerning the variable and identify the trends in its evolution.

3. Virtual Instrument for Data Acquisition

A virtual instrument consists of an interactive user interface, a dataflow diagram that serves as the source code and icon connections that allow the virtual instrument to be called from higher level virtual instruments.

More specifically, the virtual acquisition instrument has a structure as follows:

- The interactive user interface is called the front panel, because it simulates the panel of a physical instrument. The front panel contains knobs, push buttons, controls and indicators.
- The virtual instrument receives instructions from a block diagram, constructed in graphical programming language, *G*. The block diagram is a pictorial solution to the programming problem. The block diagram is also the source code for the virtual instrument.
- The virtual instrument has a hierarchical and modular structure. It can be used as top-level programs or as subprograms within other programs or subprograms. The icon and connector of the virtual instrument work like a graphical parameter list so that other virtual instruments can pass data to a subvirtual instrument.

With these features, the virtual instrument promotes and adheres to the concept of modular programming. The application is divided into a series of tasks until a complicated application becomes a series of simple subtasks.

In figure 1 is presented the block diagram of the virtual acquisition instrument, constructed by wiring together objects that send and receive data, perform specific functions and control the flow of execution.

Data are read and saved as global variables.

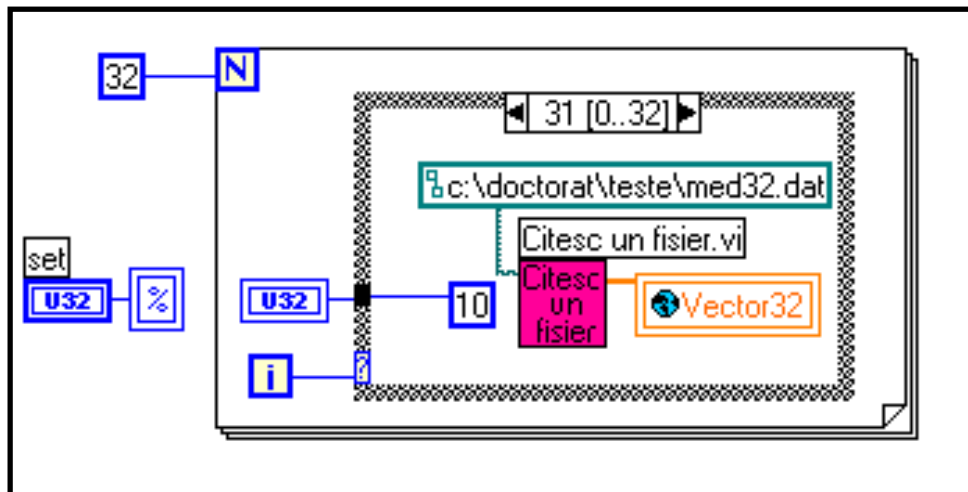


*Fig.1 The block diagram of the virtual acquisition instrument
It is build a virtual instrument to accomplish each subtask and then combine
those virtual instruments on other block diagram to accomplish the larger task*

We build a virtual instrument to accomplish each subtask and then combine those virtual instruments on other block diagram to accomplish the larger task. Finally,

the virtual instrument contains a collection of subvirtual instruments that represent application functions.

Because each subvirtual instrument is constructed by itself, apart from the rest of the application, debugging is much easier.

4. Virtual Instruments for Data Analysis

The appliance of the general scheme for monitoring uses a virtual instrument for acquisition and saving to files the signals received from the sensor.

A main program, modulated, containing four levels, makes the processing of the files' data:

- Time domain analyse;
- Frequency domain analyse;
- Amplitude domain analyse;
- Dynamic analyser.

In figure 2 is presented the block diagram of the virtual instrument for data analysis.

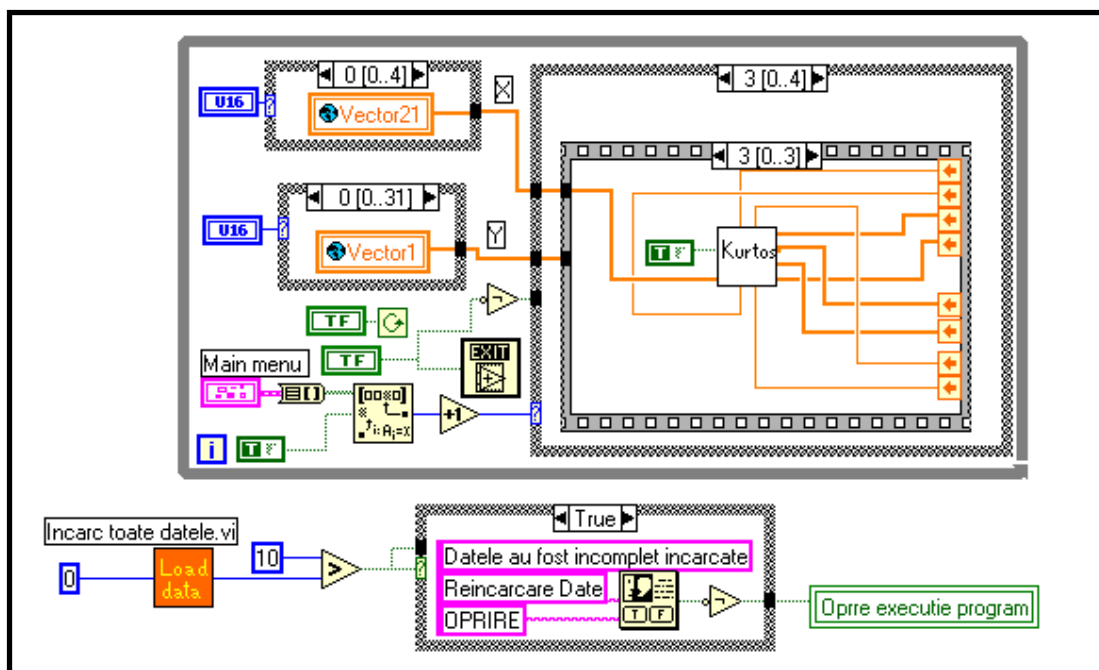


Fig. 2 The block diagram of the virtual acquisition instrument for data analysis

On main program run all the files saved using the virtual acquisition instrument. After data loading the analysis domain is chosen (figure 3). The operator can choose the reference vectors and the test vectors using selection buttons.



Fig. 3 The main program, modulated, contains four levels: time, frequency, amplitude domains and dynamic analyzer.

In each domain, the signal is process with dedicated virtual instruments. For example, the frequency domain analysis is based on the estimation of the spectra and follows these steps: obtaining the reference pattern, defining the limitative profiles, making spectra comparison and drawing the trend graph.

4. Conclusions

We have described some investigations concerning the monitoring method based on the analysis of vibration signals, using virtual instruments. All the virtual instruments are included in a main program that has four independent domain analyses: time, amplitude, frequency domains and dynamic analyzer.

The use of this program allows complex processing by selecting different functions and comparative graphical display of the variables.

Received March 14, 2005

The "Gh.Asachi" Technical University Iași

REFERENCES

1. Braun, S. - **Mechanical Signature Analysis**, Academic Press, London, 1993, **321-340**
2. Ifeacher, E., Jervis, B. - **Digital Signal Processing**, Addison- Wesley Publishing Comp., 1993, **112-135**
3. LabVIEW - **Graphical Programming for Instrumentation**, National Instruments, 1996.

CONTRIBUȚII ASUPRA INSTRUMENTAȚIEI VIRTUALE ÎN ACHIZIȚIA ȘI ANALIZA DE DATE

Rezumat: Una dintre metodele de monitorizare cele mai des întâlnite este utilizarea semnalul de vibrații ca purtător de informație asupra stării sistemului. În lucrare este prezentat un program complex de monitorizare prin achiziție și prelucrare de date în domeniile timp, amplitudine și frecvență, prin instrumentație virtuală.

HIGH SPEED DETERMINATION OF THE SPECIFIC ISOTHERMS OF THE THERMIC FIELDS CREATED IN THE PROCESS OF CASTING ALLOYS IN METALLIC MOULDS HELPED BY COMPUTER

BY

RADU DANILĂ, OVIDIU CALANCIA, AUREL FLORESCU, PETRICĂ VIZUREANU and VASILE GOANȚĂ

Abstract: The determination of the isotherm surfaces which are specific to thermal fields which appear on the alloys casting in metallic moulds according to the conditions and the way of the heat transfer within the couple casting alloy – metallic mould using LUSAS program calculations with finite elements.

Keywords: casting, alloy, the metallic mould, thermal field, isotherms, finite elements.

1. Introduction

In solidification and cooling processes of alloys castings in metallic moulds under the differences of the temperature appear a process of the heat transfer from the alloy to the mould and from the mould to outside. This heat transfer is thermodynamics processes which take place with final speed in determined conditions by space and time [1].

For high speed determination of the specific isotherms of the thermal fields created in the process of casting alloys in metallic moulds, we proposed to study the heat transfer using a calculation program with finite elements [2].

2. Work conditions and obtained results

The thermal charging conditions which are useful for the proposed study are [3]:

- the cast alloy has the initial temperature of 1350°C;
- the metallic mould before casting has the temperature of 20°C;
- the heat transfer at the outside contact, for the cast alloy as for the metallic mould, it's made through convection at 20°C temperature;
- the convection exchange rate was chosen average referring to the temperature variation and has the value $\alpha = 95 \text{ W}/(\text{m}^2\text{K})$;
- the heat transfer within the cast alloy, the metallic mould and between them took place by conduction.

Considering the given heat transfer conditions, through the continuous media made from the cast alloy and the casting metallic mould it appears a low temperature field, represented through the total amount of temperature at a certain time moment. This field is varying with (in accordance with) the considered point position and with the time.

In this way there are established isotherm surfaces which are defined as being the geometrical spot of all the temperature points from the given part (material). These isotherm surfaces have a variable position in time which characterizes a transitory heat exchange regime.

The necessary equation for the numeric simulation is the thermic transfer equation through conduction given by Fourier-Kirchhoff [3]:

$$\begin{aligned} \rho(C-l \frac{\partial f}{\partial T}) (\frac{\partial T}{\partial t} + u \frac{\partial T}{\partial x} + v \frac{\partial T}{\partial y} + w \frac{\partial T}{\partial z}) = \\ = \frac{\partial}{\partial x} (\lambda \frac{\partial T}{\partial x}) + \frac{\partial}{\partial y} (\lambda \frac{\partial T}{\partial y}) + \frac{\partial}{\partial z} (\lambda \frac{\partial T}{\partial z}) \end{aligned} \quad (1)$$

This thermic transfer equation presents a great number of solutions. Through the solving the presented differential equation, by imposing (enforcing) the limit conditions, it is obtained the exact solution of the problem. This is the analytic common way of solving, which is applicable yet in the case of relatively simple problems.

The analytic solving could be done only by creating a model so simplified that the equations could be integrated.

It's obtained, in this way, the exactly solution for a simplified model. Often is being preferred that, instead the exact solution of a simplified model, to have an approximate solution of the real model.

The approximate solutions, obtained through numeric methods, are susceptibly in many cases to mirror better the reality than the exact solutions of some simplified models, but need a bigger calculation effort. These calculations could be made by computer aid, using specialized solving programs which are using the finite elements method [2].

As a specific for the finite element method is the fact that minimising is done on sub domains, named finite elements, and linked between them in poits named nodes [4].

For the model we are proposing in sequence for study and which is presented in figure no. 1 we make the following hypothesis when analyzing finite elements:

- It is tracking the heat transfer on the interface of the cast alloy and the metallic mould. (S1 surface);
- the heat exchange with the exterior on S2 and S3 surfaces is blocked. In practice, these surfaces are covered with a refractory mixture layer which makes the heat exchange with the exterior to be insignificant. This hypothesis was imposed with a view to obtaining a constant temperature along the length of the metallic mould wall and for intensify the warm exchange between alloy and the metallic mould;
- through S4 surface is going on the convection with the air at 20°C temperature;

- the initial time for the analyze is considered then when the alloy fill in the casting metallic mould;
- It is considered that both the alloy and the metallic mould don't present heterogeneities.

Taking into account that both the alloy and the metallic mould are symmetric to the central axis, for the finite element analysis it had been used the charged model, with axis-symmetric elements.

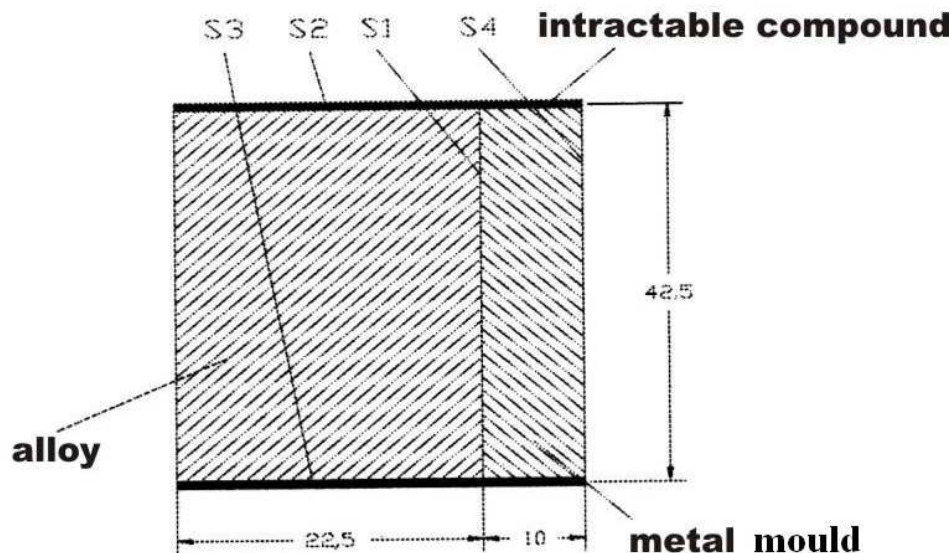


Figure 1. Pattern geometry

The analysis was made with the help of the LUSAS programmer, from its documentation using the element QFX4.

For the cast alloy (cast iron) were used the following thermo-physical constants:

- specific heat $c_s = 560 \text{ KJ}/(\text{KgK})$;
- the heat transmitting ratio $\lambda = 42 \text{ W}/(\text{mK})$;
- reference temperature $t = 20^\circ\text{C}$;
- the convection with the air ratio was chosen an average one in relation with the temperature variation $\alpha = 95 \text{ W}/(\text{m}^2\text{K})$;
- the metallic mould is cylindrical with the inside ray $r_1 = 22.5 \text{ mm}$ and the external one $r_2 = 32.5 \text{ mm}$.

The discretization network and the numbering of the nodes, it is presented in figure no. 2. Within this network, the cast alloy is inside in the rectangle accompanied by the points 1, 2, 30 and 44, but the metallic mould is inside in the rectangle accompanied by the points 30, 44, 344 and 338. After processing, it is obtained the variation in time of the temperature for every node on a side.

In figure no. 3, it is given the variation in time of the temperature for some more significant nodes. The nodes chosen from the curve in figure no. 3:

- 9 found in the center of the cast material;

- 126 belonging to the cast material and being in the immediate neighborhood of the interface between the cast material and the metallic mould;
- 51 on the surface;
- 389 belonging to the metallic mould and lying close to the interface;
- 351 belonging to the metallic mould and being at it's exterior;

It is noticed a relative high lowering of the temperature of the nodes which lie to the center of the ensemble casting alloy – metallic mould (from node 9 to node 125).

2	72	73	74	75	76	77	44	372	373	344
15	85	86	87	88	89	90	57	377	378	357
14	91	92	93	94	95	96	56	379	380	356
13	97	98	99	100	101	102	55	381	382	355
12	103	104	105	106	107	108	54	383	384	354
11	109	110	111	112	113	114	53	385	386	353
10	115	116	117	118	119	120	52	387	388	352
9	121	122	123	124	125	126	51	389	390	351
8	127	128	129	130	131	132	50	391	392	350
7	133	134	135	136	137	138	49	393	394	349
6	139	140	141	142	143	144	48	395	396	348
5	145	146	147	148	149	150	47	397	398	347
4	151	152	153	154	155	156	46	399	400	346
3	157	158	159	160	161	162	45	401	402	345
1	31	32	33	34	35	36	30	339	340	338

Figure 2. Discretization network and knots numbering

Node 126 which belongs to the alloy and it lies in the immediate neighborhood of the interface, suffers an abrupt decreasing of the temperature (figure no. 3). For node 51, which belongs to the metallic mould and lies on the interface, it is noticed a increasing of the initial temperature of the 453°C, after that it take place a slowly lowering to 20°C value. The curves presented are drawn to the total cooling of the ensemble.

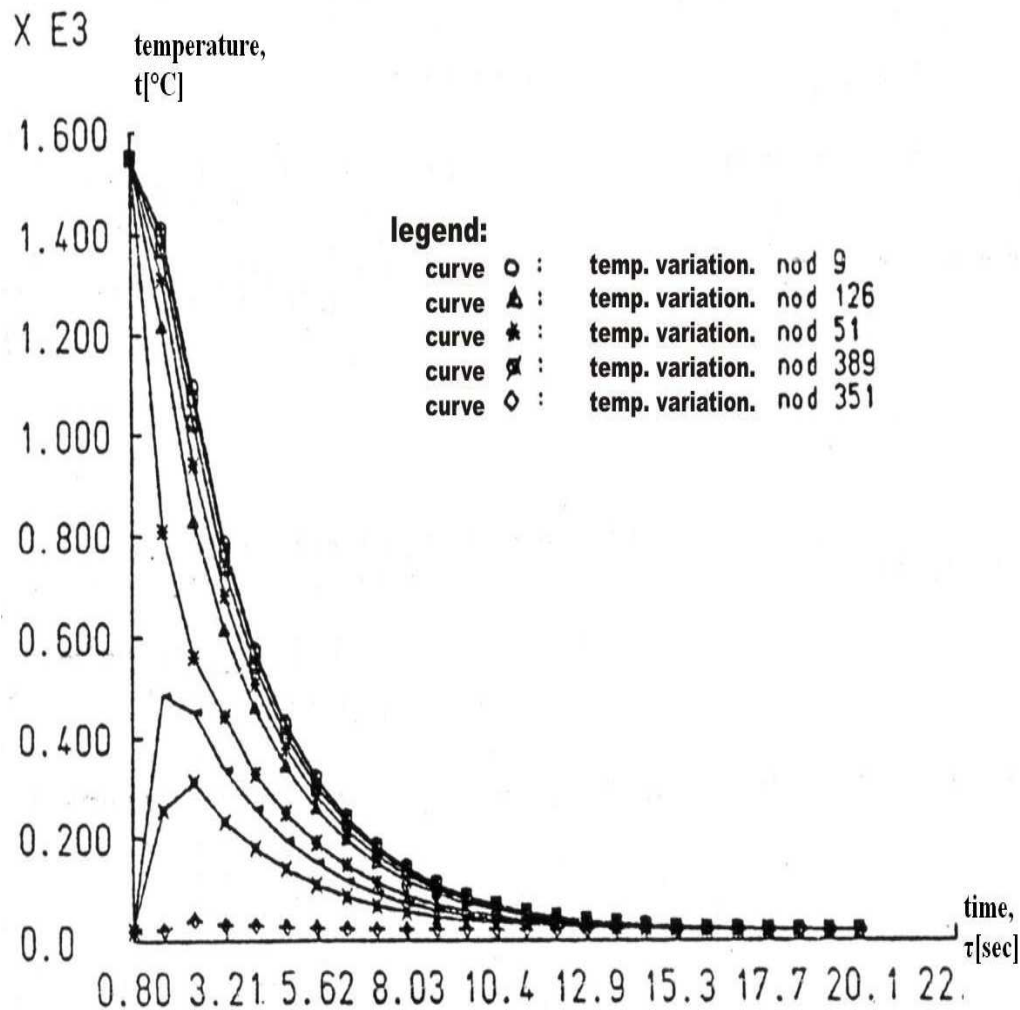


Figure 3. Temperature variation with the time

In figure no. 4, it is presented the spectrum of the isotherms established at 20000 sec. The parallelism of these isotherms is showing us that the heat exchange it's made entirely with the metallic mould. The aspect of these isotherms remains invariable for every temperature they are obtained at, only the temperature which characterizes them is modifying.

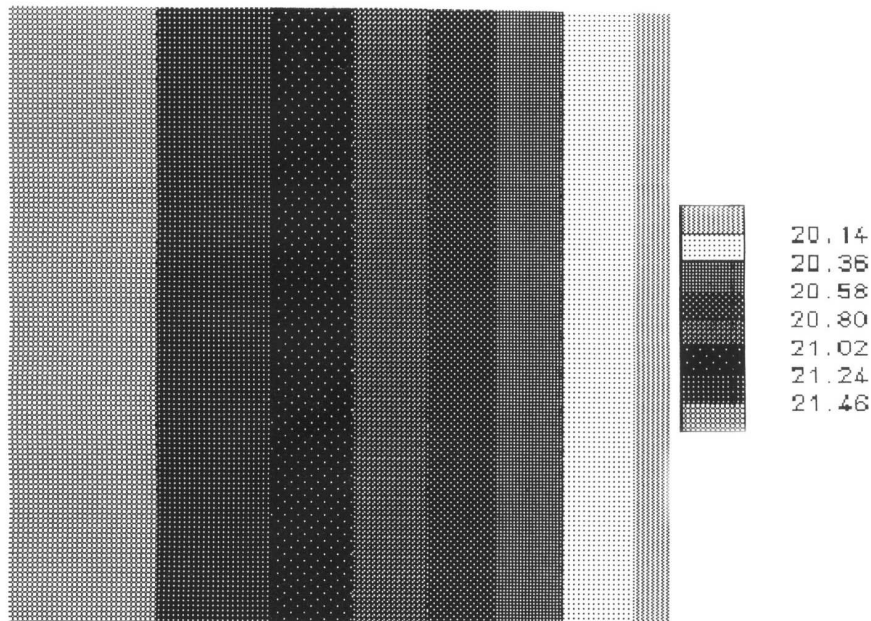


Figure 4. Isotherms spectrums at 20000 sec

To determine the variation of the temperature at the same time on the thickness of the casting metallic mould wall, therefore varying with the ray, there are chose the nodes 51, 389, 390 and 351. The time when the temperature of these nodes which belong to the metallic mould is registered is 400 sec. from of the analyze beginning.

The temperature variation for the metallic mould with the ray is given in figure no. 5. The maximum temperature is registered at the contact with the alloy (node 51) and is 453°C, and the minimum one is outside the mould and is 41°C (node 351).

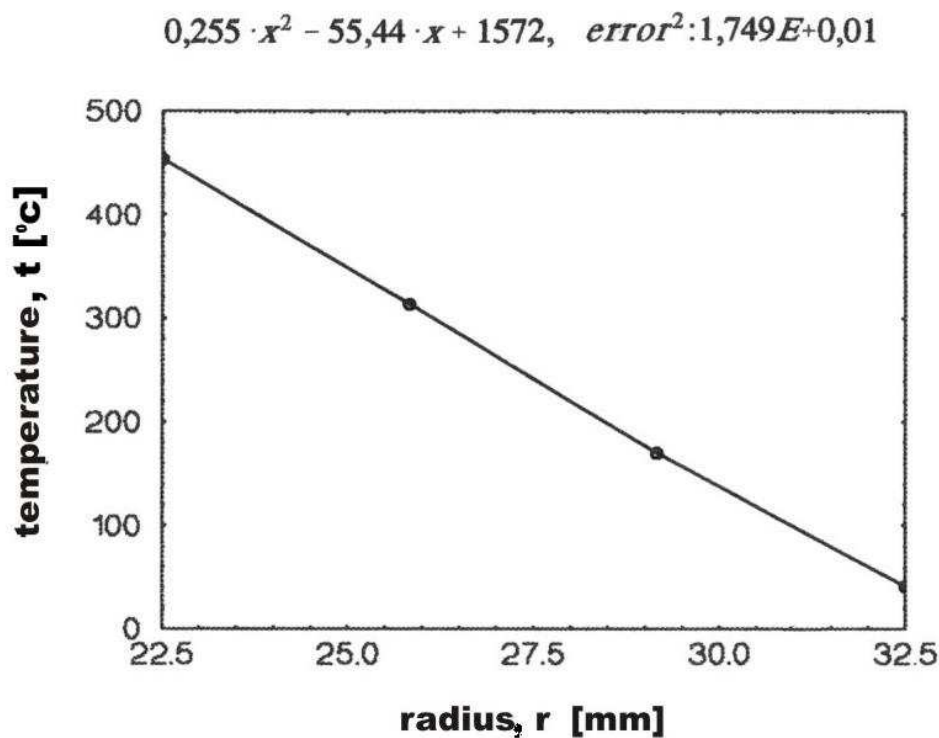


Figure 5. Temperature variation as a function of radius

The values for the temperature of the concerned nodes are taken from the listing with the variation of the temperature with the time and which is displayed after the processing ends. The represented curve (figure no. 5) is drawn by points, using the results obtained through -- the programme as a finite element. The second curve is obtained by extrapolation, approximating the first one, and it's given by the function:

$$t(r) = a x^2 + b x + c \quad (2)$$

Where:

- $t(r)$ represents the temperature variation with the ray;
- a, b, c – are the coefficients obtained after approximating the curve that gives the variation of the temperature on the thickness of the wall with the above function and have the values: $a = 0.255$, $b = -55.44$ and $c = 1572$, resulted after the interpolation;
- r – the ray measured fro the center of the ensemble to the point with t temperature.

In the figure no. 5, it can be noticed that it appears a difference of temperature between the internal and the external surface. Thus to the biggest moving tendency of the interior surface is opposing the reduced moving tendency of the neighbor and exterior surface.

3. Conclusions

The results which can be achieved using the LUSAS program calculation with finite element are [5]:

- graphical view in any moment of isotherms from different surfaces of the casting piece – metallic mould system which are necessities for establishing the preferences directions of the heat (figure no.4);
- graphical view of the discretization network knots numbering for the same system, with the possibility to adopt the dimension of the finite elements to the measure of the gradient function studied (figure no.2);
- the temperatures of every knots network in every moment of the process (figure no.3);
- the variation of the temperature on the desired direction at one moment (figure no.5) which can give the occasion of the calculation of termichal tension from metallic moulds.

REFERENCES

1. **Chiriac, F.**, *Procese de transfer de căldură și de masă în instalații industriale*, Editura Tehnică, București, 1987.
2. **Gârbea, Dan**, *Analiza cu elemente finite*, Editura Tehnică, Bucuresti 1990.
3. **Dănescu, Al.**, *Termodinamica și mașini termice*, Editura Didactică și Pedagogică, Backrest, 1985.
4. **Dănilă, R., Calancia, Ov., Ciocănel, C., Goanță, V.**, *Considerations Concerning the Use of Calculus Programs with Finite Elements "LUSAS" at the Study of Heat Transfer in Solidification and Cooling Processes of Castings Poured in Metallic Shells. Description of the Chosen Model*, Buletin I.P. Iași, Tomul XLII (XLVI), Fasc. 1 – 2, 1996, Secția IX, pag. 195 – 200.

5. **Dănilă, R.:** *Cercetări privind turnare aliajelor în forme metalice în scopul măririi durabilității acestora și al îmbunătățirii calității pieselor turnate, Teză de doctorat, Biblioteca U.T. Iași, 1996.*

**DETERMINAREA RAPIDĂ CU AJUTORUL CALCULATORULUI A IZOTERMELOR SPECIFICE
CÂMPURILOR TERMICE LA TURNAREA ALIAJELOR ÎN FORME METALICE**

(Rezumat)

În lucrare se determină suprafețele izoterme, specifice câmpurilor termice, ce apar la turnarea în forme metalice a pieselor din fontă. Condițiile și modul realizării transferului de căldură, în ansamblul aliaj – formă metalică, este studiat folosind programul LUSAS de analiză cu elementele finite.

HIGH SPEED DETERMINATION USING THE COMPUTER FOR THE THERMAL TENSIONS FROM METALLIC MOULDS AT ALLOYS CASTING

by

OVIDIU CALANCIA, RADU DANILĂ, VASILE VIOREL MOLDOVEANU,
AUREL FLORESCU and LEONACHE DRĂGOI

Abstract: The determination of the thermal tensions into the metallic moulds on the alloys casting, according to the way of variation of the temperature on the thickness of the metallic moulds wall, exactly determined through the finite elements analyze using LUSAS program.

Keywords: thermal tensions, casting, the metallic mould, alloy, thickness wall.

1. Introduction

The work is proposing a way to determine the stresses which appear in casting within metallic moulds. For this it has been used a program which uses the finite elements method, to determine the variation law of the temperature on the thickness of the casting metallic mould's wall. This equation will be inserted within the stresses expression which takes in account an axial-symmetric variation of temperature and in which the temperature doesn't vary on length.

With a view to establishing the temperature variation law on the thickness of the casting metallic mould wall, it will be considered the case of alloys casting in metallic moulds. The casting metallic mould can be considered, for the stresses analyze, as a tube with thick walls. Due to the contact between the alloy and the metallic mould, at interface it appears a heat transfer which has the sense from the alloy to the metallic mould.

2. Work conditions and obtained results

The thermic charging conditions are [1], [4]:

- the cast alloy has the initial temperature of 1350°C;
- the metallic mould before casting has the temperature of 20°C;
- the heat transfer at the outside contact, for the cast alloy as for the metallic mould, it's made through convection at 20°C temperature;
- the convection exchange rate was chosen average referring to the temperature variation and has the value $\alpha = 95 \text{ W}/(\text{m}^2\text{K})$;

- the heat transfer within the cast alloy, the metallic mould and between them took place by conduction;
- the heat transmitting ratio $\lambda = 42 \text{ W/(m K)}$;
- reference temperature $t = 20^\circ\text{C}$;
- the metallic mould is cylindrical with the inside ray $r_1 = 22.5 \text{ mm}$ and the external one $r_2 = 32.5 \text{ mm}$.

In figure no. 1, is presented a section in the metallic mould made after a perpendicular layout on the symmetry axis and, also, there are shown the radial and tangent stresses that appears as a result of the temperature variation on the wall thickness [4].

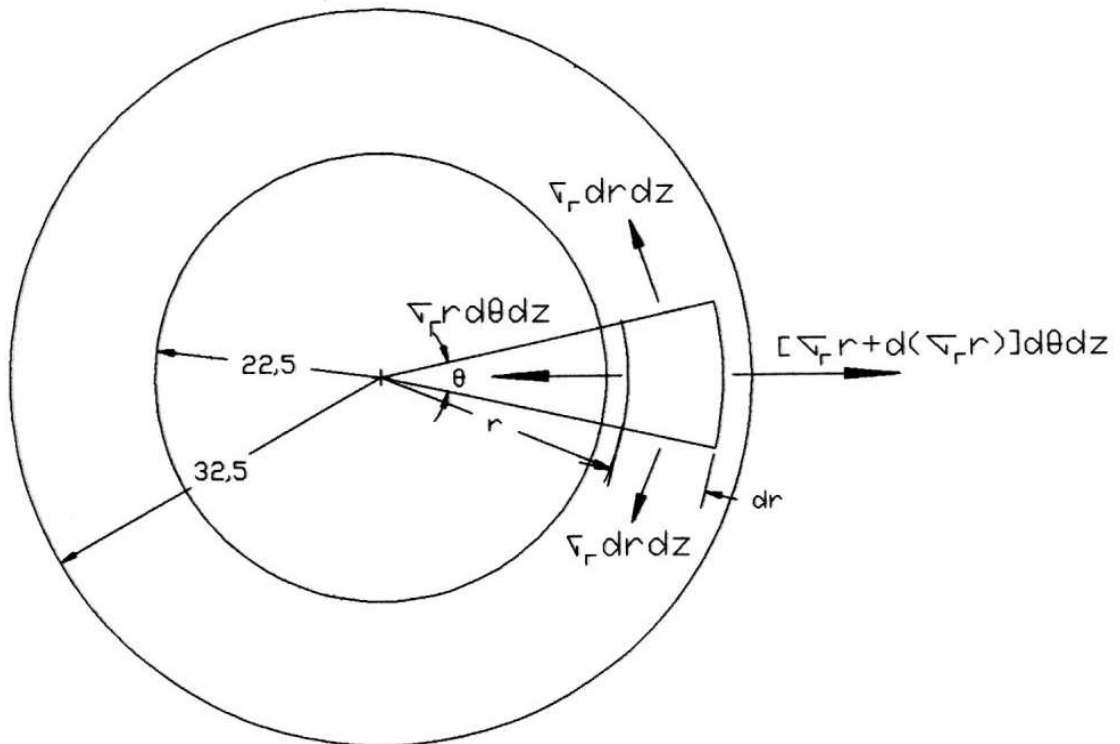


Figure 1. Thermal tensions in section through metallic mould

The relations for the unitary strains (efforts) σ_r , σ_t and σ_z that represent the tresses on the radial, tangent and longitudinal direction obtained from the deformations balance are [2]:

$$\sigma_r = \frac{E}{(1-\nu)} \left[-\frac{1}{r^2} \int_{r_1}^r \alpha t(r) r dr + \frac{r^2 - r_1^2}{r^2 (r_2^2 - r_1^2)} \int_{r_1}^{r_2} \alpha t(r) r dr \right] \quad (1)$$

$$\sigma_t = \frac{E}{(1-\nu)} \left[\frac{1}{r^2} \int_{r_1}^r \alpha t(r) r dr + \frac{r^2 + r_1^2}{r^2 (r_2^2 - r_1^2)} \int_{r_1}^{r_2} \alpha t(r) r dr - \alpha t(r) \right] \quad (2)$$

$$\sigma_z = \frac{E}{(1-\nu)} \left[\frac{2}{r_2^2 - r_1^2} \int_{r_1}^{r_2} \alpha t(r) r dr - \alpha t(r) \right] \quad (3)$$

Where:

- ν – is the Poisson coefficient;
- r_1 – the interior ray of the metallic mould;
- r_2 – the exterior ray of the metallic mould;
- E – the longitudinal elasticity module;
- $t(r)$ – the temperature variation on the metallic mould wall's thickness ($t(r) = a x^2 + b x + c$) [3].

If we replace $t(r)$ in (1), (2) and (3) equations it results the following expressions for the stresses that take into account the temperature variation on the metallic mould wall's thickness.

The variation of σ_r , σ_t and σ_z stresses given by the equations (4), (5) and (6) are presented in figure no. 2.

$$\sigma_r = \frac{\alpha E}{1-\nu} \left[-\frac{1}{r^2} \left(\frac{ar^4}{4} + \frac{br^3}{3} + \frac{cr^2}{2} - \frac{ar_1^4}{4} - \frac{br_1^3}{3} - \frac{cr_1^2}{2} \right) \right] + \frac{\alpha E}{1-\nu} \left[\frac{r^2 - r_1^2}{r^2(r_2^2 - r_1^2)} \left(\frac{ar_2^4}{4} + \frac{br_2^3}{3} + \frac{cr_2^2}{2} - \frac{ar_1^4}{4} - \frac{br_1^3}{3} - \frac{cr_1^2}{2} \right) \right] \quad (4)$$

$$\sigma_t = \frac{\alpha E}{1-\nu} \left[\frac{1}{r^2} \left(\frac{ar^4}{4} + \frac{br^3}{3} + \frac{cr^2}{2} - \frac{ar_1^4}{4} - \frac{br_1^3}{3} - \frac{cr_1^2}{2} \right) \right] + \frac{\alpha E}{1-\nu} \left[\frac{r^2 + r_1^2}{r^2(r_2^2 - r_1^2)} \left(\frac{ar_2^4}{4} + \frac{br_2^3}{3} + \frac{cr_2^2}{2} - \frac{ar_1^4}{4} - \frac{br_1^3}{3} - \frac{cr_1^2}{2} \right) - (ar^2 + br + c) \right] \quad (5)$$

$$\sigma_z = \frac{\alpha E}{1-\nu} \left[\frac{2}{r_2^2 - r_1^2} \left(\frac{ar_2^4}{4} + \frac{br_2^3}{3} + \frac{cr_2^2}{2} - \frac{ar_1^4}{4} - \frac{br_1^3}{3} - \frac{cr_1^2}{2} \right) - ar^2 - br - c \right] \quad (6)$$

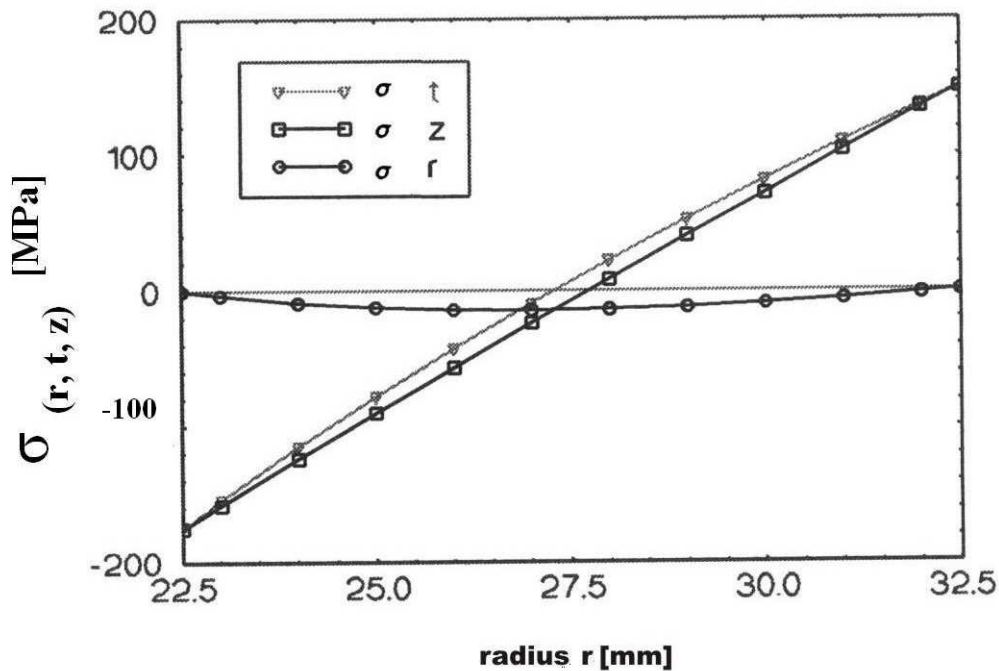


Figure 2. Variation of stresses as a function of radius

We notice that the stress on the radial direction is zero inside at outside the metallic mould and as size is much smaller than the tangent and longitudinal stresses. Also, at the interior and the exterior of the metallic mould the tangent and the longitudinal stresses have equal values.

The variation on the wall's thickness of these is likewise, with higher values of compression for σ_z then σ_t and bigger elongation values for σ_t .

The equivalent Von Misses stress has the relation [2]:

$$\sigma_{ech} = \sqrt{\frac{1}{2} [(\sigma_r - \sigma_t)^2 + (\sigma_t - \sigma_z)^2 + (\sigma_z - \sigma_r)^2]} \quad (7)$$

The variation of the equivalent stress on the metallic mould wall's thickness is shown in figure no. 3. It can be noticed that the dangerous stress appears inside the metallic mould and has the value $\sigma_{ech(r=22.5)} = 124$ MPa.

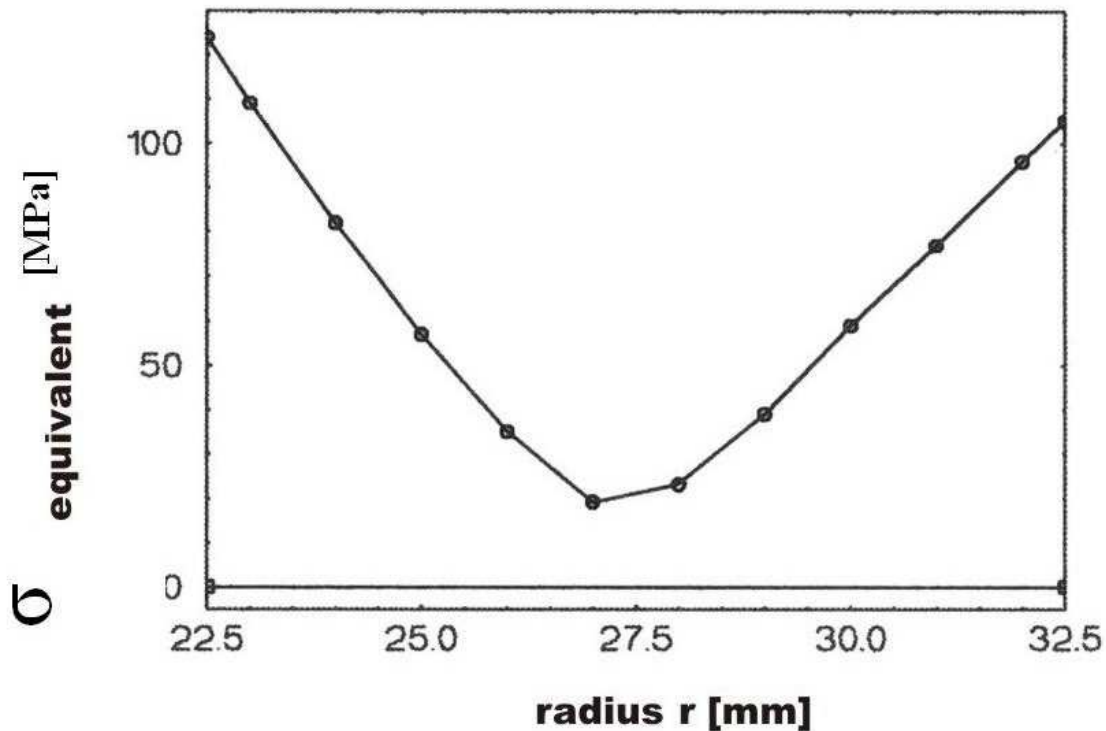


Figure 3. Variation of equivalent stress as a function of radius

3. Conclusions

Casting the alloys in metallic moulds induces within them a field of temperatures varying with time. At a certain moment of time it is established a maximum temperature difference between the warmer side of the metallic mould (node 51) and the colder side (node 351), which can be observed in figure no. 3, after 1600 sec. from the beginning of the casting [3], [4].

σ_r , σ_t and σ_z stresses that appears in this case could be calculate (estimate) with the relations specific to the materials strength [4], considering the temperature variation with the metallic mould wall thickness. The variation law of the temperature was obtained by approximating the given curve by point through the finite elements analysis. The stress variation on the metallic mould wall thickness is showing us that the dangerous strain is of compression one and it appears inside the metallic mould.

REFERENCES

1. **Dănescu, Al.**, *Termodinamica și mașini termice*, Editura Didactică și Pedagogică, Bucuresti, 1985.
2. **Ponomariov, D.**, *Calcul de rezistență în construcție de mașini*, Editura Tehnică, București, 1984.
3. **Danilă, R., Calancia, Ov., Florescu, A., Vizureanu, P., Goanță, V.**, *High Speed Determination of the Specific Isotherms of the Thermal Fields Created in the Process Casting Alloys in Metallic Moulds Helped by Computer*, Lucrările celui de-al V-lea Congres Internațional de Știința și Ingineria Materialelor, Iași, 26 – 28.V.2005.
4. **Dănilă, R.**: *Cercetări privind turnare aliajelor în forme metalice în scopul măririi durabilității acestora și al îmbunătățirii calității pieselor turnate*, Teză de doctorat, Biblioteca U.T. Iași, 1996.

DETERMINAREA RAPIDĂ CU AJUTORUL CALCULATORULUI A TENSIUNILOR TERMICE DIN FORMELE METALICE LA TURNAREA ALIAJELOR

(Rezumat)

În lucrare se determină tensiunile interne (termice) ce apar în formele metalice (tip tuburi cu pereți groși) la turnarea aliajelor, în funcție de modul de variație a temperaturii pe grosimea peretelui formei. Variația temperaturii a fost stabilită cu precizie prin analiza cu elemente finite, folosind programul LUSAS.

SEMI-PLANETARY ROLLING PROCESS AND EXPERIMENTAL SIMULATION

by

NICOLAE CANANAU, GHEORGHE GURAU, DORU HANGANU

Abstract The semi-planetary rolling is a original method for plastic deformation. The semi-planetary rolling mill consists of a planetary rolling cylinder and a massive cylinder. Into the deformed material an asymmetrical deformation state is developed. Thus the semiproduct curves. In this paper are showed the experimental researches concerning the influence of same factors on curvature of the semi-planetary rolled product.

Keywords: rolling, semiplanetary, modeling, simulation

1. Introduction

The semi-planetary rolling (Fig.1) leads to an asymmetrical stress and strain state on the thickness of the semi-product.

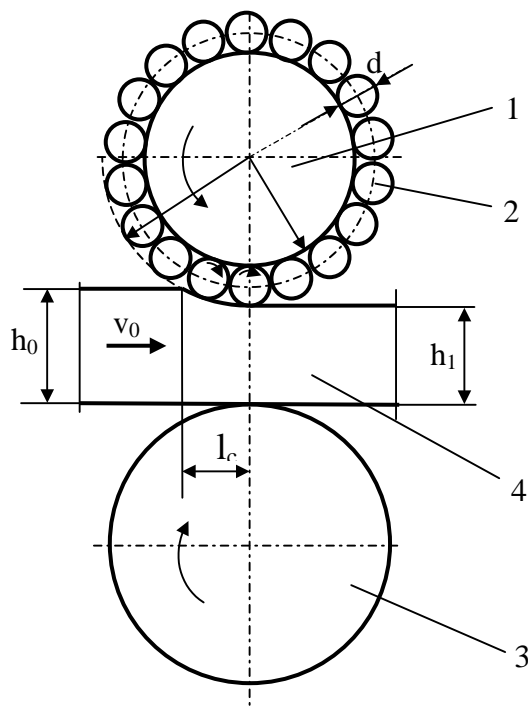


Figure 1 Scheme of semi-planetary rolling:
1-planetary cylinder, 2-satellite cylinder,
3-massive cylinder, 4-semi-product

The strain developed in the proximity of the superior planetary cylinder has greater intensity than the strains developed in the proximity of massive cylinder). As a result, after semi-planetary rolling the body, with rectilinear form, becomes a curved body. An important application of semi-planetary rolling, which may become a solution for quality assurance of the metallurgical products, may be the unbending of the continuous cast slabs of high strength steels. These steels have a reduced plasticity, in casting state and, also, at the temperature of 850 – 950 °C, they present a fragility domain.

At the same time in the unbending zone, into the proximity of the interior surface of the slab section, a plane tensile stress state is developed.

Coupled these two causes, respectively, the reduced plasticity of steel and the bi-axial tensile stress state may lead to the appearance of superficial fissures.

The semi-planetary rolling applied in

the unbending zone, to the exit of slab from curve thread of the continuous casting machine, induces an unbending moment in the condition of the compression stress state.

From the forces equilibrium (Figure 2), results:

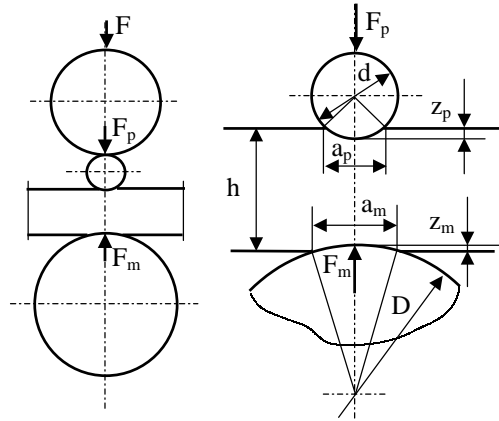


Figure 2 Forces scheme to semi-planetary rolling

$$F = F_p = F_m \quad (1)$$

In relation (1) F_p is the force developed on planetary cylinder and F_m is the force developed at the massive cylinder. It is evident :

$$F_p = p_p \cdot a_p \cdot b, \quad F_m = p_m \cdot a_m \cdot b \quad (2)$$

$$\frac{p_p}{p_m} = \frac{a_m}{a_p} \quad (3)$$

It denominated z_p the penetration depth of the satellite cylinder and z_m the penetration depth of the massive cylinder into material of body. From geometrical conditions we have:

$$a_p = 2\sqrt{2r \cdot z_p - z_p^2}, \quad a_m = 2\sqrt{2R \cdot z_m - z_m^2} \quad (4)$$

In the relations (4) r is the radius of satellite cylinder and R is the radius of the inferior cylinder. The terms z_p^2 and z_m^2 are very small then the products $(r \cdot z_p)$ and $(R \cdot z_m)$, respectively. Thus we can neglect the second terms of the radical arguments and the relations (4) become:

$$a_p = 2\sqrt{2r \cdot z_p}, \quad a_m = 2\sqrt{2R \cdot z_m} \quad (5)$$

From (3) and (5) we obtain:

$$\frac{p_p}{p_m} = \sqrt{\frac{R \cdot z_m}{r \cdot z_p}} \quad (6)$$

Using the relations (5) we can write:

$$\frac{a_p}{a_m} = \sqrt{\frac{r \cdot z_p}{R \cdot z_m}}$$

From this relation we obtain:

$$\frac{z_p}{z_m} = \frac{r}{R} \cdot \left(\frac{a_p}{a_m} \right)^2 \quad (7)$$

The strain intensity in thickness direction, in the proximity of the planetary cylinder, is greater than the strain intensity at the proximity of massive cylinder.

We denominate ϵ_{tp} , ϵ_{lp} , ϵ_{bp} the strains in the proximity of the planetary cylinder and ϵ_{tm} , ϵ_{lm} , ϵ_{bm} the strains in the proximity of massive cylinder.

Neglecting the strains in the breadth direction we obtain the conditions:

$$\epsilon_{lp} = -\epsilon_{hp} \quad \text{and} \quad \epsilon_{lm} = -\epsilon_{hm} \tag{8}$$

Because the mean strain intensity is in direct relation with the penetration depth (Fig. 3) we can write:

$$\frac{\epsilon_{lp}}{\epsilon_{lm}} = \frac{z_p}{z_m} \tag{9}$$

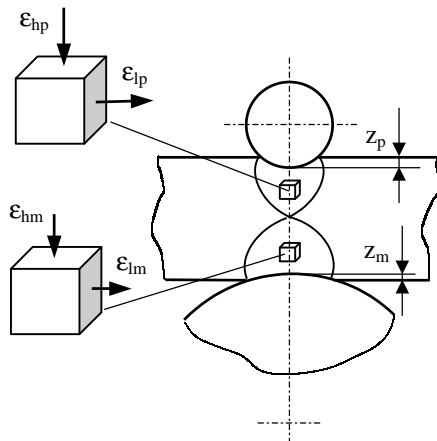


Figure 3 The local deformation states

Therefore, the strain intensity, at the length direction, developed in the proximity of the planetary cylinder is greater than the strain intensity, induced in the proximity of the massive cylinder.

Consequently, in the cross section of the semi-product will be developed the compression stress with greater intensity in the proximity of planetary cylinder.

Thus into the cross section of the body a bending moment is developed (Figure 4).

Intensity of this moment is greater, so much greater is the reduction of thickness ($\Delta h = h_0 - h_1$, h_0 is the initial and h_1 final thickness.).

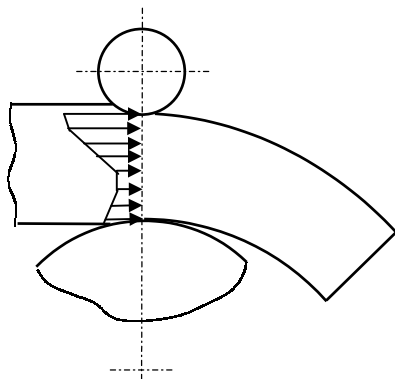


Figure 4 Bending process at semi-planetary rolling

At the same time, the bending moment is influenced by b/h ratio. For the great b/h ratio, the condition of the plan deformation state is performed and the relations (8) are satisfied. For smaller b/h ratio, relatively, the deformation in the breadth direction are different of zero and the bending moment intensity is more reduced. Thus the intensity of the bending moment is influenced by reduction of thickness Δh and b/h ratio:

$$M_i = f\left(\Delta h, \frac{b}{h}\right) \tag{10}$$

If the intensity of the bending moment is great the rolled product curves more intense. The bending intensity of the rolled product may be defined by the curvature or radius of curvature:

$$C_i = \frac{1}{R_i} = g\left(\Delta h, \frac{b}{h}\right) \tag{11}$$

where the C_i is curvature and R_i is radius of curvature of semi-product rolled of semi-planetary rolling.

In this paper are show the experimental results concerning the influence of the thickness reduction and the b/h ratio on curvature to semiplanetary rolling semi-product.

2. Experimental Conditions

The experiments were been done at a laboratory rolling mill equipped with upper planetary cylinder. The exterior diameter of the planetary cylinder is of 80mm. The diameter of the sarellite cylinders is of 12mm. The planetary cylinder includes 18 satellite cylinders.

The diameter of the inferior massive cylinder is 80mm.

The length of the active surface of cilinders is of 50mm.

The samples were processed from lead, through casting and symetrical rolling at the dimensions: the thickness of 10mm and various values for breadth. The values of the b/h ratio were: 1.15, 2.5 and 3.3.

The values of the thickness reduction were of 0.2, 0.4 and 0.6mm i.e. 2%, 4%, 6%, respectively.

Other matter of interest was the repartition of penetration depth of the sarellite cylinder and massive cylinder.

In this aim, it was prepared an equipment compused of a massive cylinder a sattelyte cylinder and a tensometer.

Also, we prepared samples with different values for b/h ratio. Loading the experimental system to the different press forces shall been induced various penetration depths of upper and lower cylinders according to their diameters.

3. Experimental Results

In the aim of evaluation of the z_p/z_m ratio they were effectuated pressing tests using the samples between the massive cylinder and satellite cylinder.

The Table 1 contents some results of these experimental researches.

The values of penetration were been calculated using the relations:

$$z_p = r - \sqrt{r^2 - \left(\frac{a_p}{2}\right)^2}, \quad z_m = R - \sqrt{R^2 - \left(\frac{a_m}{2}\right)^2} \quad (12)$$

The penetration depth for various reduction of thickness and breadth

Table 1

b_0 mm	h_0 mm	a_p mm	a_m mm	z_p mm	z_m mm	$\frac{z_p}{z_m}$
24.0	9.2	3.2	6.2	0.22	0.12	1.83
24.0	9.2	4.7	9.3	0.48	0.22	2.18
33.5	6.7	3.0	5.9	0.19	0.11	1.72
33.5	6.7	4.5	8.6	0.44	0.24	1.80

It is evident that the values of z_p/z_m ratio are 1.72 – 2.18. This proves that the penetration depth in the proximity of the planetary cylinder is greater of the penetration depth in the proximity of the inferior massive cylinder.

Consequently the effect of the asymmetrical strains repartition at semi-planetary rolling is justified.

Also we effectuated experimental tests in the aim of establishing the influence of the thickness reduction and b/h ratio on curvature and radius of curvature of the semi-planetary rolled samples.

In Figure 5 is showed the radius of curvature variation of the samples rolled at the semi-planetary rolling mill in function of thickness reduction and b/h ratio.

In Figure 6 is showed the cumulated radius of curvature variation in function of thickness reduction.

In Figure 7 is showed the curvature variation of the samples rolled at the semi-planetary rolling mill in function of b/h ratio for various thickness reductions.

The curvature of the samples increases when the thickness reduction increases and, also, when the b/h ratio increases.

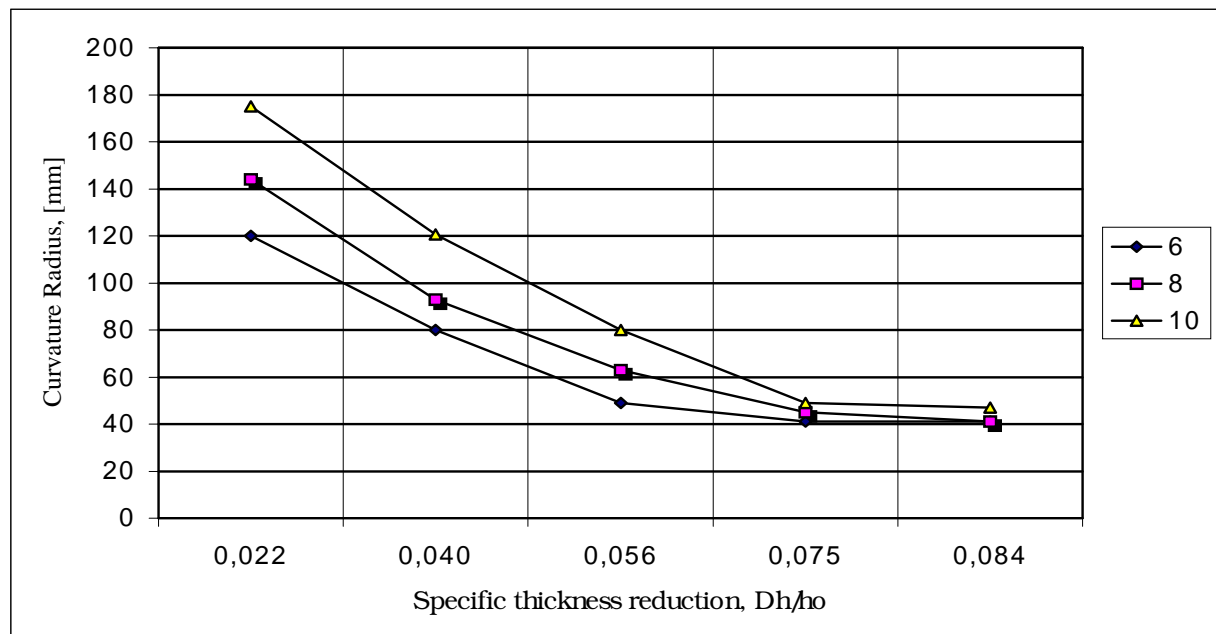


Figure 5 The variation of radius of curvature with reduction of thickness and b/h ratio

The influence of the reduction of thickness has a more important influence than the b/h ratio.

How the effect of the stress and strain fields, developed at the semi-planetary rolling, is reversible this deformation method may be used, also, for the unbending of the continuous casting slabs of high strength steels, without tensile stresses and, consequently, in conditions of the guaranteed quality of production.

Thus, the quality of continuous cast slabs shall be assured, because the unbending process is developed in same time of semi-planetary rolling, in conditions of compression stresses state. Since the critical tensile stresses are eliminated, the cause of the superficial fissures is eliminated and the surfaces of the continuous cast slabs results continuous without fissures or cracks.

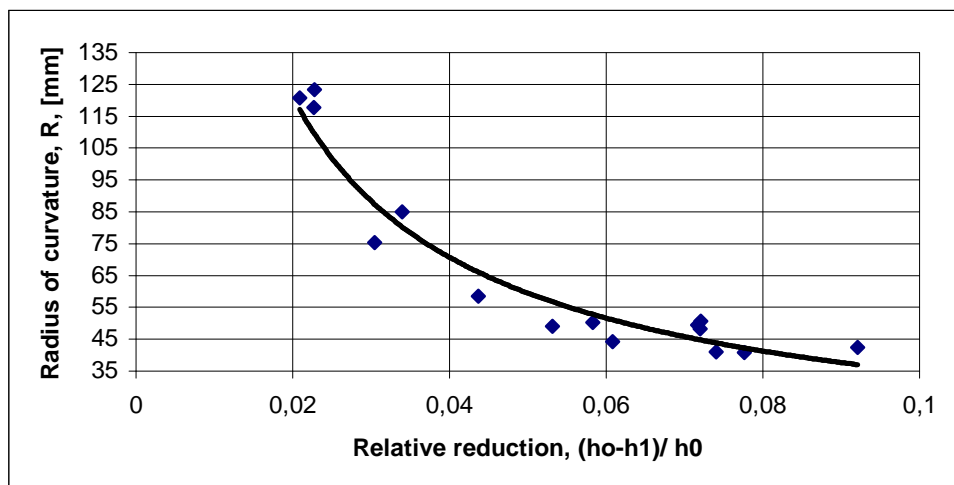


Figure 6 The variation of overall radius of curvature with reduction of thickness

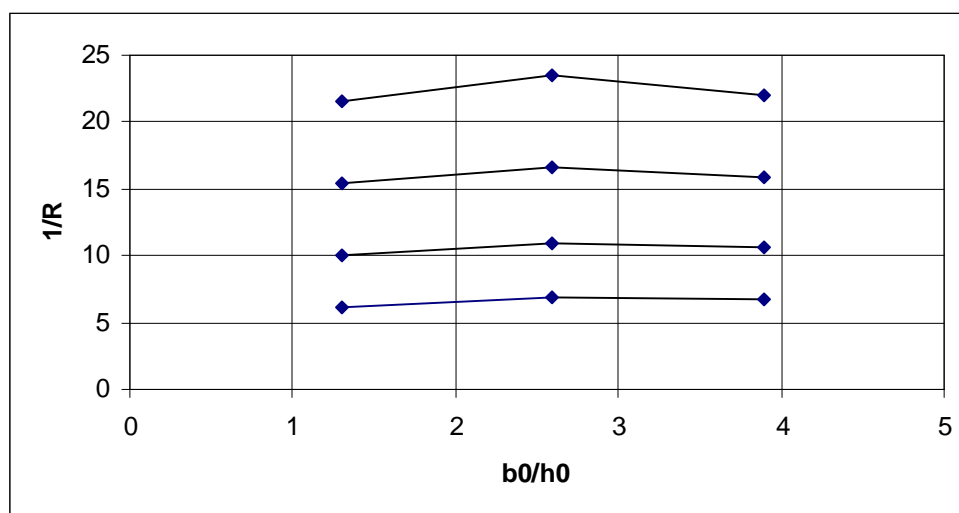


Figure 7 The variation of curvature with the b/h ratio

4. Conclusions

The semi-planetary rolling method may be applied to processing of the curve pieces or for unbending of the curved semi-product. For example the unbending of the continuous casted slabs of the high strength steels may be a favored process of semi-planetary rolling.

The researches showed in this paper prove the validity of idea of continuous cast slabs unbending. The advantage of this application is the unbending in condition of the compression stress state, this being the condition of the quality assurance of the casted slabs and, finally, the guarantee of the metallurgical products quality.

In case of curved pieces production, for the defined curvature (or radius of curvature) and b/h ratio we may be establish the optimum value of the thickness reduction.

In case of the unbending of continuous casted slab (with the b/h ratio and radius of curvature defined) we may be establish the thickness reduction necessary for its unbending.

The researches performed and showed in this paper prove that the semi-planetary rolling is a viable method for these aims.

References

- [1]. CĂNĂNĂU,N.,IVĂNESCU,A. *Studii și cercetări cu privire la defectul discontinuități la tablele groase din oțel*. Sesiunea de comunicări "Realizări și perspective în Metalurgie și Știința materialelor". Universitatea din Galați, 13-15 octombrie 2000
- [2]. CĂNĂNĂU,N.,IVĂNESCU,A. *Study on the Relation between the Quality of Continuous Cast Slabs and the Surface Discontinuities of the Steel Thick Sheet*. '01 International Conference on Advances in Materials and Processing Technologies, September 18-21, 2001, Leganes, Madrid, Spain, vol. 2, p.949-954.
- [3]. CĂNĂNĂU,N.,IVĂNESCU,A. *Technological Method of Forestall of the Superficial Cracks Network to the Continuous Cast Slabs..* '01 International Conference on Advances in Materials and Processing Technologies, September 18-21, 2001, Leganes, Madrid, Spain, vol. 2, p.955-960.
- [4] ANON, *Thin Hot Strip Using Planetary Mill*, Steel Time Intern., Sept. 1995, 33-5.
- [5] CANANAU,N.,IVANESCU,A.,CANANAU,D., *Study on the Deformation Process at the Semi-planetary Rolling*, Acta Mechanica Slovaca, Kosice, nr.3, 2001.

THEORETICAL SOLUTION OF FORGE CUTTING PROCESS

by

NICOLAE CĂNĂNĂU, DORU HANGANU, GHEORGHE GURAU

Abstract: The aim of theoretical analysis of the forging process is the calculation of the deformation force. The force developed in the forge cutting process is smaller, relatively of the force of other forge operations. Consequently, the calculation of forge cutting force is not solved and the analytical modeling of this process has not interest. However, the mathematical modeling of the forge cutting process presents interest for the theory of plastic deformation. In the present paper is showed a methodology of mathematical analysis of the forge cutting process.

Keywords: forge cutting, modeling, simulation.

1. Introduction

The forge cutting aim is the total or partial separation of a part of the semi-product. The force developed in the time of forging is small, relatively and is not important for technological calculus. But the forge cutting process has its particularities, what presents interest from the viewpoint of theory of plastic deformation.

The present paper brings a contribution to the modeling and simulation of the forge cutting process.

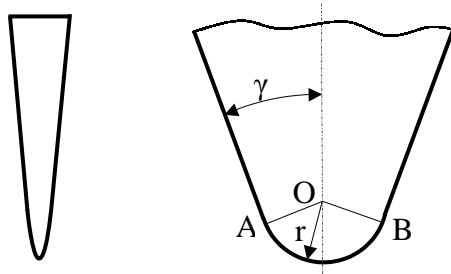


Figure 1 The aspect of cutting edge of forge tool: a-in normal conditions, b-in the theoretical approximation

The cutting forge tools, cutters and axes, have two parts: the edge and lateral surfaces. The edge of tool is the stress concentrator and determines the cutting of material. The lateral surfaces determine the separation of the parts of body. The edge is not perfect sharpened. In the time of using of cutting tool the edge uses and, consequently, it shall round, relatively quickly (Figure 1).

Thus, to the forge cutting process the stress field will developed at the contact surface between the material of semi-product and cutting tool.

The forge cutting force is the result of two components: the force developed to the edge of cutting tool and the force to lateral surfaces.

2. Establishing of Force at Edge of Cutting Tool

We consider the round form of the edge of cutting tool. We denominate r the radius of tool edge.

We admit that the material of semi-product is homogeneous and isotropic.

The calculus scheme is showed in Figure 2.

We denominate t the penetration of the cutting tool into the semi-product material.

The contact surface is limited of the angle α in relation with the point O.

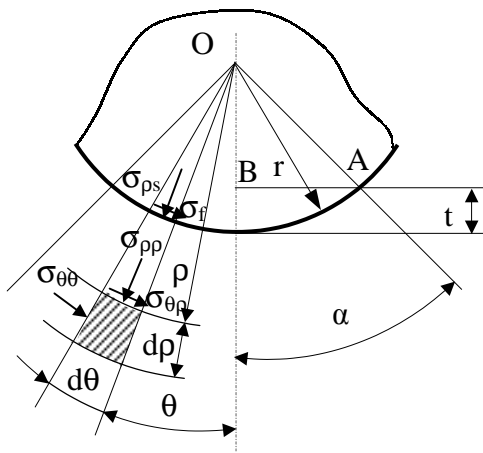


Figure 2 Calculus scheme of the section force

We consider the elementary volume at the angle θ with angular dimension $d\theta$ and radial dimension dr .

The stresses developed on the elementary volume are:

- σ_{pp} is normal stress, determined of action of the cutting tool. It is the active stress;
- $\sigma_{\theta\theta}$ is normal stress, determined of interaction of the considered mass element and the adjacent zones. It is the reactive stress.
- $\sigma_{\theta\rho}$ is tangential stress, determined of friction force, in the angular direction, to the contact surface of cutting tool and body material,
- $\sigma_{\theta z}$ is tangential stress, determined of friction force, in the direction of length to the contact surface of cutting tool and body material,

The named stresses respect the equilibrium equation: $\sigma_{ij,j} = 0$, (i and $j = 1,2,3$)

For cylindrical coordinates, in the developed form the equilibrium equation is,

$$\frac{\partial \sigma_{\theta\rho}}{\partial \rho} + \frac{1}{\rho} \cdot \frac{\partial \sigma_{\theta\theta}}{\partial \theta} + \frac{\partial \sigma_{\theta z}}{\partial z} + \frac{2\sigma_{\theta\rho}}{\rho} = 0 \quad (1)$$

The initial conditions are:

$$\sigma_{\rho\rho}^0 = \sigma_{rr}^0 = \sigma_0, \sigma_{\theta\theta}^0 = \sigma_{\theta\rho}^0 = \sigma_{\theta z}^0 = 0 \quad (2)$$

The limit conditions are:

$$\sigma_{\rho\rho}^\alpha = \sigma_{rr}^\alpha = \sigma_0, \sigma_{\theta\theta}^\alpha = \sigma_{\theta z}^\alpha = 0, \sigma_{\theta r}^\alpha = \sigma_f^\alpha \quad (3)$$

where:

σ_0 is the stress intensity characteristic stress of material at the concrete deformation conditions, and σ_f is the intensity of friction stress. For calculation of stress σ_0 is used the equation of deformation behavior,

$$\sigma_0 = \sigma(\varepsilon, \varepsilon, T), \quad (4)$$

And ε is the strain intensity $\dot{\varepsilon}$ is strain rate intensity and T is the deformation temperature.

The deformation in direction of the length may be neglected and, consequently, the stress $\sigma_{\theta z} = 0$, and $\frac{\partial \sigma_{\theta z}}{\partial z} = 0$.

Also, at hot forging the variation of $\sigma_{\theta\theta}$ with the radial coordinate ρ may be neglected.

The variation of the stress $\sigma_{\theta\rho}$ is result of the friction stress σ_f to the contact surface of cutting tool and material. From the condition of homogenous and isotropic material this is linear variation (Figure 3).

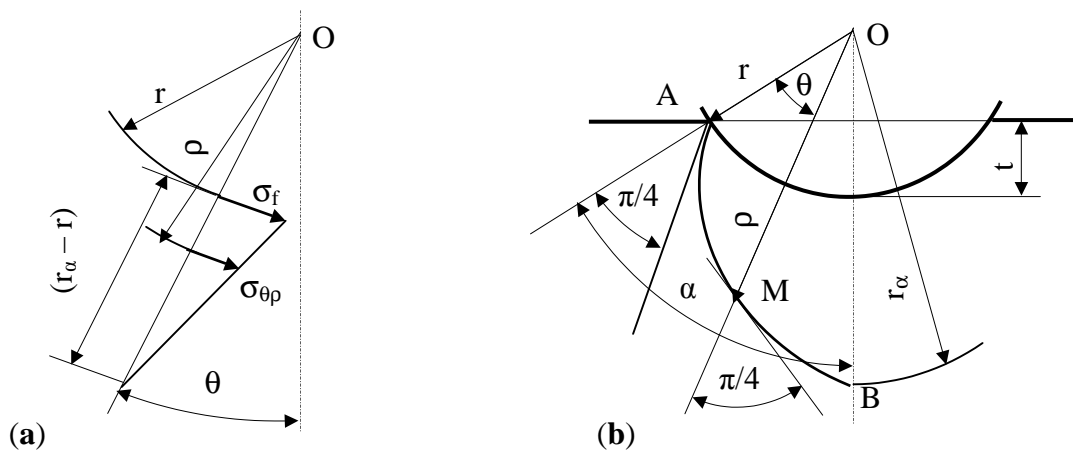


Figure 3 The scheme for calculus of stress $\sigma_{\theta\rho}$

This variation is determined of the relatively slide of the atomic layers. Consequently, we can consider the length of the zone of linear variation of the $\sigma_{\theta\rho}$ stress how the extension of the plastic deformation zone, defined by the radius r_α .

The tension $\sigma_{\theta\rho}$ has the maximum value to the contact surface (for $\rho = r$) and becomes zero at the limit of the plastic zone ($\rho = r_\alpha$).

For establishing of the radius r_α we consider the slip line, which begins in the point A, to the contact surface, and until to the point B, where the slip line intersects the symmetrical axis (Figure 3).

Because between the geometrical tangent, in the point M of slip line and the radial direction is constant and equal of $\pi/4$ the slip line is defined by logarithmic spiral and its equation is:

$$\rho = r \cdot e^\theta \quad (5)$$

For $\theta = \alpha$ we have

$$\rho(\alpha) = r_\alpha = r \cdot e^\alpha \quad (6)$$

where:

$$\alpha = \arccos\left(\frac{r-t}{r}\right) \quad (7)$$

We denominate γ the angle of the lateral surface at the symmetrical axis of the cutting tool. We have:

$$\alpha = \frac{\pi}{2} - \gamma \quad (8)$$

and:

$$r_\alpha = r \cdot e^{\frac{\pi}{2} - \gamma} \quad (9)$$

Consequently, we can write:

$$\frac{\sigma_{\theta\rho}}{\sigma_f} = \frac{r_\alpha - \rho}{r_\alpha - r} \quad (10)$$

Thus we have:

$$\frac{\partial\sigma_{\theta\rho}}{\partial\rho} = -\frac{\sigma_f}{r_\alpha - r} \quad (11)$$

And

$$\frac{\sigma_{\theta\rho}}{\rho} = \frac{\sigma_f}{\rho} \cdot \frac{r_\alpha - \rho}{r_\alpha - r} \quad (12)$$

According to the above considerations the equation (1) becomes:

$$\frac{\partial\sigma_\theta}{\partial\theta} = -\frac{\tau_f}{r_\alpha - r} \cdot (2r_\alpha - 3\rho) \quad (13)$$

The stresses σ_θ and σ_ρ are principal tensions and in base of the plasticity condition we have:

$$\frac{\partial\sigma_\theta}{\partial\theta} = \frac{\partial\sigma_\rho}{\partial\theta} \quad (14)$$

And equation (8) becomes:

$$\frac{\partial\sigma_\rho}{\partial\theta} = \frac{\sigma_f}{r_\alpha - r} \cdot (2r_\alpha - 3\rho) \quad (15)$$

For establishing of the force developed to forge cutting, the solving of the stress σ_{ps} at the contact surface is necessary.

Thus the equation (15) becomes:

$$d\sigma_{ps} = \frac{\sigma_f}{r_\alpha - r} \cdot (2r_\alpha - 3r) \cdot d\theta \quad (16)$$

We admit the friction stress σ_f of uniform repartition ($\sigma_f = \mu\sigma_0$) and we have:

$$\sigma_{ps} = \mu\sigma_0 \cdot \left(2 - \frac{r}{r_\alpha - r} \right) \cdot \theta + C \quad (17)$$

In base of the limit conditions we obtain:

$$\sigma_{ps} = -\sigma_0 \left[1 + \mu \cdot \left(2 - \frac{r}{r_\alpha - 1} \right) \cdot (\alpha - \theta) \right], \quad (18)$$

The elementary force is:

$$dF = |\sigma_\rho| \cdot a \cdot r \cdot \cos \theta \cdot d\theta \quad (19)$$

The total force is:

$$F = 2 \int_0^\theta |\sigma_\rho| \cdot a \cdot r \cdot \cos \theta \cdot d\theta \quad (20)$$

After substitution of the expression of σ_{ps} stress (equation 18) and integration, we obtain the equation for calculus of the forge cutting force into relation with the θ parameter, or with the penetration depth of the cutting tool t , where these following parameters are considered into geometrical relation:

$$F_1(\theta) = 4k \cdot a \cdot r \cdot \left[\sin \theta + \mu \cdot \left(2 - \frac{r}{r_\alpha - r} \right) \cdot [(\alpha - \theta) \cdot \sin \theta + 1 - \cos \theta] \right] \quad (21)$$

And for $\theta = \alpha$ we have:

$$F_1(\alpha) = 4k \cdot a \cdot r \cdot \left[\sin \alpha + \mu \cdot \left(2 - \frac{r}{r_\alpha - r} \right) \cdot (1 - \cos \alpha) \right] \quad (22)$$

Into above equations we denominate the dimension of the semi-product in the length of the cutting tool.

3 Establishing of the Force Developed on the Lateral Surfaces of Cutting Tool

On the lateral surface of the cutting tool are developed the perpendicular and friction forces.

We will consider elementary surfaces at the level t (Figure 4). On these surfaces are developed the perpendicular tension p and tangential tension μp , (μ is friction coefficient)

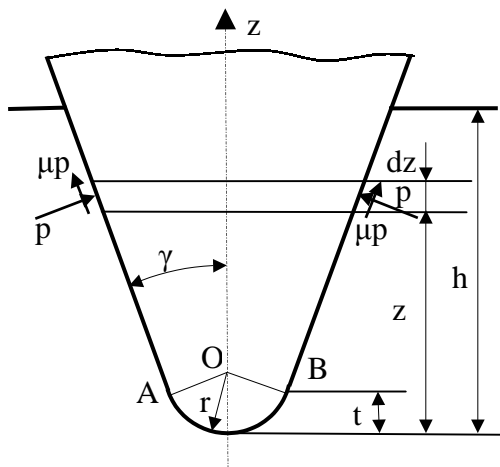


Figure 4 Scheme of forces on the lateral surfaces of cutting tool

The differential equation of elementary force developed on the lateral surfaces is:

$$dF = 2p \cdot a \cdot \frac{dz}{\cos \gamma} \cdot \sin \gamma + 2\mu \cdot p \cdot a \cdot \frac{dz}{\cos \gamma} \cdot \cos \gamma \quad (23)$$

We admit $p = \sigma_0$ and we integrate for limits t and $z-t$ and we obtain:

$$F_2(z) = 2\sigma_0 \cdot a \cdot (tg \gamma + \mu) \cdot (z - t) \quad (24)$$

For the limit value of parameter z the expression of this force is:

$$F_2(h) = 2\sigma_0 \cdot a \cdot (tg \gamma + \mu) \cdot (h - t) \quad (25)$$

The resultant force, developed into forge cutting process is the sum between F_1 and F_2 and is defined by the composed function:

$$F = \begin{cases} F_1(\theta), & \text{for } \theta \in [0, \alpha], z \leq t \\ F_1(\alpha), & \text{for } \theta > \alpha, z > t \end{cases} \quad (26)$$

4 Influence of Geometrical Factors on Forge Cutting Force

The geometrical factors what have a determinate roll on the value of forge cutting force are the radius r of the edge and the angle γ of lateral surfaces of cutting tool.

We developed a computation program for calculation of the force to the forge cutting.

Testes values are presenting in follows figures.

In figure 5 is shown variation of cutting force at vertex blade, with penetration.

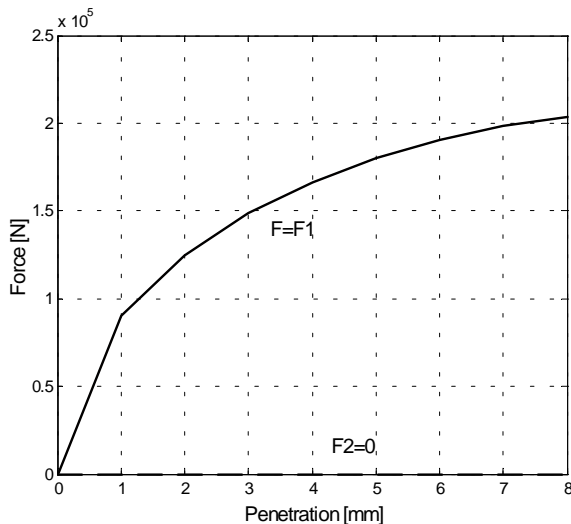


Figure 5 Force variation versus depth of penetration, less than or equal with radius of vertex blade

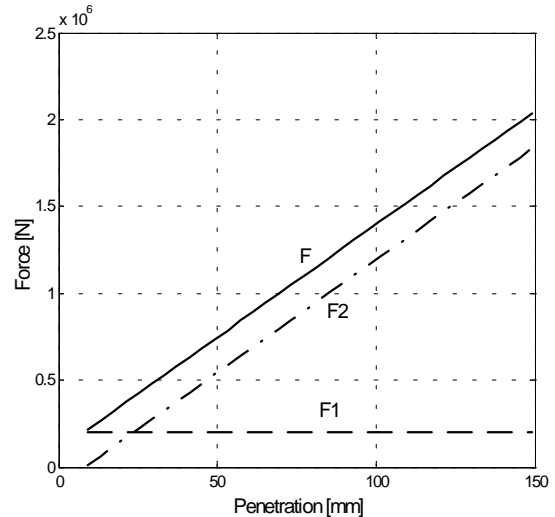


Figure 6 Force variation versus depth of penetration, greater than or equal with radius of vertex blade

Forge cutting force is definite by follows conditions: $F_1 \neq 0$ and $F_2 = 0$.

Force increases parabolic with penetration of the vertex blade. It has radius “ r ”.

In figure 6 is shown variation of cutting force, versus depth of penetration, after penetration is greater than or equal with radius “ r ”.

In figure 7 is shown radius influence versus forge cutting force.

Is possible to see that force F_1 is linear increase with radius “ r ”. F_2 force is linear decrease because when radius increasing for same depth penetration, length of contact surface between material and cutting tool is lessening.

5 Conclusions

The forge cutting consists by two successive processes. First is the effective cutting process as effect of the action of cutting tool edge. The second is the separation process of the parts of body.

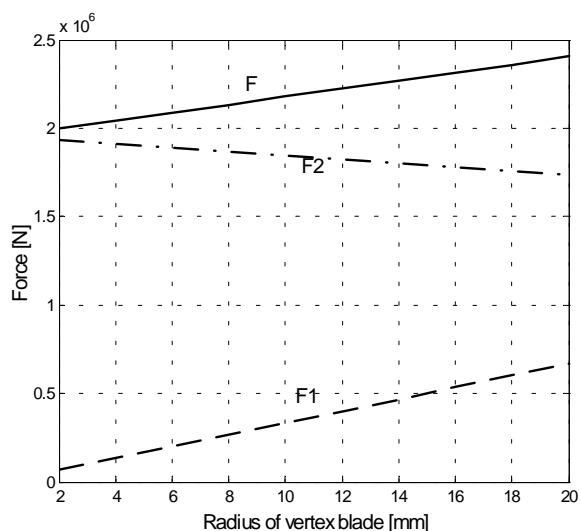


Figure 7 Radius influence versus forge cutting force

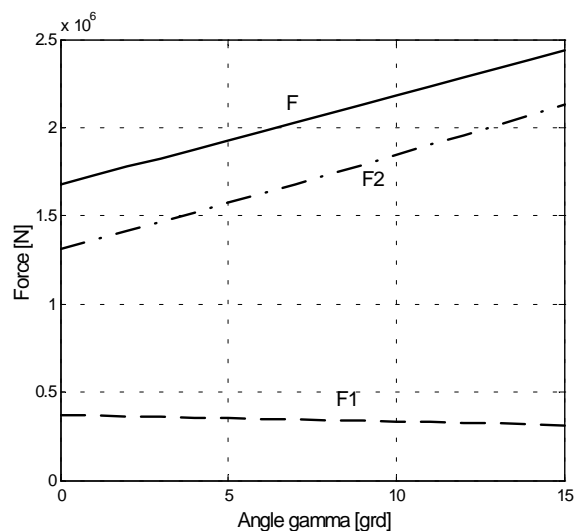


Figure 8 Angle γ influence versus forge cutting force

The cutting tool edge has a round form, what increase in the radius, in the time of use of the cutting tool, consequence of the wear.

Through the analytical modeling of the forge cutting process we established the relation of calculation of the force necessary and the evolution of this force in the time of the penetration of cutting tool into material.

The obtained results are useful for practical calculations and, also, for the theory of plastic deformation

REFERENCES

- [1] **M.ADRIAN, S.BADEA** – *Bazele proceselor de deformare plastica*, Editura tehnica, București, 1983;
- [2] **N.CANANAU** – *Teoria deformarii plastice*, Universitatea din Galati, 1994;
- [3] **M. GHINEA, V. FIREȚEANU** – *MATLAB – calcul numeric- grafică – aplicații*, Editura Teora, București, 1998
- [4] **I.DRAGAN** – *Tehnologia deformatiilor plastice*, Editura didactică și pedagogică, București, 1976.
- [5] **E.CAZIMIROVICI** – *Bazele teoretice ale deformării plastice*, Editura Bren, București, 1999
- [6] **ROWE, G.W.**, *Elements of Metalworking Theory*, Ed. Arnold, London, 1978.
- [7] **CONSTANTIN I.RADU** – *Algebră liniară, geometrie analitică și diferențială*, Editura ALL, București, 1998

VIRTUAL INSTRUMENTATION FOR SCUFFING DIAGNOSE OF BALL BEARINGS

BY

CARMEN BUJOREANU and ALINA ANGHEL

Abstract: In the metallurgical industry, one of the diagnose problem is concerned with a large number of very heavily loaded low speed rolling element bearings. Scuffing diagnose of rolling element bearings can be made by the analysis of the bearing friction forces which are the most sensitive indicator of bearing defects. Scuffing limits in angular contact ball bearings are estimated by an original algorithm and computer code. The theoretical model has been sustained by an experimental investigation. This paper presents an efficient virtual instrument in order to evidence the scuffing occurrence.

Keywords: Ball bearing, Scuffing, Test device, Virtual instrument.

1. Introduction

The means and methods of machine vibration monitoring are practically the same in all the industries and ensure similar results. Specific peculiarities for different industries occur only in the methods of detailed diagnostics.

In the metallurgical industry, the first problem is concerned with a large number of very heavily loaded low speed rolling element bearings. The traditional diagnostic methods which use the appearance of shock pulses for such bearings very often do not work because, even in non-defective bearings, at low speeds there appear many breaks of the lubrication film and the presence of defects does not change the shock pulse features significantly. So, the main possible damage is related to scuffing.

Scuffing can take place either at low sliding velocity and high normal pressure, by softening and melting a thick surface layer of the contacting bodies, or at high sliding velocities and low normal pressure, by a process of abrasion and adhesion. Also, occasionally abnormal operation causes premature bearing failure that is usually microscuffing and/or scuffing [2].

The diversity of running conditions and, implicitly, of their typical influences on scuffing failure in bearings rolling contacts is a limiting factor for researcher's options to a global study. From a strictly mechanical point of view, to estimate the bearing's scuffing risk means to settle the interdependence between the Kinematics, dynamic, lubrication and friction phenomena realized in bearing's rolling contacts subjected to an important sliding.

Our researches have been studied this interdependence by a theoretical model also sustained by an experimental simulation [3]. The defects that occur during rolling element bearing operation, first of all, influence the properties of friction forces in the

bearing [4].

A sudden increase of friction force evidences the scuffing onset. The main task of monitoring the friction force is to obtain maximum possible information and minimize the loss of information during the analysis of signals under monitoring. Such analysis is possible only when an adequate model of the monitored process is known.

Data acquisition and signal conditioning and processing of the bearing friction forces created an efficient virtual instrument to estimate the scuffing failure in ball bearings.

2. Theoretical considerations

The scuffing approaches analysis and our original experiments on bearing's contacts have been detached the idea that, any scuffing mechanism considered, there is an energetically unbalance in the rolling contact. This unbalance generates disruptions in lubrication conditions and the scuffing risk appears.

So, we consider the most adequate model to estimate the scuffing limits an energetically one.

According to lubrication regime, the amount of heat is related to the oil film parameter, λ , and can be estimated as follows:

$$q = \begin{cases} \mu \cdot p \cdot V / h_c & \lambda \geq 3 \\ \mu_{ech} \cdot p \cdot V & 1 \leq \lambda < 3 \\ \mu_a \cdot p \cdot V & \lambda < 1 \end{cases} \quad (1)$$

where: h_c is the central film thickness; p is the average contact pressure; V represents ball-race contact sliding speed. This is measurable for specimens experimental simulation, but for angular contact ball bearings tests it must be calculated.

The model also consider: μ - traction coefficient on ball-race contact for EHL regime; μ_{ech} - friction coefficient on ball-race contact for boundary lubrication regime, considering both the fluid friction (F_f) and solid friction on the asperities (F_{asp}) under the normal load Q ; μ_a - friction coefficient on ball-race contact asperities, determined by a methodology described in [10]

Therefore, a dependence between contact pressure, sliding speed and critical level of energy dissipated can be settle for any operating conditions in a ball bearing which contact geometry and lubricant properties are known.

3. Experimental considerations

Scuffing tests were performed on 7206 angular contact ball bearing included in an original test, presented in figure 3. The test rig is adapted on 4-ball machine from our laboratory.

The operating speed on the test rig was moderate (max. 2800 rpm), so the ball-inner ring sliding speed too. As the bearing scuffing risk is deeply correlated to high sliding speed (typical to high-speed ball bearings) we realised these conditions by the cage's braking. It were obtained sliding speeds enough high to initiate scuffing phenomenon for a boundary lubrication regime.

During the running process, an electromagnetic brake (figure 4) fixed on the cages of bearings system, through disk-cage device, realized the cage's braking.

The speed transducers quantify the braked cage speed ω_c and the braking torque, implicitly the force F_c between ball and cage. With these two known parameters, the correlation between experimental and theoretical investigations can be settled. The test rig also allows measuring the friction torque by means of strain gauges. The sudden increase of the friction force (as in experimental tests on disks) indicates the scuffing occurrence.

The testing conditions are the followings:

- ◆ Tested bearings were subjected to pure axial loading.
- ◆ A Raynger MX4 infrared thermometer has measured average bearing temperature.
- ◆ An electric resistance measurement device from our laboratory facilities quantified the oil film thickness. It has been imposed a poor lubrication, in order to realise a boundary regime for scuffing occurrence

A general view of the test rig is presented in figure 1.

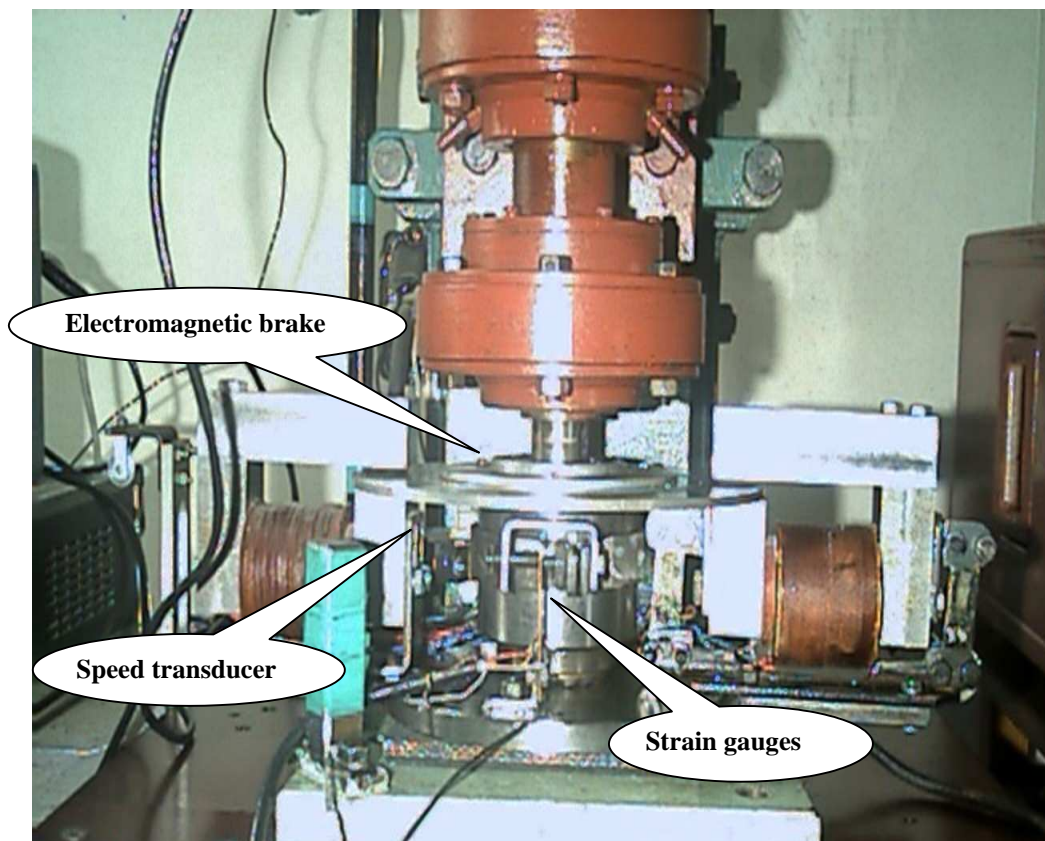


Fig.1 The test device

Observations

- Owing to the cage's braking, the ball-race sliding speeds were substantially increased (~ 3 m/s) and the scuffing appeared.
- The boundary lubrication regime potentates the scuffing risk.
- The results lead to establishment of unique scuffing limits of $1.5 \cdot 10^8$ $W \cdot m^{-2}$ (in terms of energy dissipation) in a given ball bearing (7206C), for imposed running conditions.

4. Virtual instrument for scuffing diagnose

A virtual instrument consists of an interactive user interface, a dataflow diagram that serves as the source code and icon connections that allow the virtual instrument to be called from higher level virtual instruments.

In the followings figures are presented the block diagram of the virtual acquisition instrument created, constructed by wiring together objects that send and receive data, perform specific functions and control the flow of execution. Data are read and saved as global variables.

Data acquisition and transducers signal processing were realised using NI-DAQ board and LabVIEW 5.1 soft. This virtual instrument with two channels readings monitoring the friction force respectively the braking torque is presented in figure 1.

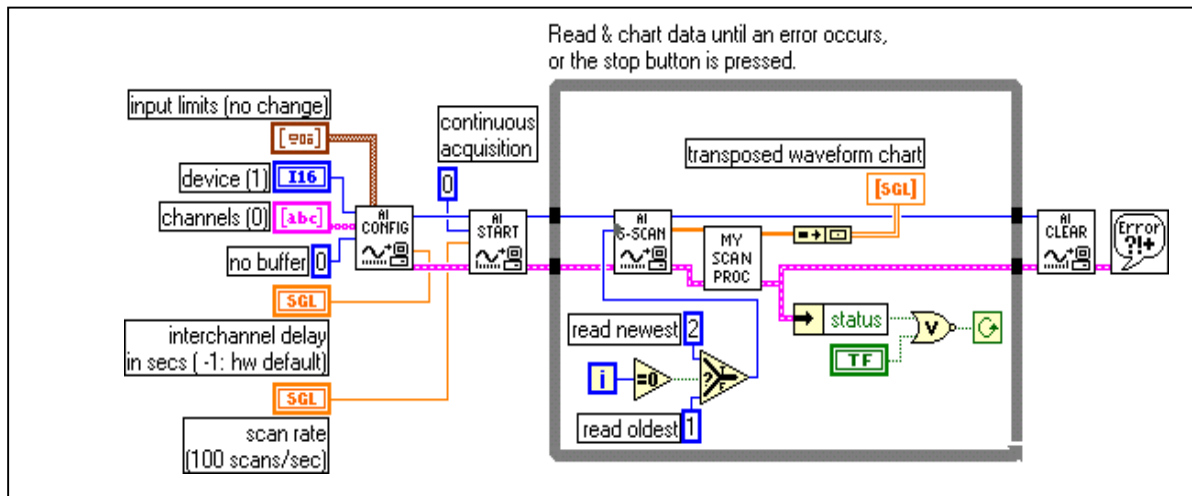


Fig.1 The block diagram of the virtual acquisition instrument

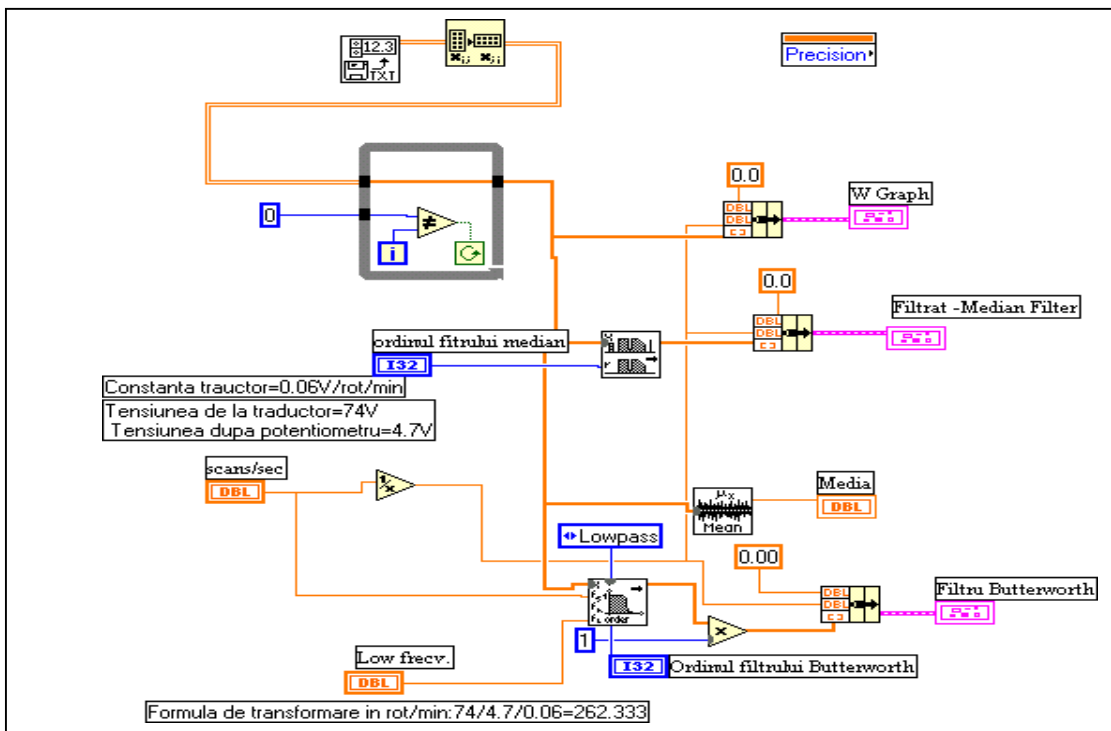


Fig. 2. Block diagram for average filtering and noise removal

The main task of monitoring is to obtain maximum possible information and minimize the loss of information during the analysis of signals under monitoring.

There is a real danger that interfering signal components may spoil the results of diagnostics. The diagnostic accuracy in this case can suffer. Therefore, in order to remove this danger, figure 2 presents the block diagram for the noise removal from acquisition chain and the signal averaging.

Figure 3 presents the scuffing initiation registered with the virtual instrument created for scuffing onset. It can be remarked the sudden friction torque increase (absolute value), accompanied by noise and vibrations. This is the moment where the machine was stopped at an earlier stage of damage process. The friction torque, in this case, was very high (around 1 N·m).

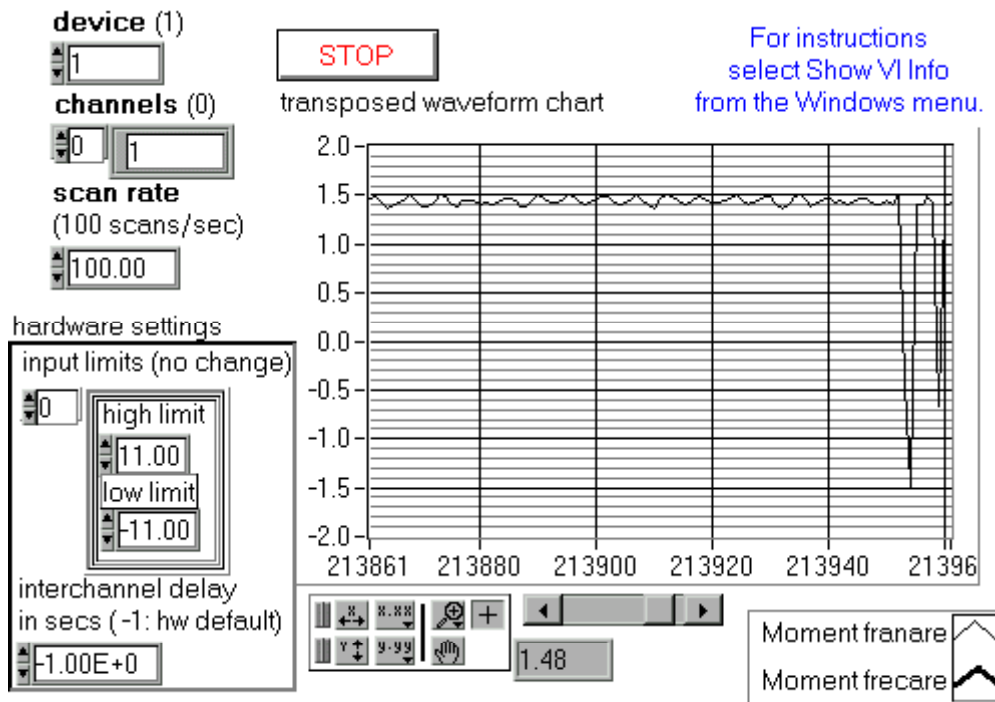


Fig.3. Scuffing onset ($F = 750 \text{ N}$; $n = 2800 \text{ rpm}$)

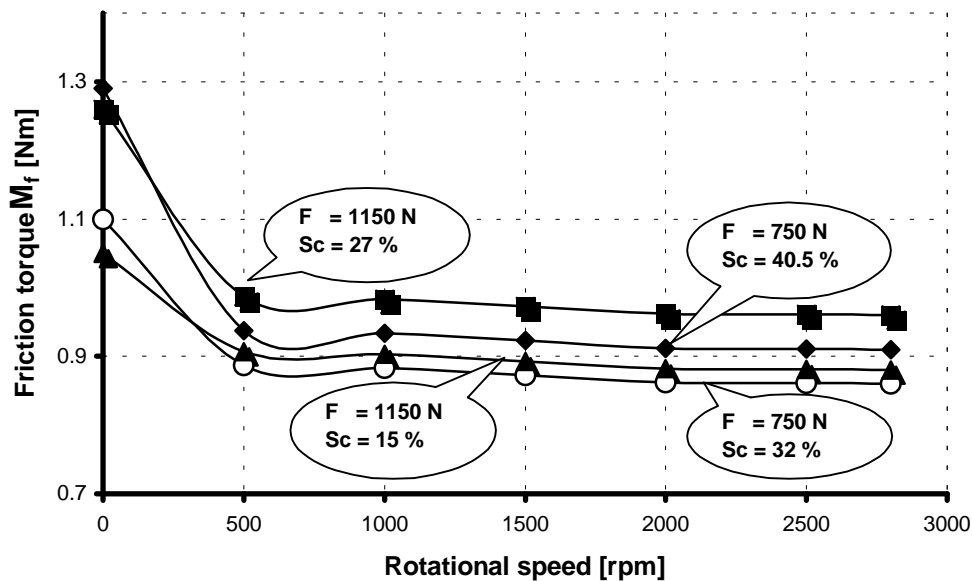


Fig.4. Friction torque with scuffing risk

5. Conclusions

The experimental results allow the evaluation of scuffing damage in angular contact ball bearing (7206C).

The algorithm established a scuffing criterion. Corroboration between the energetically criterion and the scuffing temperature leads to the bearing performance related to scuffing.

The virtual instrument created to evidence the scuffing onset is an efficient one and lead to results agreeing the literature.

The necessity to monitor rolling element bearing condition confronts the most machine users. Optimizing the combination of diagnostic methods and means to include bearing problems is one of the most important challenge.

Received March 14, 2005

The "Gh.Asachi" Technical University Iași

REFERENCES

1. S.C Lee, H.S. Cheng, - *Experimental Validation of Critical Temperature-Pressure. Theory of Scuffing*, **Tribol. Trans.**, 38, 3, 1995, **738-742**
2. Nélias, D., Nassare, F., Flamand, L., - *Etude experimentale et theorique du microgrippage dans les contacts elastohydrodynamiques*, **Rev.Gen.Therm.**, 36, 1997, **26-39**
3. C. Bujoreanu, D. Olaru, Sp. Cretu, D. Nelias, *Etude de la limite de grippage dans les roulements à billes*", *Roulements et Tribologie, Actes des Journées Internationales Francophones de Tribologie*, 2001, **195-210**
4. Alexej V. Barkov, Natalia A. Barkova , -*The artificial intelligence systems for machine condition monitoring and diagnostics* , **Proc. of the Saint Petersburg Post-graduate Institute of the Russian Federation Power Industry and Vibration Institute**, USA, Vol. 9, 1999. **1-36**
5. J.J.Chapman, -*Angular Contact Ball Bearing Dynamics, an Experimental and Theoretical Investigation*, **Lubricants and Lubrication**, 1995, **435-443**.
6. *** *LabVIEW - Graphical Programming for Instrumentation*, National Instruments, 1996.

INSTRUMENT VIRTUAL PENTRU DIAGNOSTICAREA GRIPARII IN RULMENTII CU BILE

Rezumat: Diagnosticarea fenomenului de gripare in rulmenti se efectueaza prin analizarea fortelor de frecare, ale caror variatii reprezinta un indicator sensibil al deteriorarilor. Limitele de gripare din rulmentii cu bile (intalniti in industria metalurgica) sunt estimate printr-un algoritmi si cod de calculator originale. Modelarea teoretica este sustinuta de investigatia experimentală. Lucrarea descrie instrumentatia virtuala pentru achizitia datelor referitoare la momentele de frecare si de franare in cazul in care este initiat fenomenul de gripare, in conditii critice de presiune, viteza si temperatura.

CONSIDERATIONS REGARDING THE SCUFFING FAILURE OF BALL BEARINGS

by

CARMEN BUJOREANU and SPIRIDON CRETU

Abstract: An experimental study has been performed both on the specimens and bearing test rig to estimate scuffing limits in angular contact ball bearings, often met in metallurgical industry. Some scuffing tests have been carried out on the high-speed twin-disk machine. Another series of scuffing tests were applied on the 7206 angular contact ball bearing included in an original test rig. An electromagnetic brake fixed on the cages of bearings system, through disk-cage device, realised the cage's braking. Corroboration between our experimental and theoretical results allows a scuffing criterion to estimate this type of damage. It is shown that the scuffing areas correspond to scuffing criterion $\mu \cdot p \cdot V^{0.8}$.

Keywords: Ball bearing, Scuffing, Energetically criterion, Cage braking.

1. Introduction

The literature underlines that the scuffing failure models suppose the settlement of a complex function including mechanical, physical and chemical effects of rolling contacts in running. Therefore, it is difficult to predict the solution of such a complex problem.

However, details of the circumstances and the way in which this type of distress occur are still the subject of debate, so that, various mechanisms have been proposed over the past few decades to characterize the scuffing failure. Among the multiple models, none is sufficiently effective and reliable. Over the years, there have been three major approaches to explain when sudden scuffing failure occurs. They are hydrodynamic, temperature and chemical approaches [1].

Scuffing is a complex phenomenon of severe adhesive wear generated under particular combinations including contact pressure, lubrication, speed and friction. Scuffing involves the sudden collapse of the lubricant film and is generally regarded as resulting from thermal phenomena. At this temperature, the breakdown film with local welding or adhesion of the contacting surfaces can appear. As result of local adhesion, the friction increases and causes a still higher temperature, and then the process can become catastrophic.

Scuffing can take place either at low sliding velocity and high normal pressure, by softening and melting a thick surface layer of the contacting bodies, or at high sliding velocities and low normal pressure, by a process of abrasion and adhesion.

An experimental study has been performed both on the specimens and bearing test rig to estimate scuffing limits in angular contact ball bearings. Some scuffing tests have been carried out on the high-speed twin-disk machine available at LMC facilities. Another series of scuffing tests were applied on the 7206 angular contact ball bearing

included in an original test rig. An electromagnetic brake fixed on the cages of bearings system, through disk-cage device, realised the cage's braking.

The diversity of running conditions and, implicitly, of their typical influences on scuffing failure in bearings rolling contacts is a limiting factor for researcher's options to a global study. From a strictly mechanical point of view, to estimate the bearing's scuffing risk means to settle the interdependence between the Kinematics, dynamic, lubrication and friction phenomena realized in bearing's rolling contacts subjected to an important sliding.

The scuffing appearance for the studied ball bearings is presented in figure 1.

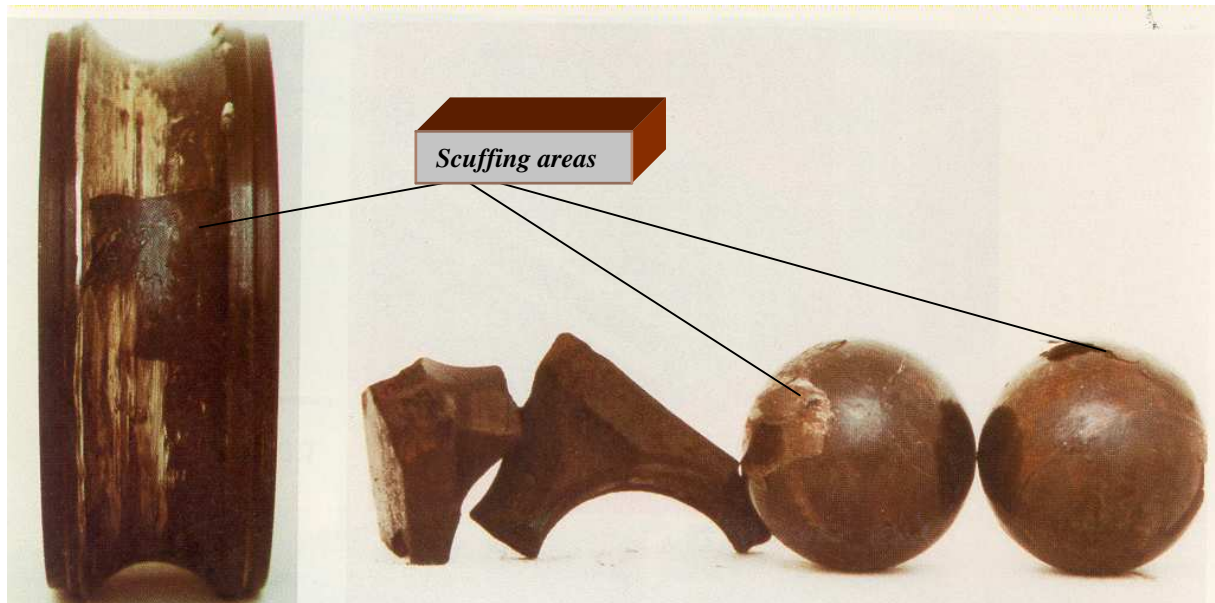


Fig.1 Scuffing appearance in ball bearings

2. Theoretical considerations

The scuffing approaches analysis and our original experiments on bearing's contacts have been detached the idea that, any scuffing mechanism considered, there is an energetically unbalance in the rolling contact. This unbalance generates disruptions in lubrication conditions and the scuffing risk appears.

So, we consider the most adequate model to estimate the scuffing limits an energetically one.

Therefore, according to lubrication regime, the amount of heat is related to the oil film parameter, λ , and can be estimated as follows:

(1) for complete EHL regime ($\lambda \geq 3$):

$$q_{fluid} = F_l \cdot \dot{\gamma} \quad (1)$$

where: q_{fluid} represents the energy dissipated in contact within the oil film; $\dot{\gamma} = V / h_c$ is the lubricant shear rate; $F_l = \int \tau dA = \mu \cdot p$ is the shear friction force within the oil film; h_c is the central film thickness; p is the average contact pressure; V represents ball-

race contact sliding speed. This is measurable for specimens experimental simulation, but for angular contact ball bearings tests it must be calculated.

(2) for boundary lubrication regime ($\lambda = 1 \dots 3$):

$$q_{mixt} = \mu_{ech} \cdot p \cdot V \quad (2)$$

where q_{mixt} represents the energy dissipated as consequence of the two friction components combined action (fluid and solid).

(3) for direct contact ($\lambda < 1$):

$$q_a = \mu_a \cdot p \cdot V \quad (3)$$

where q_a represents the energy dissipated on the asperities, when there is no lubrication.

The sliding friction is related to the degree of film formation or portion of load supported by the asperities contact.

So, the model considers:

◆ μ - traction coefficient on ball-race contact for EHL regime, determined as follows:

$$\mu = (A + B \cdot \xi) \cdot \exp(-C \cdot \xi) + D \quad (4)$$

This equation simulates the traction behaviour, taking account both of slide-to-roll ratio ξ and the lubricant rheological characteristics derived from traction curves experimentally determined using a twin-disk machine. The coefficients of the model, A , B , C , D are depending on operating conditions and are also determined from the experimental investigations.

A mineral oil (ELF 154 NS) was used as lubricant. Its rheological parameters (shear modulus G and shear stress τ_0), included in the general model for estimating scuffing risk, were predicted, pressure and temperature dependent, as described in [2].

◆ μ_{ech} - friction coefficient on ball-race contact for boundary lubrication regime, considering both the fluid friction (F_l) and solid friction on the asperities (F_{asp}) under the normal load Q :

$$\mu_{ech} = \frac{F_l + F_{asp}}{Q} \quad (5)$$

◆ μ_a - friction coefficient on ball-race contact asperities, determined by a methodology described in [3], with B_0 and C_0 experimentally estimated:

$$\mu_a = \frac{F_{asp}}{Q} = 0.18 \cdot \exp(-B_0 \cdot \lambda^{C_0}) \quad (6)$$

It can be concluded that the following relation expresses the energy dissipated:

$$q = \begin{cases} \mu \cdot p \cdot V / h_c & \lambda \geq 3 \\ \mu_{ech} \cdot p \cdot V & 1 \leq \lambda < 3 \\ \mu_a \cdot p \cdot V & \lambda < 1 \end{cases} \quad (7)$$

Therefore, a dependence between contact pressure, sliding speed and critical level of energy dissipated can be settle for any operating conditions in a ball bearing which contact geometry and lubricant properties are known.

3. Experimental considerations

Scuffing related to rolling contact in angular contact ball bearing was experimentally studied both on specimens and ball bearings.

3.1 Tests on specimens

Some scuffing tests have been carried out on the high-speed twin-disk machine described in [1]. For this simulative tribotesting, the simulation criteria refer to material, geometrical characteristics and the lubrication regime of the practical system, which is 7206 angular ball-bearing.

Testing conditions

The contacting disks, presented in figure 2, were arched performed in order to reproduce the ball-inner ring contact from 7206 ball bearing (the ellipticity factor $k = 8.964$).

The lubricant used in these tests is a mineral oil, ELF 154 NS. Its rheological behaviour is estimated from experimental traction curves obtained on the twin-disk machine [2].

In the experimental procedure the scuffing limit is reached by increasing progressively the sliding speed, other operating conditions such normal load and the rolling speed being kept constant. The evidence of disk scuffing is a sudden increase of friction force, which stops automatically the machine at an earlier stage of damage process.

Scuffing limits for mean rolling speed of 40m/s, three maximum hertzian pressures (0.8, 1.0, and 1.2 GPa) and three oil feed temperatures (40, 70 and 100 °C) have been studied on the twin-disk machine. A total of 16 tests have been carried out.

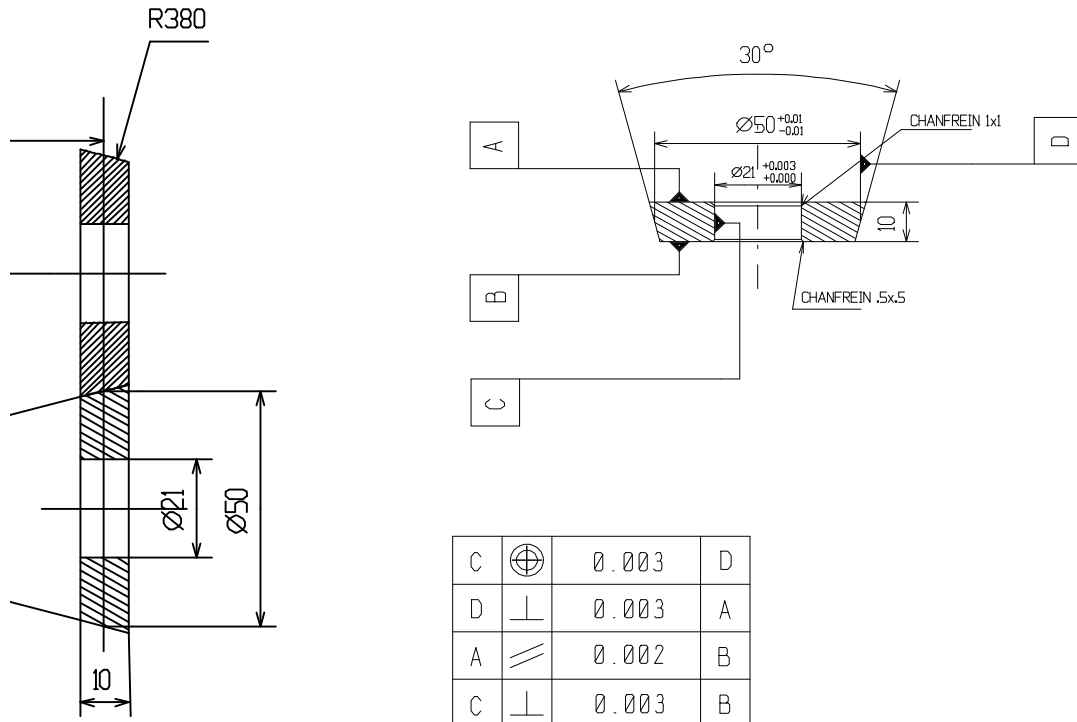


Fig.2 Scuffing test specimens

3.2 Tests on ball bearing

Scuffing tests were performed on 7206 angular contact ball bearing included in an original test, presented in figure 3. The test rig is adapted on 4-ball machine from our laboratory and was described in [4]

A general view of the test rig is presented in figure 3.

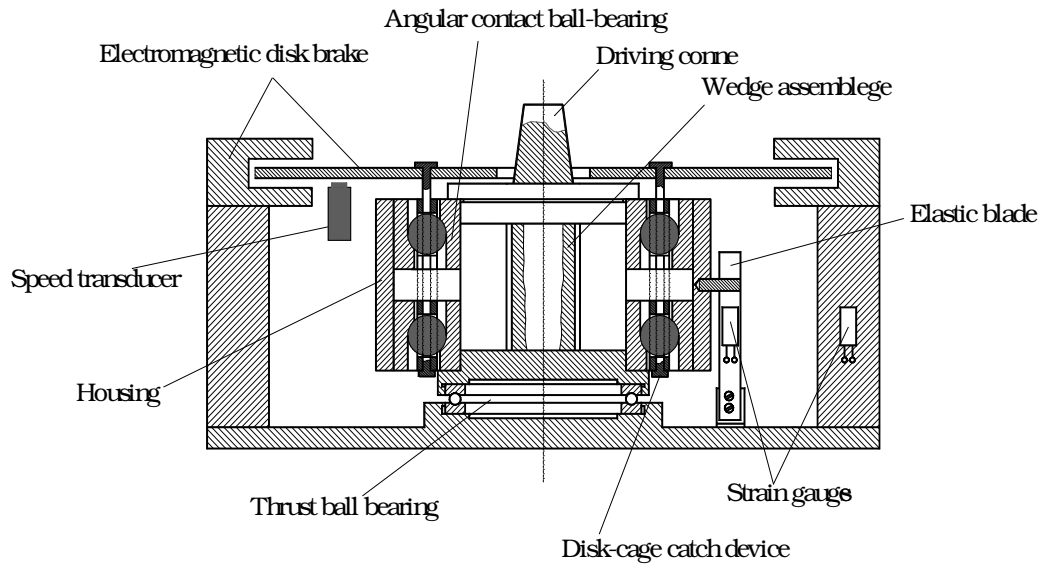


Fig.3 Scuffing test rig

4. Results

Figure 4 presents some results on scuffing limits on specimens. Scuffing sliding speed has critical value up to 9 m/s (for testing specified conditions and a complete EHL regime).

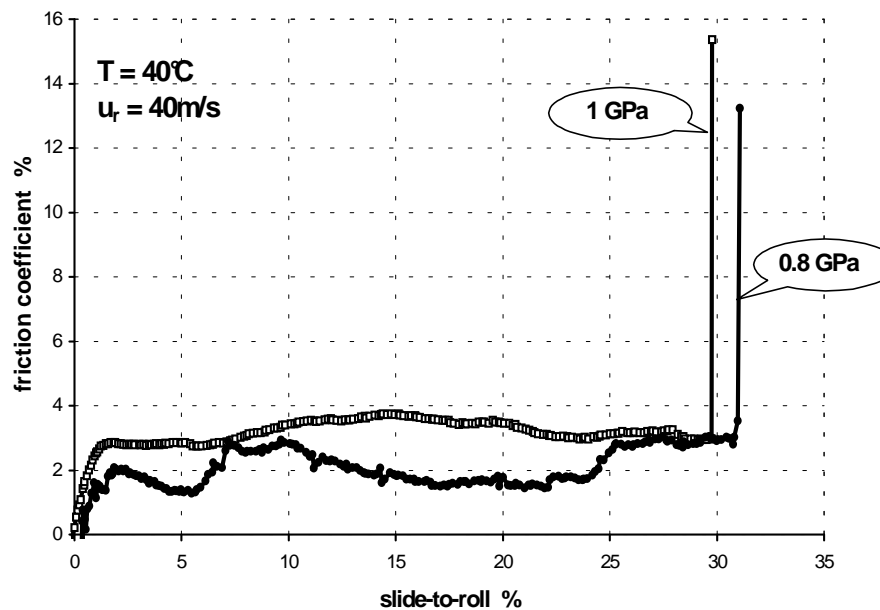


Fig.4 Scuffing limits in specimens

Figure 5 presents some scuffing limits on ball bearings. The operating speed on the test rig was moderate (max. 2800 rpm), so the ball-inner ring sliding speed too. As the bearing scuffing risk is deeply correlated to high sliding speed (typical to high-speed ball bearings) we realised these conditions by the cage's braking. It was obtained sliding speeds enough high to initiate scuffing phenomenon for a boundary lubrication regime.

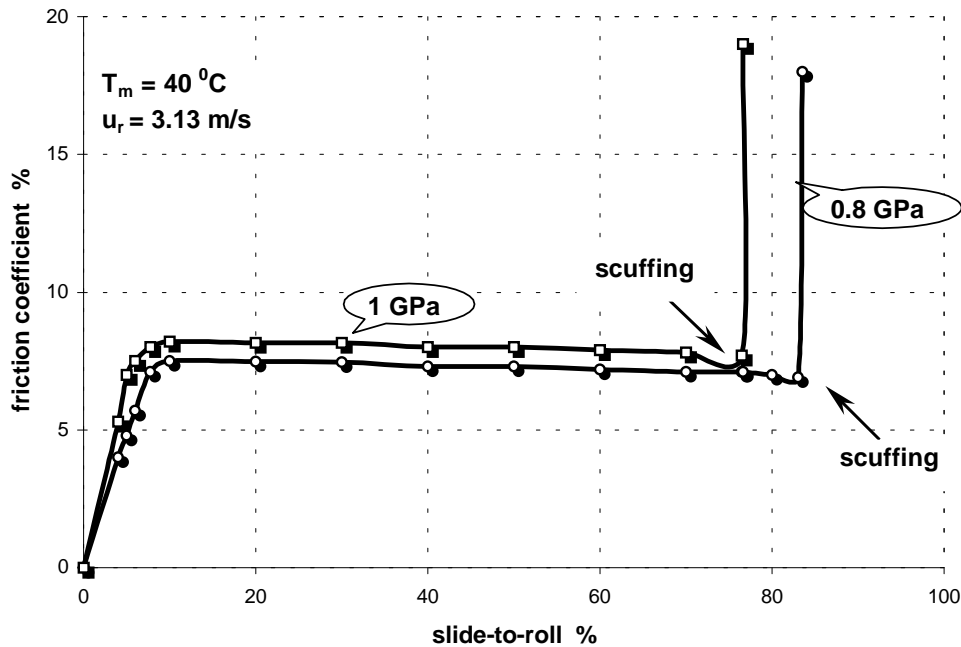


Fig.5 Scuffing limits in ball bearings

These results lead to establishment of unique scuffing limits of $1.5 \cdot 10^8 \text{ W} \cdot \text{m}^{-2}$ (in terms of energy dissipation) in a given ball bearing, for imposed running conditions (figure 6)

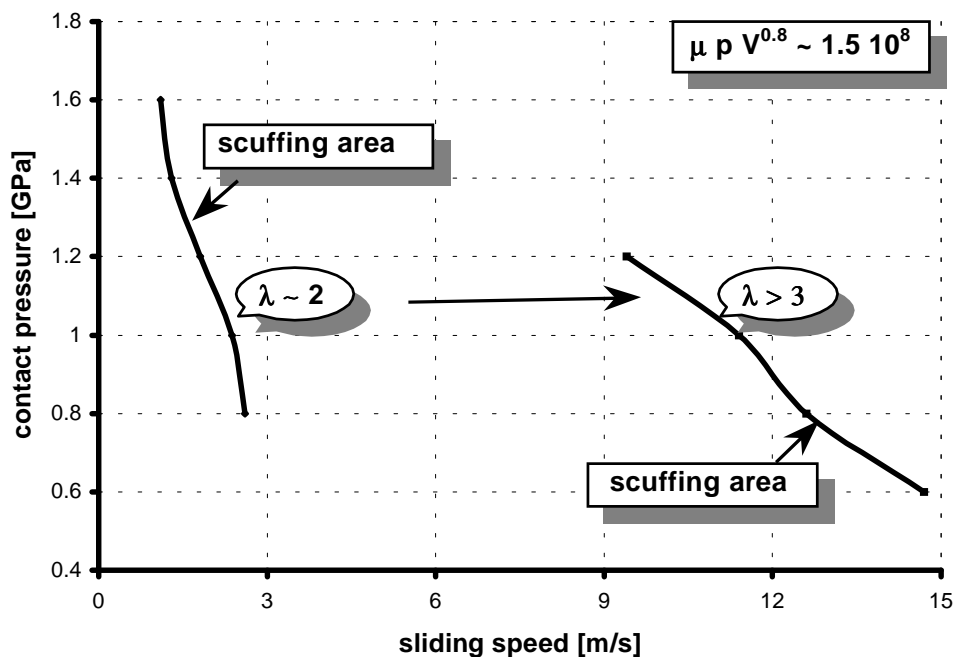


Fig. 6 Scuffing estimation in ball bearings

5. Conclusions

It can be remarked that the tests on angular contact ball bearing (7206C) lead to scuffing limit around 3 m/s in a gross sliding context (boundary lubrication regime).

Contact pressure and also oil temperature increasing lead to decreasing the scuffing limit for sliding speed.

Sliding speeds enough high to initiate scuffing phenomenon were obtained by cage's braking, despite moderate rolling speed performed on the test rig.

Corroboration between all these experimental results allows a scuffing criterion to estimate this type of damage in ball bearings.

Received March 14, 2005

The "Gh.Asachi" Technical University Iași

REFERENCES

1. Bowman, W.F., Stachowiak, G.W., -*A Review of Scuffing Models*, **Tribology Letters**, no.2, 1999, **113-131**
2. C. Bujoreanu, D. Olaru, Sp. Cretu, D. Nelias, *Etude de la limite de grippage dans les roulements à billes*", *Roulements et Tribologie, Actes des Journées Internationales Francophones de Tribologie*, 2001, **195-210**
3. Aihara, S., -*A New Running Torque Formula for Tapered Roller Bearings Under Axial Load*, **Trans. of ASME, J. of Tribol.**, 109, july, 1997, **471-476**.
4. Nélias, D., Nassare, F., Flamand, L., - *Etude expérimentale et théorique du microgrippage dans les contacts elastohydrodynamiques*, **Rev.Gen.Therm.**, 36, 1997, **26-39**

CONSIDERATII PRIVIND DETERIORAREA PRIN GRIPARE IN RULMENTII CU BILE

Rezumat: Lucrarea descrie cercetarile autorilor privind deteriorarea prin gripare in rulmentii cu bile, deseori intalnita in industria metalurgica. S-a proiectat si realizat un stand original pentru testarea rulmentilor. Prin coroborarea rezultatelor teoretice si experimentale se stabileste un criteriu de gripare specific acestor rulmenti, cu caracter practice pentru proiectantii si utilizatorii de rulmenti.

ANALYTICAL STUDY ABOUT THE TRANSITORY WORKING CONDITIONS BEHAVIOUR OF THE ELECTRIC RESISTANCE FURNACE

BY

ELENA CHIRILĂ and CONSTANTIN CĂRĂUȘU

Abstract: The paper represents a theoretical and experimental analysis about the behaviour of the electric resistance furnace in transitory working conditions. So, it studies, in an analytical and experimental way, the dynamical characteristics of the transitory working conditions (the time constant and the dead time) and the answer of the automatic system when the entering values and the perturbation values are variable for the automatic adjustment of the parameters of the processes which take place in these equipments.

Keywords: transitory working conditions, electric resistance furnace, time constant, dead time, automatic adjustment

1. Introduction

This theoretical and experimental study about the behaviour of the electric resistance furnace in transitory working conditions is necessary for automatic adjustment of the functional variable parameters of the processes in these equipments. The automatic adjustment is strictly necessary in a correct lead of the heating processes. Wanting a stationary working condition of the processes for a long time, it must quickly and precisely observe the errors of the functional parameters out of the reference values.

2. General considerations

Analysing the most important parameters of these kind of equipments it can be observe that all of them are variable in time because of the different kind of perturbations (the current and productivity variations, the false air admission, the calorific losses etc.).

For a correct automatic adjustment, it must study the interdependence between the variations of the parameters. Therefore, during the working of the equipment, there are independent variable parameters (their automatic adjustment is made in simple circuit, for each independent parameter), but there are interdependent parameters, too (their automatic adjustment is made in complex circuit). The automatic adjustment will also going to an automatic measurement, a long distance transmission, an indication and recording of the parameters, an automatic checking including audio or video signals and commands for some of the parameters.

In modern technologies, the heating processes, which take place in electric resistance furnace, impose very strictly conditions for the performances. So, a constant value for the vat temperature must take place not only in all the space of the vat, but in

time, too.

The automatic adjustment of the vat temperature for the electric resistance furnace is very important because the vat temperature is the most important parameter in well working conditions of the furnace and on the other side, the adjustment of this parameter takes place in typical conditions connected with the heating transfer phenomenon.

For the electric resistance furnace, the dead time, T_m , depends on: the type and size of the heating source; the way of the heating generation and its transfer to the walls of the furnace and to the load (depending on the design and the material of the heating surface and on the placement of the heating source); the thickness and the material of the walls; the type, the construction and the placement of the measure elements into the furnace.

The time constants, T_1 and T_2 , are a measure for the answer time of the furnace. This means that all furnaces are inertia elements (the answer of the automatic process is not in the same time with the variation of the entrance parameters but after a transitory working and the exit parameter has an aperiodic variation). The existence of the time constants depends on the properties of the adjustment elements to accumulate energy or masses (capacity) – the capacity of the walls to accumulate heating. The time constants depend on: the volume of the vat; the power of the heating source; the material of the walls; the type, the construction and the placement of the measure element into the furnace.

The amplification factor of the furnace, K , shows the effects of the execution parameters or of the perturbation parameters. It depends on: the dimensions of the furnace, the type of the execution organ and of the measure element of the automatic adjustment system.

3. Theoretical Study of the Transitory Working

Analysing the behaviour of the electric resistance furnace in stationary working conditions, these equipments are generally real nonlinear elements (certain parts of the static characteristic have nonlinearities – the saturation and the curved parts being the most important). So, the furnace is a linear element only in a part of the $m(t)$ characteristic – so called linear zone.

For the linear zone (generally, the working zone of the furnace), the behaviour of the transitory working conditions is described by linear differential equations (the coefficients of the equation are constant values).

Knowing that heating processes are generally show aperiodical processes, the electric resistance furnace can be assimilated to a second degree superamortized element. So, the behaviour of this equipment is described by the following general equation:

$$a_0 \frac{d^2 T}{dt^2} + a_1 \frac{dT}{dt} + a_2 \cdot T = b_1 \cdot m, \quad (1)$$

where a_0 , a_1 , a_2 , b_1 are characteristic constants of the furnace.

The equation (1) represents the interdependence between the vat temperature $T(t)$ and the execution variable of the system, $m(t)$.

In particular case, equation (1) becomes:

$$T_2 \frac{d^2 T}{dt^2} + T_1 \frac{dT}{dt} + T = K \cdot m, \quad (2)$$

where: $T_2 = \frac{a_0}{a_2}$ and $T_1 = \frac{a_1}{a_2}$ are time constants; $K = \frac{b_1}{a_2}$ - amplification factor.

The amortized factor (the superamortization) is $\xi = \frac{T_1}{2\sqrt{T_2}} = 2 \dots 3$.

The equation is the same when the perturbation variables have their action to the furnace.

If the furnace is an experimental one (a laboratory equipment having a thin brickwork), the constant T_2 has negligible values considering it null. So, in this conditions, the furnace can be assimilated to a first degree element and its behaviour is described by the following equation:

$$T_1 \frac{dT}{dt} + T = K \cdot m, \quad (3)$$

So, after the variations of the execution and the perturbation variables, the vat temperature tends to a new stationary value (a final constant value). So, the equipment can be considered as a autoadjustable element. This property is conditioned to the heating transfer phenomenon of the process.

In a good approximation, the electric resistance furnace is similar to a superamortized second degree element ($\xi > 1$) and its transfer function (the complex answer of the automated process) is:

$$Y(S) = \frac{K}{T_2 \cdot S^2 + T_1 \cdot S + 1}, \quad (4)$$

where S is superadjustment.

But in reality, the dynamic behaviour of these equipments is more complex because, excepting the inertia of the answer (because of the time constants), there is a strong influence of the dead time, T_m . The value of this constant is not negligible.

As a conclusion, when the vat temperature of the electric resistance furnace is automatic adjustment, these equipments can be similar to:

- first degree elements with dead time (for a laboratory equipment). Their equation is:

$$T_1 \frac{dT}{dt} + T = K \cdot m \cdot (t - T_m), \quad (5)$$

- second degree elements with dead time. Their equation is:

$$T_2 \frac{d^2 T}{dt^2} + T_1 \frac{dT}{dt} + T = K \cdot m \cdot (t - T_m), \quad (6)$$

For a practical estimate of the complex behavior of these equipments, in transitory working conditions, wanting to find the dynamic characteristics, the real indicial functions are replaced by the equivalent indicial functions, the error of this approximation being smaller when the degree of the furnace is higher. This approximation is based on the replacement of one real element by two ideal elements in series in this way:

- one element with dead time having:

$$\text{➤ the equation: } T = m \cdot (t - T_m) \quad (7)$$

$$\text{➤ the transfer function: } Y_m(S) = e^{-S \cdot T_m} \quad (8)$$

- one first degree element having:

$$\text{➤ the equation: } T_1 \frac{dT}{dt} + T = K \cdot m \cdot (t - T_m), \quad (9)$$

$$\text{➤ the transfer function: } Y_1(S) = \frac{K}{1 + T_1 \cdot S}, \quad (10)$$

So, the ineffectual element has the following transfer function:

$$Y(S) = \frac{K \cdot e^{-S \cdot T_m}}{1 + T_1 \cdot S}, \quad (11)$$

4. Experimental Study of the Transitory Working

The experimental researches of the dynamic of the heating processes in electric resistance furnace show that this equipment has the following transfer function:

$$Y(S) = \frac{K}{1 + S \cdot T} \cdot e^{-T_m \cdot S}, \quad (12)$$

For the identification of the process, must find in an experimental way, K , T and T_m parameters.

The identification is based on the indicial answer of the process obtained when a stage (step) signal is applied. Analysing this answer it can find the model of the process using the graphic method.

The amplification factor, K , is:

$$K = \frac{\Delta Y}{\Delta U} = \frac{Y_2 - Y_1}{U_2 - U_1}, \quad (13)$$

where: Y_1 – the value of the exit parameter in a stationary working, when a stage signal was applied;

Y_2 – the value of the exit parameter in a stationary working before the stage signal was applied;

U_1 – the initial automatic drive (before the stage signal was applied);

U_2 – so-called automatic drive.

The dead time, T_m , was calculated knowing that it is the time after the exit parameter is more than $0,01 \cdot Y_1$ from the initial value of the exit parameter.

The time constant, T , was calculated knowing that it is the time after the exit parameter is $y = 0,632 \cdot y_{st}$, y_{st} is the stationary component of the answer.

The graphs showed in fig. 1 (a, b, c, d, e) represent the answers of the process when different values stages were applied.

For each answer the values of the parameters of the mathematical model determined and they were noted in table 1.

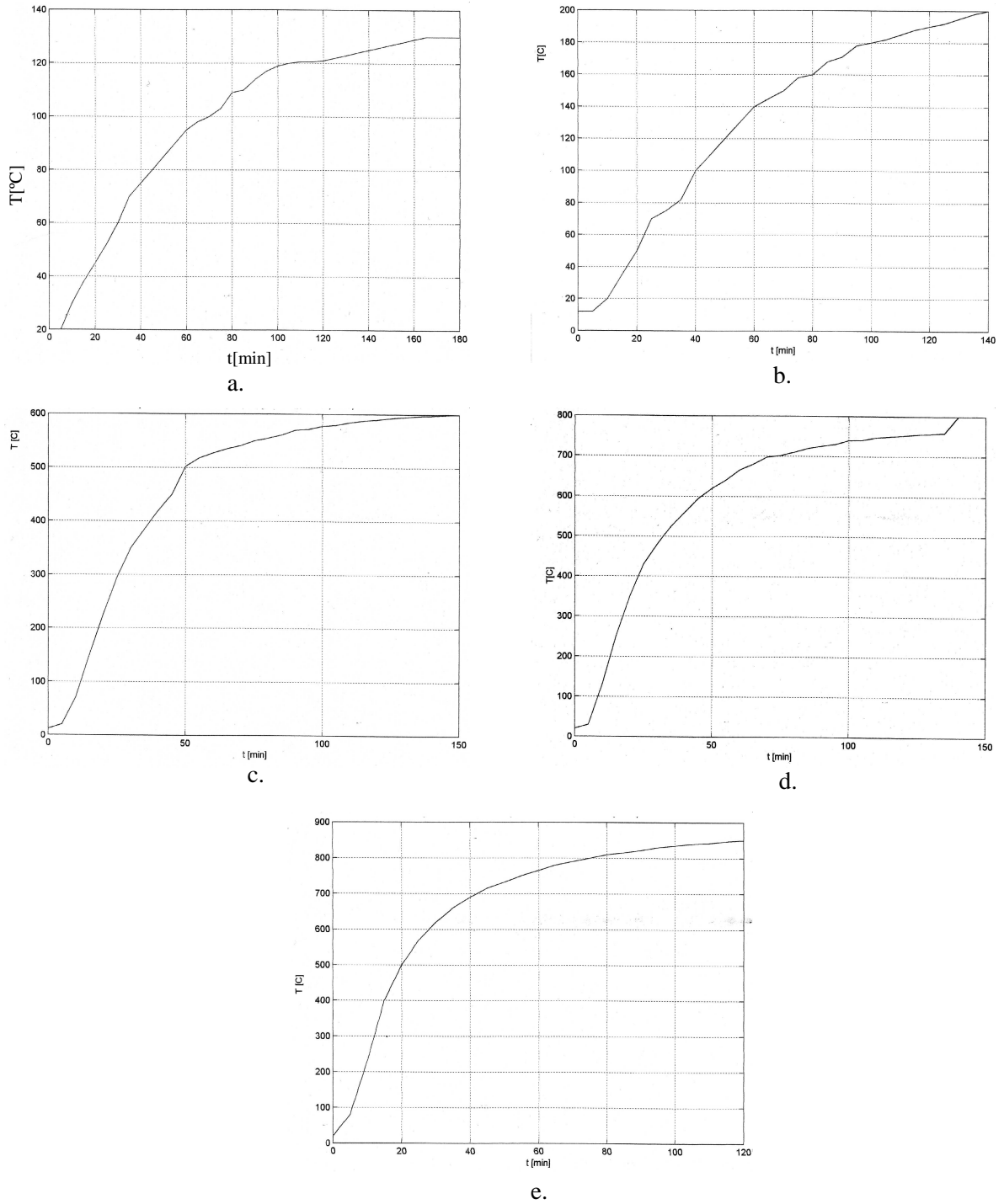


Fig. 1. The answers of the system applying stages with: a. 15%; b. 30%; c. 40%; d. 50%; e. 60%

Table 1. The values of the parameters of the mathematical model

U [%]	T [min]	K	T_{\min} [min]
15	55	7,33	10
30	42	14	2,5
40	41,5	14,55	2
50	34	14,8	1
60	24	13,83	0,5

Doing the calculations of the mean values of the parameters of the mathematical model for these five answers of the process, the transfer function is:

$$Y(S) = \frac{12,31}{1+39,4 \cdot S} \cdot e^{-3,95 \cdot S}, \quad (14)$$

But $0,1 < \frac{T_m}{T} \leq 1$, so the period of samples has the following values:
 $T \simeq (0,32 \div 1,2) \cdot T_m$.

We have chosen $T = 0,76 \cdot T_m = 3 \text{ min}$.

5. Conclusions

It will take into consideration all of the compound elements of the automatic adjustment circuit for the vat temperature, all of them having influence over the dynamic behaviour of all system; each of the elements influences which its transfer function. So, the dynamic characteristics of the system depend on by the characteristics of each compound element.

The total amplification factor of the system is the product of the amplification factors of the elements in series; the total time constant and the total dead time also depend on the inertias of the elements of the automatic equipment.

Usually, the dynamic characteristics of the transitory working are experimental found on a real industrial equipment varying the stage, the ramp or the sinusoidal signal of the execution variable.

Received April 20, 2005

The "Gh.Asachi" Technical University Iași

REFERENCES

1. Olah, I. – *Echipamente și structuri convenționale*. Ed. „Gh. Asachi” (rotaprint), Iași, 1996.
2. Oprescu, I., Vârcolacu, I. – *Automatizări metalurgice în instalații de deformare plastică și tratamente termice*. Ed. Didactică și Pedagogică, București, 1983.
3. * * * - *DAQ 6023E/6024E/6025E. User Manual*. National Instruments Corporation. 2000 (format electronic).
4. * * * - *The Measurement and Automatization*. Catalog 2000, Austin. National Instruments Corporation.

THE CONCEIVING OF THE AUTOMATIC MEASURING AND ADJUSTMENT BLOCK, ASSISTED BY THE COMPUTER, FOR THE VAT TEMPERATURE OF THE ELECTRIC RESISTANCE FURNACE

BY

ELENA CHIRILĂ and CONSTANTIN CĂRĂUȘU

Abstract: After a short analysis of the elements and the conditions of the vat temperature measurement for an electric resistance furnace, the paper presents the conception of the authors about the automatic measuring and adjustment block, assisted by the computer, of the most importance parameter of this equipment process (the vat temperature).

Keywords: electric resistance furnace, vat temperature, automatic adjustment block

1. Introduction

The vat temperature is the most important constructive-functional parameter of the electric resistance furnace.

As a matter of fact, the vat temperature is the temperature in the emplacement point of the measurement sensitive element (the thermocouple). So, it is difficult to provide a uniform variation for the temperature in all the space of the vat using classic adjustment system for automatic adjustment. It can realize only a pre-established variation in time of the temperature measured with a sensitive element.

The uniformity of the temperature into the furnace depends on a correct designing and exploitation of this kind of equipment.

2. General considerations

The sensitive elements used in temperature measuring (usually, thermocouples) influence the dynamic behaviour of the process, so, they influence the process which will be adjust in two ways:

- the emplacement of the thermocouple into the furnace;
- the own thermocouple dynamic behaviour depending on the constructive peculiarity.

The thermocouples can be emplace in the centre of the load that heats in the furnace, or inside of the walls (for the adjustment of the conventional temperature) or, in extreme case, near by the heating source. This last solution is justified on the necessity for the source (the resistances) and the sensitive element to be closely connected. This means that the heating transfer time and the temperature variation are shorter when the thermopower of the furnace is variable. Obviously, this kind of emplacement used for the discontinuous adjustment of the temperature goes to the

variations of the temperature with oscillations having very small amplitudes on the load, but having, in the same time, many contacts in unit time. In the same time, the oscillations near by resistances can have high amplitudes which are more different from the amplitude on the load; so, when the furnace heats on, after the door opens (for ex.: when the charge is loaded), the temperature on the load has not the wanted value (the energy stored in the walls could be the energy that source released in the short time of the connecting, so the thermic flood to the charge is in fact zero). But, the emplacement of the thermocouple near by the source has the advantage of the superheating source protection. Wanting to avoid the disadvantage but to use the advantage of this situation, it can use a supplementary safe thermocouple emplaced near by the resistance used for the disconnected of the furnace when the superheating takes place; the thermocouple of the adjustment circuit will be emplace a little for off the source.

So, wanting an optimum emplacement of the thermocouple will be respect the following conditions:

- the real heating of the load with the technological prescribe temperature;
- the superheating source protection;
- oscillations with minimum amplitudes in the interest point;
- minimum connectings of the furnace in unit time (discontinuous adjustment case).

3. The automatic measuring and adjustment block, assisted by computer for the vat temperature

When the authors have conceived this block, they take into account the dynamic behaviour of the sensitive temperature elements – aperiodical elements having one or two degrees, constant time, T , and dead time, T_m . The values of these dynamic characteristics depend on the construction of the thermocouple (material, the thickness of the protection sheath, etc.) and they influence the dynamic characteristics of the furnace.

The block contains the sensitive temperature element (the thermocouple) and the automatic measuring and adjustment equipment (fig. 1).

The automatic measuring equipment includes a regulator and an execution element. The regulator may be a continuous (P, PI, PD or PID) or a discontinuous one (biposition, triposition or with impulses).

Introducing the computer, the automatic drive of the process is provided.

The automatic adjustment of the vat temperature can be realized for a fixed entering value or for a diagram entering signal. The medium precision of this kind of automatic adjustment is $5\div 10$ °C for thermal treatment processes, $0,2\div 0,5$ °C for laboratory processes and $10\div 25$ °C for the melting processes and for the heating plastic deformation processes.

It can be apply any of the automatic adjustment method (continuous, discontinuous or semicontinuous). The discontinuous method is recommended because the electric resistance furnaces have high temperature inertia. This method is also the simplest, the cheapest and the most precise one (the relative precision is $1\div 3\%$).

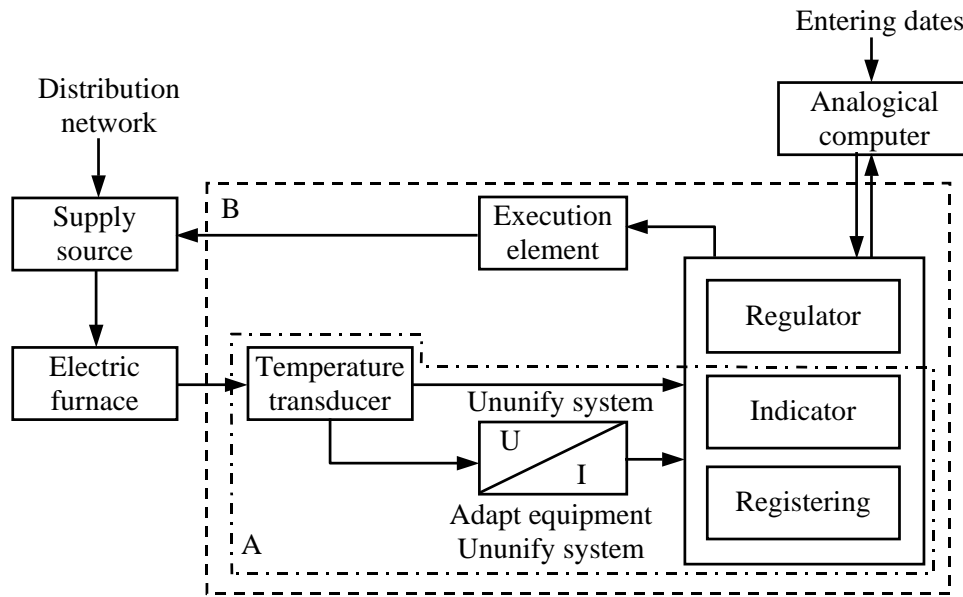


Fig. 1. The scheme of the automatic measuring and adjustment assisted by computer equipment: A – the automatic measuring equipment; B – the automatic measuring and adjustment block equipment

When the vat temperature of the electric resistance furnace is automatic adjusted, everybody knows that this equipment is feeded usually in mono or three-phase alternative current (the electric mains has maximum 500 V. The temperature adjustment is made varying the electric power of the descending transformer.

When the automatic measuring and adjustment is made assisted by the computer, it can be used a LabView software – a power and flexible software system.

Using the solutions given by LabView it can obtain a lot of information, it can realize applications for the acquisitioned information analyse or this information may be presented in different ways (graphic interferences, Web pages, based information files).

Using LabView software it can create and demonstrate fast programmes for the generation and acquisition of the signals from integrate circuits, USB equipments or Ethernet systems. The acquisition of information offers more facilities, such as: automatic configuration and testing panels for the verification of the operation, configurations channels for scanning of the data series, generator for the watch signals, events numerator, clock for the events measuring, etc. These entrance-exit facilities combined with types of special data and virtual equipments for the analysing of the measurements are very fast special acquisitions data from the sensories.

In the same time, LabView gives hardware equipments for direct connecting equipments. So, it can configure and use in virtual any kind of measuring equipment including instruments, integrate equipments for data acquisitions, motion controllers, systems for images acquisitions, logical programmable (PCL), etc.

Knowing that LabView drives for the instruments have ordinary architecture and interface, the connecting and the communications are easy, without cod program lines.

A virtual instrument (the identical reproduction of the real instruments behaviour using the computer) has a frontal panel (represents the user interface and the block diagram - so called program). So, LabView is an editor, an compiler and a run time operating system, in the same time.

To begin the work with a LabView application means to chose the respective instrument using LabView library. Automatically, the screen of the monitor shows the panel for an interactive operation realizing for the data introduction, the fixing of an entrance, the visualing of an exit, the selecting of the working way, etc. The aspect of the virtual panel is identical with the panel of the real instrument.

In the back site of the frontal panel there is the block diagram selecting Window – Block Diagram option (so called the program of the application). As a matter of the fact DB is a source cod containing inferior level instruments such as: circuits For or While, arithmetical or trigonometric functions, case structures, signal generation or processing, statistical calculations, etc. These elements – so called nodes – are wired, so the flow of date takes place.

A nod has a graphical representation (icon) and some terminals which connect different nodes with other subroutine of the program.

Each of the windows contains the title bar, the main bar, a palette with buttons for the virtual instrument action (Panel Palette), a work site and a icon.

4. Conclusions

The computer replaces the classical automatic adjustment equipment including the regulators functions, with a lot of advantages, such as: the decreasing of the price of the adjustment equipment, the possibility to replace a lot of different kind of regulations using the same software.

Received April 20, 2005

The “Gh.Asachi” Technical University Iași

REFERENCES

1. * * * - *DAQ 6023E/6024E/6025E. User Manual*. National Instruments Corporation. 2000 (format electronic).
2. * * * - *The Measurement and Automatization*. Catalog 2000, Austin. National Instruments Corporation.
3. * * * - *LabVIEW Basic Course Manual*. Austin, 1994. National Instruments Corporation.

NUMERICAL MODEL TO COMPUTE THERMAL STRESS-RELIEF PROCESSES AT CARBON STEEL

BY

**CONSTANTIN DUMITRACHE, CORNELIU COMANDAR, ADRIAN SABĂU, NICUȘOR
 AMARIEI**

Abstract: *In the article [3] the authors propose a mathematical model of optimization thermal stress-relief process which are conditioned by the plastic yield speed phenomenon. These actual models take in advance experimental results but don't reflect another practical phenomenon, the plastic yield speed is increasing in the vicinity of material yield point. In this paper is computed using numerical method Runge-Kutta [1] the time variation law $\sigma(t)$ of thermal residual stresses at OLC45 steel.*

Keywords: *Residual Stresses, Thermal Stress-Relief*

1. Mathematical model of thermal stress-relief process

The authors' article [3] propose a new equation for the plastic yield speed calculus:

$$\frac{d\varepsilon_p}{dt} = \frac{K \cdot \sigma}{\sigma_c - \sigma} \quad (1)$$

where is the time functions like K –steel creep coefficient [1/h], σ –residual stress [MPa] with the initial value $\sigma(0)=\sigma_0$ and σ_c –the material yield point [MPa].

In the stress relaxation process the specific elongations there are in equation:

$$\varepsilon_0 = \varepsilon + \varepsilon_p \quad (2)$$

where ε_0 –initial specific elongation which is caused by internal stress value, ε –elastic specific elongation and ε_p –specific plastic elongation.

Through derivation with the time, equation (2) become:

$$\frac{d\varepsilon}{dt} + \frac{d\varepsilon_p}{dt} = 0 \quad (3)$$

where elastic specific elongation $\varepsilon = \frac{\sigma}{E}$ and through derivation with time is getting:

$$\frac{d\varepsilon}{dt} = \frac{\frac{d\sigma}{dt} \cdot E - \frac{dE}{dt} \cdot \sigma}{E^2} \quad (4)$$

and E –longitudinal elastic modulus. With the equations (1) and (4) in (3) can get the differential equation of thermal stress-relief process:

$$\frac{d\sigma(t)}{dt} + \frac{K(t) \cdot E(t) \cdot \sigma(t)}{\sigma_c(t) - \sigma(t)} - \frac{dE(t)}{dt} \cdot \frac{\sigma(t)}{E(t)} = 0 \quad (5)$$

with the solution $\sigma(t)$ check initial condition $\sigma(0)=\sigma_0$. All the functions from equation (5) are variation laws with the time.

2. The calculus model of function $E(t)$, $\sigma(t)$, $K(t)$

For determining the time laws variation it's necessary to use:

- the values of $E(T)$, $\sigma_c(T)$ and $K(T)$ with temperature which represent analytical functions;
- the relation of $T=f(t)$ from cycle of stress-relief annealing.

The values of $E(T)$ and $\sigma_c(T)$ at the different temperatures have experimentally determined and the variation laws are presented in [2] using suitable approximation functions.

The coefficient $K(T)$ is calculated using relation (1) and the creep limit $\sigma_{1/10000}(T)$ which is representing the stress, produce a specific plastic elongation $\frac{d\varepsilon_p}{dt} = 1\% = 0,01$ in 10000 hours at the temperature T . This stress produces plastic deformation with the medium speed:

$$\frac{d\varepsilon_p}{dt} = \frac{0,01}{10000} = 10^{-6} \left[\frac{1}{h} \right] \quad (6)$$

From the relations (1) and (6) result:

$$K(T) = 10^{-6} \cdot \frac{\sigma_c(T) - \sigma_{1/10000}(T)}{\sigma_{1/10000}(T)} \quad (7)$$

with the temperature law variation in [2].

Using relation (1) it can get accurately determination of steel creep coefficient $K(t)$ if it use creep curves, which are drawing at 50-100 hours who are corresponding at time stress-relief period.

Between temperature and time could be written a linear expression:

$$T = a \cdot t + b \quad (8)$$

where the parameters a and b have different values on the thermal stress-relief annealing (fig. 1).

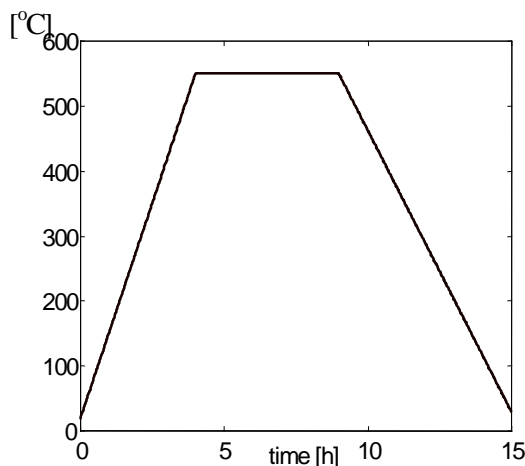


Fig. 1. The cycle of thermal stress-relief annealing for OLC45 steel [1]

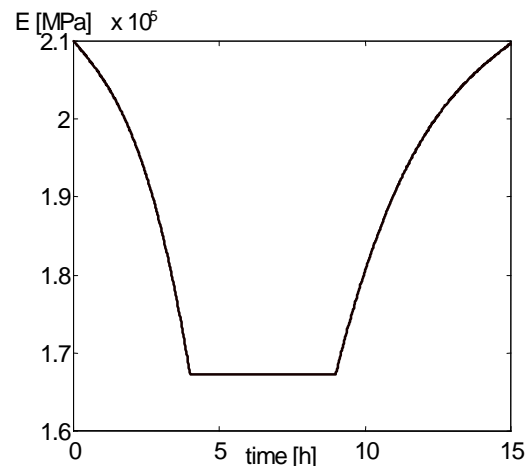


Fig. 2. The time variation law of $E(t)$ for OLC45 steel [1]

The parameter a represents heating/cooling rate and during the heat treatment, at the maintain time process, the parameter $a=0$.

With the relation (8) in the temperature laws variation for $E(T)$, $\sigma_c(T)$ and $K(T)$ it can get the time variation laws $E(t)$, $\sigma_c(t)$ and $K(t)$ (fig. 2, 3, 4).

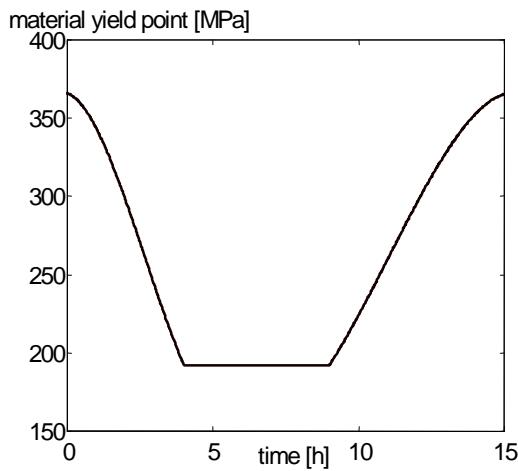


Fig. 3. The time variation law of $\sigma_c(t)$ for OLC45 steel [1]

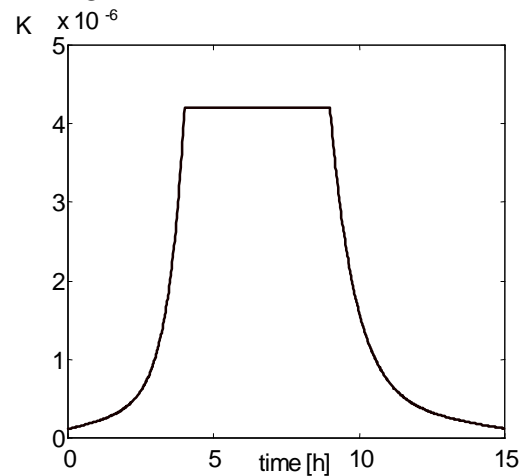


Fig. 4. The time variation law of steel creep coefficient $K(t)$ for OLC45 steel [1]

It consider that the initial temperature of heating for OLC45 steel type is $T_0=20^\circ\text{C}$ and the maximum stress-relief temperature is $T_{\max}=550^\circ\text{C}$. Near the end of the treatment, the cooling temperature with the furnace become $T_{\text{fin}}=30^\circ\text{C}$ [4].

The time period of heating is 4 hours, maintain period at the maximum temperature T_{\max} is 5 hours and the period of cooling is 6 hours.

3. Numerical method to compute thermal residual stresses

All these time variations laws could be introduced in relation (5) and the function $\sigma(t)$ represents the solution of differential equation of thermal stress-relief process:

$$\frac{d\sigma(t)}{dt} = f(t, \sigma(t)) \quad (9)$$

$$f(t, \sigma(t)) = -\frac{K(t) \cdot E(t) \cdot \sigma(t)}{\sigma_c(t) - \sigma(t)} + \frac{dE(t)}{dt} \cdot \frac{\sigma(t)}{E(t)}$$

$$\sigma_{i+1} = \sigma_i + \frac{1}{6} \cdot (K_1 + 2 \cdot K_2 + 2 \cdot K_3 + K_4) \quad i = 0, 1, 2, \dots$$

$$K_1 = h \cdot f(t_i, \sigma_i);$$

$$K_2 = h \cdot f\left(t_i + \frac{1}{2} \cdot h, \sigma_i + \frac{1}{2} \cdot K_1\right); \quad (10)$$

$$K_3 = h \cdot f\left(t_i + \frac{1}{2} \cdot h, \sigma_i + \frac{1}{2} \cdot K_2\right);$$

$$K_4 = h \cdot f(t_i + h, \sigma_i + K_3)$$

Because didn't find any analytical solution of this equation I used the numerical method Runge-Kutta [1] and finally obtained table values solution. For computing,

I've started using the initial known value of stress and I applied the algorithm no. 4 (10) of this method, where h –represents the time computing step.

4. Conclusions

Residual stresses during thermal stress-relief process (fig. 5, 6) will change in time and they depend with initial residual stress σ_0 and cycle' parameters of thermal stress-relief annealing (the maximum stress-relief temperature, maintain period at the maximum temperature):

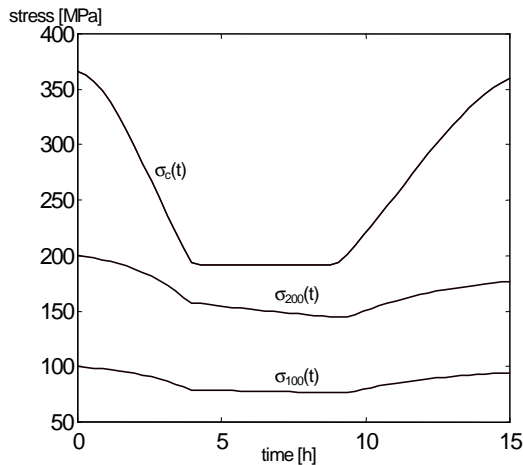


Fig. 5. Material yield point and residual stresses variation during thermal stress-relief process obtained with computational numerical method Runge-Kutta [1]

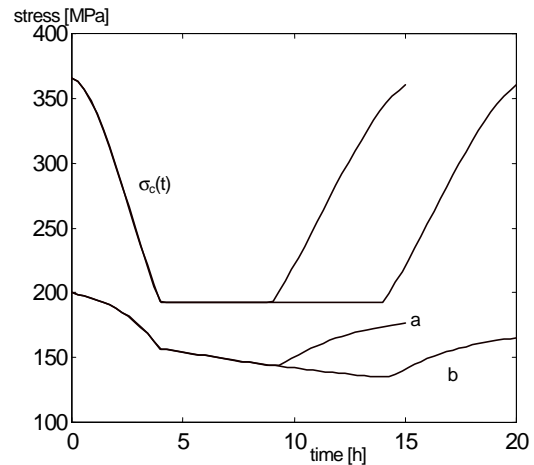


Fig. 6. Material yield point and residual stresses variation during thermal stress-relief process at the different maintain period at stress-relief temperature: a- $T_{detens}=550^{\circ}\text{C}$ and maintain period $t_{maint}=6$ hours; b- $T_{detens}=550^{\circ}\text{C}$ and maintain period $t_{maint}=10$ hours [1]

REFERENCES

- [1]. Dumitrache C. - **Cercetări privind influența ultrasunetelor asupra elementelor de substructură și tensiuni ale construcțiilor sudate**, Teză de doctorat, Iași, 2000;
- [2]. Dumitrache C., Comandar C., Sabău Adrian Amariei N. – **Computational model of optimization thermal stress-relief processes at carbon steel**, 3rd International Conference “Research and development in mechanical industry” RaDMI 2003, 19-23 sept. 2003 Herceg Novi, Serbia and Montenegro
- [3]. Hopulele I., Leon D., Amariei N., Ștefan M. - **Un nou model matematic de analizare și de optimizare a proceselor de detensionare termică**, Timișoara, 1993
- [4]. Vermeșan G. – **Îndrumar de tratamente termice**, Ed. Dacia, Cluj Napoca, 1987

METODĂ NUMERICĂ DE REZOLVARE A ECUAȚIEI DIFERENȚIALE A PROCESULUI DE DETENSIONARE TERMICĂ PENTRU UN OȚEL OLC45

REZUMAT: Această lucrare constituie continuarea articolului [2] și pune în evidență rezolvarea numerică a ecuației diferențiale de ordinul I din relația 5 prin metoda Runge-Kutta. Soluția care se obține este sub forma unui tabel de valori, iar pentru determinarea acesteia s-a pornit de la valoarea inițială cunoscută a tensiunii remanente și aplicând algoritmul de ordinul patru al metodei. Aceasta rezolvare computerizată permite reglarea parametrilor ciclogramei de tratament termic astfel încât să se obțină o anumită valoare a tensiunii remanente finale. Se poate modifica temperatura de detensionare T_{max} care însă nu poate depăși o anumită limită; de asemenea se poate modifica durata de menținere la temperatura de tratament.

**EXPERIMENTAL RESULTS REGARDING THE PRECISION AND THE
UNIFORMITY OF THE TEMPERATURE IN AN ELECTRICAL FURNACE
FOR HEAT TREATMENT USING AN AUTOADAPTIVE CONTROL
SYSTEM**

by

CRISTINA ALBU-IACOB

Abstract

The paper presents a few experimental results regarding the diagrams of applied heat treatments obtained at heat treatments applied to some copper alloys, heat treatments which have been effected in two situations: at first using the classic equipment of process control and then using a system of autoadaptive control of the heat treatment, made up of a computer (endowed with specialised soft), a power control unit with silicon controlled rectifiers and an electronic interface between them. It comes out that the precision and the uniformity of the temperature are of $\pm 2^{\circ}\text{C}$ using a system of autoadaptive control. Moreover, the experiments effected have pointed out both the savings of electrical energy and the improvement of the results of the heat treatment applied, shown by comparing the microstructures of the machine parts which were heat treated in the improved installation to those obtained in the initial installation.

Keywords

Temperature uniformity, temperature precision, heat treatment, autoadaptiv control

In order to confirm through experiments the precision and uniformity of the temperature in an electrical furnace for heat treatment endowed with a system of autoadaptive control I have performed both light/idle tests and load tests, using charges of copper alloys mentioned in the fabrication protocol of S.C. "COMES" S.A. Săvinești. A few of the load tests are presentet in this paper.

The diagrams of heat treating obtained for annealing of homogenizing of the machine parts made of bronze with aluminium CuAl9-B, SR CR 1338:2000, in two situations, are presented in figures 1-4:

- using the classic instalation of heat treating (figure 1 and the detail in figure 2);
- using the installation of heat treating endowed with a system of autoadaptive control (figure 3 and the detail in figure 4).

Analysing the detailed representation it comes out that the temperature regulation performed by the initial control of the furnace is done with high deviations, the values of temperature in the vault being between 863°C and 888°C , instead of a value of 875°C required by the heat treatment (that is a deviation of up to 13°C).

In the case of utilisation of the improved control system, a deviation of up to 5°C (between 873°C and 880°C) from the assigned temperature has been recorded, the higher deviations being recorded at the begining of the maintenance period.

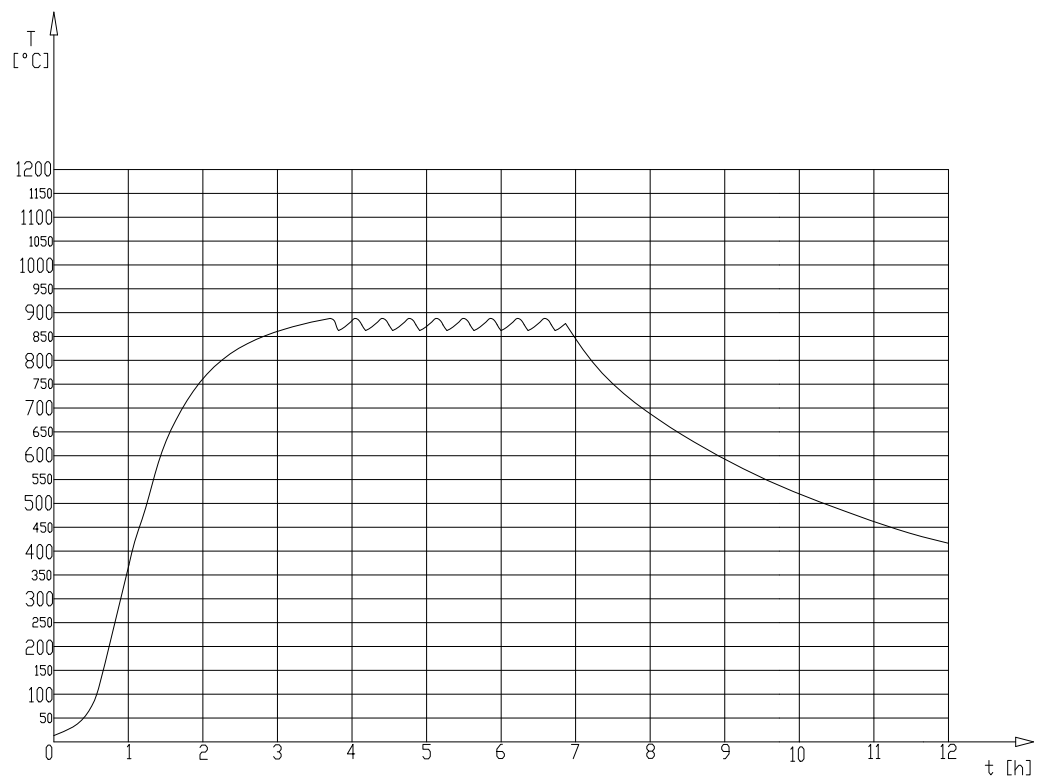


Figure 1. Heat treatment diagram obtained for annealing of homogenizing of the machine parts made of bronze with aluminium CuAl9-B using the initial installation

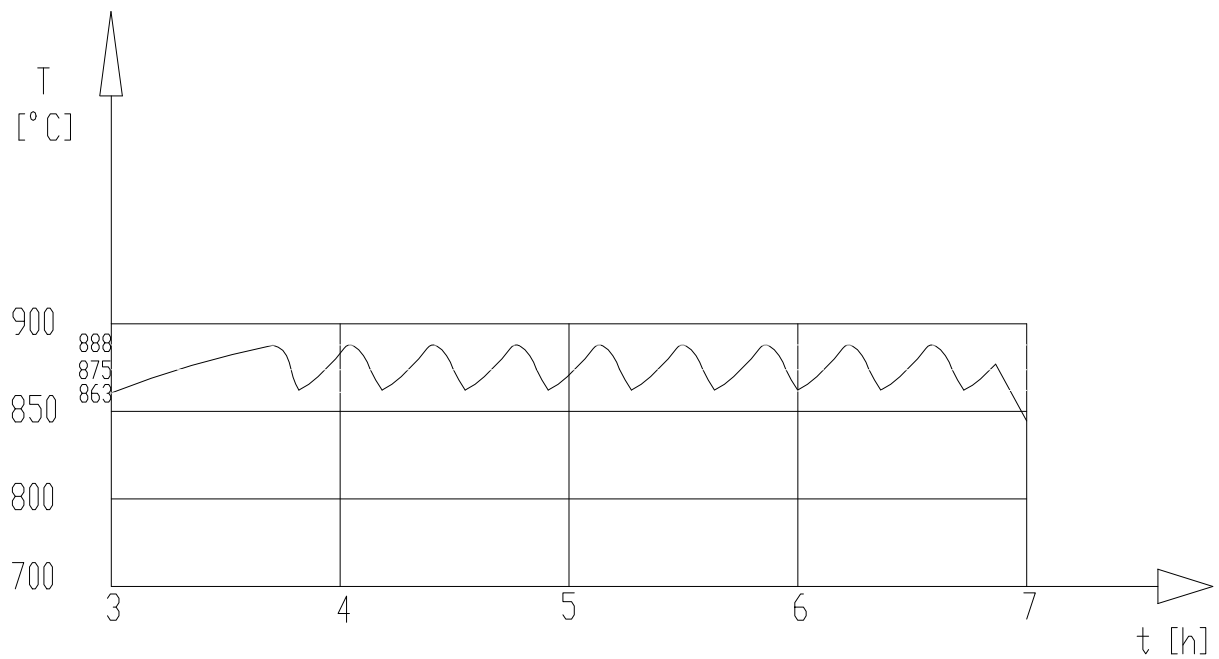


Figure2. Detail of figure 1

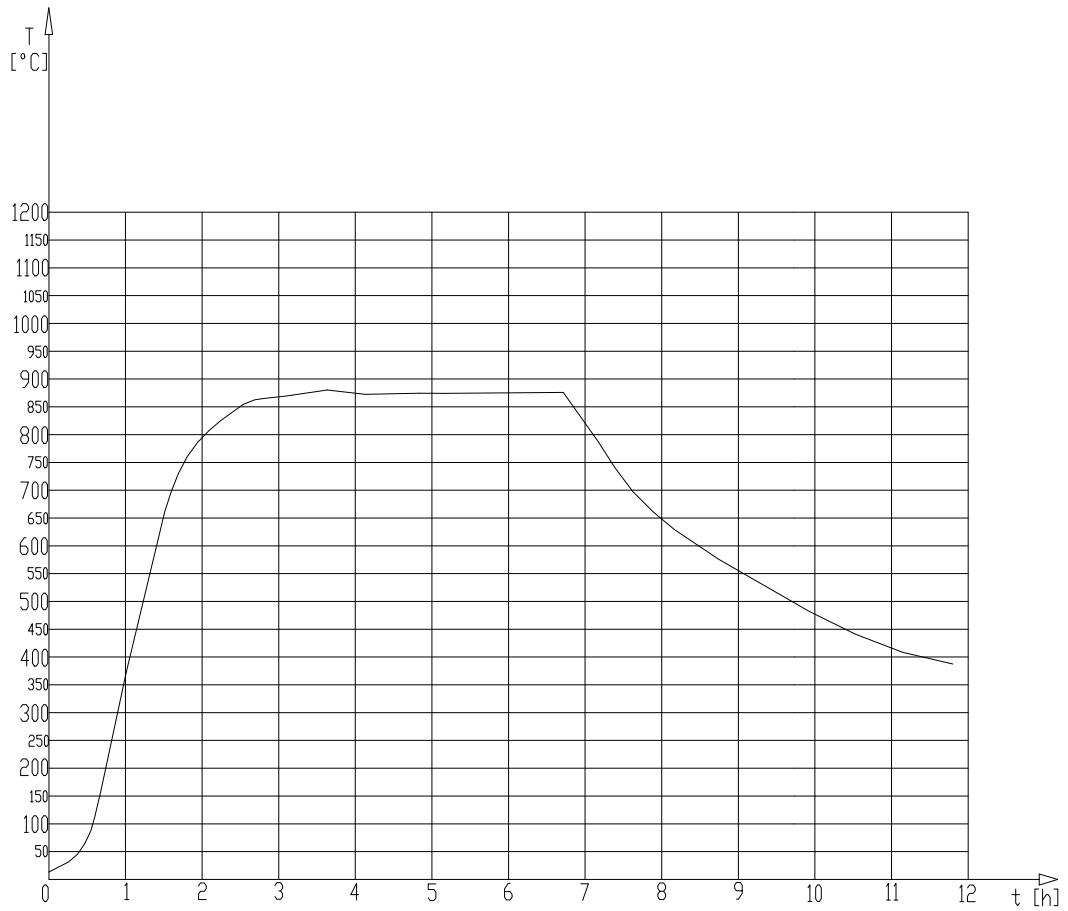


Figure 3. Heat treatment diagram obtained for annealing of homogenizing of the machine parts made of bronze with aluminium CuAl9-B using the improved installation

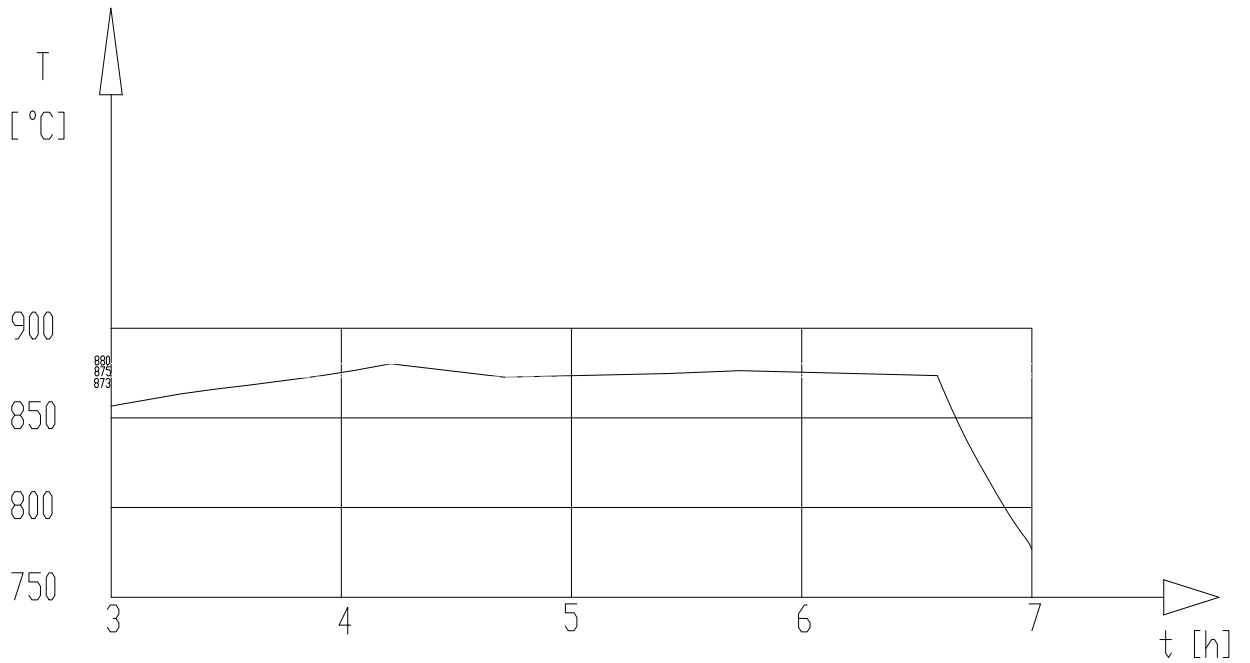


Figure 4. Detail of figure 3

The technological requirements impose in some situations cooling speeds which are lower than the one of natural decreasing of the temperature of the furnace, through the variation of the amount of energy supplied to the resistors, especially in the case of the furnaces having low temperature delay. The controlled cooling requires so much the more a competitive system of control, compared to the maintenance period in the cycle of heat treatment. This is the case of the heat treatment presented in figures 5-9, namely annealing of homogenizing of the complex biphase brass CuZn39PbAl-B, SR CR 1338:2000.

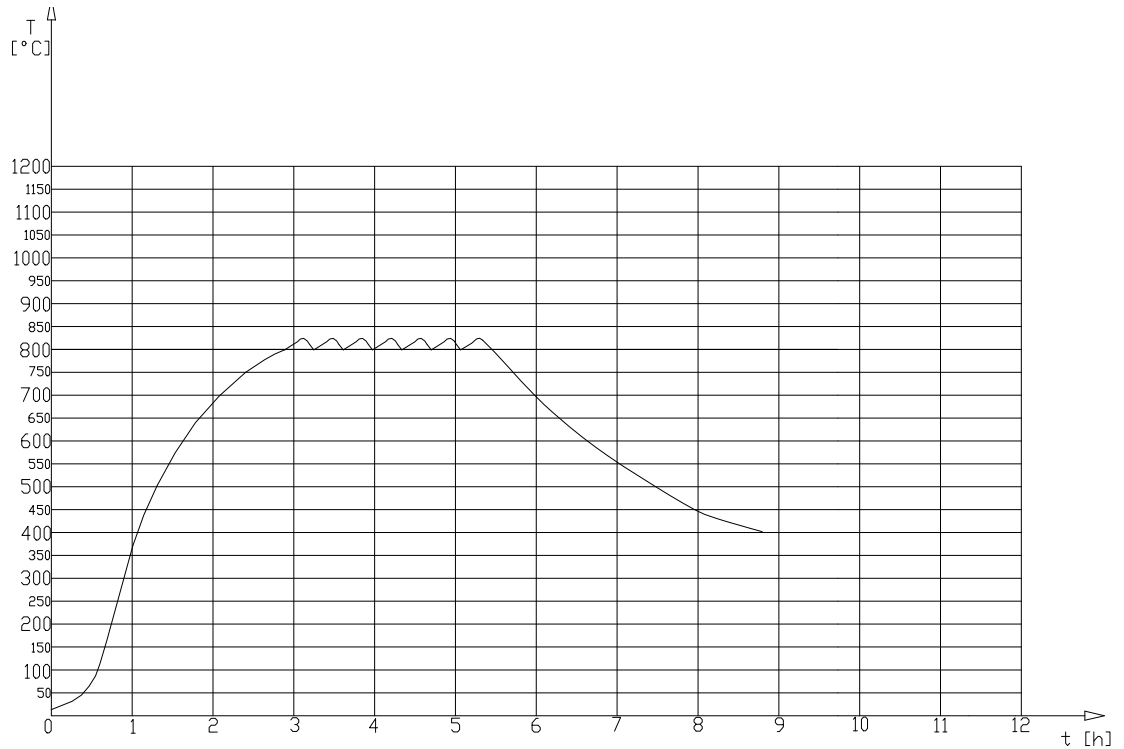


Figure 5. Heat treatment diagram obtained for annealing of homogenizing of the machine parts made of CuZn39Pb-B using the initial installation

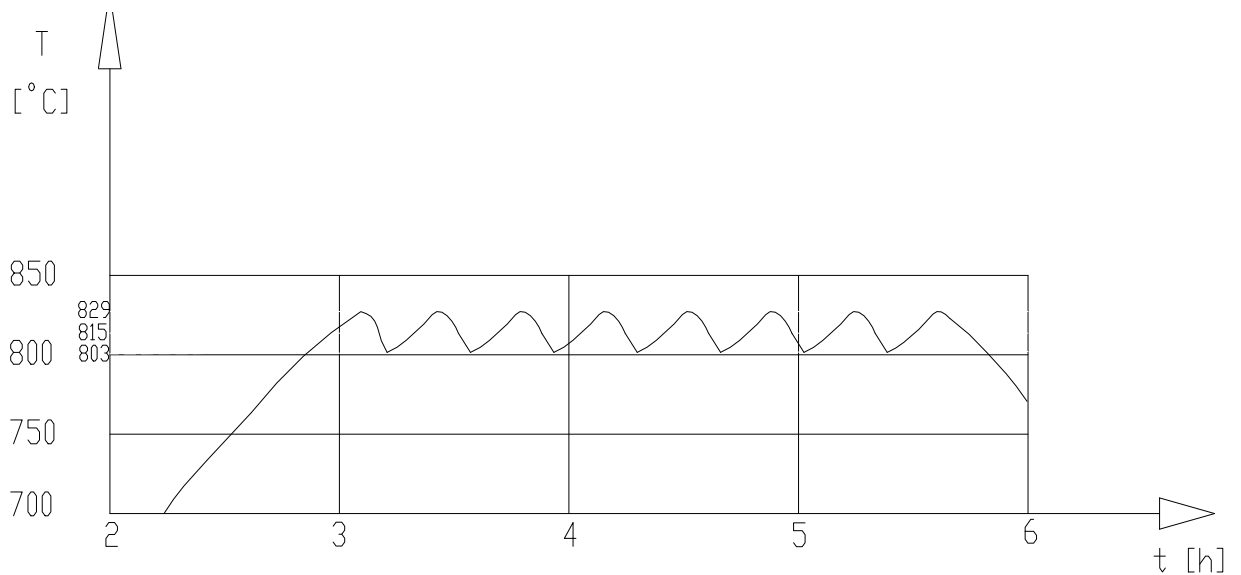


Figure 6. Detail of figure 5

Using the initial installation, the diagram presented in figure 5 and the detail in figure 6 has been obtained. Using the autoadaptive system, the diagram in figure 7 and the details presented in figure 8 (maintaining) and in figure 9 (controlled cooling) has been obtained.

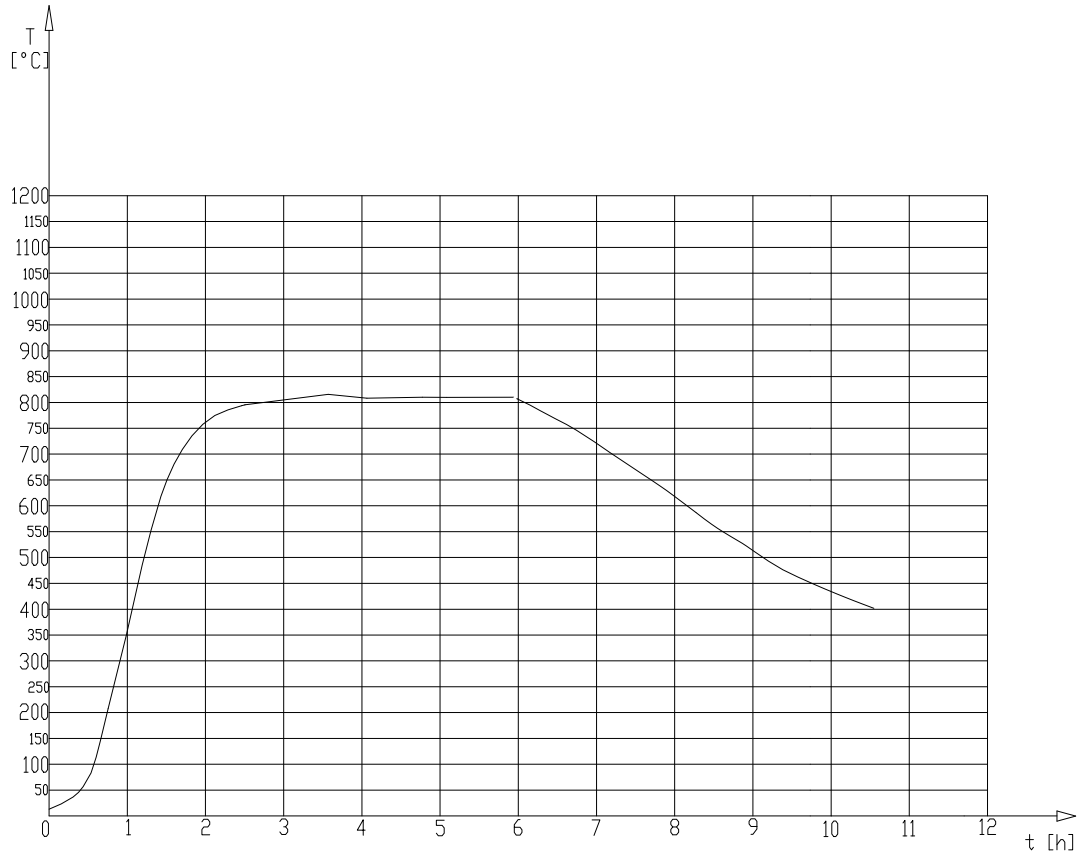


Figure 7. Heat treatment diagram obtained for annealing of homogenizing of the machine parts made of CuZn39Pb-B using the improved installation

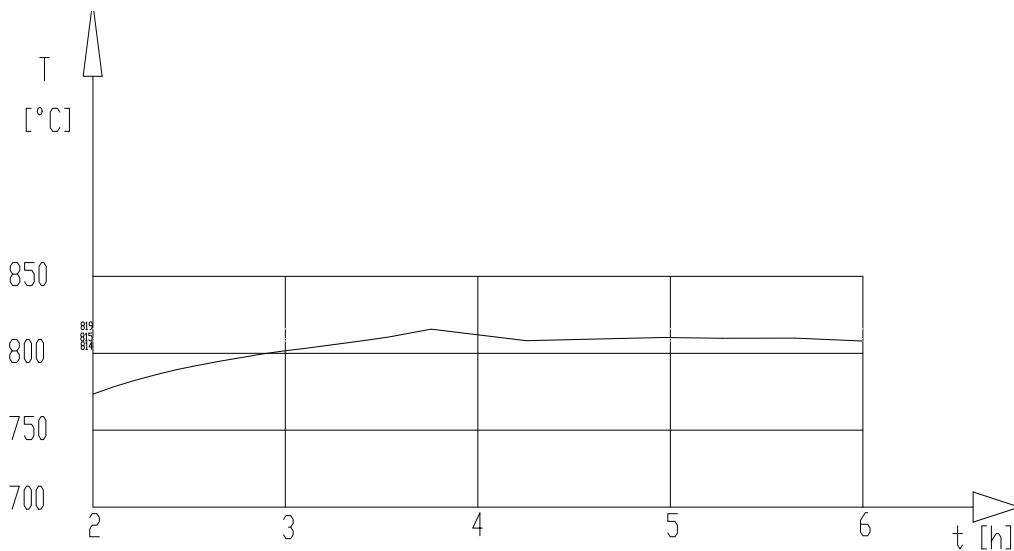


Figure 8. Detail of figure 7

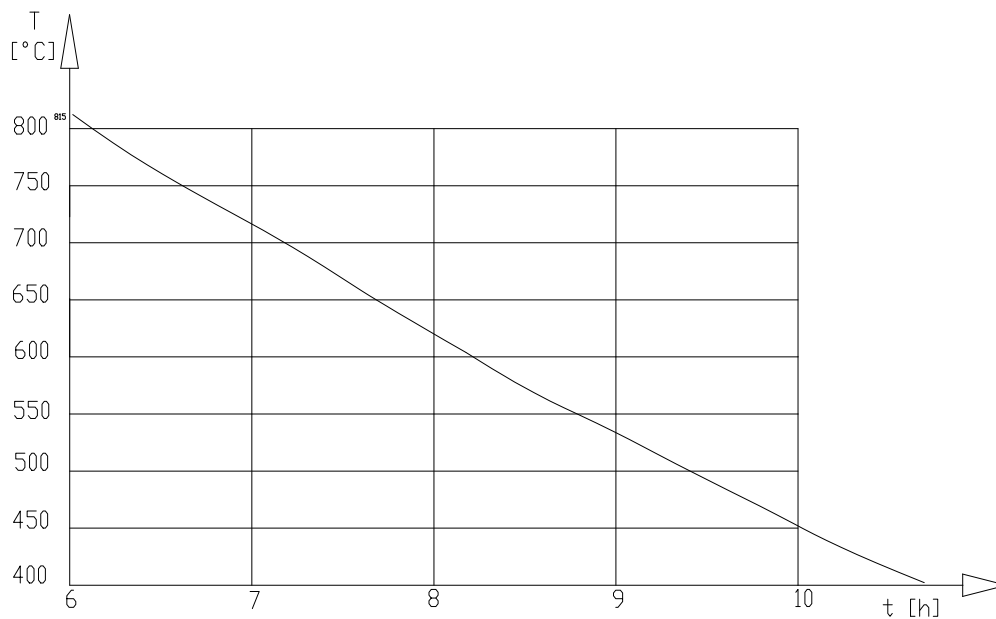


Figure 9. Detail of figure 7

References:

Cristina Albu-Iacob- Teza de doctorat „ Contributii privind imbunatatirea constructiv-functionala a instalatiilor de tratament termic al aliajelor de cupru”, Iasi, 2002

Received May 2, 2005

Technical Coledge of Transport, Piatra Neamt, Neamt, Romania

**REZULTATE EXPERIMENTALE PRIVIND PRECIZIA SI UNIFORMITATEA TEMPERATURII
IN CUPTOARELE ELECTRICE**

Rezumat. Lucrarea prezinta cateva rezultate experimentale privind diagramele de tratament termic aplicat obtinute la tratamentele termice aplicate unor aliaje de cupru , tratamente termice care s-au efectuat in doua situatii:mai intai folosind un echipament de conducere clasica a procesului si apoi folosind un sistem de conducere autoadaptiva a tratamentului termic, format dintr-un calculator(dotat cu soft specializat),o unitate de comanda a puterii cu tiristori si o interfata electronica intre acestea. Se constata ca folosind un sistem de conducere autoadaptiva precizia si uniformitatea temperaturii sunt de $\pm 2^{\circ}\text{C}$.In plus, experimentările efectuate au scos în evidență atât economia de energie electrică, cât și îmbunătățirea rezultatelor tratamentelor termice aplicate, ilustrată prin compararea microstructurilor pieselor tratate în instalația îmbunătățită cu cele obținute în instalația inițială.

PROGRAMME CARRIED OUT FOR AUTOADAPTIVE CONTROL OF AN ELECTRIC FURNACE OF HEAT TREATING USING A COMPUTER

by

CRISTINA ALBU-IACOB

Abstract

The equipment for ordering, controlling and regulating the technological process of heat treatment must enable the continuous regulation of the input voltage of the resistors in order to obtain a time-temperature dependence according to the given diagram of heat treating. This condition can be obtained using a command system <<on-line>> in closed circuit for the process of heat treatment. Controlling the process of heat treatment, taking into account the particularities of all the factors involved, can be done using the outfit consisting in a numerical computer which should communicate with the control unit endowed with silicon controlled rectifiers through a specialised interface, instead of the conventional equipment of controlling. The computer uses a specialised soft which should observe as well as possible the concrete aspects of the controlled process, which confers both an increase of the power efficiency of the installations and better results regarding the quality of the machine parts heat treated.

Keywords

Programme, autoadaptive control, electrical furnace, heat treatment

The programme carried out ensures the autoadaptation for the parameters of the thermoregulator device having a PID behaviour through the method of the unit step response of the furnace. Taking into account the necessity of the experimental knowledge of the constructive-functional characteristics of the furnace, a first experiment in order to determine the unit step response of it was performed. The gradual control of the heating power was achieved using silicon controlled rectifiers operated in a phase angle. In this case the relation between power and the control angle

is (1):
$$P = \frac{U_s^2}{R} \left(1 - \frac{\psi}{\pi} + \frac{\sin 2\psi}{2\pi} \right) \quad (1)$$

A variation of π radians of the control angle ψ corresponds to a variation of the cue voltage U_{com} from the exist of the analogue-digital converter of 10 V, thus $U_{com} = 0$ V corresponds to the angle $\psi = \pi$ (rad), and $U_{com} = 10$ V corresponds to the angle $\psi = 0$ V. Therefore, there is a relation (2):

$$\psi = \pi - \frac{U_{com}}{10} \pi \quad (2) \quad \text{or} \quad \frac{\psi}{\pi} = 1 - \frac{U_{com}}{10} \quad (3), \quad \text{whence} \quad 2\psi = 2\pi - U_{com} \frac{\pi}{5} \quad (4)$$

The relation (5) results:
$$P = \frac{U_s^2}{R} \left(\frac{U_{com}}{10} + \frac{\sin\left(\frac{\pi U_{com}}{5}\right)}{2\pi} \right) \quad (5)$$

The relation between the theme of the variator U_{com} and the number of the bits (binary units) applied to the analogue-digital converter on 8 bits is: $U_{com} = 10 \text{ V}$ – corresponds to a number of 256 bits, $U_{com} = 0 \text{ V}$ – corresponds to a number of 0 bits.

One can conclude that N bits will correspond to a voltage U_{com} according to the

$$\text{formula: } N = \frac{U_{com} \cdot 256}{10} \text{ (bits) or } U_{com} = \frac{10N}{256} \quad (6)$$

The power $P = \frac{U_s^2}{R} = P_{max}$ will correspond to an angle $\psi=0$ and the power $P=0$ will correspond to the angle $\psi = \pi$.

$$P = P_{MAX} \left(1 - \frac{\psi}{\pi} + \frac{\sin 2\psi}{2\pi} \right) \quad (7) , P = P_{MAX} \left(\frac{U_{com}}{10} + \frac{\sin \left(\frac{\pi U_{com}}{5} \right)}{2\pi} \right) \quad (8)$$

$$\text{Expressed by means of the number of bits: } P = P_{MAX} \left(\frac{N}{256} + \frac{\sin \left(\frac{2\pi N}{256} \right)}{2\pi} \right) \quad (9)$$

I. Activation parameters:

- 1°. Target temperature (TARGET) (°C)
- 2°. Proportionality band (BP) (%): 5% ... 40%
- 3°. Hysterezis (HYSZ), $\max |\theta_{measured}(t) - \theta_{programed}(t)|$: 2°C ... 5°C
- 4°. The initial power applied to the furnace (EF) (%): $(60 \dots 80) \times P_{MAX}/100$
- 5°. Time (TIME), (min)
- 6°. Sampling quantum (K): 10 ... 15 seconds
- 7°. Estimation time (TIME_ESTIM) for the parameters T_u and V_{MAX} : 3 ... 4 min
- 8°. Maximum deviation (DEVIATION) : $\max |\theta_{m\acute{a}surat}(t) - \theta_{estimat}(t)|$: 1...3°C

II. The furnace being at the ambient temperature, we apply an initial power equal to the one settled at the point 4° from above (EF).

III. When the temperature in the furnace, $\theta(t)$, reaches the value:

$$\theta(t) \geq \text{TARGET} - \frac{75}{100} \times \text{BP} \times \text{TARGET} \quad (10), \text{ we shell check up the condition of}$$

$$\text{hysterezis: } |\text{TARGET} - \theta(t)| \leq \frac{\text{HISZ}}{2} \quad (11)$$

If the temperature observes this condition, the power will not have to be modified again ($\Delta P=0$).

If the temperature measured doesn't observe this condition, a supplementary step of power will have to be applied following the algorithm given below:

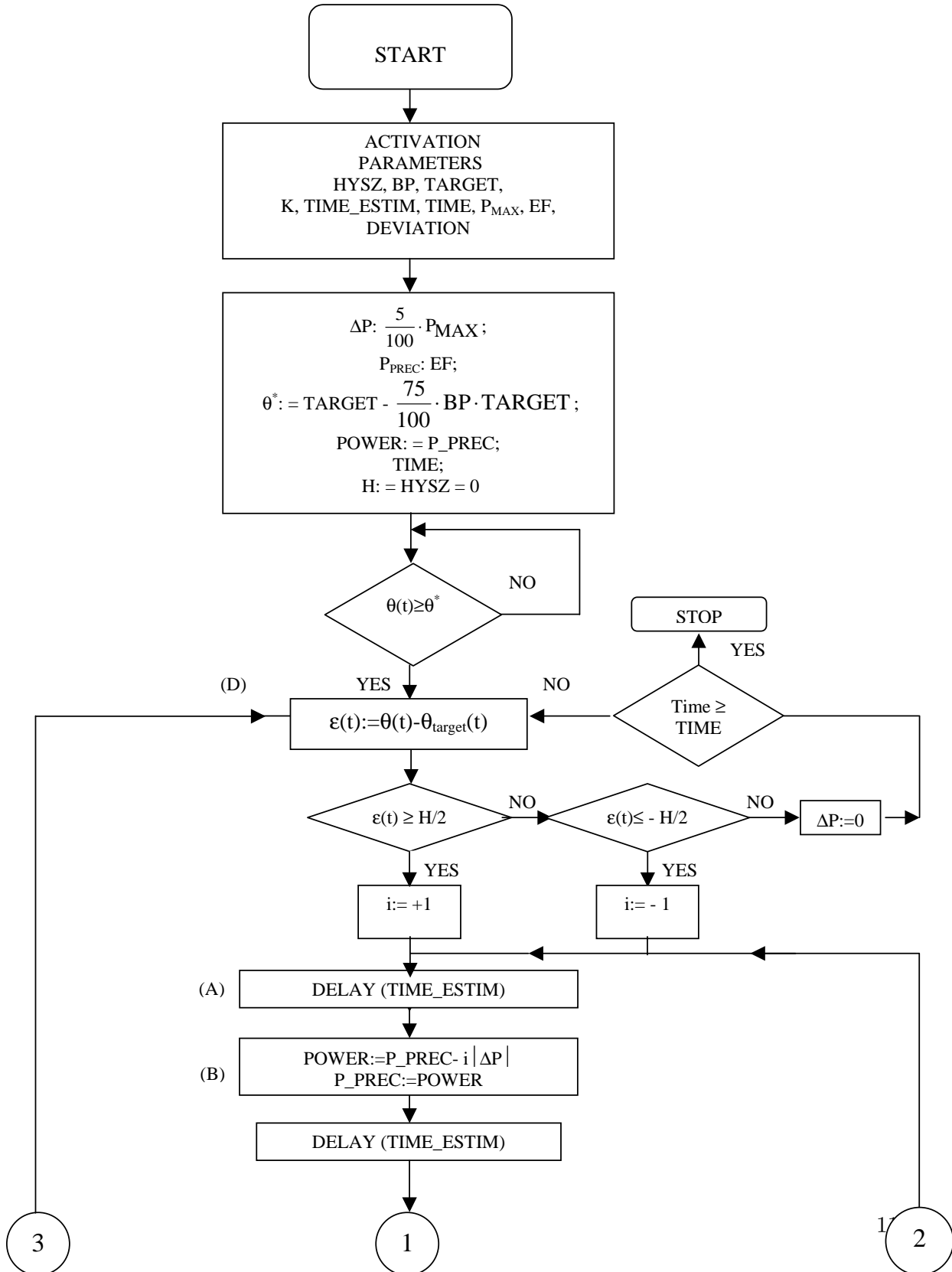
1°. The sampling quantum (expressed in seconds) being K and the time of estimation (TIME_ESTIM), expressed in minutes, a number of quanta will results:

$$\text{number} = \frac{\text{TIME_ESTIM} \times 60}{K} \quad (12)$$

In the time interval TIME_ESTIM we shall memorize the values of the temperatures measured at the equal intervals of time (K) in the sequence : TEMP_TC₂[j], in which

the index j varies from 0 to the maximum value of the number of quanta, number given above (in the logical scheme-see block A).

The logical scheme of programme is presented in the figure1.



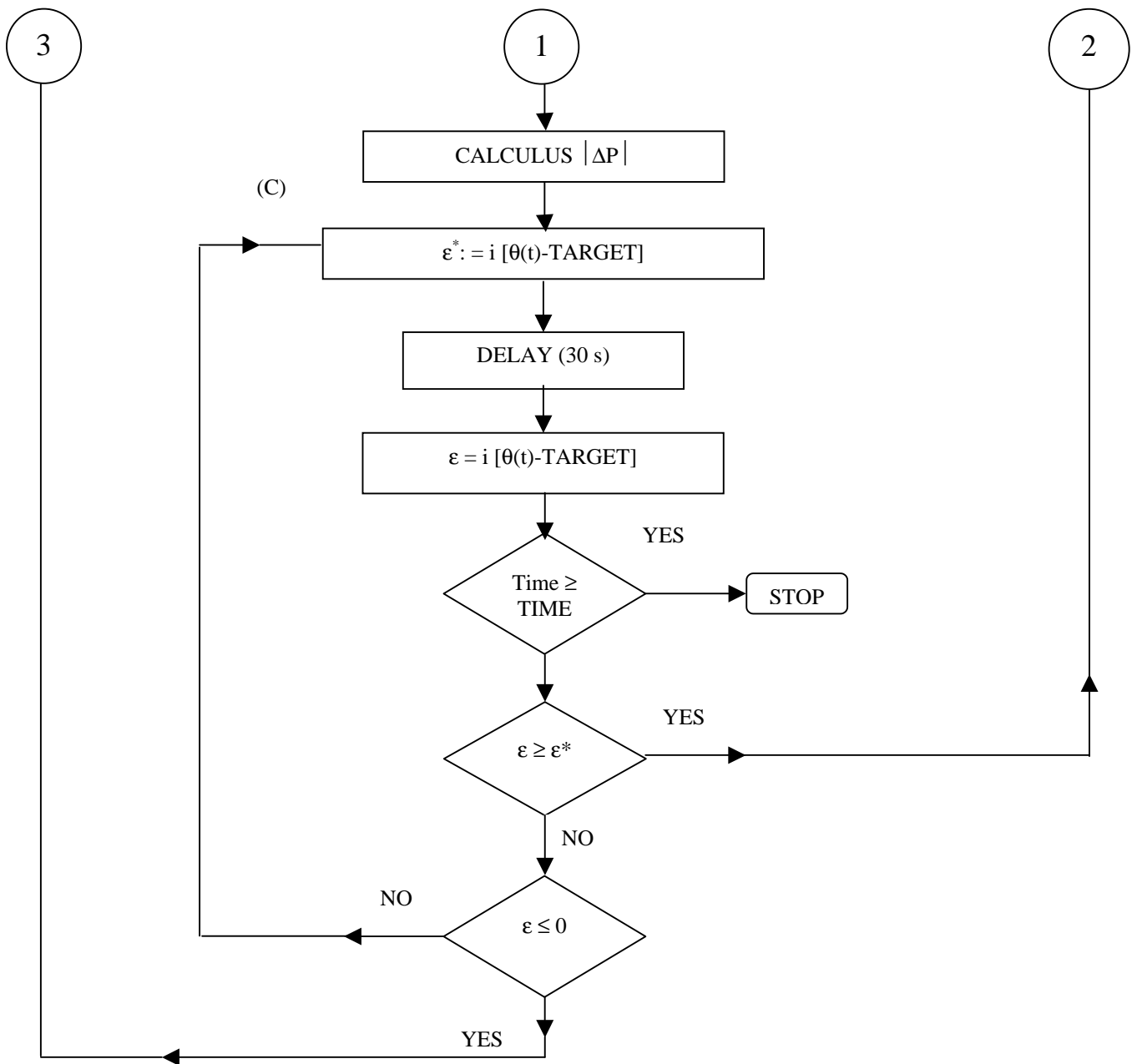


Figure 1. Logical scheme of the programme

2°.A supplementary step of power $5/100 P_{MAX}$ will be applied to the furnace. Taking into account the variations that are in line approximately on short intervals of time($TIME_ESTIM$), that is 3-4 minutes, we can estimate having a good approximation how the temperature in the furnace would have evolved if the step of power from above hadn't been applied.

In figure 2 we note with (1) the variation of the temperature in the furnace, temperature measured in the interval 0-T ($T= TIME_ESTIM$).

Without the applying of the supplementary step of power, the temperature would have evolved in the interval $(T-2T)$ following the curve (1), which we can approximate

with the straight line AB, noted with (2) on the shorter interval of time ($T-3T/2$). The slope of the straight line (2) can be calculated in this way:

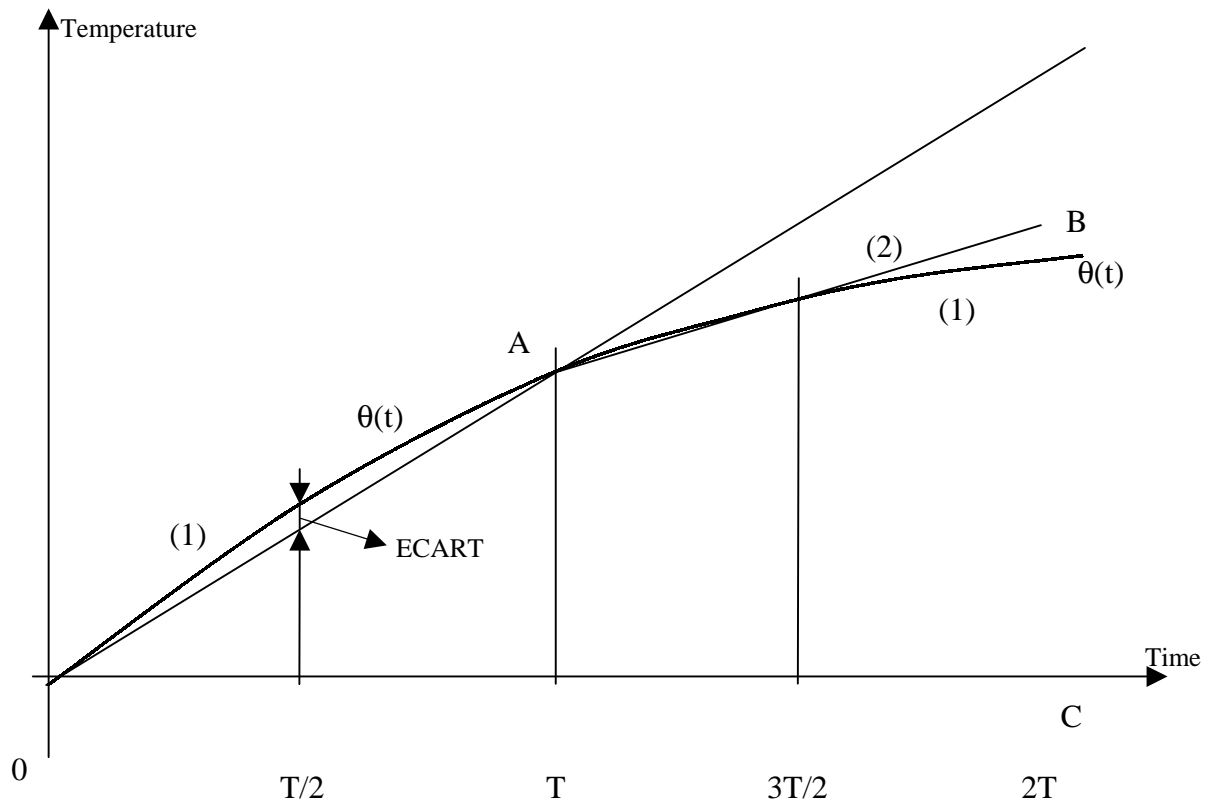


Figure 2. Graphic representation of the model for the estimation of the evolution of the temperature

- we draw the straight line OA and then we measure a difference at the moment $T/2$:

$$\theta\left(\frac{T}{2}\right) - \frac{\text{TEMP_TC}_2[0] + \text{TEMP_TC}_2[T]}{2} = \text{ECART} \quad (13)$$

- we prolong the straight line OA up to the point C in which the value of the y-coordinate will be:

$$\text{STRAIGHT LINE}[2T] = 2 \times \text{TEMP_TC}_2[2T] - \text{TEMP_TC}_2[0] \quad (14)$$

We find out the point B if we diminish the value of the temperature gap/separation five times, experimentally determined value for variations of the temperature tangent line which are not higher than $1^\circ\text{C}/\text{min}$. In order to estimate the temperature we have made the sequence:

$$\text{BETA}[q] = \text{STRAIGHTLINE}[\text{number}] + q \times ((\text{STRAIGHTLINE}[2 \times \text{number}] - 5 \times \text{ECART}) - \text{STRAIGHTLINE}[\text{number}]) / \text{number} \quad (15)$$

The index q varies from 0 to the maximum value = number (in the logical scheme see block B).

3°. In the time interval $(T-2T)$ we check up the condition (16) for $q=1\dots\text{number}$, that is the maximum deviation between the value measured and the estimated one should not overreach the value settled. The last index q which satisfies the condition (16) will provide us T_u at a first estimation $T_u=q \times K$:

$$\text{TEMP_TC}_2[q] - \text{BETA}[q] \leq \text{DEVIATION} \quad (16)$$

4°. At the end of the period T we can calculate $\text{tg}\alpha_{\max} = V_{\max}$, according to figure 3 which represents graphically the method of determination for the calculus of the parameters involved in the calculus of the parameters of the continuous regulator PID.uu.

$$V_{\max} = \frac{\theta(T) - \theta(i \cdot K)}{T - i \cdot K}, \quad (17), \quad \text{where } i \cdot K = T_u, \quad \text{the one in the first estimation (point } 3^\circ).$$

$$\text{But } V_{\max} \text{ can be expressed in this way, too: } V_{\max} = \frac{\theta(i \cdot K)}{i \cdot K - t_m} \quad (18).$$

This relation will enable us to recalculate the time T_u :

$$T_u = t_m = i \cdot K - \frac{\theta(i \cdot K)}{V_{\max}} \quad (19)$$

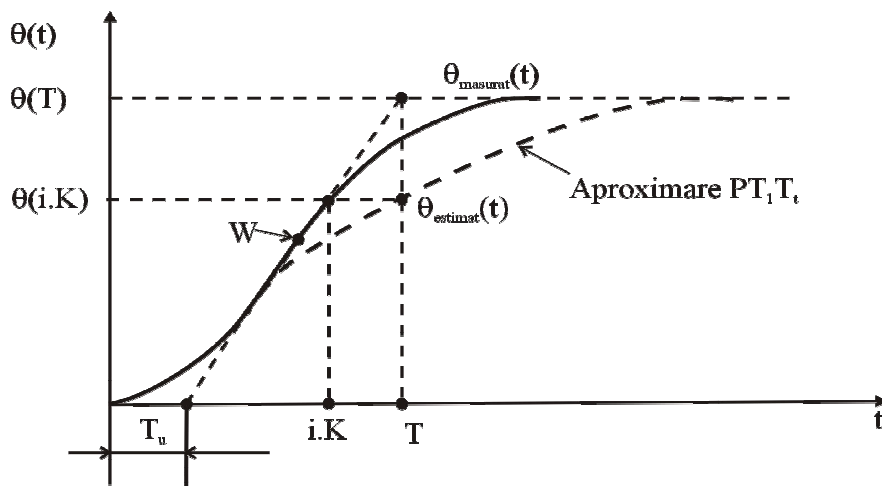


Figure 3. Graphic model of calculus used for the determination of the parameters of the continuous regulator PID

IV. At the end of the period T we can calculate:

$$\int_0^T \theta_{\text{measured}}(t) dt \quad \text{and} \quad \int_0^T \theta_{\text{estimated}}(t) dt.$$

$$\Delta W = K_R \left(\int_0^T \theta_{\text{measured}}(t) dt - \int_0^T \theta_{\text{estimated}}(t) dt \right) \quad (20), \quad \frac{\Delta W}{T} = P(T) - P(0) \quad (21)$$

In the relation(21), $P(0)$ is the old step of power and $P(T)$ the new power applied to the furnace.It means that: $K_R = \frac{T[P(T)-P(0)]}{\int_0^T \theta_{measured}(t)dt - \int_0^T \theta_{estimated}(t)dt}$ (22)

We know now, at the end of T period, the following parameters: T_u , V_{max} and K_R , the essential parameters in order to recalculate the parameters K_P , T_I and T_D for a continuous PID regulator.

V. In order to reach the desired temperature θ_{target} it is necessary that we should apply a step of power:

$$\Delta P = K_R \cdot \left[K_P (\theta_{target} - \theta(T)) + \frac{1}{T_I} \cdot \int_0^T (\theta_{target} - \theta(t))dt + T_D \cdot \frac{d(\theta_{target} - \theta(t))}{dt} \right] \quad (23), \text{ where } K_P, T_I \text{ and } T_D$$

will be calculated according to the following empiric rules deduced by the the application of the Ziegler-Nichols method (the unit step response method):

$$K_P = \frac{\theta_{consemn}}{1,7 \cdot V_{max} \cdot T_u \cdot 100}, \quad T_I = 2T_u, \quad T_D = 2T_u$$

It means that:

$$\Delta P = K_R \cdot \left[\frac{\theta_{target}}{1,7 \cdot V_{max} \cdot T_u \cdot 100} (\theta_{target} - \theta(T)) + \frac{1}{2T_u} \cdot \frac{\theta(0) - \theta(T)}{2} T + 2T_u \frac{\theta(0) - \theta(T)}{T} \right] \quad (24)$$

VI.After we have calculated the step of power ΔP which is necessary in order to reach the target temperature assigned (TARGET), we shall measure a difference $\varepsilon^* = \theta(t) - TARGET$ and after 30 seconds we shall measure again : $\varepsilon = \theta(t) - TARGET$. If the time overreach the settled value TIME, the process of regulation will end (block STOP in the logical scheme).If not, we shall keep on testing if a diminution of the distance between the temperature measured and the one prescribed, $\varepsilon \geq \varepsilon^*$, takes place in these 30 seconds.If the distance increase, we shall obviously have to recalculate the step f power ΔP .If the distance decreases, ($\varepsilon < \varepsilon^*$), but $\varepsilon > 0$, we shall recalculate ε^* and ε (we go back to block (C) in the logical scheme).If, this time, $\varepsilon \leq 0$ it is the moment to resume the testing of the interval of hysterezis (block D in the logical scheme)

In conclusion, controlling the process using a computer offers the possibility to have the repeatability of the cycles of heat treating, owing to the computer programme conceived, which enables monitoring, memorizing and stocking the parameters which can be settled and the real temperatures in the charge in graphic and numerical form.

References:

Cristina Albu-Iacob- Teza de doctorat „ Contributii privind imbunatatirea constructiv-functionala a instalatiilor de tratament termic al aliajelor de cupru”, Iasi, 2002

Received May 2, 2005

Technical Coledge of Transport, Piatra Neamt, Neamt, Romania

CONTROLUL AUTOADAPTIV AL UNUI CUPTOR ELECTRIC

Rezumat. Echipamentul pentru comanda, controlul și reglarea procesului tehnologic de tratament termic trebuie să permită reglarea continuă a tensiunii de alimentare a rezistorilor pentru a obține o dependență temperatură – timp în conformitate cu diagrama de tratament termic dată. Această condiție se poate obține folosind un sistem de conducere « on-line » în circuit închis a procesului de tratament termic. Conducerea procesului de tratament termic, ținând cont de particularitățile tuturor factorilor implicați, se poate face prin utilizarea, în locul echipamentului de conducere convențional, a unui echipament folosind un calculator numeric care să comunice cu unitatea de comandă cu tiristori printr-o interfață specializată. Calculatorul folosește un soft specializat care să respecte cât mai mult aspectele concrete ale procesului condus, ceea ce conferă atât o creștere a eficienței energetice a utilajului, cât și rezultate mai bune privind calitatea pieselor tratate termic.

STUDY OF MECHANICAL BEHAVIOR OF DENTAL RESTORATIONS BY USING DATA ACQUISITION SYSTEMS

by

R.COMANECI*, A.M.VITALARIU, L.ZAHARIA*, R.CHELARIU***

ABSTRACT: *The restoration of endodontically treated teeth with dental materials that have similar properties with dental tissues became a major aim in the restorative dentistry. Thus, today are available on the market different kind of non-metallic post, made from zirconium oxide ceramics or composite resins reinforced with carbon, glass and quartz fibers. Unfortunately, there are few information about the influence of the post material on the fracture resistance of endodontically treated teeth.*

This study was undertaken to characterize the fracture resistance and mode of failure of endodontically treated incisors restored with prefabricated titanium, or carbon/glass/quartz fibers-reinforced composite posts. Because of their brittle behavior, it would be more appropriate to study the fracture resistance and mode of failure of a post-and-core system at its initial failure. Accurate recording of the first sign of failure is possible only by modern data acquisition equipment.

KEYWORDS: *fiber reinforced posts, post and core system, fracture resistance, data acquisition*

INTRODUCTION

The high success rate for modern endodontics have resulted in an increased demand for clinically convenient post and core systems to help restore lost tooth structure. It is well known that the use of a post does not increase the strength of the remaining tooth. Its role is to provide retention to the core material. The price for this retention, however, may be an increased risk of root fracture.

Many specialists agree that the design and the material of the post have a certain influence on the fracture resistance of endodontically treated teeth (1, 2, 3, 4). An ideal post should have similar shape to the prepared root canal, mechanical properties identical to dentin to resist to occlusal forces and to induce minimal tensions on dental root. In addition, a post should provide a good retention for the core material and should be easily removed from the root it is necessary.

Due to composition and structure of dental tissues, and to their mechanical characteristics, teeth have a brittle behavior. Because that, it is difficult to determine the moment of failure threshold by classic methods. In this context, the failure point was recording by using modern data acquisition equipment.

MATERIALS AND METHOD

Forty freshly extracted human maxillary central incisors free of cracks, caries, fractures, abrasion and restorations, were selected based on dimensional requirements and randomly divided into four groups of 10 specimens:

- group 1 – teeth restored with carbon fiber posts (Carbopost)
- group 2 – teeth restored with glass fiber posts (Snowlight)
- group 3 – teeth restored with prefabricated titanium posts (Ancorextra)
- group 4 (control) – endodontically treated teeth but without posts.

Preparation of the samples:

- the anatomic crowns of teeth from experimental groups (1,2 and 3) were sectioned horizontal to the long axis, 2 mm coronal to the cemento-enamel junction (CEJ), figure 1a, using a diamond bur
- after endodontic instrumentation, all roots were obturated with gutta percha and resin sealer AH-26 (DeTrey), Figure 1b
- post space was prepared removing gutta percha with appropriate drills; 3 mm was kept on the apex region to ensure a good endodontic seal

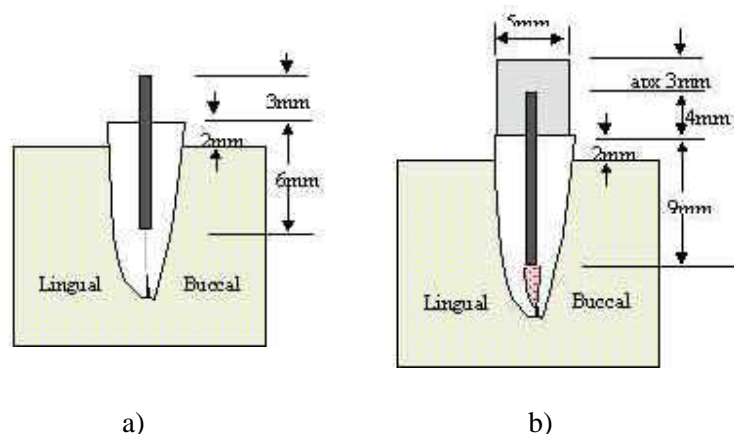


Figure 1. Preparation of the samples

- the posts were placed into the roots leaving 4 mm above the tooth section and were cemented with a dual-cure resin cement (Panavia F), Figure 2

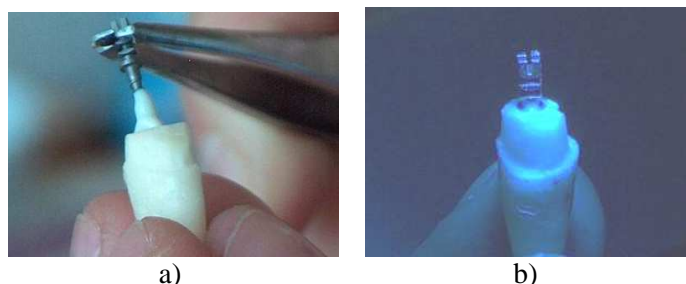


Figure 2. a) Post cementation; b) light-curing of the cement

- the crown portion was built up with a light-curing composite (Blend-a-lux) until a 6 mm height core is achieved, Figure 3

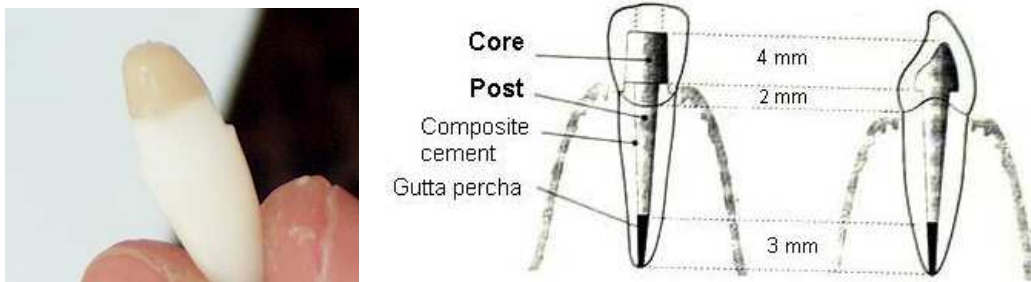


Fig. 3. a) the core build-up; b) schematic drawing of a tooth restored with a post-and-core

- the roots were embedded in clear self-cure acrylic resin (Superacryl/Spofa) surrounded by stainless steel cylinders (20 mm high, 20 mm diameter), Fig. 4.



Figure 4. The roots are embedded in self-cure resin

- finally, metal cast crowns were cemented on all specimens
- on the oral surface of each metal crown was made a notch (0,3 mm deep and 1 mm wide), right above the cingulum, in order to place there the compressive load during the test, Figure 5



Figure 5. The specimen mounted in metallic cylinders

TEST PROCEDURE

All specimens were screwed into a custom-made stainless steel mounting device (Figure 6) and loaded until fracture. Compressive load was applied with an universal load-testing machine with nominal forces of 25kN to the teeth at a cross-head speed of 19mm/min. Loads were applied at an angle of 45 degrees at the oral surface of the crown, in order to reproduce the normal transmission of occlusal forces on the anterior teeth, Figure 7.



Figure 6. a)The specimen mounted in the testing device;

b) the specimen mounted in the testing machine

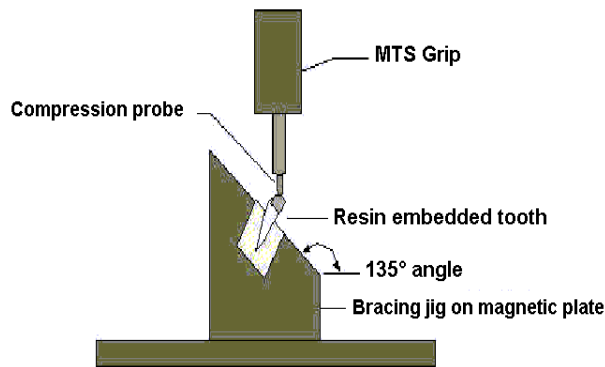


Figure 7. The principle of compressive test



Figure 8. Data acquisition equipment

Force measurements were recorded with a compressive force transducer - load cell - (nominal forces of 100kN) with strain gauges connected as full Wheatstone bridge. Each strain gauge - type 3/350 LG11 HBM Hottinger Baldwin Messtechnik - have an internal resistance of 350Ω.

The testing apparatus was connected to a measuring amplifier N2302 and to PCI6023E National Instruments data acquisition board respectively, Figure 8. LabVIEW 6.0 National Instruments software was used to perform a data acquisition virtual instrument for measurement with a scan rate of 1000scan/sec (5, 6).

All data was recorded from the first fracture point that were represented on the paper chart by the first drop of the load, Figure 9 and 10.

The load testing-machine was not interrupted after the drop of load. Waiting for complete destruction of the crown post-and-core system would

interfere with final result when investigating the mode of fracture. All specimens failed with teeth fracture.

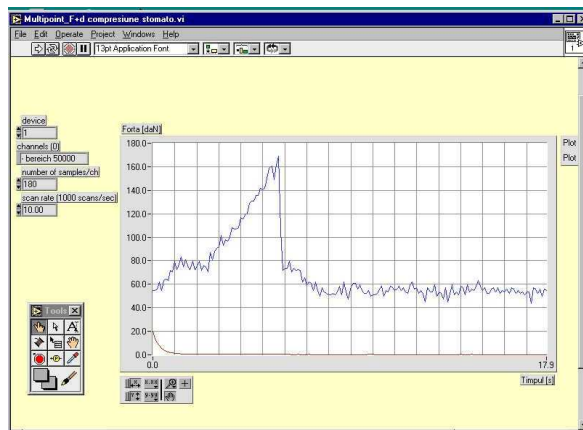


Figure 9. Recorded load forces by data acquisition.

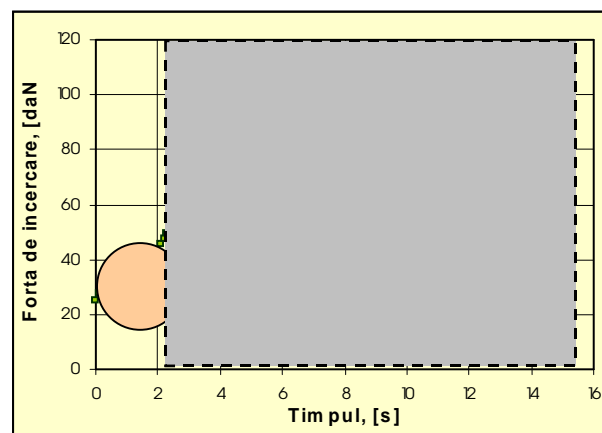


Figure 10. Filtered values of load forces

EXERIMENTAL RESULTS AND CONCLUSIONS

The range of load resistance of the teeth to the point of fracture was about 31-35daN, Table 1. The load values for all specimen groups are graphically illustrated in Figure

11. By using data acquisition, we be able to accurately determine the initial moment of failure by first drop of the force on the paper chart. Comparison of resistance showed no significant differences between titanium and carbon or glass fiber reinforced composite posts.

Table1. The fracture resistance of restored teeth

Group	F_r , [daN]
Control (M)	31 ÷ 34,9
Carbon (C)	31,8 ÷ 32,2
Glass (S)	31,3 ÷ 35,1
Titanium (T)	31,75 ÷ 35,25

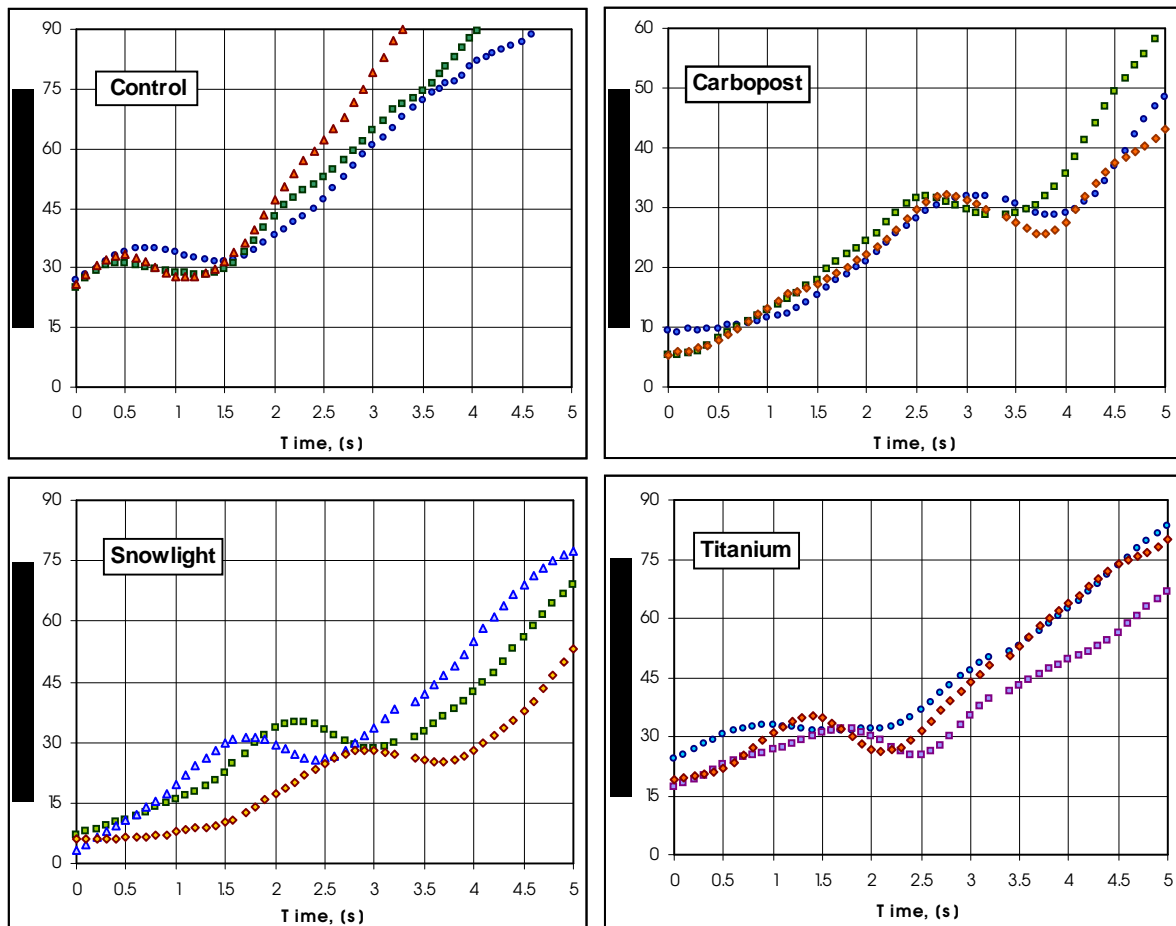
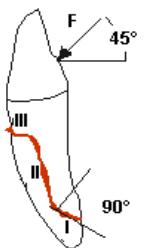
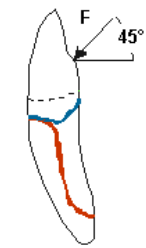


Figure 11. Compressive loads for each studied group of specimens

Differences were observed among the groups regarding the mode of failure of the different posts studied. The fracture patterns of all test groups are presented in Table 2. The fracture loads were determined and the mode of failure was recorded and classified as favorable (repairable) or catastrophic. The number of catastrophic

fractures was higher in group of metallic posts restorations (titanium) – 50% vertical root fractures, 30% combined root fractures. In this case, less rigid dentin are not able to absorb stresses and are therefore susceptible to failure.

Table 2. The patterns of teeth fractures

Group	Number of specimens	Repairable fractures 	Vertical root fractures 	Combined root fractures 
Carbopost	10	5	3	2
Snowlight	10	8	-	2
Titanium	10	2	5	3
Control	10	5	-	5

The greatest number of restorable fractures were recorded in Snowpost group (80%) and in the Carbopost group (50%). These results may be attributable to the fact that carbon/glass fiber reinforced posts have the modulus of elasticity closer to the dentin.

Received May 6, 2005

*) Technical University “Gh. Asachi” Iasi, Faculty of Science and Materials Engineering

***) University of Medicine and Pharmacy „Gr.T. Popa” Iasi, Faculty of Dental Medicine

REFERENCES

1. Akkayan B., Gülmez T. – Resistance to fracture of endodontically treated teeth restored with different post systems – J Prosthet Dent 2002; 87: 431-437
2. Assif D., Bitenski A., Pilo R., Oren E. – Effect of post design on resistance to fracture of endodontically treated teeth with complete crowns – J Prosthet Dent 1993; 69:36
3. Maccari PC, Conceicao EN, Nunes MF – Fracture resistance of endodontically treated teeth restored with three different prefabricated esthetic posts – J Esthet Restor Dent 2003;15(1):25-30
4. Möllersten L., Lockowandt Paul, Lindén Lars-Åke – A comparison of strengths of five core and post-and-core systems – Quintessence Int. 2002,vol.33,nr.2, 140-149.
5. The Newsletter for PC-Based Data Acquisition and Control, December 2002, ISSN 1472-0221.
6. A. Bruce Buckman - Computer-Based Electronic Measurement: An Introductory Electronics Laboratory Workbook Based on LabVIEW and Virtual Bench, Prentice Hall, 1999, 0-20-136182-5.

ACHIZITIA DE DATE IN STUDIUL COMPORTARII MECANICE A RESTAURARILOR DENTARE

Rezumat. Restaurarea dinților tratați endodontic cu materiale ce au proprietăți apropiate de cele ale dentinei a devenit un obiectiv major în dentistica restaurativă. În acest context, au apărut pe piață pivoturile din material compozit armat cu fibre de carbon, sticlă (cuart) și polietilenă, precum și pivoturi din ceramică pe bază de oxid de zirconiu. La ora actuală există un număr relativ limitat de informații privind influența materialului pivotului asupra rezistenței la fracturare a dinților tratați endodontic, cu reconstituiri corono-radiculare (RCR).

Prezentul studiu a fost realizat în scopul determinării rezistenței la fracturare și a modului de fracturare a dinților cu reconstituiri corono-radiculare cu pivoturi din titan sau cu pivoturi compozite cu fibre de carbon, respectiv sticlă. Datorită comportării mecanice prin excelență fragile a RCR, este recomandată determinarea rezistenței la rupere în momentul inițial al propagării fisurii. Determinarea cu precizie a primului semn de fracturare este posibilă numai prin utilizarea echipamentului modern de achiziție de date.

MUFFLER DESIGN USING FINITE ELEMENT MODELING AND SIMULATION

by

RADU DROSESCU

ABSTRACT: *Computer simulation offers the possibilities to achieve better values for all factors that will minimize the production efforts and costs of a muffler design and fabrication process. The most important factors involving in muffler design are noise level attenuation, back pressure, size and weight. In order to obtain the optimal solution for a specifically muffler design, many prototypes involving material, time spend and expensive costs are necessary, including acoustic tests and measurements. Precise computer modeling and simulation using FE programs can replace all this operations resulting considerable improvement in shorting the design time and cost production.*

KEY-WORDS: muffler, silencer, acoustic, finite element, modeling, simulation

1. Introduction

Considerable effort has been directed over the years in connection with attempting to optimize the design of muffler for internal combustion engines in which there is a flow of gases having a noise component entrained or accompanying the gases. There are many factors which are considered in determining whether or no a particular muffler design is a success, the most commonly considered parameters being size, weight, back pressure and, perhaps most important, noise reduction. Reductions of size offer the designers greater flexibility in the positioning of the muffler and also, the possibility in its use on other combustion engines.

Existing exhaust systems have attained a noise reduction level, which is satisfactory for today's requirements, but the future NVH standards demand lower noise levels, which will be tolerated in parallel with the increase in standards as to reduction of pollutants in exhaust gases. Another factor that competes directly with noise reduction is the effect of the muffler on engine performance. More particularly, mufflers inherently impede the flow of exhaust gases from the engine. This obstacle creates a back pressure between the engine and the muffler, with a negative resulting effect upon the power production of the engine. Hence, increasing back pressure as a results of noise and weight reduction solutions decrease the engine efficiency and will defeat the effects of these improvements. Automotive designers therefore must make design decisions that will achieve a selected noise level while minimizing back pressure and its effect on the engine performance.

2. Muffler geometry

Mufflers are radiating structures emitting sounds into the surrounding space. Modeling the acoustics of a muffler implies the mathematical descriptions of the pressure wave propagation and the analysis of damping for propagation of harmonic acoustic waves. Mathlab and Simulink are valuable platforms used to develop

simulation finite element type programs used in acoustic waves modeling. FEM programs like Nastran or Fluent can be also used to model the pressure wave propagation into a muffler.

In Fig.1 and 2 are shown two muffler with semblable 3D geometries used to meet the customer demands.

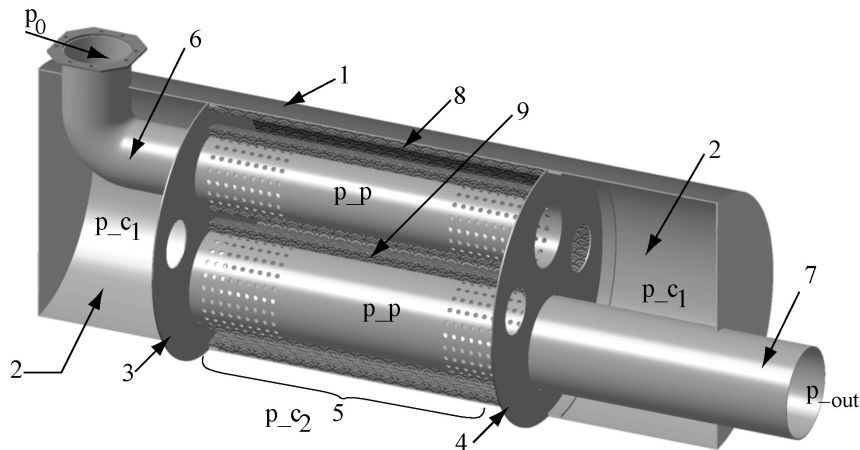


Fig.1 Muffler- 3D geometry representation

For this application we have choose a classical silencer construction with two expansion chamber 2 and a middle resonance chamber 5 known as a low frequency tuning chamber [2]. These chambers are formed from the muffler shell 1 with two internal baffles 3 and 4 which also support two pipes (tubes) 6 and 7 used to conduct the exhaust gaze. The inlet tube 6 will extend through the inlet chamber 2 and the central chamber 5 and will enter into the outlet chamber 2. The inlet tube must be of solid wall construction through the inlet end chamber but will be perforated in the central chamber of the muffler. Similarly, the outlet tube 7 opens in the inlet chamber 2 and passes through the central and outlet chambers 5, respectively 2. The outlet tube is typically of solid wall construction in the outlet chamber 2 and perforated in the central chamber. The communication of the flow between these tree chambers is made with circular perforations in the baffle walls or with one or two transfer tube as can be seen in Fig.2.

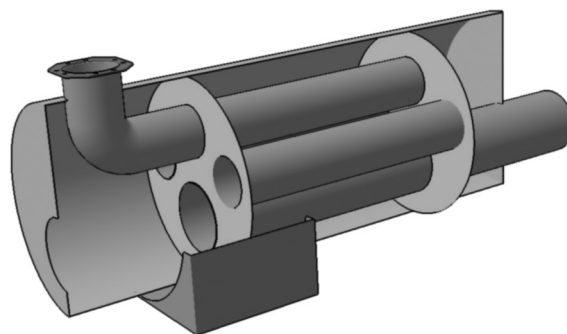


Fig.2 Muffler-with two expansion and one resonance chambers and internal transfer tubes

The transfer tube(s) may be also perforated, as it passes through the resonance chamber. The resonance chamber is packed with a sound absorbing material 9 around the passing tubes and around the shell wall, 8. Typical absorbing materials used in muffler construction are fiberglass, steel fibers or ceramic fibers. Fiberglass at high

temperatures and high speeds tends to blown out from the absorbent coating and in time, will degrade the acoustic characteristics of the muffler.

Many muffler design parameters can affect the acoustic behavior as the back pressure evolutions. Between them, the most important are the chamber sizes, the number and diameter of the perforations, tube diameters, wall thickness, and the offset position of the tubes in respect with the muffler centerline [3]. Same rules must be kept in mind when design a muffler.

- Hence, the varying size chambers each have their own noise attenuation characteristics. More particularly, the small chambers are efficient in attenuating high frequency noise, while the larger chambers tend to be effective in attenuating low frequency noise. However, the resonance chamber is slightly larger than either expansion chambers.
- The perforations of the tubes in the region of the resonance chamber contribute to the sound attenuation of the muffler. The size and density of these holes must be selected to achieve the desired attenuation of low frequency noise produced by the exhaust gases passing through the tubes.
- High frequency tuning chamber can be obtained with little space consumption by surrounding the central tube portion by a solid wall generally having a circular or tubular structure as can be seen from Fig.3.

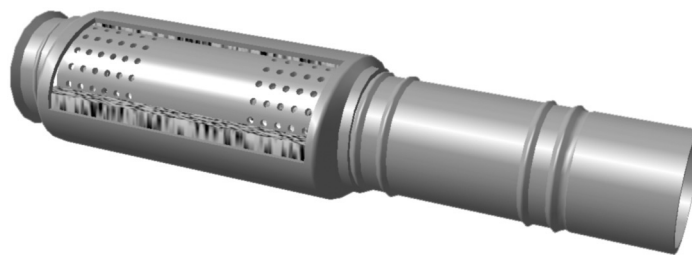


Fig.3 High frequency tuning chamber

The external added tubular member is provided with pinches adjacent fixed in the tube rims in order to achieve a secure positioning. The interspace between the tube and the high frequency tuning chamber wall is filling with a sound absorbing material as fiberglass.

3. Modeling equations

The model equation most frequently used in muffler simulation is a slightly modified Helmholtz's relation [1] for acoustic pressure, p_{ac} :

$$\nabla \cdot \left(-\frac{\nabla p_{ac}}{\rho} \right) - \frac{\omega^2 \cdot p_{ac}}{c_s^2 \cdot \rho} = 0 \quad (1)$$

where ρ is the exhaust gases density which must be explicitly considered in cases that variations in density in different material exist, c_s is the sound speed and $\omega = 2 \cdot \pi \cdot \text{freq}$ being the angular frequency. This equation must be adapted to the boundary conditions, which include the external and internal walls of the muffler.

For this reasons, modeling process begins with the geometry design of the muffler in 3D space. We can use for that a lot of CAD programs like SolidWorks (used in this case), ProEngineer, Mechanical Desktop, CATIA, which can generate an

output file in one of the graphical format accepted from FE meshing programs (igs, iges, stl, vrm, etc.). All these programs offer the meshing options for the 3D geometries with different levels of accuracy and refinement. In Fig.4 is shown the meshing used in FE modeling for the selected muffler geometry.

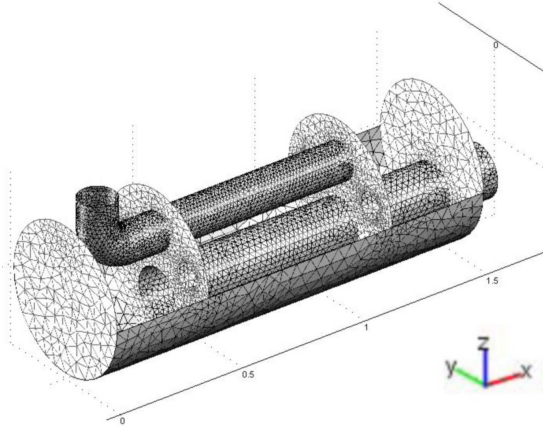


Fig.4 Meshing geometry for the tree chambers muffler

Tree different boundary equations are necessary for the outer wall of the muffler, at the baffle walls between the expansion and resonator chambers, and for the tubes walls. The sound pressure variables are noted for these bounds with p_{c1} , p_{c2} , respectively p_p . At the outlet boundary, the radiating wave plane is described by equation:

$$\left(-\frac{\nabla p}{\rho}\right) \cdot \mathbf{n} - \frac{i \cdot \omega}{c_s \cdot \rho} \cdot \mathbf{p} = 0 \quad (2)$$

At the inlet boundary is a combination of incoming and outgoing plane waves described with equation:

$$\left(-\frac{\nabla p}{\rho}\right) \cdot \mathbf{n} - \frac{i \cdot \omega}{c_s \cdot \rho} \cdot \mathbf{p} + 2 \cdot \frac{i \cdot \omega}{c_s \cdot \rho} \cdot \mathbf{p}_0 = 0 \quad (3)$$

where p_0 is the outer pressure applied at the muffler input and i is the imaginary unit.

Replacing variables with the notes one results the following equations:

$$\nabla \cdot \left(-\frac{\nabla p_{c1}}{\rho_0} + q_s\right) - \frac{\omega^2 \cdot p_{c1}}{c_s^2 \cdot \rho_0} = 0 \quad (4)$$

for the expansion chambers with $\rho_0 = 1.25$, $c_s = 343$ m/s and q_s dipole source. Similarly for the resonance chamber:

$$\nabla \cdot \left(-\frac{\nabla p_{c2}}{\rho_0} + q_s\right) - \frac{\omega^2 \cdot p_{c2}}{c_s^2 \cdot \rho_0} = 0 \quad (5)$$

and for the pipes:

$$\nabla \cdot \left(-\frac{\nabla p_p}{\rho_0} + q_s\right) - \frac{\omega^2 \cdot p_p}{c_s^2 \cdot \rho_0} = 0 \quad (6)$$

In order to appreciate the noise attenuation, a damping variable is defined as the ratio between the acoustic energies on the muffler outlet and inlet using relation:

$$ac_d = 10 \cdot \log \left(\frac{w_{outlet}}{w_{inlet}} \right) = 10 \cdot \log \left(\frac{\int \frac{|p_{out}|^2}{2 \cdot \rho \cdot c_s} \cdot dA}{\int \frac{|p_0|^2}{2 \cdot \rho \cdot c_s} \cdot dA} \right) \quad (7)$$

4. Simulation results

The objectives of this project consist in founding muffler architectures, which will improve the existing customer silencer by at least 20 dB. As can be seen from Fig.5

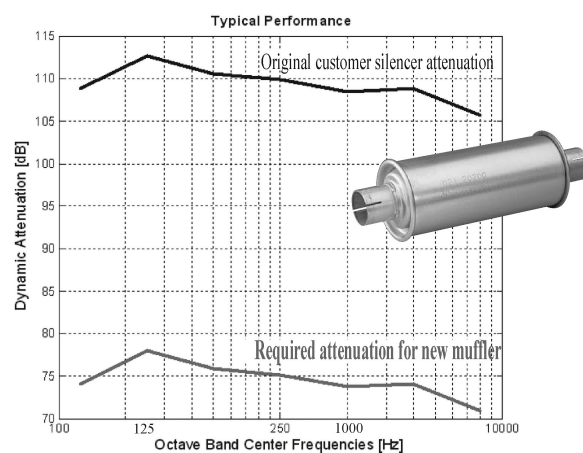


Fig.5 Dynamic attenuation for the customer silencer and proposed muffler

It must be known that a coarse meshing as can be seen in fig. 4 implies 29182 elements and 47776 degree of freedoms and the simulation time on a Pentium 4, 2.8 GHz with 1 Gb memory is approximately 5 hours without the consideration of tubes perforations. The frequency range was 100 – 1000 Hz with 10 Hz working interval. In normal meshing mode, the number of elements is 53836 and it became 80461, 109769 and 178933 for the fine, finer, respectively extra fine meshing mode necessary to simulate the perforations in tubes. All this resolutions beginning with the normal mode override the computing and memory capacities and are not possible to be run on the existing computer.

The attenuation characteristic for the proposed muffler is depicted in figure 6. It can be seen that the 30 dB objective can be reached for most of the frequency ranges, the worse behavior being recorded in the 400-500 Hz range with the 470 Hz the resonance frequency. This plot reveals that the damping is better at higher frequencies with the exception of several deep peaks throughout the selected frequency range. The dips correspond to the resonance frequencies for different parts on the muffler system.

By choosing adequate sizes for the tree chambers, these levels can be significantly reduced. It must also consider the attenuation in the low frequency range added by using the resonance tube perforations and absorption materials.

In order to enhance attenuations in frequencies higher than 900 Hz, additional piggyback chamber like that of Fig. 3 could be used. Better results are obtained by

replacing the muffler wall fiberglass coating with steel or ceramic fibers but the production prices will be higher.

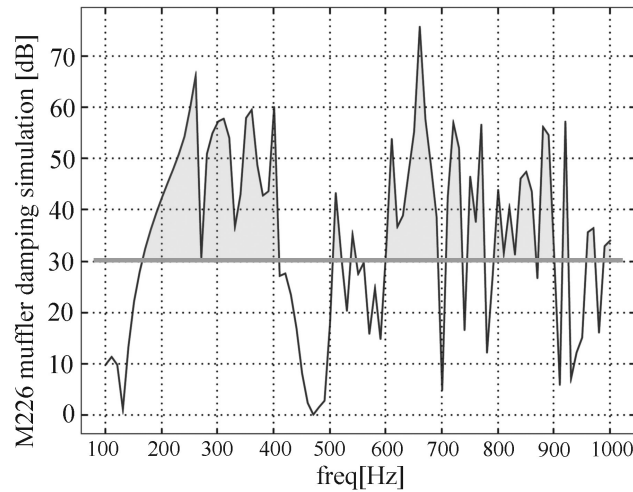


Fig.5 Dynamic attenuation for the customer silencer and proposed muffler

The acoustic pressure plot varies with the resonance frequency selected. For, example, at the 470 Hz the pressure plot is shown in Fig.6 with the real values of the pressure being plotted as isosurfaces, and the absolute value of the pressure being displayed as a boundary plot on the inner walls of the muffler.

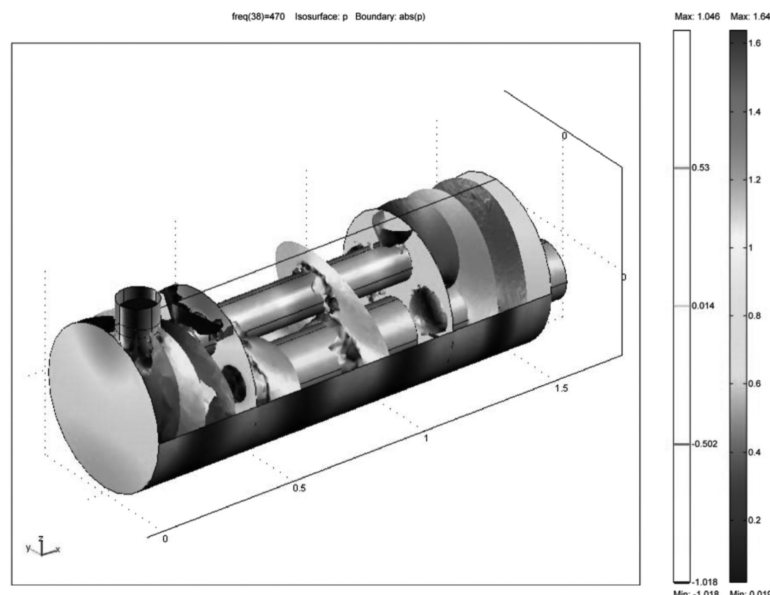


Fig.6 Projection on the x-y plane of the acoustic pressure solution at 470 Hz resonance frequency

The dip in the damping around the 470 resonance frequency is caused by the resonance in the central chamber 5. For other resonance frequencies it can be seen the resonance in the expansion chambers, for example in Fig.7 for the 590 Hz, and Fig.8 for 700 Hz.

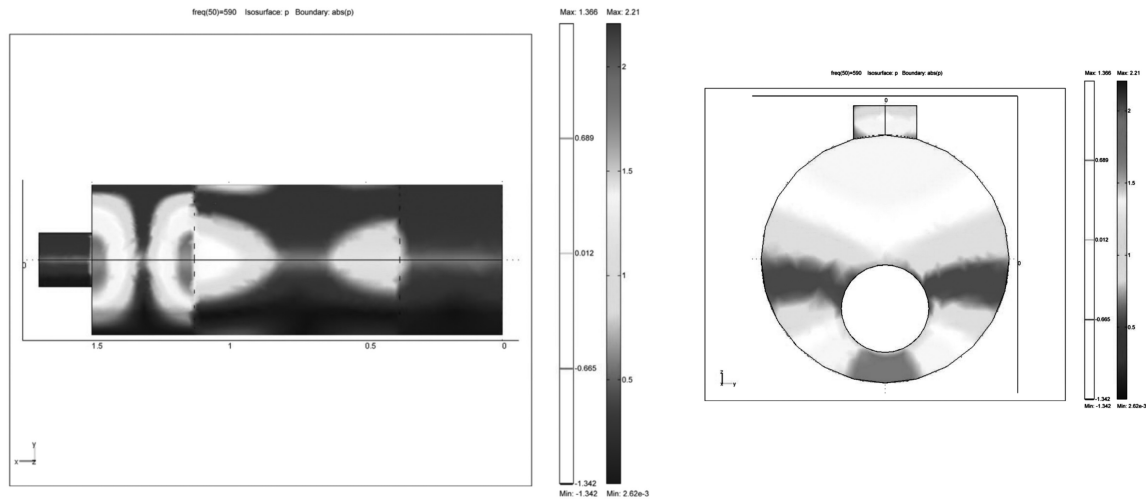


Fig.7 Projection on the x - y plane of the acoustic pressure solution at 590 Hz resonance frequency

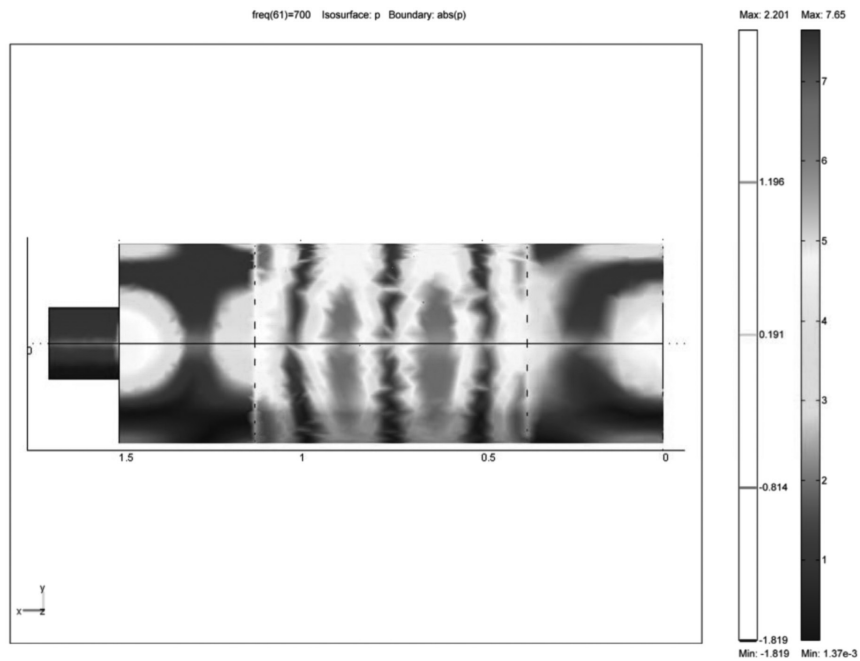


Fig.8 Projection on the x - y plane of the acoustic pressure solution at 700 Hz resonance frequency

5. Conclusions

The advantages of the finite element simulation as a design tool in the muffler design become clear, especially its accuracy in all frequency range and its resultant high reliability and availability, as well as its ability to record all the negative resonance frequencies.

The measure range of 100-1000Hz with 10 Hz tick interval is sufficient to determine the muffler attenuating behavior in most disturbing acoustic interval.

Accurate resultants can be obtained without the time, material and cost spends only by replacing some programming parameters in the computer system modeler. Test and analysis time has been short so dramatically that development engineers must use these FE simulations extensively.

REFERENCES

1. L. Beranek., “*Noise Reduction*”, New-York, McGraw-Hill, 1960, p.227-250
2. C.H., Harris., “*Handbook of Noise Control*”, McGraw-Hill, 1957, p.18-24
3. Don. D. Davis Jr., et al., “*Theoretical & Experimental Investigation of Muffler with Comments on Engine-Exhaust Muffler Design*”, Report 1192, Langley Aeronautical Laboratory, 1980

MODELARE CU ELEMENT FINIT ȘI SIMULARE

Rezumat Lucrarea analizează câteva metode de îmbunătățire a comportamentului acustic al unei tobe furnizată de fabricant axate în principal pe alegerea unei geometrii cu trei camere și două tuburi parțial perforate, precum și a unor îmbrăcămînți utilizând materiale sono-absorbante precum fibre de sticlă, fibre ceramice sau sârmă de oțel. Validarea modelului propus se face pe calculator cu ajutorul ecuațiilor de tip element finit. Este analizată atenuarea în banda 100-1000Hz, fiind propuse și soluții de îmbunătățire a acestora.

**THE CONTRIBUTION OF THE MATHEMATICAL MODELLING
OF HOT AND COLD ROLLING AND OF COOLING REGIME TO
THE IMPROVEMENT OF THE PLASTICITY CHARACTERISTICS
OF LOW-CARBON STEEL SHEETS**

by

V. MIRON, G. GHERGHISOR, R. PAUNESCU

Abstract. *The fabrication of deep-drawing cold-rolled sheets with high plasticity characteristics – according to the European norm EN 10130-92 – depends greatly on the granulation size and on the texture of hot-rolled sheet.*

An increase of the granulation (size: 7-8) and an intensifying of the (111) texture have been obtained by imposing a final hot-rolling temperature of minimum 860° C and a reduction ratio of maximum 15% on the last two finishing passes, as well as by imposing a quick and intense cooling of the rolled sheet; this cooling must assure a passing temperature of 520° - 560° C.

The optimization of the temperatures and of reductions has been obtained by the mathematical modelling of the hot rolling regime and of the cooling after rolling.

The experimental results confirmed that the Anan model is the most adequate one to the industrial conditions.

Keywords: flat products, cold rolled sheets

1. INTRODUCTION

The deep-drawing cold-rolled plates and sheets are made, generally, of low-carbon non-alloyed steel, aluminium-killed.

The specific problems of their fabrication are, apart the obtaining of surface aspects and of size tolerances, the plasticity mechanical characteristics (A_{80} – min. 38%) and the drawing capacity (r_{90} – min. 1.60 and n_{90} – min. 0.180) of the material.

The obtaining of mechanical characteristics is greatly influenced by the granulation size and by the texture of hot-rolled sheet.

A granulation of sizes 7 – 8 (20 – 30 μm) and the intensifying of (111) texture constantly involve high mechanical characteristics [1, 2].

For these steels, a correlation of the hot-rolled sheet granulation size to the temperature and reduction ratio, as well as a correlation of its granulation to the cold-rolled sheet granulation are encountered [3].

2. EXPERIMENTS

The steel used in our tests has been elaborated in a combined - blast converter, using low - sulphur cast iron; it was continuous cast in slabs of 200 mm in thickness.

The steel chemical composition, compared to the European norm EN 10130-92, is presented in table 1.

Table 1. The chemical composition of cold-rolled sheet

Chemical composition, %							
Elements	C	Mn	Si	P	S	Al	N
According to EN 10130-92	max. 0.080	max. 0.40	-	max. 0.030	max. 0.030	-	-
Existing	0.040	0.30	0.01	0.012	0.008	0.040	0.006

Based upon the analysis of several mathematical models of the hot-rolled regime, it is stated that the Anan model [4] is the most adequate for the industrial rolling condition.

Various reduction regimes and rolling temperatures have been computer simulated, based on this model. Two variants of rolling, for two different thicknesses of the hot rolled sheet have been chosen and experimentally tested.

In view to intensify the (111) texture and to avoid the precipitation, in this stage, of the recrystallization inhibitor AlN, the sheet has been quickly cooled after hot-rolling, the passing temperature being 520 - 560°C.

The hot rolled sheets of 2.3 and 3.0 mm in thickness have been cold - rerolled to 0.8 and 1.0 mm, annealed in a bell-furnace at 680 - 700°C and levelled to an elongation ratio of 1.5 – 2.0%.

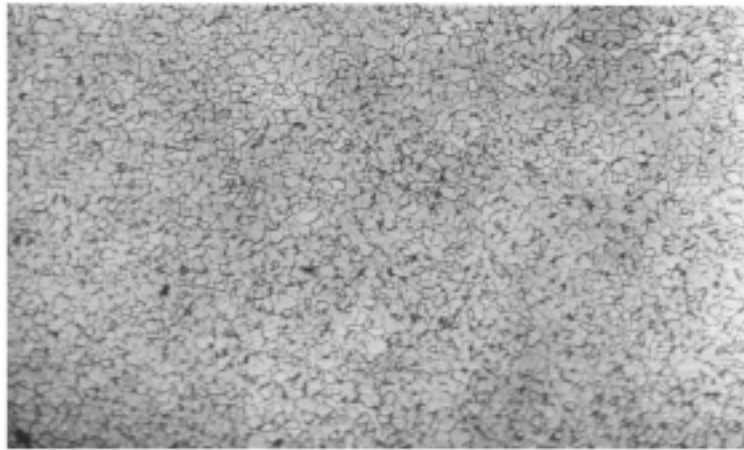
3. RESULTS

3.1. The metallographical analysis of hot-rolled sheet

The results obtained in the microstructural analysis of hot-rolled sheet, compared to the simulated variants analysis, are presented in figures 1 and 2.

A fine granulation of 9 – 10 size, with an average diameter of maximum 20 µm, is obtained when the final temperature is maximum 830° C and the reduction ratios for the two last passes are 20 – 25% (variant no.1), indifferently of the thickness of hot-rolled sheet (figure1).

An increase of the granulation up to 20 – 30 µm (size 7-8) is noticed in variant no. 2 – with a final rolling temperature of minimum 860° C and with reduction ratios on the last two passes of maximum 15% (figure 2).

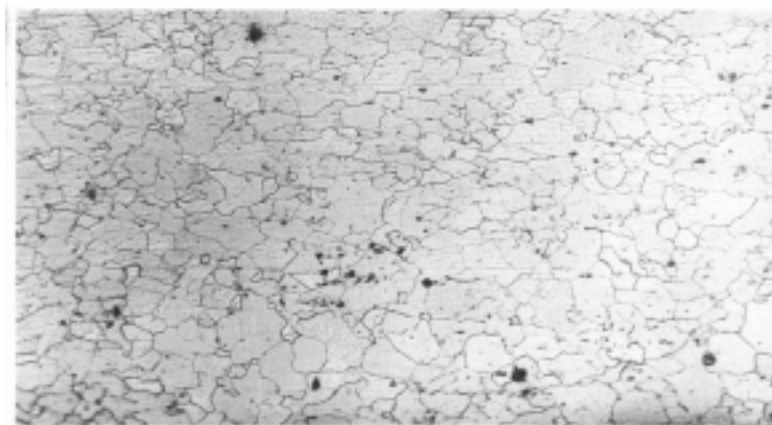


5% Nital etching

100:1

Medium grain diameter: 18 - 22 μm (size 9 – 10)

Fig. 3. The cold rolling strip microstructure achieved after recrystallization annealing (variant no. 1)



5% Nital etching

100:1

Medium grain diameter: 26 - 31 μm (size 7 - 8)

Fig. 4. The cold rolling strip microstructure achieved after recrystallization annealing (variant no. 2)

Table 2. The influence of hot-rolling regime upon the mechanical characteristics of cold-rolled sheet

Technological variant	Thickness of hot rolling sheet (mm)	Thickness of cold rolling sheet (mm)	Mechanical characteristics				
			$R_{p0,2}$ N/mm ²	R_m N/mm ²	A_{80} %	r_{90}	n_{90}
FePO ₄ EN10130-92	-	-	max. 210	270 - 350	min. 38	min. 1.60	min. 0.180
Variant 1	2.30-3.00	0.80-1.00	226 - 232	337 - 348	36.5- 37.0	1.49- 1.62	0.162- 0.170
Variant 2	2.30-3.00	0.80-1.00	158 - 164	276 - 285	40.0- 42.0	1.74- 1.82	0.200- 0.215

It can be noticed that in variant no.2 the increasing of granulation size is connected to a decrease of yield stress, $R_{p0.2}$, to values under 165 N/mm^2 and to an increase of fracture elongation, A_{80} , from 37% to above 40%.

The increase of hardening coefficient, n_{90} , to 0.200 and above, is also noticeable, the prescribed value in EN 10130-92 being minimum 0.180.

An increase of the normal anisotropy coefficient, r_{90} , to values of 1.70 and above are also encountered in the variant no. 2, due to intensifying of the (111) texture.

4. CONCLUSIONS

An improvement of the plasticity and deep-drawing characteristics of the cold-rolled sheets, above the prescribed level in the European norm EN 10130-92, can be obtained by:

- The optimization of reduction and temperature regime in hot-rolling on the bases of a mathematical modelling of the plastic deformation process;
- Adequate condition of cooling after hot rolling.

REFERENCES

1. Wolfgang Bleck, Rolf Bode: Stahl und Eisen 114 (1994) nr. 3, p. 61 - 67
2. Wolfgang Bleck: Stahl und Eisen 115 (1995) nr.4, p. 55 – 63
3. Pârvu Gh.: Teza doctorat 1980
4. Anan S: ISIJ International nr.3 / 1992

Received May 2, 2005

**METALLURGICAL RESEARCH INSTITUTE – ICEM S.A.
UNIVERSITY POLITEHNICA BUCHAREST**

ASPECTE PRIVIND CONTRIBUȚIA MODELĂRII MATEMATICE ASUPRA REGIMULUI DE
LAMINARE LA CALD ȘI LA RECE ȘI ASUPRA CONDIȚIILOR DE RĂCIRE ÎN VEDEREA
ÎMBUNĂTĂȚIRII CARACTERISTICILOR DE PLASTICITATE ALE BENZILOR DIN OȚELURI CU
CONȚINUT SCĂZUT DE CARBON

Rezumat

Realizarea unor caracteristici superioare de plasticitate a benzilor laminate la rece pentru ambutisare adâncă, la nivelul normei europene EN 10130 - 92, depinde în mare măsură de mărimea granulației și textura benzii laminate la cald.

Impunând o temperatură finală de laminare la cald de minim 860°C și grade de reducere de maxim 15% pe ultimele două treceri finisoare, precum și o răcire rapidă și intensă a benzii după laminare, care să asigure o temperatură de rulare de $520^\circ - 560^\circ \text{C}$, s-a putut obține o creștere a granulației (punctaj 7 - 8) și o intensificare a texturii (111), favorabilă ambutisării adânci.

Optimizarea reducerilor pe trecere și a temperaturilor a fost posibilă prin modelarea matematică a regimului de laminare la cald și a răcirii după laminare.

Din analiza mai multor modele matematice s-a confirmat de către rezultatele experimentale faptul că modelul propus de Anan este cel mai apropiat de condițiile industriale.

THE COMPUTER ASSISTED ESTABLISHING OF CREEP BEHAVIOUR AT 500 °C FOR THE STEEL 33MOCR11

by

DUMITRU MIHAI, MIHAI STEFAN AND GHEORGHE BADARAU

Abstract: The paper shows a new method of determination of the family of creep curves and its application for a 33 MoCr 11 steel. This computer assisted method enables more accuracy and reliability for the results obtained by using an original high quality mathematic apparatus.

Introduction

The use of steels at the building of some installations from the energetic industry, operated for a long time at high temperatures, imposes the knowing of their creep behaviour. In view of designing, machining and operating in safety conditions of such installations there are necessary many experimental determinations. A special place is being held by the long duration tests, the traction creep tests being the most used. A wide use is specific for the mild alloyed steels; in these steels Mo and V are being introduced for enhancing the creep behaviour and Cr is added to enhance the resistance to oxidation.

Methodology for establishing the function of a family of creep curves

For the evolution in time of the accumulation of plastic deformation at the constant temperature and constant tension it is proposed a function like:

$$\varepsilon_{plastic}(t) = Q.t + M(1 - e^{-N.t}) \quad (1)$$

where:

$\varepsilon_{plastic}$ - is the specific plastic deformation;

t - time ;

Q,M,N coefficients that depend on material, tension and temperature.

The values of the coefficients Q,M,N are determined on the basis of experimental results, applying the method of the smallest squares. For this purpose it was used a calculus program. Making creep tests for several initial tensions σ_i (four as a minimum), one can obtain the functions:

$$\varepsilon_{i\,plastic}(t) = Q_i.t + M_i(1 - e^{-N_i.t}) \quad (2)$$

In view of establishing a function for the creep family curves one extrapolates the results obtained for the coefficients Q_i, M_i, N_i .

$$\varepsilon_{plastic}(t) = Q.t + M(1 - e^{-N.t})$$

This relation represents the equation of a surface generated by the creep curves at the T temperature.

Developing in a Mac- Laurin series:

$$e^{-N.t} = 1 - \frac{N.t}{1!} + \frac{(N.t)^2}{2!} - \frac{(N.t)^3}{3!} + \dots + \frac{(-1)^n}{n!} (N.t)^n + R_n \quad (3)$$

$$\varepsilon_{plastic}(t) = A_0 + A_1.t + A_2.t^2 + A_3.t^3 + A_4.t^4 + A_5.t^5 + A_6.t^6 + A_7.t^7 \quad (4)$$

The specific plastic deformation can be computed with the relations (1) and (4), from the graphs, it result they are convergent.

The determination of the function of the family of creep curves for the steel 33MoCr11 at 500 °C

The chemical composition of the studied steel, determined by the spectral method with a Quantovac type equipment is shown in table 1.

Table 1 The chemical composition of the steel 33MoCr11

33MoCr11	C %	Si %	Mn %	Cr %	Mo %
STAS 791-80	0,3-0,37	0,17-0,37	0,40-0,80	0,90-1,30	0,15-0,25
Sample	0,36	0,35	0,63	1,26	0,18

For determining the mechanical characteristics there have been made tests for traction at two temperatures 20⁰ C and 500⁰ C . Tests were made according to the prescriptions from SR EN 10002-1994 for the tests at environmental temperature and SR EN 10002-5 - 1995 for the tests made at high temperatures. Tests results are given in table 2.

Table 2 Mechanical properties in given testing condition

Material	Temperature [⁰ C]	R _{p02} [MPa]	R _m [MPa]	A _{11,3} [%]
33MoCr11	20	650	850	12
	500	425	610	21

For the creep tests there were used samples having the shape and the sizes foreseen in STAS 6596-81 and there were conducted on a MF – 300 installation.

The heating of the sample was achieved by using an electric furnace, the temperature being measured with three thermocouples Pt – PtRh . The maintaining and the regulation of the temperature were done with an electronic regulator that ensures the nominal testing temperature $\pm 2^0 C$ during the whole period of the test.

The measurement of the deformations (elongations) was done with a mechanic extensometer that ensures a precision of 1µm. There were made creep tests at the following tensions 200 MPa, 300 MPa , 350 MPa and 400 MPa . The results of these tests are shown in figures 1, 2,3,4 .

One can see that the creep speed enhances very much at tensions overcoming 400 MPa.

Tests made at the tensions 430 MPa and 500 MPa were made until breaking. The breaking elongations A_n and the creep necking Z , as well as the duration until breaking t_R are given in table 3.

Table 3 The breaking elongations A_n , the creep necking Z and the duration until breaking t_R as a function of tension

Tension [MPa]	t_R [min]	A_n [%]	Z [%]
430	295	25	70
500	26	18	68

The following creep curves were obtained:

- for $\sigma = 200MPa$

$\varepsilon_{plastic}(t) = \beta(t)$; $\varepsilon_{plastic}(t) = o(t)$, time is given in hours (h).

ORIGIN $\equiv 1$

x := $\left(\begin{array}{c} 0 \\ 0.833 \\ 1.66 \\ 2.5 \\ 3.33 \\ 4.166 \\ 5 \\ 5.83 \\ 6.66 \\ 7.5 \\ 8.33 \\ 9.66 \\ 10 \end{array} \right)$

$$y := \begin{pmatrix} 0 \\ 0.714 \cdot 10^{-3} \\ 1.071 \cdot 10^{-3} \\ 1.3214 \cdot 10^{-3} \\ 1.42 \cdot 10^{-3} \\ 1.4285 \cdot 10^{-3} \\ 1.785 \cdot 10^{-3} \\ 1.7857 \cdot 10^{-3} \\ 1.9642 \cdot 10^{-3} \\ 1.9928 \cdot 10^{-3} \\ 2.142 \cdot 10^{-3} \\ 2.1428 \cdot 10^{-3} \\ 2.3214 \cdot 10^{-3} \end{pmatrix}$$

$$n := \text{length}(x)$$

$$m := 7$$

$$i := 1..n$$

$$k := 1..2 \cdot m + 1$$

$$s_k := \sum_i [(x_i)^{k-1}]$$

$$k := 1..m + 1$$

$$b_k := \sum_i y_i \cdot [(x_i)^{k-1}]$$

$$i := 1..m + 1$$

$$j := 1..m + 1$$

$$a_{i,j} := s_{i+j-1}$$

$$c := a^{-1} \cdot b$$

$$c = \begin{pmatrix} -1.334 \times 10^{-6} \\ 1.166 \times 10^{-3} \\ -4.412 \times 10^{-4} \\ 1.007 \times 10^{-4} \\ -1.484 \times 10^{-5} \\ 1.683 \times 10^{-6} \\ -1.325 \times 10^{-7} \\ 4.657 \times 10^{-9} \end{pmatrix}$$

$$w(t) := 4.657 \cdot 10^{-9} \cdot t^7 - 1.325 \cdot 10^{-7} \cdot t^6 + 1.683 \cdot 10^{-6} \cdot t^5 - 1.484 \cdot 10^{-5} \cdot t^4$$

$$n(t) := -4.412 \cdot 10^{-4} \cdot t^2 + 1.166 \cdot 10^{-3} \cdot t - 1.334 \cdot 10^{-6} + 1.007 \cdot 10^{-4} \cdot t^3$$

$$o(t) := w(t) + n(t)$$

$$t := 0, 0.0543 \dots 10$$

$$\beta(t) := 1.25980149421483 \cdot 10^{-4} \cdot t + 1.0578699617622 \cdot 10^{-3} (1 - e^{-Ct})$$

$$C := 1.01869818391696$$

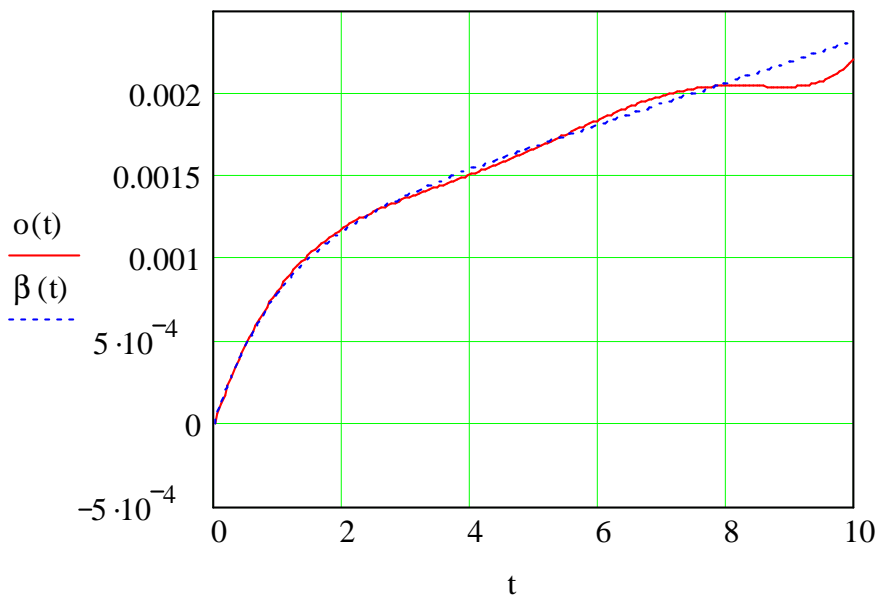


Figure 1

- for $\sigma = 300MPa$

$$\varepsilon_{plastic}(t) = \beta(t); \quad \varepsilon_{plastic}(t) = o(t)$$

ORIGIN $\equiv 1$

$$x := \begin{pmatrix} 0 \\ 0.833 \\ 1.66 \\ 2.5 \\ 3.33 \\ 4.166 \\ 5 \\ 5.83 \\ 6.66 \\ 7.5 \\ 8.33 \\ 9.66 \\ 10 \end{pmatrix}$$
$$y := \begin{pmatrix} 0 \\ 2.1428 \cdot 10^{-3} \\ 2.8928 \cdot 10^{-3} \\ 3.5714 \cdot 10^{-3} \\ 4.2857 \cdot 10^{-3} \\ 4.6428 \cdot 10^{-3} \\ 5.3571 \cdot 10^{-3} \\ 5.7142 \cdot 10^{-3} \\ 6.4285 \cdot 10^{-3} \\ 6.7867 \cdot 10^{-3} \\ 7.5 \cdot 10^{-3} \\ 7.8571 \cdot 10^{-3} \\ 8.5714 \cdot 10^{-3} \end{pmatrix}$$
$$n := \text{length}(x)$$
$$m := 7$$

$$i := 1..n$$

$$k := 1..2 \cdot m + 1$$

$$s_k := \sum_i [(x_i)^{k-1}]$$

$$k := 1..m + 1$$

$$b_k := \sum_i y_i \cdot [(x_i)^{k-1}]$$

$$i := 1..m + 1$$

$$j := 1..m + 1$$

$$a_{i,j} := s_{i+j-1}$$

$$c := a^{-1} \cdot b$$

$$c = \begin{pmatrix} 2.014 \times 10^{-7} \\ 4.513 \times 10^{-3} \\ -3.408 \times 10^{-3} \\ 1.582 \times 10^{-3} \\ -4.022 \times 10^{-4} \\ 5.6 \times 10^{-5} \\ -3.997 \times 10^{-6} \\ 1.141 \times 10^{-7} \end{pmatrix}$$

$$w(t) := 1.141 \cdot 10^{-7} \cdot t^7 - 3.997 \cdot 10^{-6} \cdot t^6 + 5.6 \cdot 10^{-5} \cdot t^5 - 4.022 \cdot 10^{-4} \cdot t^4$$

$$n(t) := 1.582 \cdot 10^{-3} \cdot t^3 - 3.408 \cdot 10^{-3} \cdot t^2 + 4.513 \cdot 10^{-3} \cdot t + 2.014 \cdot 10^{-7}$$

$$o(t) := w(t) + n(t)$$

$$t := 0, 0.0543..10$$

$$\beta(t) := 6.51819504563946 \cdot 10^{-4} \cdot t + 1.99574903419039 \times 10^{-3} (1 - e^{-Ct})$$

$$C := 1.84161907030211$$

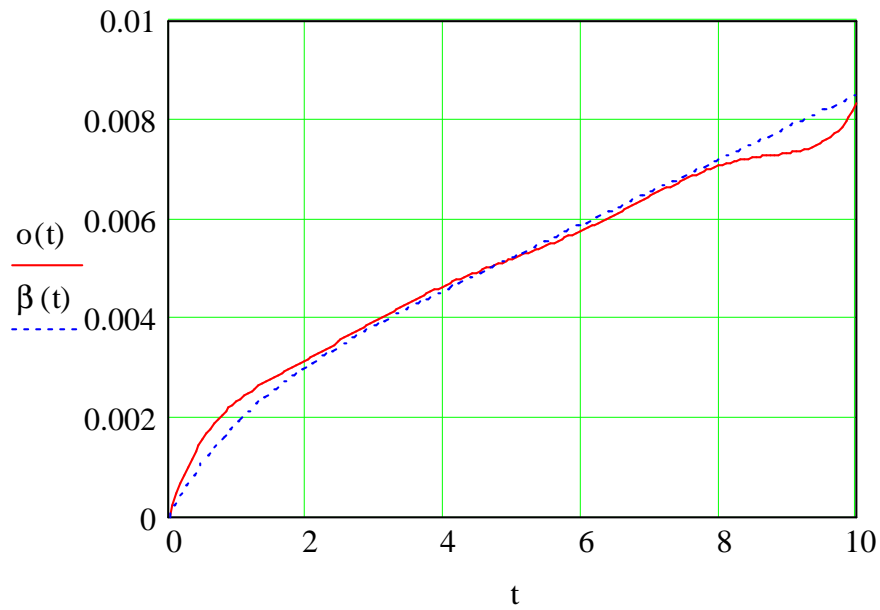


Figure 2

- for $\sigma = 350MPa$

$$\varepsilon_{plastic}(t) = \beta(t); \quad \varepsilon_{plastic}(t) = o(t)$$

ORIGIN \equiv 1

x :=

0
0.833
1.66
2.5
3.33
4.166
5
5.83
6.66
7.5
8.33
9.66
10

$$y := \begin{pmatrix} 0 \\ 3.75 \cdot 10^{-3} \\ 4.8214 \cdot 10^{-3} \\ 6.25 \cdot 10^{-3} \\ 6.964 \cdot 10^{-3} \\ 7.678 \cdot 10^{-3} \\ 8.75 \cdot 10^{-3} \\ 9.821 \cdot 10^{-3} \\ 10.535 \cdot 10^{-3} \\ 11.25 \cdot 10^{-3} \\ 12.85 \cdot 10^{-3} \\ 13.75 \cdot 10^{-3} \\ 14.64 \cdot 10^{-3} \end{pmatrix}$$

$n := \text{length}(x)$

$m := 7$

$i := 1..n$

$k := 1..2 \cdot m + 1$

$s_k := \sum_i [(x_i)^{k-1}]$

$k := 1..m + 1$

$b_k := \sum_i y_i \cdot [(x_i)^{k-1}]$

$i := 1..m + 1$

$j := 1..m + 1$

$a_{i,j} := s_{i+j-1}$

$c := a^{-1} \cdot b$

$$c = \begin{pmatrix} 9.424 \times 10^{-6} \\ 7.371 \times 10^{-3} \\ -4.999 \times 10^{-3} \\ 2.085 \times 10^{-3} \\ -4.855 \times 10^{-4} \\ 6.304 \times 10^{-5} \\ -4.251 \times 10^{-6} \\ 1.157 \times 10^{-7} \end{pmatrix}$$

$$w(t) := 1.157 \cdot 10^{-7} \cdot t^7 - 4.251 \cdot 10^{-6} \cdot t^6 + 6.304 \cdot 10^{-5} \cdot t^5 - 4.855 \cdot 10^{-4} \cdot t^4$$

$$n(t) := 2.085 \cdot 10^{-3} \cdot t^3 - 4.999 \cdot 10^{-3} \cdot t^2 + 7.371 \cdot 10^{-3} \cdot t + 9.424 \cdot 10^{-6}$$

$$o(t) := w(t) + n(t)$$

$$t := 0, 0.0543 \dots 10$$

$$\beta(t) := 1.1502697426546 \cdot 10^{-3} \cdot t + 3.05171457769499 \times 10^{-3} (1 - e^{-Ct})$$

$$C := 2.89842273492303$$

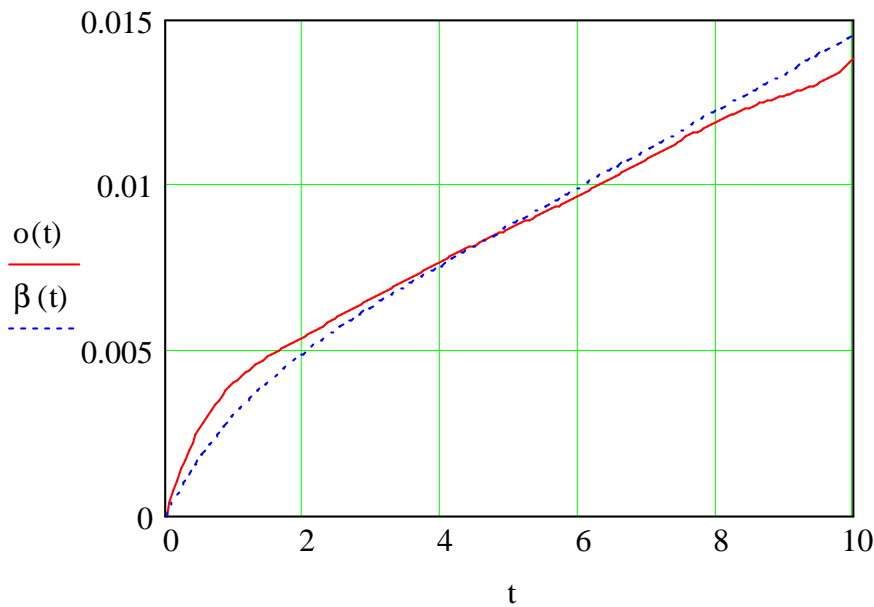


Figure 3

- for $\sigma = 400MPa$

$$\varepsilon_{plastic}(t) = \beta(t); \quad \varepsilon_{plastic}(t) = o(t)$$

ORIGIN \equiv 1

$$x := \begin{pmatrix} 0 \\ 0.833 \\ 1.66 \\ 2.5 \\ 3.33 \\ 4.166 \\ 5 \\ 5.83 \\ 6.66 \\ 7.5 \\ 8.33 \\ 9.66 \\ 10 \end{pmatrix}$$
$$y := \begin{pmatrix} 0 \\ 5.178 \cdot 10^{-3} \\ 6.928 \cdot 10^{-3} \\ 8.392 \cdot 10^{-3} \\ 9.821 \cdot 10^{-3} \\ 10.535 \cdot 10^{-3} \\ 12.321 \cdot 10^{-3} \\ 13.75 \cdot 10^{-3} \\ 14.821 \cdot 10^{-3} \\ 16.071 \cdot 10^{-3} \\ 17.857 \cdot 10^{-3} \\ 19.285 \cdot 10^{-3} \\ 20 \cdot 10^{-3} \end{pmatrix}$$

$n := \text{length}(x)$

$m := 7$

$i := 1..n$

$k := 1..2 \cdot m + 1$

$s_k := \sum_i [(x_i)^{k-1}]$

$k := 1..m + 1$

$b_k := \sum_i y_i \cdot [(x_i)^{k-1}]$

$i := 1..m + 1$

$j := 1..m + 1$

$a_{i,j} := s_{i+j-1}$

$c := a^{-1} \cdot b$

$$c = \begin{pmatrix} 8.49 \times 10^{-6} \\ 9.925 \times 10^{-3} \\ -6.195 \times 10^{-3} \\ 2.355 \times 10^{-3} \\ -5.019 \times 10^{-4} \\ 6.043 \times 10^{-5} \\ -3.826 \times 10^{-6} \\ 9.874 \times 10^{-8} \end{pmatrix}$$

$w(t) := 9.874 \cdot 10^{-8} \cdot t^7 - 3.826 \cdot 10^{-6} \cdot t^6 + 6.043 \cdot 10^{-5} \cdot t^5 - 5.019 \cdot 10^{-4} \cdot t^4$

$n(t) := 2.355 \cdot 10^{-3} \cdot t^3 - 6.195 \cdot 10^{-3} \cdot t^2 + 9.925 \cdot 10^{-3} \cdot t + 8.49 \cdot 10^{-6}$

$o(t) := w(t) + n(t)$

$t := 0, 0.0543..10$

$\beta(t) := 1.59659754874751 \cdot 10^{-3} \cdot t + 4.3107448362346 \times 10^{-3} (1 - e^{-Ct})$

$C := 2.69918925716663$

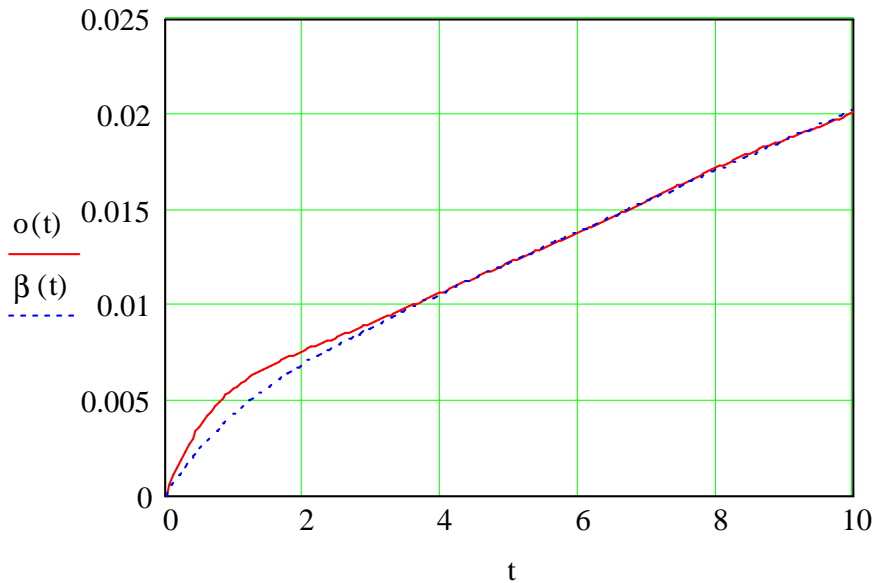


Figure 4

Conclusions

The methodology shown is especially useful for the establishing of the function of the family of creep curves at a certain temperature, by making a restrained number of tests. Having in view the lack of experimental data referring to the creep behaviour of the mild alloyed steels it is necessary to extend it to other steel brands and other temperature recommended for thermal power plants.

Received March 12, 2005

Faculty of Mechanics
Faculty of Materials Science and Engineering

References

1. Constantinescu, A., rotenstein, B., Lascu-simion, N., Fluajul metalelor, Editura Tehnica, Bucuresti, 1970
2. Mocanu, D.R., s.a., Incercarea materialelor, vol 1, Editura Tehnica, Bucuresti, 1982
3. Vernon, J, Testing of materials, McMillan, London, 1992
4. Mihai, Dtru., Influence of the exposure temperature and time on some pipe steels used for live steam transport, European journal of Mechanical and Environmental engineering, vol. 46, nr. 3, 2001, p. 185, Bruxelles 5, Belgia
5. Mihai, Dtru., Bujoreanu, L.Gh., Mechanical properties degradation in a Cr-Mo low alloy steel pipe after prolonged use for gas transport in a power station, Rev. Metalurgia, Madrid 38 (2002)
6. Mihai, Dtru., Effects of a long exposure at elevated temperatures and pressures 151211 steel, 15 - 175, Ostrava, Metal 2001, Czech republic
7. Mihai, Dtru., fiabilitatea conductelor din otel 15123, utilizate la transportul aburului viu in termocentrale, Cercetari metalurgice si de noi materiale, vol IX, nr. 3, 2001.

COMPORTAREA LA FLUAJ LA 500 °C A OTELULUI 33MOCR11

Rezumat: Lucrarea prezinta o noua metoda de determinare a curbelor de fluaj si aplicarea ei la otelul 33MoCr11. Aceasta metoda asistata de calculator permite obtinerea cu mai mare acuratete si incredere a rezultatelor. Prin utilizarea unui aparat mathematic original de inalta calitate.

THE MYTHOLOGY OF METALS IN MIRCEA ELIADE'S WORK

by

GHEORGHE COMAN

***Abstract.** The paleoanthropics' and the hominians' mythologies are based on the interpretation that everything is the result of a love between a masculine entity and a feminine entity, that everything grows, and dies. This concept witnesses the lapse of time until our ages through the Hellenic and Arabic alchemic texts which tell about the "torture" of metals in order to reach their "maturation" from ores, and then their processing. The phenomenon is taken over from the elaborated mystics itself of the Alexandrian and Christian world – that eternal life cannot be achieved but with sufferings and death.*

Object and motivation of this study

In an interview about Mircea Eliade (1907-1986), the French philosopher, Edgar MORIN, said: "For me, Eliade was not simply a mythologist, but an authentic myth". And, indeed, Mircea Eliade became a legend, a myth while he was still alive.

Why mythology? Because, as Mircea Eliade mentions: "The myths are perfectly true histories which explain how a reality, be it the cosmos in its entirety, or one of its aspects, came into being as a consequence of the super-human beings' deeds. The myth is eminently a sacred history because it tells about the gods' and the other superhuman beings' activity. The myths also depict the emergence of the sacred into the world, an emergence which, in fact, founds the world. The myths always refer to a creation; they show how something came into being: the cosmos, the earth, the human being, an institution, or a behaviourist pattern. In this regard, the myths represent paradigms for fundamental human acts".

In his vast work, among the mythical topics he was interested in there is one concerning the mythology of metals. It seems natural to us just by considering the fact that metals had and still have an important place in the development, progress, and maintenance of the human civilization. The periodization of human history itself is thought, from a certain point of view, in accordance with the nature of the used materials for the tools making: the stone age, the age of bronze and the age of iron which, considered as a whole, may merge into the age of metals, resulting in the "Civilisation of Metal", as a TV show was named after.

The mythology of metals seems fascinating to us, first of all because in its context one may encounter the still unseparated "practices" related to mythological rites and other ones related to the handicrafts norms which will generate the bases of science founding in time. In Mircea Eliade's language, we find a sort of "underground conflict" here. From his point of view, "to follow the history of the underground conflict between the "mystical" experiencing and the "scientific" experiencing means to acknowledge all transformations which led to the birth of modern world. It is a fascinating and dangerous issue, which cannot be dwelled upon but by resorting to a whole arsenal of facts and documents, and a lot of sense of criticism".

In the current study we will refer to some ideas which present this “underground conflict“ between mythology and science throughout the long history of discovering and using the metals existing in the surrounding nature with a human purpose.

The Civilisation of Metals: the First Manifestations

The transition from the civilisation of stone to the bronze one meant a gigantic step for the human civilisation. The civilisation of bronze follows the iron one which provides the germs of modern civilisation. This is known as the civilisation of the cast iron and steel, both of them based on the preponderant use of iron in their structure.

The first iron samples known by the people originated in the meteoritic iron. Mircea Eliade mentioned that “the meteorites made a strong impression on the primitive man’s mind”[1]. Concerning this topic, Mircea Eliade writes as follows: “The meteoritic origin of the metals bestow them, of course, various magic qualities. The metals – be they directly from the Sky (by meteors) or discovered in the core of the Earth – were infused with magic powers. That is why not everyone could work with them. The metallurgical rites [...] had a very well established magic function. In fact, these beliefs related to metallurgy are met not only in the Mesopotamian cultures. In China and in India, the boiling vessels for melting the ores and the “initiates” in know of the rites maintained a sacred aura around them, fed and guarded by magic powers... Those who work with metals are in connection with mysterious forces, be they of meteoric origin or from the earth. In the first instance, the metal is charged with all the Sky’s virtue from whose canopy it was separated, and the second instance, the ore is uprooted from the matrix of Mother Earth before time, and this almost gynaecologic operation was extremely dangerous because of the magic power which was discharged during the said intervention”[2]. “In metallurgy, the Indian proved to be exquisite technicians. The iron column in Kutab of at least 1,500 years is the most thick column which could be obtained in the whole world until the 17th century A.C. The chemical analyses proved that the iron was pure, unmixed. Metallurgy was one of the ancient India glories. The metallurgic texts available to us present us a highly advanced technique, empiric, almost industrial. In spite of all that, we should not forget that in India, like in other regions, too, metallurgy was a “sacred” activity from the very the beginning. It is true there are not many texts left; nevertheless, Rig Veda keeps the tradition of some vegetable drugs owned by the blacksmiths and which allow us to infer the obscure connections between magic, mystics, and metallurgy”[7].

Metallurgy was a sacred art everywhere. That was due to the fact that metals were not one of the “profane gifts“ of human’s existence. They originated in extraterrestrial areas: they were send either by Heaven or uprooted from the “underground matrix” – the metals always came from “the other world”. From this point of view, the primitive logic of the archaic cultures seems to be coherent in the case, too. Everything which does not belong naturally to man, everything which cannot be found around him, everything which does not participate in the “Adamic condition of existing” is mysterious, sacred, or daemonic, because it changes its nature. This is the authentic, primordial significance of all faiths as far as metallurgy is concerned: metals change the human’s nature by modifying his existence conditions. And, on the one hand, this modification is fulfilled because it annuls the paradisiac

state (the stage of fruit and seed reapers) by creating a new state – and, on the other hand, because the presence of metals itself in the human society brings along unknown magic forces which are out of number, belonging to other cosmic levels, and the game of these obscure forces (sacred or daemonic) reveals other horizons to the human soul and it allows him to have other experiences [3].

The discovery of metals and the invention of metallurgic methods of smelting them from ores, as well as their subsequent processing by altering the form and casting, had as a consequence important modifications in the structure of the human community mental.

First of all, it was considered that, in comparison with the meteoric iron, the ores represent an incomplete “gestation” of the metal, and the metallurgical process acts as an accelerating factor in the process of the product maturation. This maturation and perfection of the finished product is achieved after a suffering and sacrifice process endured by the subject, therefore it was transposed in the human being's "maturation" process. “Each new modification of the human structure means a new fructification of conscience in a certain way - thus the man having acquired new experience fields and having discovered analogies between different cosmic levels”[4]. From this point of view, maybe it is significant the fact that the first systematic studies on man and his ages combine with the image of the historical ages named after the used metals. We refer to Hesiod and his *Days and Nights*.

The modification of the human mental based on some mythology of the surrounding nature which comprises not only the metallurgical phenomenon seems to be the factor which led to discovering the sacred. Mircea Eliade stated that each manifestation of the sacred is important in assessing the evolution of human mental; any rite, any myth, any faith or divine character reflects the experience of the sacred and, implicitly, the concepts of being, significance, and truth. “It is difficult for us to imagine how the human spirit might function without having the conviction that something irreducibly real exists in the world; and it is impossible to imagine how conscience may appear without conferring a certain significance to human's impulses and experiences. The awareness of a real and significant world is closely related to the discovery of the sacred. Through the existence of the sacred, the human spirit noticed the difference between what is revealed as being real, powerful, rich, and significant, and what is deprived of these qualities, that is the chaotic and perilous passing of things, their fortuitous apparitions and disappearances deprived of any significance”. On the most archaic levels of culture, to live like a human being is a religious act in itself, because the alimentation, the sexual life and labour have a sacramental value. In other words, to be or rather to become human means to be “religious”.

In the agriculturalists' religions, the origin of cereals is divine; the cereal offering to the people is often related to a herogamy relation between the god of heaven and Mother Earth, or to the mythical drama involving copulation, death, and resurrection. The fertility of the earth is solidary with the feminine fecundity. The agricultural civilisations elaborate what might be called a cosmic religion, because the religious activity is focused on the main mystery: the periodical renewal of Moon.

This herogamy is taken into consideration in the case of metals, too. The following lines are from the period of the middle ages alchemy: “The world conceived seven metals / as planets seven are alike, / And the cosmos gave us to use / Both the

iron and the copper, and the silver. / Both the tin and the gold, and the lead... / My child! / Their father is the sulphur. / And now, hurry, son, to find out / That the mother of all is the mercury”.

These lines reverberate of the medieval belief according to which the growth or the regeneration of a metallic ore requires a parent and a matrix who should be capable of receiving the generating action. These functions were carried out by the two chemical elements mentioned in the lines, the sulphur and the mercury. By mixing the mercury and the sulphur with the ore, the sulphur behaves as masculine seed, and the mercury as feminine seed in conceiving and “giving birth to a child”. For the “easy confinement of the ore” it is required a kind of natural vessel, like the lodes, where the ore is conceived. The golden ore is confined by the action of Heaven, especially that of the Sun, without the intervention of fire. The copper ore is conceived under the influence of planet Venus, the iron ore under the influence of Mars, the lead ore grows under the influence of Saturn, etc. Each known metallic element was the beneficiary of a cosmic association: gold-sun; silver-moon; mercury-mercury; copper-Venus; iron-Mars; tin-Jupiter; lead-Saturn [8]. There can be noticed a harmonious association between the alchemic mysticism and the metallurgical techniques.

Since the Neolithic age and till the iron age, the history of ideas and religious beliefs is the same with the history of civilisation. Each technological discovery, each economical and social invention, etc. seems to be “doubled” by a religious significance and value.

The “mythology of metals” followed the “mythology of grinded stone”, the richest and the most characteristic one being elaborated and based on iron. The metallurgy of the terrestrial iron is what made this metal be suitable for everyday use. This aspect had important religious consequences. The metals “grow in the core of the earth”. The caves and the mines are associated to the matrix Mother-Earth.

All the mines and mountains mythologies, the numerous fairies, genii, elves, phantoms, and spirits are multiple epiphanies of the sacred presence the man is faced with in his intent to reach the geological levels of Life. In numerous mythologies, the divine blacksmiths make at a forge the gods' weapons, thus insuring their victory against the Dragons and other monstrous Beings. All these ideas and beliefs focused on the profession of mine workers, metallurgists, and blacksmiths considerably enriched the *homo faber's* mythology as it was inherited from the stone age.

Mircea Eliade's philosophy has been always concerned about discovering the sacred. For him, the sacred is an element in the structure of conscience and not a stage in the history of this conscience.

It cannot be written a history of a spiritual creation category before presenting its structure and morphology. “The History of Beliefs and Religious Ideas” is, above all, a history, and not a personal interpretation of the different religions presenting it. Mircea Eliade stated when referring to this book – “I have written this book to present what happened during the historical time, resorting to some intuitions, experiences and religious ideas which contributed to the human condition building from the prehistoric times and until the beginning of our age”.

The paleoanthropics' and the hominians' mythologies are based on the interpretation that everything is the result of a love between a masculine entity and a feminine entity, that everything grows, and dies. This concept witnesses the lapse of

time until our ages through the Hellenic and Arabic alchemic texts which tell about the “torture” of metals in order to reach their “maturation” from ores, and then their processing. The phenomenon is taken over from the elaborated mystics itself of the Alexandrian and Christian world – that eternal life cannot be achieved but with sufferings and death. According to the Arabic alchemy, one cannot hope for the Eternal Life without enduring suffering and death – and the archaic traditions of the Creation tell that man and all living things were made out of god’s blood, through his death, through his sufferings. Also, the buildings raised by the man’s hand cannot last (cannot have an “eternal life” in the matter sense of speaking) unless someone, human or animal, is sacrificed at their foundation. We talk here about the redeeming suffering, the voluntarily experienced death so that one may be granted eternal life – significances which were discovered and made more profound with the emergence of Christianity. But, however, they were preceded by a long Oriental tradition[5].

As a first conclusion, we present one of Mircea Eliade’s remarks: “... the great discoveries – metallurgy, agriculture, the calendar, the “law” etc. – significantly modified the human condition. But the subtle dynamics of this modification and its implications failed to be understood. Indeed, for each fundamental new discovery, the human being enlarges not only the domain of empiric knowledge and renews his means of subsistence, but he discovers a new cosmic level, he experiences another order of reality. It was not the discovery of metals as such the fact which entailed the mental evolution, but the “presence” of metals, by means of which the human being discovers another cosmic level, that is he gets in touch with unknown realities or realities left unknown until then. In other words, metallurgy – like agriculture, etc. – causes mental syntheses which radically modify the human condition by modifying its representation about the Cosmos”. He appreciates that: “... metals change the human nature by modifying his existence conditions. And the said modification is fulfilled, on one hand, because it annuls the paradisiac stage (the stages of the fruit and seed reapers) creating instead a new stage – and on the other hand, because the presence of metals itself in human society brings along numerous unknown magic forces belonging to other cosmic levels, and this game of obscure forces (sacred or daemonic) reveals to the human soul other horizons and allows it to have new experiences”[6].

Received May 3, 2005

Universitatea „Ștefan Lupășcu” Iași

References.

- [1] **Eliade Mircea**, *Babylonian Cosmology and Alchemy*, Iasi, “Moldova” Publishing House, 1991, p.49
- [2] **Eliade Mircea**, *Babylonian Cosmology and Alchemy*, Iasi, “Moldova” Publishing House, 1991, p.52-54
- [3] **Eliade Mircea**, *Babylonian Cosmology and Alchemy*, Iasi, “Moldova” Publishing House, 1991, p.58
- [4] **Eliade Mircea**, *Babylonian Cosmology and Alchemy*, Iasi, “Moldova” Publishing House, 1991, p.79
- [5] **Eliade Mircea**, *Babylonian Cosmology and Alchemy*, Iasi, “Moldova” Publishing House, 1991, p.81
- [6] **Eliade Mircea**, *Asian Alchemy*, Bucharest, “Humanitas” Publishing House, 1991, p.73, 117
- [7] **Eliade Mircea**, *The Way to the Core*, Bucharest, “Univers” Publishing House, 1991, p.602
- [8] **Coman Gheorghe**, *The Study of Metals*, Polytechnic Institute of Iasi, I – 1986; II – 1987.

MITOLOGIA METALELOR ÎN OPERA LUI MIRCEA ELIADE

Mitologiile paleantropilor și hominienilor au la bază interpretarea că totul se naște din iubire între o entitate masculină și o entitate feminină, crește și moare. Această concepție străbate timpul până la noi prin textele alchimice helenistice și arabe care vorbesc de „tortura” metalelor pentru „maturizarea” lor din minereuri și apoi prelucrarea acestora. Fenomenul este preluat chiar de mistica elaborată de lumea alexandrină și creștină – că viața eternă nu poate fi obținută fără suferință și fără moarte.

**AUTHENTICATION OF ANCIENT BRONZE COINS
I. ASPECTS CONCERNING
THE COMPOSITION OF THE PATINA**

by

**ION SANDU¹, DAN GELU GĂLUSCĂ², IOAN CARCEA², MIHAI ȘTEFAN², ANDREI
VICTOR SANDU²**

***Abstract** – The paper presents the chemistry of the main compounds from the structure of patina of ancient bronze coins, which results from the corrosion, respectively from pedological processes and also from contamination, while are held in collections or in archeological sites. The comparative study of the main types of compounds resulted from corrosion and from contamination permits the selection of mineral phases by microscopy and their chemical analysis.*

***Keywords:** surface corrosion, pedological process, corrosion products, contaminants, mineral phases*

1. Introduction

There is known that the ancient bronze coins have in the main alloy composition, among the fourth elements: Cu, Sn, Zn and Pb a series of microelements, resulted from minerals, as are: Fe, Si, As, Sb, Al, P and others. In time, those suffer two types of proceses: surface corrosion and pedological processes. The corrosion is happening at the exposure in the museum and also in archeological sites. The pedological processes are happening just in archeological sites [1-3].

In the conservation and valorization of ancient coins, from collections and new discovered in archeological sites, the knowledge of the composition of the patina has an important role, with multiple practical implication in authentication and in restoration processes [1-3]. So, the problem is related to the question: are the materials corrosion products, are they common outdoor contaminants or are they from a past treatment? The results presented here provide an example of what materials can be found on outdoor bronzes and, more importantly, there is a discussion of the possible source of these materials.

This paper is intended to form part of a series of reviews on current knowledge concerning the corrosion products of copper alloys, their occurrence on ancient coins.

2. Compounds resulted from copper corrosion

The main copper compounds identified in the patina ancient bronze coins were: oxides, hydroxides, carbonates, sulphides, chlorides, sulphates and other.

2.1. Copper oxides and redeposited copper

Cuprite (Cu_2O , a copper(I) oxide) was a common corrosion product, identified in the patina layer. Cuprite is almost equally distributed between exposed, partly exposed and sheltered areas, and the greatest quantity of cuprite was identified on bronze coins. **Tenorite** (CuO) was identified only on some surface of ancient coins. On out-door copper and copper alloys, cuprite is a common corrosion product [4], usually found next to the metal surface [5].

Along with the copper oxides identified, copper metal was also detected in low quantities. The copper is probably redeposited metal resulting from the decomposition of cuprite. Thermodynamically, cuprite is stable with respect to tenorite and copper [5], but in dilute acids cuprite becomes unstable and copper(I) ions can disproportionate into copper(II) ions and metallic copper [5,6]. Light may also play a role in promoting the photoreduction of cuprite to metallic copper [6]. A factor contributing to copper formation may have been corrosion processes that took place during indoor storage of the samples before they were analyzed.

2.2. Copper carbonates

Ancient bronze coins (before Xth century) contain copper carbonates. After the Xth century non contain copper carbonates in any of the surface samples. The basic copper carbonates, **green malachite** $\text{Cu}_2(\text{OH})_2\text{CO}_3$ and **blue azurite** $\text{Cu}_3(\text{OH})_2(\text{CO}_3)_2$, are often identified on archaeological bronzes coins [7] but only rarely are they found on outdoor bronzes coins [8]. The formation of azurite and malachite on buried copper alloys is promoted by high levels of carbonate ions in groundwater, with azurite favoured at higher carbonate levels [9]. Although basic copper carbonates can form on copper exposed to the atmosphere, the formation of other basic copper compounds is usually favoured because of the higher relative concentrations of sulphate ions and chloride ions.

2.3. Copper sulphides

Ten of the 25 coins contained crystalline copper sulphides. **Chalcocite** (Cu_2S) was identified six times, **Geerite** (Cu_8S_5 or $\text{Cu}_{1.6}\text{S}$) was detected three and **djurleite** ($\text{Cu}_{31}\text{S}_{16}$ or $\text{Cu}_{1.94}\text{S}$) was found once. These sulphides were identified on coins made after Xth century and were identified about equally in samples from exposed, partly exposed and sheltered areas. It has been suggested that the black areas on outdoor bronze coins consist principally or partly of copper sulphides [10], which are hard to be identified. Although crystalline copper sulphides have been identified in other studies, they were usually only minor componenta. There are several different ways these copper sulphides could have formed. **Chalcocite** is known to form when copper is exposed to air containing hydrogen sulphide (H_2S) [11], a common pollutant from pulp and paper mills. (Another possible, although unlikely, source of H_2S could have been sulphate-reducing bacteria growing in anaerobic conditions under the surface corrosion. Such copper sulphide formation due to sulphate-reducing bacteria has been noted on archaeological bronzes [12].) Chalcocite could also have formed through

oxidation-reduction reactions involving copper and sulphur dioxide [13], Finally, a dark layer of copper sulphides could have been produced artificially by the chemical patination of the bronze surface using potassium, sodium or ammonium sulphides [14].

2.4. Copper chlorides

Seven copper chlorides were identified in 10 surface samples (70%), generally on coins from sea sites. This high percentage was surprising because chloride-containing corrosion products are normally associated with a marine environment [4]. If the site is not close to the sea and its precipitation does not contain significant amounts of chloride ions, the copper chlorides must not be present in the patina. In the areas where precipitation contained an average chloride ion concentration of $0,2 \text{ mg}\cdot\text{l}^{-1}$ compared to an average sulphate ion concentration of $3,0 \text{ mg}\cdot\text{l}^{-1}$, there could be found copper chlorides [3]. From the copper chlorides the most frequent found are Cu_2Cl_2 (**nantokite**) and CuCl_2 . Out of 100 ancient coins, extracted from sea, more than 30 contained cuprous chloride or nantokite. This particular sample also contained calcium chloride hydrate. Nantokite is a naturally occurring, pale grey, wax-like mineral [15] with low solubility in water [16]. It forms under conditions of plentiful chloride ion concentration, acidity and reducing (low oxygen) conditions [17]. In moist air, nantokite is unstable and it reacts with oxygen and water to produce basic copper chlorides and hydrochloric acid [16]. Only rarely has nantokite been identified on outdoor bronzes [3]. It is believed, however, that the long-term existence of nantokite on an outdoor bronze requires isolation from moisture and air, possibly by a relatively thick corrosion layer.

2.5. Copper chloride hydroxides

The four copper chloride hydroxides, also called basic copper chlorides, were **atacamite** $\alpha\text{-Cu}_2(\text{OH})_3\text{Cl}$, **paratacamite** $\gamma\text{-Cu}_2(\text{OH})_2\text{Cl}$, the **copper chloride hydroxide** $\text{Cu}(\text{OH})\text{Cl}$, and another **copper chloride hydroxide** $\text{Cu}_2(\text{OH})_3\text{Cl}$. Atacamite was detected in 6 of 10 surface samples, paratacamite was detected in 2 of 10 surface samples, and the other two were each detected in one surface sample. Atacamite and paratacamite have been detected previously on outdoor copper and copper alloys [18]. They are naturally occurring minerals with the same chemical formula but different crystal structures, and they have green colours and hardnesses similar to **brochantite** and **antlerite** [19, 20].

Atacamite and paratacamite were mostly found in sheltered and partly exposed areas. These are the areas not readily washed by rain, where enough chlorides, probably from road salt, could have accumulated. Laboratory studies have shown that if brochantite is placed in a solution containing high levels of chloride ions, it will convert to atacamite through a mechanism of dissolution and precipitation [21]. Atacamite was identified approximately three times more frequently than paratacamite. An increased abundance of atacamite over paratacamite has also been observed by *Mourrey* [3]. Although the formation of these minerals must depend on kinetic factors, because the difference in their free energies of formation is so small [21], the important factors are not well understood [22].

2.6. Copper chloride hydroxide hydrates

Two copper chloride hydroxide hydrates were identified: **anthonyite** $\text{Cu}(\text{OH},\text{Cl})_2 \cdot \text{H}_2\text{O}$, and $\text{Cu}_7\text{Cl}_4(\text{OH})_{10} \cdot \text{H}_2\text{O}$. Anthonyite is a naturally occurring mineral that is soft (2 on the Mohs scale) and insoluble in water but readily soluble in cold, dilute acids [3]. It is subject to dehydration as are other hydrated basic copper salts. The presence of these two hydrated copper chloride hydroxides may indicate recent corrosion on the statues or other processes occurring during sample storage prior to analysis.

2.7. Copper sulphates

A small fraction (24%) of the coins contained one or more of eight different copper sulphates (three copper sulphate hydroxides, three copper sulphate hydroxide hydrates, and two others).

2.7.1. Copper sulphate hydroxides

Copper sulphate hydroxides, also called basic copper sulphates, occurred in 100 coins with **brochantite** $\text{Cu}_4(\text{SO}_4)(\text{OH})_6$ in 83, **antlerite** $\text{Cu}_3(\text{SO}_4)(\text{OH})_4$ in 16, and the copper sulphate hydroxide $\text{Cu}_2(\text{SO}_4)(\text{OH})_2$ in one. Brochantite and antlerite are naturally occurring green minerals; antlerite is brittle and somewhat softer (3,5 on the Mohs scale) than brochantite (3,5 to 4 on the Mohs scale) [19]. They are common corrosion products in the green patina on outdoor bronze coins [3].

Brochantite was identified in roughly equal numbers of surface samples from exposed, partly exposed or sheltered areas, and it was identified in surface samples with a wide range of macroscopic colours, including green, black, yellow, red, brown or grey. It was observed that, in general, the longer a coin remained outside, the greater the fraction of its surface samples containing brochantite, although there were three exceptions. Antlerite, identified in only 16% of the surface samples, was found mainly on recent coins. The surface samples containing antlerite were from sheltered or partly exposed areas. Robbiola *et al.* also detected antlerite in sheltered areas on outdoor bronzes [18]. In 1984, Nielsen suggested that acid rain was attacking brochantite and converting it to the more soluble (and therefore less projective) antlerite [23]. However, laboratory experiments failed to provide evidence for any direct conversion of brochantite to antlerite in acid Solutions [24]. Nassau *et al.* proposed, instead, that the two crystalline materials form independently as a result of localized corrosion conditions, such as differences in pH [24].

2.7.2. Copper sulphate hydroxide hydrates

Six surface samples contained hydrated copper sulphate hydroxides: four contained **posnjakite** $\text{Cu}_4(\text{SO}_4)(\text{OH})_6 \cdot \text{H}_2\text{O}$, one $\text{Cu}_5(\text{SO}_4)(\text{OH})_6 \cdot 5\text{H}_2\text{O}$ and one $\text{Cu}_2(\text{SO}_4)_2(\text{OH})_2 \cdot 2\text{H}_2\text{O}$. These six samples came from sheltered or exposed areas. The mineral posnjakite is light blue, has a hardness of 2 to 3 on the Mohs scale [24], and has been detected on outdoor bronzes [3]. It differs from brochantite only in having

water of hydration [24], and is thought to be a precursor to brochantite formation, Posnjakite and the other copper sulphate hydroxide hydrates may indicate recent active corrosion on these statues. On the other hand, their presence may also be the result of reactions occurring during storage after sampling and before analysis.

2.7.3. Other copper sulphates

The two remaining copper sulphates were *ammonium copper sulphate hydrate* $\text{Cu}(\text{NH}_4)_2\text{SO}_4 \cdot 2\text{H}_2\text{O}$ and *devilline* $\text{CaCu}_4(\text{SO}_4)_2(\text{OH})_6 \cdot 3\text{H}_2\text{O}$, a calcium copper sulphate hydroxide hydrate. The ammonium copper sulphate hydrate was detected in a surface sample from an exposed coins. A similar compound, known as Tutton salt $\text{Cu}(\text{NH}_4\text{SO}_4)_2 \cdot 6\text{H}_2\text{O}$, has been detected on two pieces in sheltered areas where the salt, despite being highly soluble, was not easily washed away [3]. Possible sources of ammonia are insects excrement or atmospheric dust containing ammonium sulphate particles [3]. The devilline was found on a sheltered area; gypsum ($\text{CaSO}_4 \cdot 2\text{H}_2\text{O}$) was present in the same sample. Gypsum and its solubility are discussed in more detail below.

3. Compounds resulted from tin corrosion

The only tin compounds identified were tin oxides. The stannic oxide **cassiterite** (SnO_2) was detected six times, another **stannic oxide** (SnO_2) was detected once, and the stannous oxide **romarchite** (SnO) was detected twice from 10 ancient coins, mainly in green-coloured samples. Cassiterite, a naturally occurring mineral with a hardness of 6 to 7 on the Mohs scale, is white when pure but it is often stained by impurities. Romarchite is black or blue-black [25]. Cassiterite has been detected by others on outdoor bronzes [3].

When exposed outdoors, tin readily develops a thin film of essentially insoluble Cassiterite which slows further corrosion by passivating the tin surface [26]. Surface studies have detected higher levels of tin at the outer surface of green areas than at the outer surface of black areas [18]. It is thought that, in areas not regularly washed by rain, the tin oxide formed initially becomes covered with extraneous deposits and corrosion products. On the other hand, in areas regularly washed by rain, any extraneous materials or slightly soluble corrosion products are washed away, leaving the less soluble materials such as tin oxide, brochantite or atacamite. This process would explain why the tin oxides were identified mainly in green-coloured samples.

4. Compounds resulted from zinc corrosion

The only zinc compound, zinc oxide or **zincite** (ZnO), was identified in five coins. When zinc is exposed outdoors, it initially forms zinc oxides and hydroxides [27] which transform slowly to one of several basic zinc compounds [3]. The corrosion products of zinc tend to be soluble in weakly acidic solutions [27] and so are readily dissolved. It is possible that the zincite identified on these five statues results from corrosion of freshly exposed zinc. It is also possible, however, that the zincite is not a corrosion product but an extraneous deposit of windblown paint; zincite is a common white pigment in paint.

5. Compounds resulted from lead corrosion

The lead compounds identified were **anglesite** PbSO_4 , **cerussite** PbCO_3 , **hydrocerussite** $\text{Pb}_3(\text{CO}_3)_2(\text{OH})_2$, **lead oxide hydrate** $\text{PbO}\cdot x\text{H}_2\text{O}$, **lead oxide hydroxide hydrate** $\text{Pb}_{13}\text{O}_8(\text{OH})_{10}\cdot\text{H}_2\text{O}$ and **lead oxide sulphate hydrate** $\text{Pb}_4\text{O}_3(\text{SO}_4)\cdot\text{H}_2\text{O}$. These compounds occurred in few coins. Lead was identified in metal samples from about half of the ancient coins.

Anglesite was the most frequently identified lead corrosion product. The presence of anglesite is not surprising because it is the principal atmospheric corrosion product on lead [28]. Stockle *et al.* have detected anglesite on copper and bronze test pieces after only one year of outdoor exposure [3]. Anglesite forms white crystals which are slightly soluble in water but less soluble at lower pH [28].

The lead carbonates, cerussite and hydrocerussite, were detected mainly on the ancient coins (before Xth century). Cerussite was detected three times and hydrocerussite twice. Lead carbonates are common corrosion products on lead exposed to atmospheric conditions [28]. Cerussite forms colourless crystals; hydrocerussite, also known as basic lead carbonate or white lead, forms white crystals. The partial pressure of carbon dioxide in the atmosphere favours hydrocerussite formation [26], but lower pH values favour cerussite formation [28].

On the ancient coins, significantly more lead corrosion products were detected than other common corrosion products such as brochantite. These lead corrosion products could be from a patination process based on lead compounds, such as lead acetate or lead dioxide [14]. A contributing factor may have been car exhaust.

6. Compounds resulted from contamination

Most of the compounds discussed in this section are believed to be deposited from pedological processes rather than formed by corrosion of the coins bronzes. The inorganic compounds are discussed first, followed by the organic ones. Some of these compounds are not harmful (silicates, iron compounds); others may promote corrosion (gypsum, organic materials).

6.1. Silicates

Most of these silicates were identified in six out of then coins, from archaeological sites. Of importance is quartz (40%), in sheltered, partly exposed and exposed areas. The abundance of quartz on outdoor bronze pieces has been noted by others [3].

Quartz, a colourless mineral often tinted by impurities, is harder (7 on the Mohs scale [25]) than most copper corrosion products (2-5 to 4 on the Mohs scale [19]). Quartz is often the main constituent of sand, which is used in large quantities in building materials. Quartz and other silicates could be residual sand from a sand-casting process [3], or they could result from the accumulation of airborne particulate material. In future, it would be useful to analyze the shapes and sizes of the quartz grains and study the layering of material on the surface, to try and identify the source of the quartz.

6.2. Iron compounds

Iron oxides and iron oxide hydroxides, various iron sulphates and iron sulphate hydroxides, one iron carbonate and one iron chloride were identified. The largest numbers of iron-containing compounds were identified on coins from archaeological sites with mobile chemical deposits. The iron compounds are probably from other iron pieces, which are in the same site as the coins. The iron oxides, were two forms of FeO, four forms of Fe₂O₃ and Fe₃O₄; **haematite** (α -Fe₂O₃), the iron oxide identified most frequently, was detected mainly in exposed areas. The iron oxide hydroxides, consisted of four different crystal forms of FeOOH; the predominant one was **goethite**. Most of these iron oxides and iron oxide hydroxides form naturally when iron corrodes outdoors [3]. They are also common pigments.

Many different sulphate-containing iron compounds were detected. The six iron sulphates, each found only once, were two ferrous sulphates, K₂Fe(SO₄)₂·6H₂O and (NH₄)₂Fe₂(SO₄)₂ three ferric sulphates, Na₃Fe(SO₄)₃, Fe₂(SO₄)₃·H₂O and (NH₄)₃Fe(SO₄)₃, and one mixed ferrous-ferric sulphate Fe₂(SO₄)₄·22H₂O. The three iron sulphate hydroxides were two crystal forms of Fe(OH)SO₄·2H₂O (parabutlerite and butlerite) and amarantite Fe(OH)SO₄·3H₂O. Sulphate ions accelerate iron corrosion and become incorporated into the rust layer [3]. The ammonia component may originate from particulate matter [3] or insects excrements [3]; ammonia forms soluble complexes with copper and stimulates copper corrosion.

Other iron compounds were an iron chloride hydrate FeCl₃·7H₂O and siderite FeCO₃. The iron chloride hydrate is deliquescent and water-soluble. The siderite it has low solubility in water and is normally formed in slightly alkaline, carbon-ate-rich and oxygen-poor conditions.

6.3. Gypsum

Calcium sulphate hydrate (gypsum, CaSO₄·2H₂O) was present in the surface of the pieces from archaeological sites. Gypsum is a soft (1,5 to 2 on the Mohs scale), naturally occurring mineral that is colourless when pure. It was found mainly in sheltered or partly exposed areas; only rarely was it identified in samples from exposed areas, probably because gypsum is slightly soluble in water [29].

A possible source is the formation of gypsum from the reaction of calcium carbonate with sulphate ions [29], from sites with high chemical deposits. Burmester and Koller, who identified gypsum on sheltered bronze doors, were concerned at damage caused by expansion as calcium carbonate converts to gypsum [3]. As mentioned earlier for quartz, it would be useful in the future to analyze the shapes and sizes of gypsum grains to determine their exact source.

6.4. Other inorganic calcium compounds

The four calcium carbonates were **calcite** CaCO₃, another crystal form of CaCO₃, **fairchildite** K₂Ca(CO₃)₂ and **ankerite** Ca(Fe,Mg)(CO₃)₂.

In total, 80% of the coins from archaeological sites contained one or more of these carbonates; they were detected in samples from sheltered, partly exposed and exposed areas. Calcium carbonates are used as fillers for paint [3] and as building materials (for example, limestone, cement) and so they are probably wind-blown material. As discussed above, calcium carbonates are susceptible to conversion to calcium sulphates. Furthermore, fairchildite is deliquescent [30] and will promote corrosion under conditions of high humidity.

One calcium chloride, the hydrate $\text{CaCl}_2 \cdot 4\text{H}_2\text{O}$, was identified in a surface sample from a partially exposed area on the National War Memorial. This hydrate is usually formed from another hydrate, $\text{CaCl}_2 \cdot 6\text{H}_2\text{O}$, when the relative humidity is low. Therefore the presence of calcium chloride may result from the sea water. It may also result from a reaction between sodium chloride and calcium-containing material such as calcite. Because calcium chloride deliquesces at a relative humidity above about 33%, its presence on the coins will promote corrosion [30].

6.5. Organic compounds

The organic compounds identified at the surface of the patina are humic acid, oxalates, uric acid and others which speed up the corrosion processes [3].

7. Conclusion

This paper has documented the surface compounds on the ancient bronze coins and has attempted to discuss the possible sources of these materials. It is hoped that this information can be used as a resource by conservators and conservation scientists involved with all aspects of the treatment of ancient bronze coins.

References

1. I. Sandu, A. Dima, I.G. Sandu, **Conservarea și restaurarea obiectelor metalice**, Ed. Corson, Iași 2002;
2. I. Sandu, I.G. Sandu, **Aspecte moderne privind conservarea bunurilor culturale, vol.I, Nomenclatură, tipologii și cazuistici**, Ed. Performantica, Iași, 2005;
3. W. Mourey, **Conservarea antichităților metalice – de la săpătură la muzeu**, Ed. Tehnică, București, 1998;
4. E. Matson, R. Holm, “*Copper and copper alloys*”, in **Metal Corrosion in the Atmosphere**, ASTM Special Technical Publications, 435, American Society for Testing and Materials, Philadelphia, 1968, p. 187;
5. R.L. Opila, „*Copper patinas: an investigation by Auger electron spectroscopy*”, în **Corrosion Science**, 27, (1987), p. 685;
6. H. W. Richardson, “*Copper compounds*” in **Kirk-Othmer Encyclopedia of Chemical Technology**, 4-th edn, vol. VII, Ed. John Wiley & Sons, New York, 1993, p. 505;
7. R.J. Gettens, “*Patina: Noble and vile*” in **Art and Technology: A Symposium on Classical Bronzes**, ed. S. Doeringer, D.G. Mitten and A. Steinberg, MIT Press, Cambridge MA (1970), p. 57;
8. J.D. Meakin, D.L. Ames, D.A. Dolske, “*Degradation of ancient bronze*”, in **Atmospheric Environment**, 26B, (1992), p. 207;
9. R.M. Garrels, C.L. Christ, **Solutions Minerals and Equilibria**, ed. Jones and Barlett, Boston, 1990, p. 154;

10. P.D. Weil, P. Gaspar, L. Gulbransen, R. Lindberg, D. Zimmerman, "*The corrosive deterioration of outdoor bronze*", in **Science and Technology in the Service of Conservation**, Ed. IIC, London, (1982), p. 130;
11. S.P. Sharma, "*Reaction of copper and copper oxide with H_2S* " in **J. Electrochemical Society**, 127, 1980, p. 21;
12. W.A. Oddy, N.D. Meeks, "*Unusual phenomena in the corrosion of ancient bronzes*" in **Science and Technology in the Service of Conservation**, Ed. IIC, London, (1982), p. 119;
13. S.K. Chawla, J.H. Payer, "*The early stage of atmospheric corrosion of copper by sulfur dioxide*" in **J. Electrochemical Society**, 137, 1990, p. 60;
14. R. Hughes, M. Rowe, **The Colouring, Bronzing and Patination of Metals**, Ed. Crafts Council, London, 1982;
15. R.J. Ghetts, "*Mineral alteration products on ancient metal objects*" in **Recent Advances in Conservation**, Ed. Butterworths, London, 1963, p. 89;
16. D. Scott, "*Bronze disease: a review of some chemical problems and the role of relative humidity*", in **J. American Institute for Conservation**, 29, (1990), p. 193;
17. M.B. Mcneil, "*Interpretation of bronze disease and related copper corrosion mechanism interms of log-activity diagrams*", in **Materials Issues in Art and Archeology**, III, Ed. Materials Research Society, Pittsburg, 1992, p. 1055;
18. L. Robbiola, C. Fiaud, S. Pennec, "*New model of outdoor bronze corrosion and its implications for conservation*", in **ICOM Committee for Conservation 10-th Triennial Meeting**, Washington D.C., 1993, p. 796;
19. C. Palache, H. Berman, C. Frondel, **The System of Mineralogy, 7th edn**, Volumul II, Ed. John Wiley & Sons, New-York, 1951;
20. H.R. Oswald, J.R. Gueter, "*Crystal data on paratacamite*", in **J. Applied Crystallography**, 4, (1971), p. 530;
21. T. L. Woods, R.M. Garrels, "*Use of oxidized copper mineral as environmental indicators*", in **Applied Geochemistry**, 1, (1986), p. 181;
22. A. M. Pollard, R.G. Thomas, P.A. Willeams, "*Synthesys and stabilities of the basic Cu(II) chlorides atacamite, paratacamite and botallackite*", in **Mineralogical Magazine**, 53, (1989), p. 557;
23. N. Nielsen, "*Keeping the torch lit*", in **Materials Permormance**, 23, (1984), p. 78;
24. K. Nassau, P.K. Gallancher, A.E. Miller, T.E. Graedel, "*The Characterisation of patina components by X-ray diffraction and evolved gas analysis*" in **Corrosion Science**, 27, (1987), p. 669;
25. R.C. Weast (editor), **CRC Handbook of Chemistry and Physics**, Ed. CRC Press, Boca Raton, 2004;
26. S. Turgoose, "*The corrosion of lead and tin: before and after escavation*" in **Lead and Tin: Studies in Conservation and Technology** (ed. G. Miles, S. Pollard), Ed. United Kingdom Institute for Conservation, London, 1985, p. 15;
27. T.E. Graedel, "*Corrosion mechanism for zinc exposed the atmosphere*", in **J. Electrochemical Society**, 136, (1989), p. 193;
28. T.E. Graedel, "*Corrosion mechanism for lead exposed the atmosphere*", in **J. Electrochemical Society**, 141, (1994), p. 922;
29. E.M. Winkler, **Stone: Properties, Durability in Man's Environment**, Ed. Springer – Verlag, New York, 1973, p. 94;
30. R. Waller, "*Temperature and humidity sensitive mineralogical and petrological specimens*", in **The Care and Conservation of Geological Materials**, (ed. F.M. Howie), Butterworth – Heinemann Ltd., London, 1992, p. 36;

Received March 12, 2005

¹⁾ „Al.I.Cuza” University of Iasi, Department of Cultural Heritage

²⁾ „Gh. Asachi” Tehnical University of Iasi, Faculty of Material Science and Engineering

AUTENTIFICAREA MONEDELOR VECHI DIN BRONZ
I. ASPECTE PRIVIND COMPOZIȚIA PATINEI

***Rezumat** – Lucrarea prezintă chimismul principalilor componenți din structura patinei monedelor vechi din bronz, care au rezultat prin procese de coroziune și pedologice, dar și prin contaminare, la expunerea în colecții sau în situri arheologice. Studiul comparativ al principalelor tipuri de compuși rezultați din coroziune și prin contaminare permite selectarea fazelor minerale prin microscopie în vederea analizării lor chimice.*

AUTHENTICATION OF ANCIENT BRONZE COINS II. MICROCHEMICAL, IR AND XRD ANALYSES

by

IOAN GABRIEL SANDU¹, IRINA CRINA ANCA SANDU², ADRIAN DIMA¹, ION SANDU³,
ION NEACȘU⁴

Abstract – The paper deals with the experimental results obtained from the micro-chemical, IR and XRD analyses for the identification of the corrosion products and of the surface contaminants, formed in time or during pedological processes. These results can converge to establish correlations useful for age determination and for authentication.

Keywords: microchemistry, micro-stratigraphy, corrosion products, contaminants

1. Introduction

The authentication expertise of ancient coins, new discovered or from different collections, uses in the analytical system one or more of the attributes of authentication: material, conception or engraver, coin factory, efigies etc. The material, under the two aspects, the basic alloy (the metal composition) and its corrosion products formed in time on the surface, under the action of the exogenous factors and first of all under the pedological ones, is a very important indication for authentication. The analysis of their composition, based on chronological systems of comparison, allows the obtaining of data concerning the age and the processes undergone in time from the loss phase to the discovery.

The aggressivity of the physical-chemical systems in the archaeological site influences both the composition of the corrosion products on the surface of artifact and the contamination materials.

In this respect, the present paper deals with the authentication of old bronze coins, discovered on the territory of our country, through the analysis of the composition of the corrosion products and of the surface contaminants using the micro-chemical, IR and XRD techniques of investigation.

2. Experimental techniques

Three groups of ancient bronze coins, discovered on the territory of Romania or from private collections, were studied. In order to analyze the corrosion products and the surface contaminants four techniques were applied: microphotography on normal cleaned samples, with or without nital attack and on stratigraphical sections (transversal sections), micro-chemical analysis, IR spectroscopy and X-ray diffraction.

2.1. Sampling and processing of materials. Materials and methods

Samples were taken from three groups of ancient bronze coins: coins in a collapse state discovered in the village of Nufărul (Constanța county) in 2000, dated from IV-Vth century, with christian symbols (fig. 1-a), 6 Austrian coins (Kreutzer) from 1813-1815, of different values (fig. 1-b) and 6 of the first Romanian coins from 1867-1881 – having the value of 5 bani and 10 bani respectively (fig. 1-c), noted MA, MO and MR. Two of the coins in collapse of IV-Vth century were broken in order to put in evidence the metallic bulk (fig. 2).

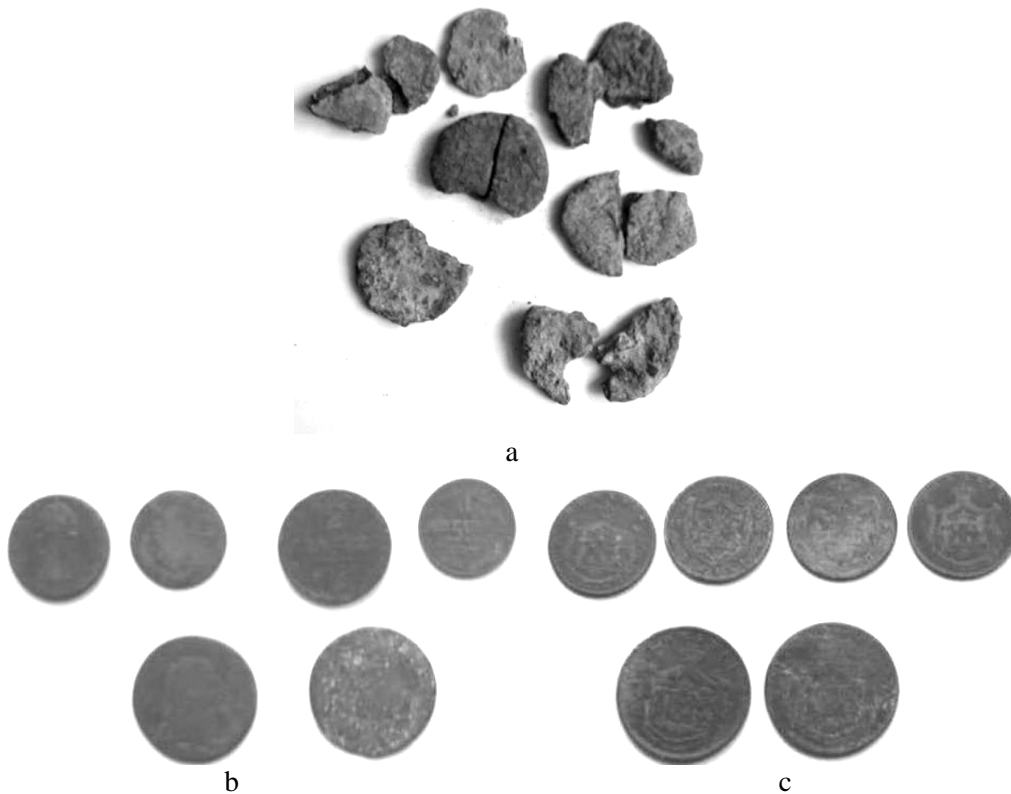


Fig. 1. The three groups of bronze coins taken into study:
 a – fragments of coins from IV-Vth century, with christian symbols (MA);
 b – Austrian Kreutzers from 1813-1815 (MO), and
 c – Romanian coins from 1867-1880 (MR).

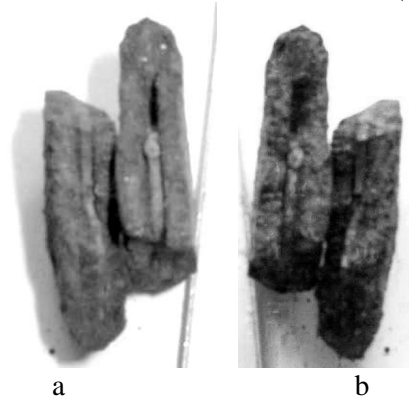


Fig. 2. Photography of two fragments of old coins (MA) broken in middle in order to put in evidence the metallic bulk (pre-collapse): a – in VIS; b – in UV

2.2. Micro-chemical and stratigraphical analysis

Both the transversal sections and the surfaces of the coins were analyzed by optical microscopy using a OLYMPUS CX21 microscope under reflected light (Vis) followed by micro-chemical tests. The micro-photographies were taken with an OLYMPUS digital camera, adapted to the microscope. The nature of the corrosion products and of the contaminants was established by micro-chemical reactions on surfaces or transversal sections, in a native state or after previous mechanical or chemical cleaning (nital attack). The nature of the structural components of the corrosion products and contaminants, disposed in concentrated areas as beautifully colored crystals, was directly attributed, based on the color and crystallographic system.

2.3. IR Spectroscopy

The IR analysis was done using fine dispersed samples as KBr pellets. The IR spectra were registered in the field of 200-4000 cm^{-1} , using a SPECORD M80 Carl Zeiss Jena spectrophotometer.

2.4. X-Ray Diffraction (XRD)

The X-ray diffraction analysis was done on powders of crystallites, finely grinded. Or this purpose a Philips 1130/00 diffractometer equipped with a Cu anode and a Ni filter (for high resolution), at 1200 W and vertical goniometer with an angular resolution bigger than 0,005 degrees.

3. Results and discussions

Considering that the old bronzes are mainly composed of four metals: Cu, Sn, Zn and Pb and small quantities of microelements: Fe, Sb, Al, As, Si and P, the visual microscopical analysis studied the morphology of the micro-crystallites on the surfaces and in the sections and successively the micro-chemical tests with specific reagents contributed to the determination of the mineral components of the corrosion products and contaminants, formed in time or by pedological processes.

In the figures 3 and 4 the micro-photographies of the surface structures and on transversal sections, subject to micro-chemical tests are given. These are showing the presence of main cations and of alloy-forming cations or induced by pedological processes (table 1), but also the morphology and the color of the micro-crystallites.

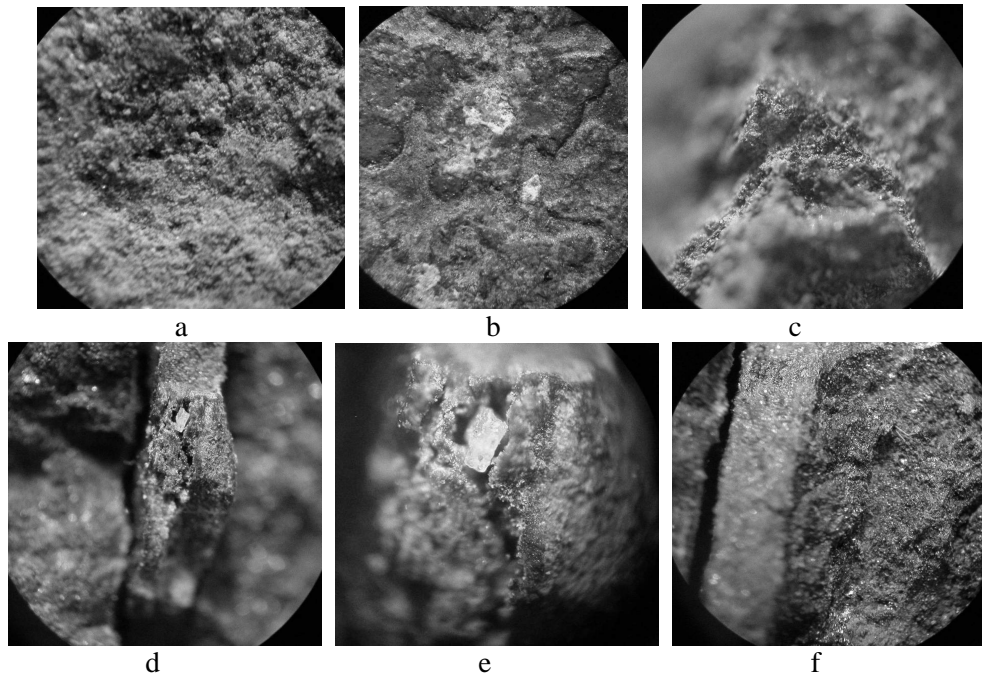


Fig. 3. Micro-photographies of the surface structured and on sections, analyzed by micro-chemical reactions: a – MA coin (160X); b – MO coin (240X); c – MR coin (300X); d – section of MA coin (16X), e – structure after nital attack of the MO coin (16X), f – micro-stratigraphy of the deposit on a MR coin (160X)

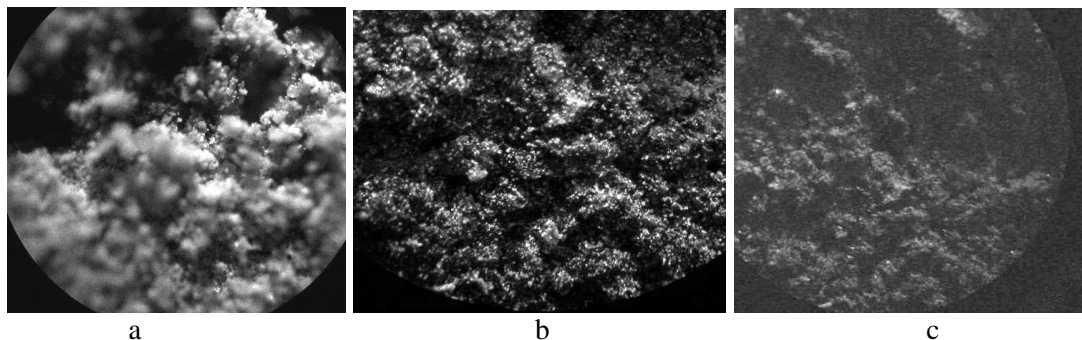


Fig. 4. Microphotographs in VIS (300X) of the surface structures microscopically analyzed for the study of the crystallites' morphology with specific colors due to the corrosion products or contaminants: a – MA coins; b – MO coins; c – MR coins.

It should be underlined that the coins dated from IV-Vth century have a corrosion layer very loosen, with an important quantity of organic and inorganic contaminants. The metallic bulk, observed in the stratigraphical section (fig. 3-a and d) presents a segregation effect of Zn with its accumulation in the area of shrink on the surface. The same phenomenon, but less visible, was observed in the Austrian coins fig. 3-b and e). The last, because of the complex composition in the alloying process forms in time large, non-uniform corrosion structures, with zonal repartition of certain components. In exchange, the Romanian old coins, with a limited alloying composition (95% Cu, 4% Sn and 1% Zn) and rigorously elaborated, have an uniform patina, compacted and very thin, made mainly of oxydes, sulphides, carbonates and weakly hydrated sulphates (fig. 3-c and f).

The IR spectra (fig. 5) and X-ray diffractograms (fig. 6) put in evidence the complex nature of the corrosion products of the three groups of coins. In the obtained diffractograms for the three groups of coins, 20 mineral compounds were

identified, the main part of them being formed by corrosion, but also by contamination, such as: gypsum, quartz, calcite and a limited series of organic compounds (table 2).

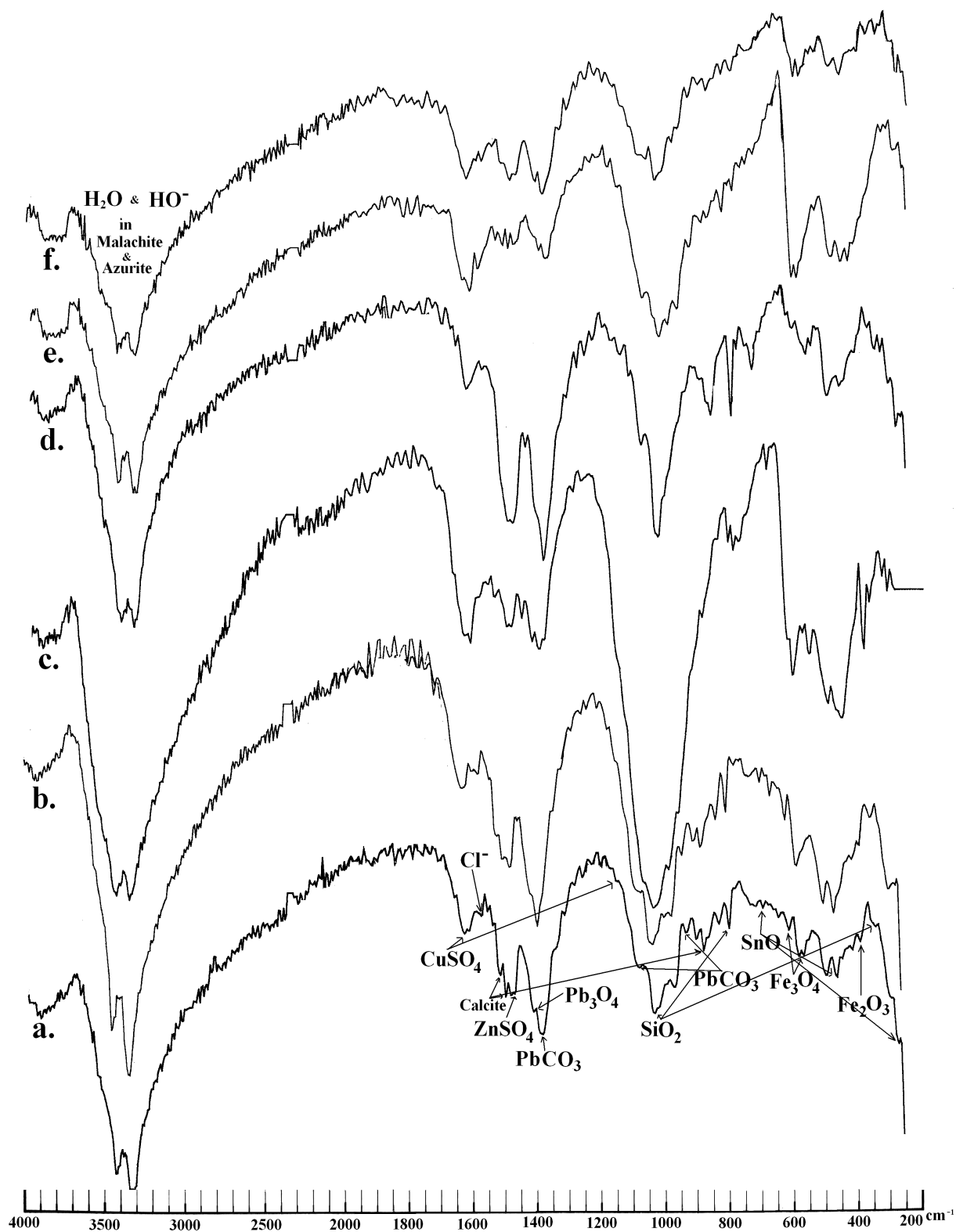


Fig. 5. IR spectra: a – MA (a), b – MA(b), c – MO(1813),
d – MO(1815), e – MR (1867), f – MR (1881)

Table 1. Cations found in the corrosion products and contaminants, analyzed by micro-chemical and IR spectroscopy

Coins	Cu(II)	Sn(II)	Zn(II)	Pb(II)	Fe(II)	Sb(III)	Al(III)	As(III)	Si(IV)	P(V)
MA (a)	++++	++++	++	++	++	+	+	+	++	+
MA (b)	++++	++++	++	++	++	+	-	+	++	+
MO (1813)	++++	++++	++	+	+	-	-	-	+	-
MO (1815)	++++	++++	++	+	+	-	-	-	+	-
MR (1867)	++++	++++	++	+	+	-	-	-	-	-
MR (1881)	++++	++++	++	+	+	-	-	-	-	-

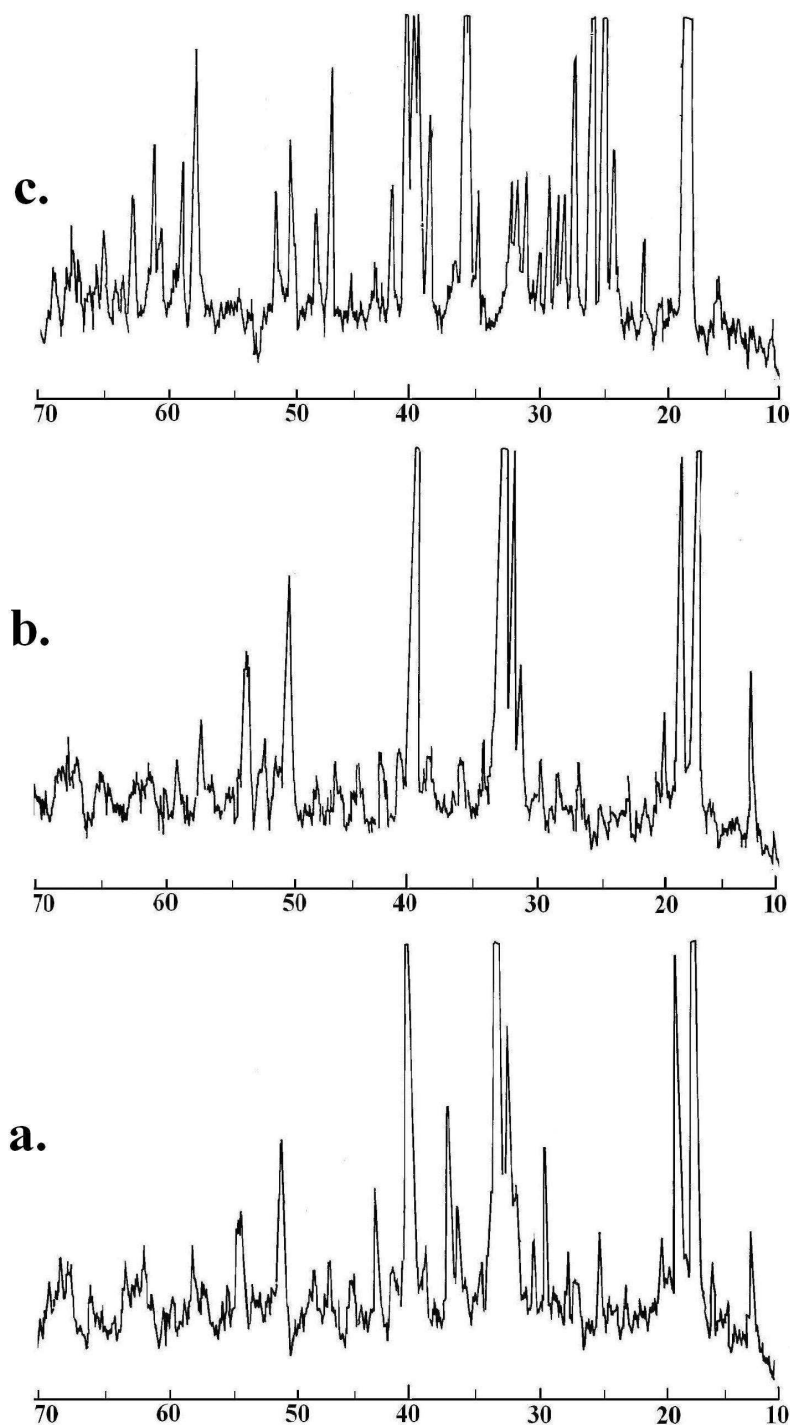


Fig. 6. X-ray diffractograms:
a – MA coins, b – MO coins, c – MR coins.

Table 2. Chemical compounds determined by IR spectroscopy and XRD in the corrosion products and contaminants

Mineral phase	Chemical formula	Color and aspect	N. pick	PDF	MA (a)	MA (b)	MO 1813	MO 1815	MR 1867	MR 1881
Malachite	$\text{CuCO}_3 \cdot \text{Cu}(\text{OH})_2$ or $\text{Cu}_2(\text{OH})_2\text{CO}_3$	Green, with a characteristic vitreous aspect	22	10-399	+++	+++	++	++	+	+
Azurite	$2\text{CuCO}_3 \cdot \text{Cu}(\text{OH})_2$ or $\text{Cu}_3(\text{OH})_2(\text{CO}_3)_2$	Dark blue	20	11-136 11-682	++	++	++	++	-	-
Athacamite	$\text{Cu}_2(\text{OH})_3\text{Cl} \cdot n\text{H}_2\text{O}$ or $\text{CuCl}_2 \cdot 3\text{Cu}(\text{OH})_2 \cdot n\text{H}_2\text{O}$	Emerald-green with more or less dark tones in function of n and with a vitreous aspect	62	2-0146 25-0269	++	++	+	+	-	-
Parathacamite	$\text{Cu}_2(\text{OH})_3\text{Cl} \cdot \text{CuCl}_2 \cdot 3\text{Cu}(\text{OH})_2$	Green-blue	20	15-694 19-389 25-1427	++	++	+	+	-	-
Nantokite	Cu_2Cl_2	Waxy gray-white	1	6-0344	+	+	+	+	+	+
Cuprite	Cu_2O	Brick-Red, with gray-brownish or yellowish to orange tones	76	5-0667	++	++	++	++	++	++
Tenorite	CuO	Black-gray to brown	1	41-0254	+	+	+	+	+	+
Cassiterite	SnO_2	Shiny white	2	6-0395	+	+	-	-	-	-
Minium	Pb_3O_4	Red	1	29-0781	+	+	+	+	-	-
Calcocite	Cu_2S	Pb-like gray, with metallic brightness	2	9-0328 33-0490	+	+	++	++	++	++
Calconite	$\text{CuSO}_4 \cdot 5\text{H}_2\text{O}$	Clear blue	33	21-0816 36-0432	++	++	+	+	+	+
Anthlerite	$\text{Cu}_3(\text{OH})_4\text{SO}_4$ or $\text{CuSO}_4 \cdot 2\text{Cu}(\text{OH})_2$	Blackish with green tones	16	7-0407	++	++	+	+	-	-
Brochantite	$\text{Cu}_4(\text{OH})_6\text{SO}_4$ or $\text{CuSO}_4 \cdot 3\text{Cu}(\text{OH})_2$	Blue to clear green	83	13-0398 43-1458	++	++	+	+	+	+
Langite	$\text{Cu}_4(\text{OH})_6\text{SO}_4 \cdot \text{H}_2\text{O}$ or $\text{CuSO}_4 \cdot 3\text{Cu}(\text{OH})_2 \cdot \text{H}_2\text{O}$	Dark bright green	4	20-0364	++	++	++	++	++	++
Anglesite	PbSO_4	Grey – greenish gray	20	5-0577 36-1461	+	+	+	+	-	-
Cerrusite	$\text{Pb}_2(\text{OH})_2\text{CO}_3$	White	2	13-0131	+	+	+	+	-	-
Gloslarite	$\text{ZnSO}_4 \cdot 7\text{H}_2\text{O}$	Grey with opalescent reflexes	5	36-1451	+	+	+	+	+	+
Gypsum	$\text{CaSO}_4 \cdot 2\text{H}_2\text{O}$	White-gray	33	21-0816 36-0432	+	+	-	-	-	-
Quarz	SiO_2	Translucid gray	7	5-0490	+	+	-	-	-	-

Calcite	CaCO ₃	White-gray	14	5-0586 24-0027	++	++	-	-	-	-
Organic substances		Black-brownish	2	28-2016 31-1982	+	+	-	-	-	-

The complexity of the spectra and diffractogramms patterns increments from the old coins (MA) to the Romanian ones (MR). This aspect is interpreted as a result of the alloy composition and age of the artifact, but also as an effect of the aggressive action of the exogenous factors, that modified the material. It is true that some endogenous factors, related to the material and the creation technology, together with the exogenous ones, determines in most cases the mechanism of the degradation and deterioration processes. Many ancient coins were exposed to strong pedological processes (erosions and corrosions, until the collapse) or to thermal processes, that made them fragile and caused phases modifications, in most cases irreversible.

Conclusions

The paper is the third part of a series of notes that aims to establish correlations between the composition of the basic material (alloy) and the corrosion products, contaminants respectively, by analyzing the surface distribution and in the volume phase of the structures that form the natural patina of a coin. This study will allow to elaborate an experimental method for authentication.

The obtained experimental data allow the study of the corrosion and erosion mechanisms to which the coins and all the numismatic pieces are subject in time, when the so-called natural patina is formed. Its characteristics allow to draw up correlations between the composition and the distribution of the main alloy components and of those induced by the aggressive external environments or by pedological processes.

In this way, using the micro-chemical and morphological analysis on surface and sections of coins, together with the IR spectroscopy and X-ray diffraction, data concerning the composition and the distribution of the corrosion products and contaminants from the patina was obtained. These results will be applied in a complex system of age and oldness evaluation, using other modern techniques and methods of analysis.

References

1. I. Sandu, A. Dima, I.G. Sandu, **Conservarea și restaurarea obiectelor metalice**, Ed. Corson, Iași 2002;
2. I. Sandu, I.G. Sandu, **Aspecte moderne privind conservarea bunurilor culturale, vol.I, Nomenclatură, tipologii și cazuistici**, Ed. Performantica, Iași, 2005;
3. W. Mourey, **Conservarea antichităților metalice – de la săpătură la muzeu**, Ed. Tehnică, București, 1998;
4. A. Dima, I. Sandu, I. G. Sandu, I.C.A. Sandu, „*Valorization of metallic objects belonging to the national and world cultural heritage*”, în **Buletinul Institutului Politehnic din Iași**, Tomul XLVII (LI), Fasc. 1-2, Secția Știința și Ingineria Materialelor, (2001), p. 141 - 150;
5. I. Sandu, A. Dima, I.G. Sandu, I.C.A. Sandu, „*Effects and stages experienced by old metallic artefacts from creation to museum exhibition*”, în, **Buletinul Institutului Politehnic din Iași**, Tomul XLVIII (LII), Fasc. 3-4, Secția Știința și Ingineria Materialelor, (2002), p. 83;
6. C. Palache, H. Berman, C. Frondel, **The System of Mineralogy, 7th edn**, Volumul II, Ed. John Wiley & Sons, New-York, 1951;

7. R.A. Nyquist, R.O. Kagel, **Infrared Spectra of Inorganic Compounds**, Academic Press, New-York and London, 1971;
8. * * * , **The Sadtler Standard Spectra**, Ed. Stadler Research Laboratories, Philadelphia PA, 1972;
9. * * * **JCPDS Mineral File: Joint Committee for Powder Diffraction Inorganic Search Manual**, International Centre for Diffraction Data, Swarthmore, 1992;
10. H.P. Klug, L.E. Alexander, **X-ray Diffraction Procedures for Polycrystalline and Amorphous Materials**, Ed. Wiley, New-York, 1974;
11. F.M. Helmi, „X-ray study, geochemistry and mineralogy of some ancient Egyptian coins (Graeco-Roman period) and their natural raw materials” în **MSc Dissertation**, Aimshams University, Cairo, 1973;
12. K. Nassau, P.K. Gallancher, A.E. Miller, T.E. Graedel, „The Characterisation of patina components by X-ray diffraction and evolved gas analysis” în **Corrosion Science**, 27, (1987), p. 669;
13. L.S. Selwyn, N.E. Binnie, J. Poitras, M.E. Laver, D.A. Downham, „Outdoor Bronze Statues: Analysis of Metal and Surface Samples” în **Studies in Conservation**, vol. 41, nr. 4 (1996), p. 205;
14. D.A. Scott, J. Podany, „Ancient copper alloys: some metallurgical and technological studies of Greek and Roman bronzes” in **Small Bronzes from the Ancient World**, Ed. J. Paul Getty Museum, Malibu, California (1990), p. 31;
15. T.E. Graedel, K. Nassau, J.P. Franey, „Copper patinas formed in the atmosphere. I. Introduction” în **Corrosion Science**, nr. 27 (1987), p. 639.

Received May 3, 2005

¹⁾ „Gh. Asachi” Technical University of Iasi, Faculty of Material Science and Engineering

²⁾ Consiglio Nazionale delle Ricerche, ICVBC, Firenze

³⁾ „Al.I.Cuza” University of Iasi, Department of Cultural Heritage

⁴⁾ National Military Museum, București, Conservation Laboratory

AUTENTIFICAREA MONEDELOR VECHI DE BRONZ II. ANALIZA MICROCHIMICĂ, IR ȘI XRD

Rezumat– *Lucrarea se refera la rezultatele experimentale obținute din analizele microchimice, IR și XRD pentru identificarea produșilor de coroziune și a contaminanților de suprafață, formați în timp sau în urma proceselor pedologice. Aceste rezultate pot stabili unele corelații folositoare la determinarea vârstei și pentru autentificare.*

AUTHENTICATION OF ANCIENT BRONZE COINS III. COLORIMETRIC AND THERMOGRAVIMETRIC ANALYSES

by

IOAN GABRIEL SANDU¹, ȘTEFANIA STOLERIU², ION SANDU³, ADRIAN DIMA¹, IRINA
CRINA ANCA SANDU⁴, ION NEACȘU⁵

Abstract – The paper deals with the experimental results obtained through colorimetry by reflection and thermogravimetry in a dynamic regime, in order to identify the corrosion products and the surface contaminants, formed in time or following pedological processes. These data are useful for establishing correlations used in the age determination and authentication respectively.

Keywords: colorimetry by reflection, thermal derivatography, weight loss in a dynamic thermal regime, thermal effects, corrosion products, contaminants

1. Introduction

The natural patina and the composition of the basic alloy are among the main aspects studied by the scientific researchers, due to the implications regarding the conservation state, the valorization by exhibition and treasuring, the age determination and the quota of value indication [1,2].

The patina, with any of its obvious forms on ancient coins (the layer of corrosion products, the surface polishing due to the use and so on) [3], is one of the most important patrimonial elements that can be used for authentication [4]. For this purpose, a series of experimental methods and modern analytical techniques, mostly destructive and invasive, can be applied, such as: thermogravimetric analysis, XRD, mass spectrometry, metallography and other [5-12]. In the last years, a series of methods were studied and these are using direct non-invasive techniques on the object, without sampling. Among these, our research group is mainly applying the colorimetry by reflection [13]. This technique allows the determination of the conservation state and of the oldness of the objects by measuring the deviations and the chromatic alterations.

This method needs of rigorously studied reference systems and therefore in most cases it is necessary to correlate it with other techniques.

In this respect, the present paper deals with the experimental data obtained by reflection colorimetry and thermogravimetry, in view of establishing the composition of the corrosion products and of the contaminants that form the patina of the ancient bronze coins. These experimental data will be used for an expert system of age determination, that will allow the elaboration of an authentication method by comparison of two groups of characteristics: composition and physical-structural,

mechanical and optical properties of the basic alloy of the layer that forms the natural patina.

2. Experimental techniques

Three groups of ancient bronze coins, from various archaeological sites or private collections, were taken into study. In order to analyze the corrosion products and the surface contaminants, two techniques, one non-destructive, the colorimetry by reflection and another one invasive (with sampling), thermal derivatography.

2.1. Sampling and processing of materials. Materials and methods

For the derivatographic analysis, samples of three groups of ancient bronze coins were chosen, as it follows: MA – ancient coins (dated from IV-Vth century, with christian symbols), in a collapse state, from the treasure discovered in the village of Nufărul (Constanța county) in 2000, (fig. 1-a), MO – Austrian coins (Kreutzers) from 1813-1815 (fig. 1-b) and MR – Romanian coins from 1867-1881 (fig. 1-c).

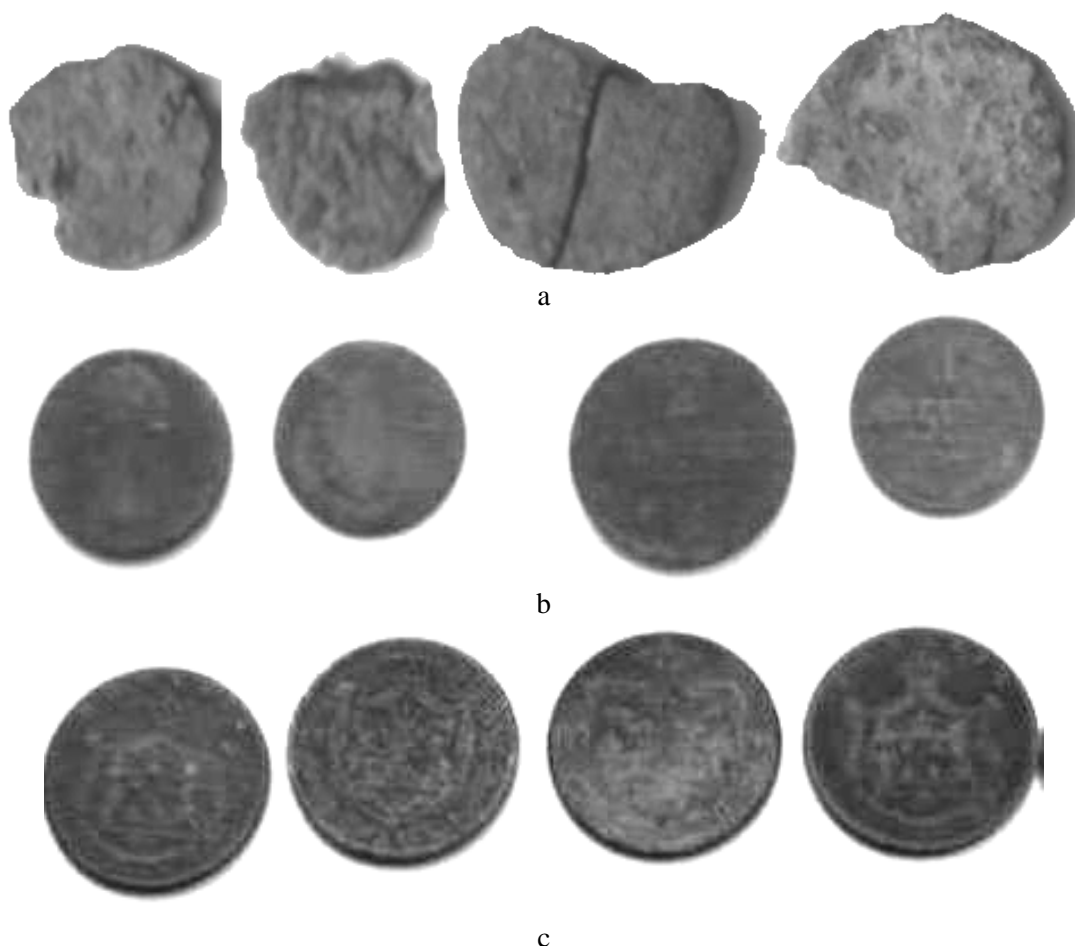


Fig. 1. Bronze coins taken into study:
a – MA; b – MO and c – MR.

The colorimetric analysis, being a non-invasive technique, was done directly on each coin.

2.2. Colorimetry by reflection

The colorimetric study was done by selecting on the surface of the coins the areas with corrosion products and area with an uniform passivated patina. A digital colorimeter with two types of optical devices (based on optical fibers) with different illumination geometries and observation angles (fig. 2 and 3), coupled with a computer with which the values R G B of the CIE colorimetric triangle were established. The analyzed areas were covered with *mylar* (PET), foreseen of small holes that delimit the measuring areas. The number of 3-5 points is corresponding to the comparison areas (basic alloy and patina). In each point the transducer was positioned directly on the material, protecting in this way its color from the contact.

Because the colorimetric analysis was applied on a non-shining surface, with rough areas, using the same light spot projected in one point, 3-5 determinations were done, in order to eliminate the errors of the measure.

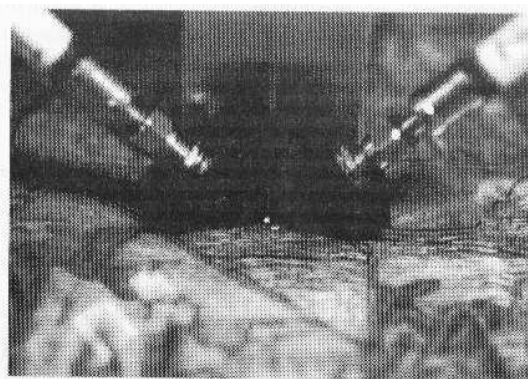


Fig. 2. Sonde 2x45°/0°

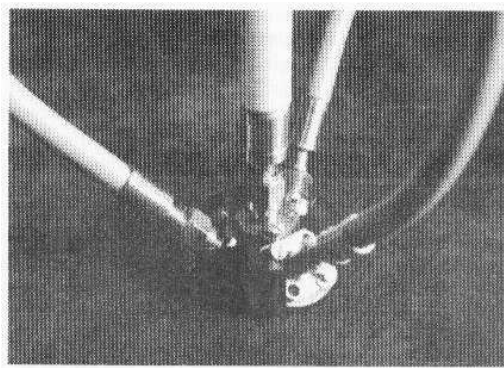


Fig. 3. Sonde d/8°

The colorimetric calculation was done on the average spectrum of each point, for which the standard deviation was successively determined. It has to be said that the analyzed areas were first cleaned with aqueous and alcohol solutions and for the alloy a side area with active corrosion was chosen for being treated with nitric acid (40%) in order to remove the corrosion layer from the metal. After the nital attack with acid, the coin was attentively cleaned with water and acetone and afterwards desiccated on filter papers.

2.3. Thermal Derivatography

The thermal processes that occurs in the samples taken into study were analyzed with a Analyser SHIMADZU DTG-TA-51H Complex instrument which simultaneous measure - thermogravimetry (TG)/ differential thermo-analysis (DTA); temperature range: room temperature to 1500°C, mass measurable range: ± 20 up to ± 200 mg; readability: 0.001 mg; DTA measurement range: ± 0.15 to ± 1000 μ V, sample quantity: max 1g; heating speed: 0.1 to +50°C/hour; hold time: 0 to 999 min or 0 to 999 hours, cooling method by ventilation; signal output: analog and digital; atmosphere: air; reference material: Al_2O_3 .

These experimental parameters were the same for the samples made of high porosity corrosion material from the MA coins and for the thin patina of the MO and MR coins.

3. Results and discussions

Based on the experimental results of the I note [14], regarding the chemical nature of the corrosion products mainly as beautifully colored minerals, the areas for the colorimetric analysis by reflection were selected under an OLYMPUS CX21 optical microscope (fig. 4).

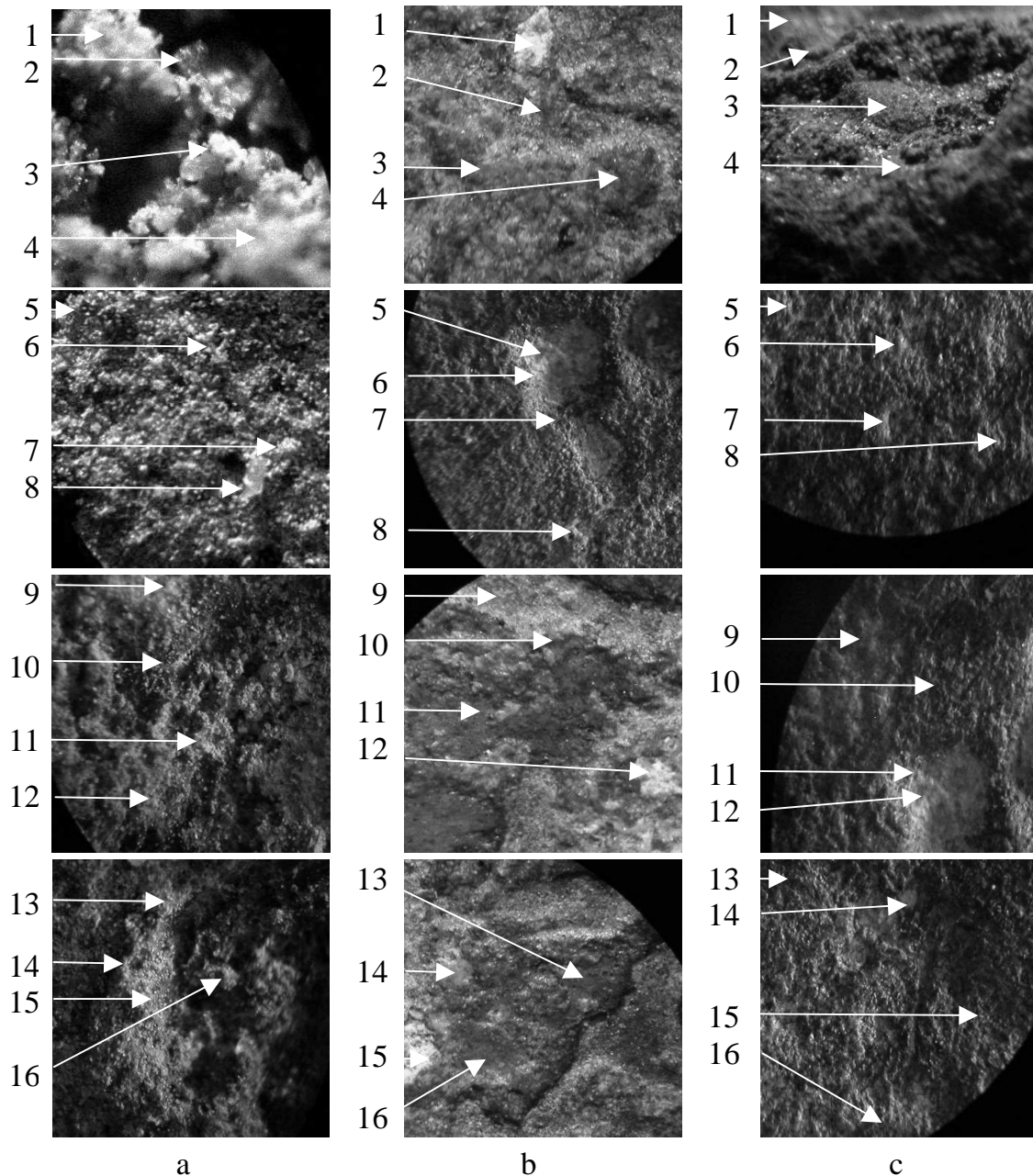


Fig. 4. Sampling areas for the colorimetric analysis: a – MA, b – MO, c – MR.

The points selected for analysis are represented by mineralogical entities more or less unpurified, both during the corrosion processes and by contamination after the pedological processes (recrystallizations, dehydrations, segregations, osmoses, carbonations, sulphations, chlorination etc.).

The colorimetry has the advantage that allows a punctual analysis of the color of the microcrystallites. In this respect, the mineralogical phases, studied also with other methods [14] were identified in their major part (table 1).

Table 1. The colorimetric results (RGB) for the minerals in the structure of the patina analyzed by groups of coins

Nr. crt.	Mineral	MA coins			Mineral	MO coins			Mineral	MR coins		
		R	G	B		R	G	B		R	G	B
1	Calcite	231	246	57	Quartz	234	244	122	Antlerite	100	76	6
2	Malachite	75	140	14	Cuprite	138	58	9	Langite	159	147	27
3	Malachite	58	117	51	Malachite	62	125	21	Calcocite	165	118	28
4	Calcite	251	241	109	Cuprite	140	49	5	Cuprite	158	75	7
5	Cuprite	211	55	0	Anglesite	104	85	0	Antlerite	106	36	0
6	Cuprite	215	82	15	Gloslarite	242	206	84	Brocantite	57	55	6
7	Calcite	255	236	209	Tenorite	211	109	24	Cuprite	170	95	2
8	Quartz	216	157	39	Calcite	219	183	63	Cassiterite	231	157	60
9	Paratachamite	159	136	30	Tenorite	180	100	5	Brocantite	63	61	13
10	Minium	220	125	41	Brocantite	78	84	10	Tenorite	184	80	9
11	Tenorite	175	88	9	Cuprite	195	62	17	Atacanite	135	130	10
12	Calcocite	125	114	22	Ceruză	249	255	157	Cassiterite	236	212	62
13	Tenorite	160	116	7	Cuprite	153	45	0	Nantokite	63	31	8
14	Atacanite	149	152	19	Atacanite	139	164	36	Anglesite	112	99	7
15	Malachite	84	108	24	Gypsum	241	252	124	Cuprite	192	100	35
16	Paratachamite	134	135	31	Cuprite	182	56	16	Cuprite	180	83	41

From the table 1 the deviations and chromatic alterations can be evaluated with the relative color modifications of micro-crystallites morphologically similar in the same group of coins (table 2) or between groups (table 3).

According to the results of the table 2, only some mineralogical phases, derived from the corrosion and pedological processes, can be used for the study of the evolution of these processes in time. Malachite, cuprite, tenorite etc. are among these minerals and are formed during the corrosion processes, while calcite derives from contamination.

Table 2. Differences between the R G B values in the variation field, relative to a mineral from the patina of the analyzed coins

Mineral	ΔR			ΔG			ΔB		
	MA	MO	MR	MA	MO	MR	MA	MO	MR
Malachite	26	0	-	32	0	-	37	0	-
Cuprite	4	57	86	27	17	64	15	16	34
Atacamite	0	0	0	0	0	0	0	0	0
Paratacamite	25	-	-	1	-	-	1	-	-
Tenorite	15	31	0	28	9	0	28	19	0
Calcocite	0	-	0	0	-	0	0	-	0
Anglesite	-	0	0	-	0	0	-	0	0
Nantokite	-	-	0	-	-	0	-	-	0
Brocantite	-	0	6	-	0	6	-	0	7
Antlerite	-	-	6	-	-	40	-	-	6
Gloslarite	-	0	-	-	0	-	-	0	-
Ceruse	-	0	-	-	0	-	-	0	-
Minium	0	-	-	0	-	-	0	-	-
Cassiterite	-	-	5	-	-	65	-	-	2
Calcite	24	0	-	10	0	-	52	0	-
Gypsum	-	0	-	-	0	-	-	0	-
Quartz	0	-	-	0	-	-	0	-	-

The R G B values for the same compounds (table 3) allow also the determination of characteristics with chronological value, that together with the study

of the evolution in time of the alteration processes can be used as quantitative parameters for authentication.

Tableul 3. Differences between the R G B values relative to the same mineral from the patina of the three groups of coins

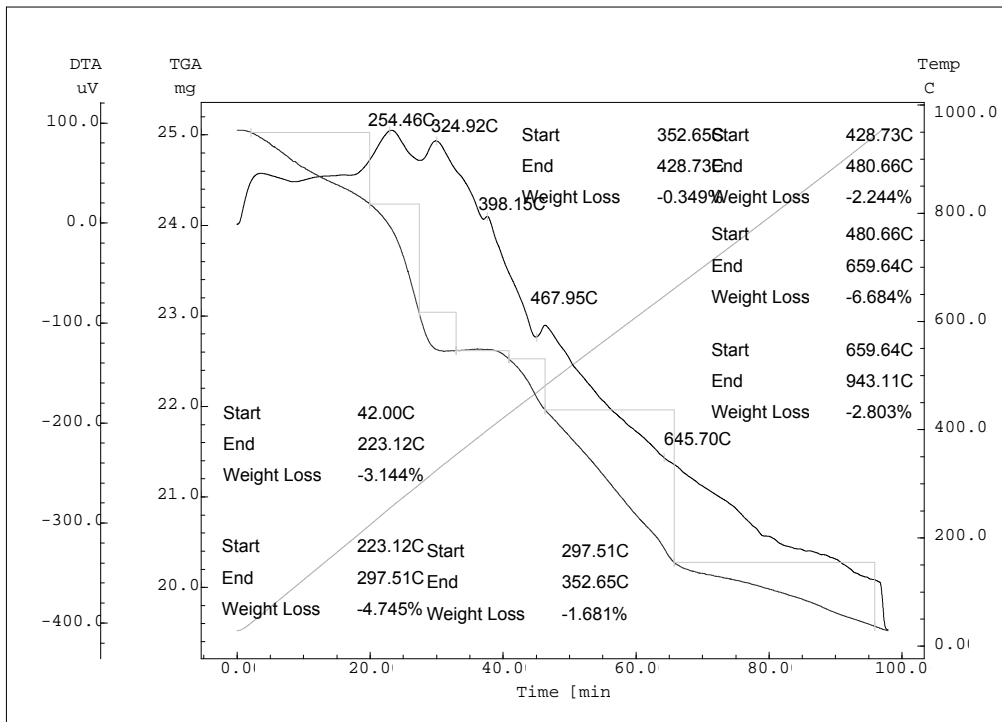
Mineral	ΔR (MA-MO)	ΔG (MA-MR)	ΔB (MO-MR)
Malachite	22	-	-
Cuprite	78	67	41
Atacamite	10	14	26
Tenorite	51	24	29
Calcocite	-	40	-
Anglesite	-	-	7
Brocantite	-	-	4
Calcite	32	-	-
Quartz	18	-	-

We should also mention that the chromatic analysis did not covered all the micro-crystallites from the structure of the patina of the analyzed coins, because it was not the intention of the present paper. The main purpose was the correlation between the colorimetric data concerning the identification of phases and their thermal behavior, studied through gravimetry.

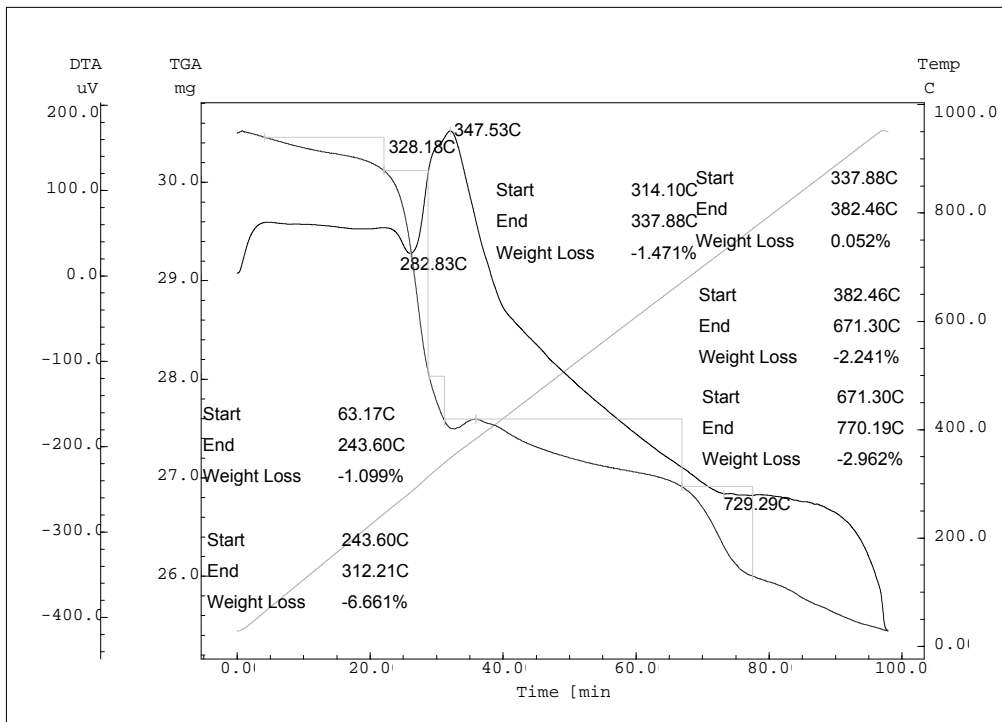
The thermal analysis, in a dynamic regime through the study of the TGA and DTA curves, allows the characterization of the weigh loss and thermal effects evolution during the gradual heating of the samples and puts in evidence the complexity of the composition of the analyzed materials. Studying the thermograms from the figure 5, important differences between the three groups of coins are obvious. In this respect, the MA coins (fig. 5) are containing besides the hygroscopic water also an important quantity of water chemically bounded (constitutive water), under the forms of coordination water, crystallization water, zeolitic water and as OH groups, that are eliminated generally under 315°C. In exchange, the MO coins (fig. 6) present over the area of water elimination a series of oxidation processes of active metallic structures, sulphides and inferior oxides. The MR coins (fig. 7), more recent, with an uniform patina and a poor composition in corrosion products, present, in a limited manner, both the interval of water elimination and the interval related to the processes of thermal decomposition of some oxides, carbonates etc.

At every group of coins can be observed that the external structures are well hydrated (fig. 5b, 6b and 7b). The hydration process rate grows with the age.

The thermogravimetry together with DSC, even they are destructive methods, allow the mathematical elaboration of the DTA curves and the obtained data can be chronologically correlated. Therefore our research group is paying a special attention to these methods. It should be underlined that these methods should be correlated with others when they have to be applied for authentication.

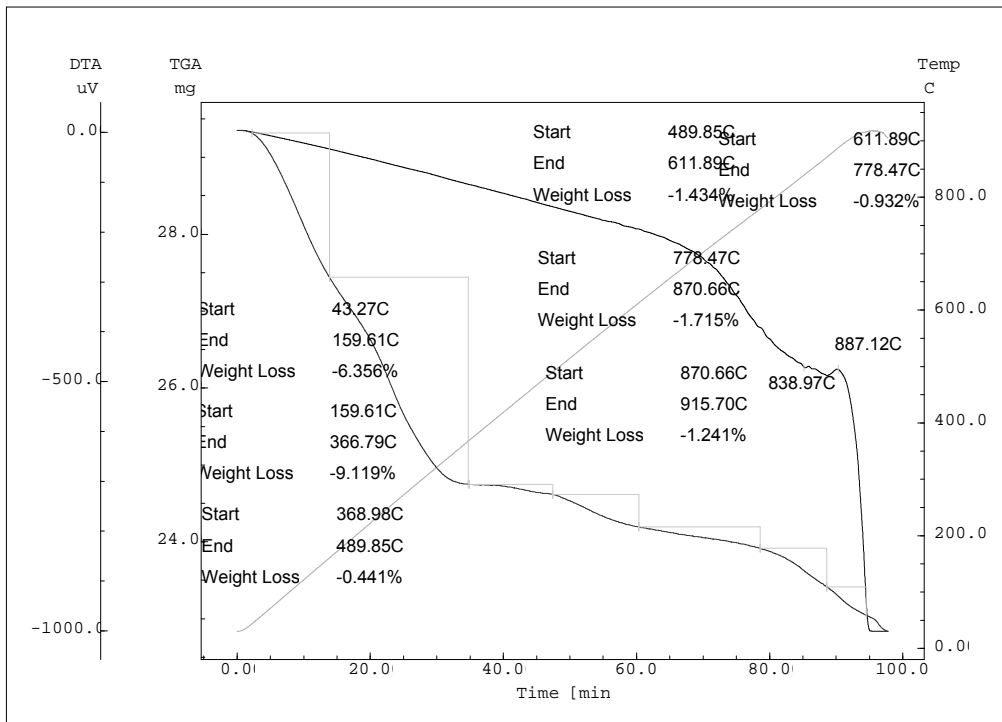


a.

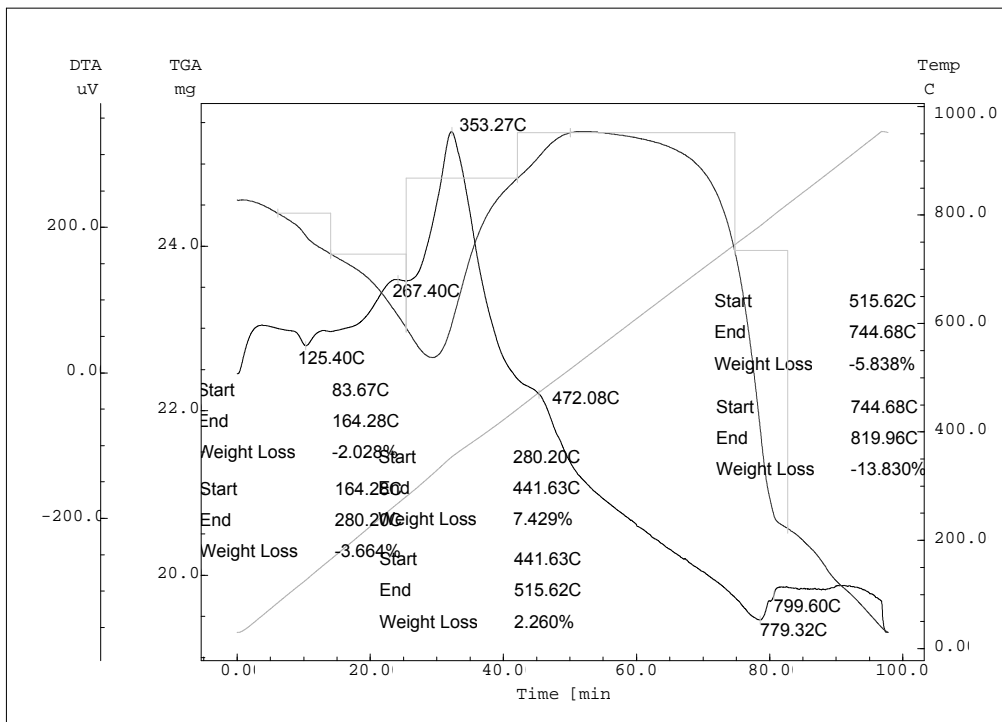


b.

Fig. 5. Derivatograms of the corrosion products in the structure of the patina for MA coins: a – inside coin; b – at surface

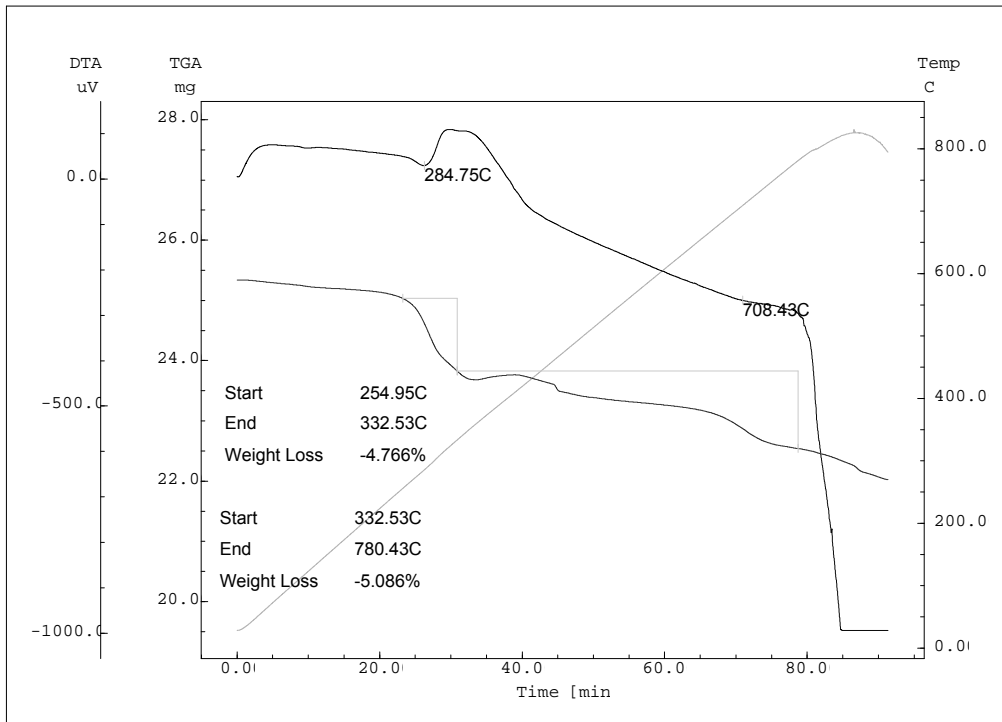


a.

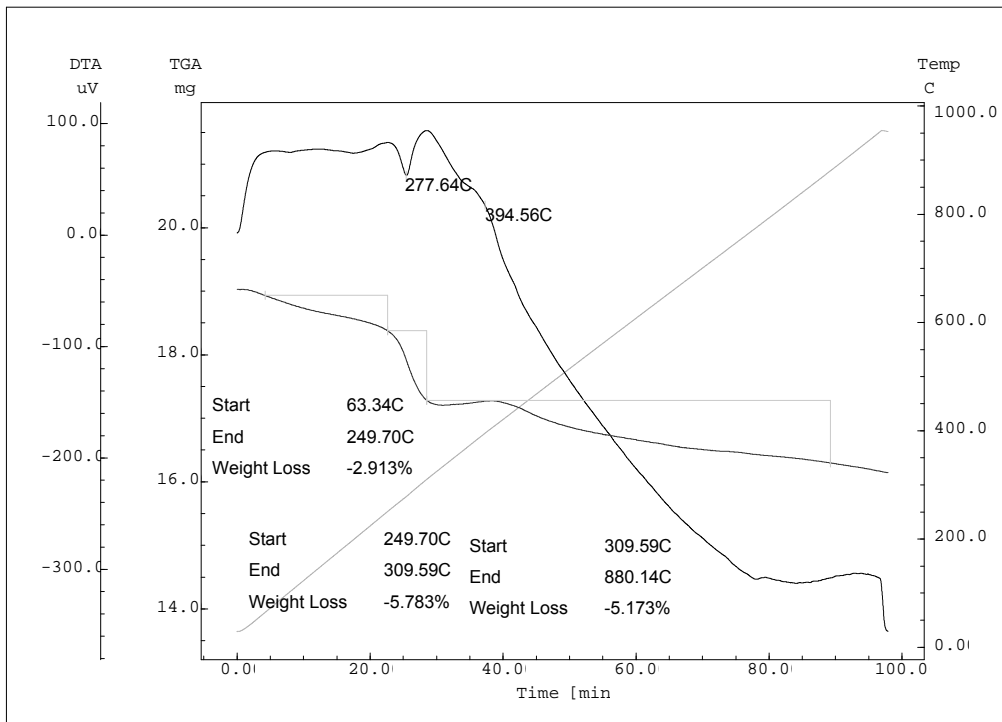


b.

Fig. 6. Derivatograms of the corrosion products in the structure of the patina for MO coins: a – inside coin; b – at surface



a.



b.

Fig. 7. Derivatograms of the corrosion products in the structure of the patina for MR coins: a – inside coin; b – at surface

Conclusions

The paper is the second note from a series that has the purpose of establishing correlations between the composition of the basic alloy and the corrosion products, respectively of the contaminants found in the structure of the patina of the ancient bronze coins, using the analysis of their chemical, physical, optical and structural characteristics. This study will allow the elaboration of an experimental method, as base for an expert system for authentication of ancient bronze artifacts.

The experimental data allow the deeper knowledge of the mechanisms of the corrosion and pedological processes that the coins are subject to during exhibitions or in the archaeological sites when the so-called natural patina is formed. Its characteristics are important in establishing the correlations between the composition and the distribution of the main components of the alloy and those induced by the aggressive exogenous environments or by the pedological processes.

In this way, using two analytical techniques completely different: colorimetry by reflection and thermogravimetry, the difference and the complexity of the corrosion products and contaminants formed in time as a more or less passivant layer (patina) were put in evidence for the three groups of bronze coins, of different époques.

References

1. I. Sandu, A. Dima, I.G. Sandu, **Conservarea și restaurarea obiectelor metalice**, Ed. Corson, Iași 2002;
2. I. Sandu, I.G. Sandu, **Aspecte moderne privind conservarea bunurilor culturale, vol.I, Nomenclatură, tipologii și cazuistici**, Ed. Performantica, Iași, 2005;
3. L. Kockaert, R.H. Marijijnissen, **Dialogue avec l'oeuvre ravagee apres 250 ans de restauration**, Ed. Bibliotheque des Amis du Funds Mercator, Paribas, 1996;
4. F. Schweizer, „*Bronze objects from lake sites: from patina to biography*”, în **Ancient and Historic Metals** (ed. D.A. Scott, J. Podany, B. Considine), Ed. Getty Conservation Institute, Marina del Rey, California, 1994, p.33;
5. I. Sandu, I.C.A. Sandu, A. van Saanen, **Expertiza științifică a operelor de artă**, vol. I (Autentificarea și stabilirea paternității), Ed. Univ. „Al.I. Cuza” Iași în colaborare cu Ed. Trinitas, Iași, 1998;
6. D.A. Scoott, **Metallography and Microstructure of Ancient and Historic Matalls**, Ed. Getty Conservation Institute, Marina del Rey, California, 1991, p.23;
7. K. Nassau, P.K. Gallancher, A.E. Miller, T.E. Graedel, „*The Characterisation of patina components by X-ray difraccition and evolved gas analysis*” în **Corrosin Science**, 27, (1987), p. 669;
8. H.P. Klug, L.E. Alexander, **X-ray Diffraction Procedures for Polycrystalline and Amorphus Materials**, Ed. Wielely, New-York, 1974;
9. N.H. Tennent, K.M. Antonio, „*Bronze disease: synthesis and characterization of botallackite, paratacamite and atacamite by IR spectroscopy*”, în **ICOM Committee for Conservation 6th Triennial Meeting**, Ottawa, (1981), p. 11;
10. R.L. Opila, „*Copper patinas: an investigation by Auger electron spectroscopy*”, în **Corrosion Science**, 27, (1987), p. 685;
11. L.S. Selwyn, N.E. Binnie, J. Poitras, M.E. Laver, D.A. Downham, „*Outdoor Bronze Statues: Analysis of Metal and Surface Samples*” în **Studies în Conservation**, vol. 41, nr. 4 (1996), p. 205;
12. D.A. Scott, J. Podany, „*Ancient cooper alloys: some metallurgical and technological studies of Greek and Roman bronzes*” in **Small Bronzes from the Ancient World**, Ed. J. Paul Getty Museum, Malibu, California (1990), p. 31;
13. I. Sandu, I.C.A. Sandu, I.G. Sandu, **Colorimetria în artă**, Ed. Corson, Iași, 2002;

14. I.G. Sandu, I.C.A. Sandu, A.Dima, I. Sandu, I. Neacșu, „Ancient bronze coins authentication. I. Histochemic, mineralogic, IR and XRD Analysis”, in în **Buletinul Institutului Politehnic din Iasi**, Tomul XLXI (LV), Fasc. 1-2, Secția Știința și Ingineria Materialelor, (2005), p.;
15. D. Costache, **Analiza chimică prin metoda cinetică**, Ed. Academiei RSR, București, 1974.

Received May 4, 2005

- ¹⁾ „Gh. Asachi” Technical University of Iasi, Faculty of Material Science and Engineering
²⁾ Universitatea Politehnica București, Facultatea de Chimie Industrială
³⁾ „Al.I.Cuza” University of Iasi, Department of Cultural Heritage
⁴⁾ Consiglio Nazionale delle Ricerche, ICVBC, Firenze
⁵⁾ Muzeul Militar Național București, Laboratorul de Restaurare

AUTENTIFICAREA MONEDELOR ANTICE DIN BRONZ III. ANALIZA COLORIMETRICĂ ȘI TERMOGRAVIMETRICĂ

Rezumat – În lucrare se prezintă datele experimentale obținute prin analiza colorimetrică prin reflexie și termogravimetrică în regim dinamic, pentru identificarea produșilor de coroziune de interior și exterior și a contaminanților de suprafață, rezultați în timp la expunere în colecții sau prin procese pedologice în situri arheologice, în vederea stabilirii unor corelații implicate în determinarea vechimii, respectiv în autentificare.

STUDY OF THE ARTIFICIAL PATINA OF THE RESTORED ANCIENT BRONZE ARTIFACTS

by

IOAN GABRIEL SANDU¹, ADRIAN DIMA¹, ION SANDU², NICOLAE SULIȚANU³,
STEFANIA STOLERIU⁴, FLORIN DIACONESCU¹

Abstract – The paper deals with the study of the patina obtained by chemical passivation of the ancient coins surfaces that were subject to interventions of restoration. A series of structural characteristics of the patina obtained with a patented procedure are compared with the characteristics of the natural patina and the cleaned basic alloy. Several modern techniques are used in the present study, such as: SEM, AFM, metallographic analysis and colorimetry by reflection.

Keywords: natural and artificial patina, passivation, mineralogical phases, SEM, AFM, metallographic analysis, colorimetry.

1. Introduction

The role and the importance of the natural patina of the ancient cultural goods, especially those made of metal that acquire it in time, either in the archaeological site either during the conservation and exhibition in a museum. This patina gives a noble value to the object and is one of the basic patrimonial elements used in authentication and has also a positive role in protecting the artefact with a passivant layer [1, 2].

Usually, the craftsmen practice of metallic artifacts used as artistic elements made of copper's alloys or with other uses (coins, medals, frames, guard life-lines chandeliers, statues and statuary groups etc.) and the conservation practice of ancient pieces of cultural heritage for obtaining polychrome patinas apply the method of artistic painting with protective layers, by brushing in a thin layer or by immersion or spraying the product. This methods have the great disadvantage of "imitating" the patina, that successively needs a complex elaboration for tones, textures and drawing. On other hand this patina has a limited resistance in time, the product used being easily altered by exfoliation, alveolization, cracking etc., and forming deposits and pellicles that become adherent and monolithic [1, 2, 3].

There are also known the passivation processes for metallic surfaces of bronze and brass, that make use of chemical passivation by oxidation and of electrochemical (anodic oxidation) passivation with aqueous acid or alkaline solutions or with alkaline melting mixtures and oxidizing salts. These procedures can be easily applied on pieces or objects of cultural heritage that have corrossions extended to all the surface, because the technique implies the total immersion in solution or melt and therefore cannot be

applied locally on limited surfaces [6 - 8]. These have also the disadvantage of a very thin, transparent passivant layer that is formed. This layer has a non-uniform unique tone, that is affected chromatically by the oxidized spots formed „in situ” or successively to passivation, in the presence of humid climatic environments.

In the last few years the restoration practice introduced pastes or a wet layer with high porosity that contain oxidizing dispersions of oxides or silver salts [9], calchonatronite, benztriazol and others [10, 11]. These procedures have the disadvantage of giving passivant structures very thin and difficult to be chromatically integrated that in time change their colour due to contamination with sub-products formed in reagents used for treatments.

The present paper deals with a patination procedure by chemical surface passivation patented by the authors [12, 13], that allows the obtaining of an uniform layer as thickness and colour, climatically resistant and adherent to metallic substrata made of copper alloys, using an alcoholic dispersion of ethylic or isopropyl alcohol , that contains Sb penta-sulphide as passivant reagent (with redox and acid-base activity) and two additives, ammonium sulphide and thiourea, structurally characterized by AFM, SEM and colorimetry by reflection. In order to render easier the experiments the samples taken into study are ancient coins, that are the smallest pieces made of copper alloys from, among the objects of cultural heritage. Moreover, their abundance as number, the diversity as alloy composition and casuistic indicate the coins as more appropriate for various studies and researches.

2. Experimental techniques

2.1. Sampling and obtaining the patina of the restored areas

The analyses were done on a group of Romanian bronze coins that circulated between 1867 and 1888 and that presented a very good natural patina.

Half of the front and back sides was treated by immersion in an aqueous solution of nitric acid 40%, in this way being removed the patina and the corrosion products. Afterwards the coins were washed, cleaned and dried. Half of the cleaned area and was re-varnished by brush with a dispersion containing ethylic alcohol and Sb penta-sulphide as passivant reagent (with redox and acid-base activity) and two additives, ammonium sulphide and thiourea. The alcoholic dispersion was obtained by finely grinding the three components and mixing them with gradually added quantities of alcohol. Successively the dispersion was applied on the cleaned surface by brush and friction, at the room temperature for 5 minutes. After the washing with alcohol of the treated area and drying with compressed air device, a protective was applied in a very thin, transparent layer of alcoholic solution of propolis [14].

The so treated coins were analysed by Scanning electron microscopy (SEM), high force microscopy (AFM), metallography (MM) and colorimetry by reflection (CR).

2.2. Scanning Electron Microscopy (SEM)

Scanning Electron Microscopy was done with an electron microscope HITACHI S2600N with EDAX spectrometer, with two functions:

- Image analysis with secondary electron detector (SE): resolution: up to 4.0 nm (at 25 kV in high vacuum mode); magnification range: 15x to 300,000x; accelerating voltage: 0.5 kV to 30kV; 300,000x
- Element mapping with energy dispersive x-ray spectrometer (EDAX): 72 elements from sodium to uranium (up to 8 elements simultaneously) are displayed and automatically overlaid.

2.3. Atomic Force Microscopy (AFM)

An atomically sharp tip is scanned over a surface with feedback mechanisms that enable the piezo-electric scanners to maintain the tip at a constant force (to obtain height information), or height (to obtain force information) above the sample surface. The force between the tip and the sample surface is very small, usually less than 10^{-9} N. AFMs can achieve a resolution of 10 pm, and unlike electron microscopes, can image samples in air. By using AFM can be obtained information on 3-Dimensional topography of surfaces, metrology and analysis of sub-micron phase distribution in metals, thin film mechanical and physical property characterization, defect imaging in metal failure analysis etc.

2.4. Metallographic analysis

For the metallographic analysis a Zeiss – Neophot metallographic microscope was used, and for the nital attack solutions of 25 cm³ HCl (1,19 g/cm³) and 75 cm³ HNO₃ 40% were prepared. The samples were immersed for 5-10 seconds, and successively washed under water jet.

2.5. Colorimetry by reflection

The colorimetric study was done by selecting on the surface of the coins the areas with corrosion products and area with an uniform passivated patina. A digital colorimeter with two types of optical devices (based on optical fibers) with different illumination geometries and observation angles, coupled with a computer with which the values R G B of the CIE colorimetric triangle were established. The analyzed areas were covered with *mylar* (PET), foreseen of small holes that delimit the measuring areas. The number of 3-5 points is corresponding to the comparison areas (basic alloy and patina). In each point the transducer was positioned directly on the material, protecting in this way its colour from the contact.

Because the colorimetric analysis was applied on a non-shining surface, with rough areas, using the same light spot projected in one point, 3-5 determinations were done, in order to eliminate the errors of the measure.

The colorimetric calculation was done on the average spectrum of each point, for which the standard deviation was successively determined. It has to be said that the analysed areas were first cleaned with aqueous and alcohol solutions and for the alloy a side area with active corrosion was chosen for being treated with nitric acid (40%) in order to remove the corrosion layer from the metal. After the nital attack with acid, the coin was attentively cleaned with water and acetone and afterwards desiccated on filter papers.

3. Results and discussions

A group of coins, that circulated on our territory between 1867 and 1888, now in a private collection, was taken into study. The coins have the natural patina very well preserved on the entire surface. The analysts considered also coins with areas affected by active corrosion processes (fig. 1.), that were cleaned, some on half of the surface (for comparison) and others on the entire surface, being removed both the natural patina and the corrosion products and contaminants.

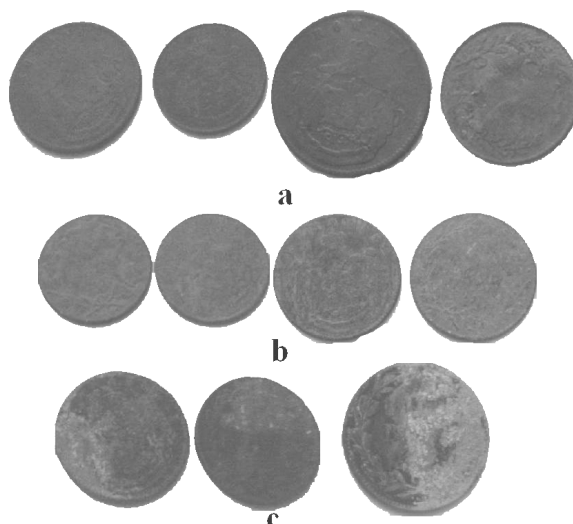


Fig. 1. Coins taken into study: a – with well preserved patina ;
b – with patina and slow extended corrosion ; c – with patina and active corrosion

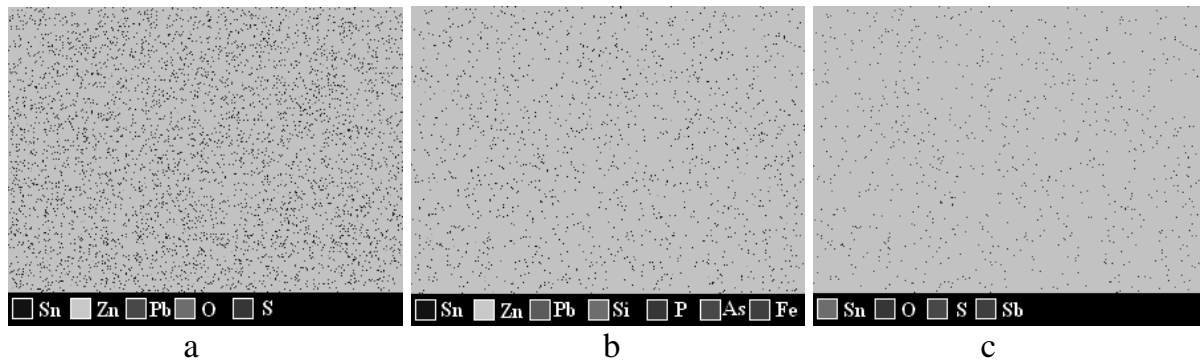


b

Fig. 2. Cleaned and varnished coins:

a – on half of the surface for comparison; b – on the entire surface;

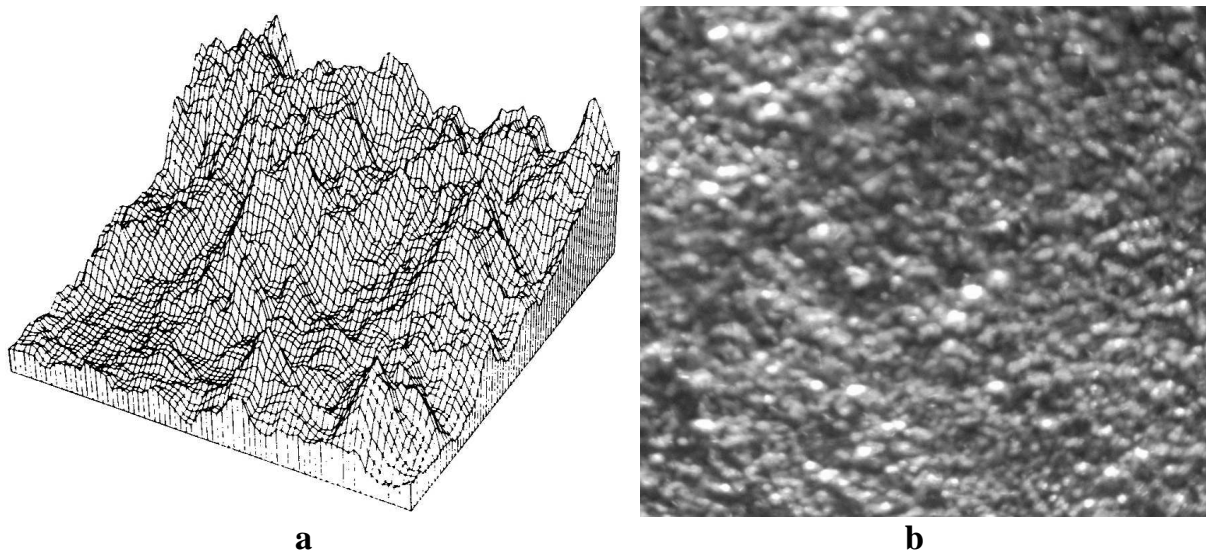
The SEM analysis put in evidence the distribution of the structural components in the natural patina (coin as collection piece), in the basic alloy (cleaned coin) and in the re-varnished structure (Fig. 3).

**Fig. 3.** Distribution of atoms by SEM analysis for:

a – ancient patina; b – basic cleaned alloy; c – re-varnished structure

It can be observed the presence of the oxygen and sulphur atoms both in the ancient patina and in the newly obtained artificial patina, the last having also Sb atoms in composition (a limited number). It can be also observed the uniform distribution of passivant microelements and their crowding in function of the type of patina, natural or artificial.

Figure 4 shows the AFM topography of passivated surface. The AFM images emphasized the uniform distribution of the surface structures after the repatination.

**Fig. 4.** AFM topography of the repatinated surface:

a -3D surface profile image; b – top view surface image.

The figure 5 gives the compared images obtained by metallographic analysis, in which the structures of natural patina under the form of cracked, eroded surface (fig.

5a), the crystalline phases of basic alloy (fig. 5b) and the homogenous structures of the artificial patina (fig. 5c).

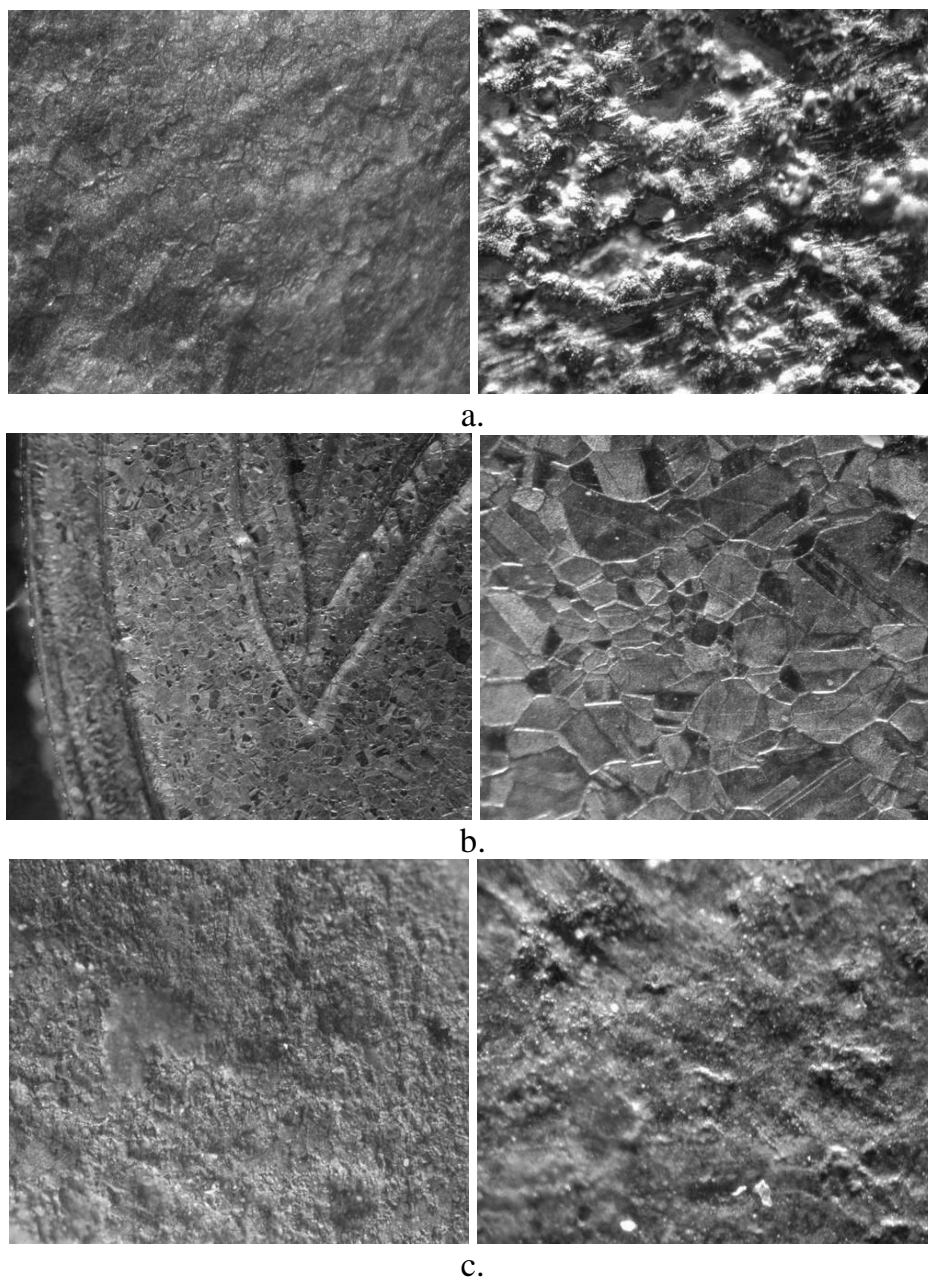


Fig. 5. Metallographic images (40X and 200X):
a – natural patina, b – metal cleaned by nital attack; c – re-varnished surface

The colorimetric analysis took into consideration areas of structures with a homogenous colour. In this respect, for the natural patina (fig. 6a) the measures were done in the points corresponding to some minerals of similar background colour (cuprite, calcocite and tenorite), for the cleaned coin (fig. 6b), in the points with an homogeneous colour corresponding to brass, and for the re-varnished areas (fig. 6c) in the points corresponding to the same minerals as for the natural patina (cuprite, calcocite and tenorite).

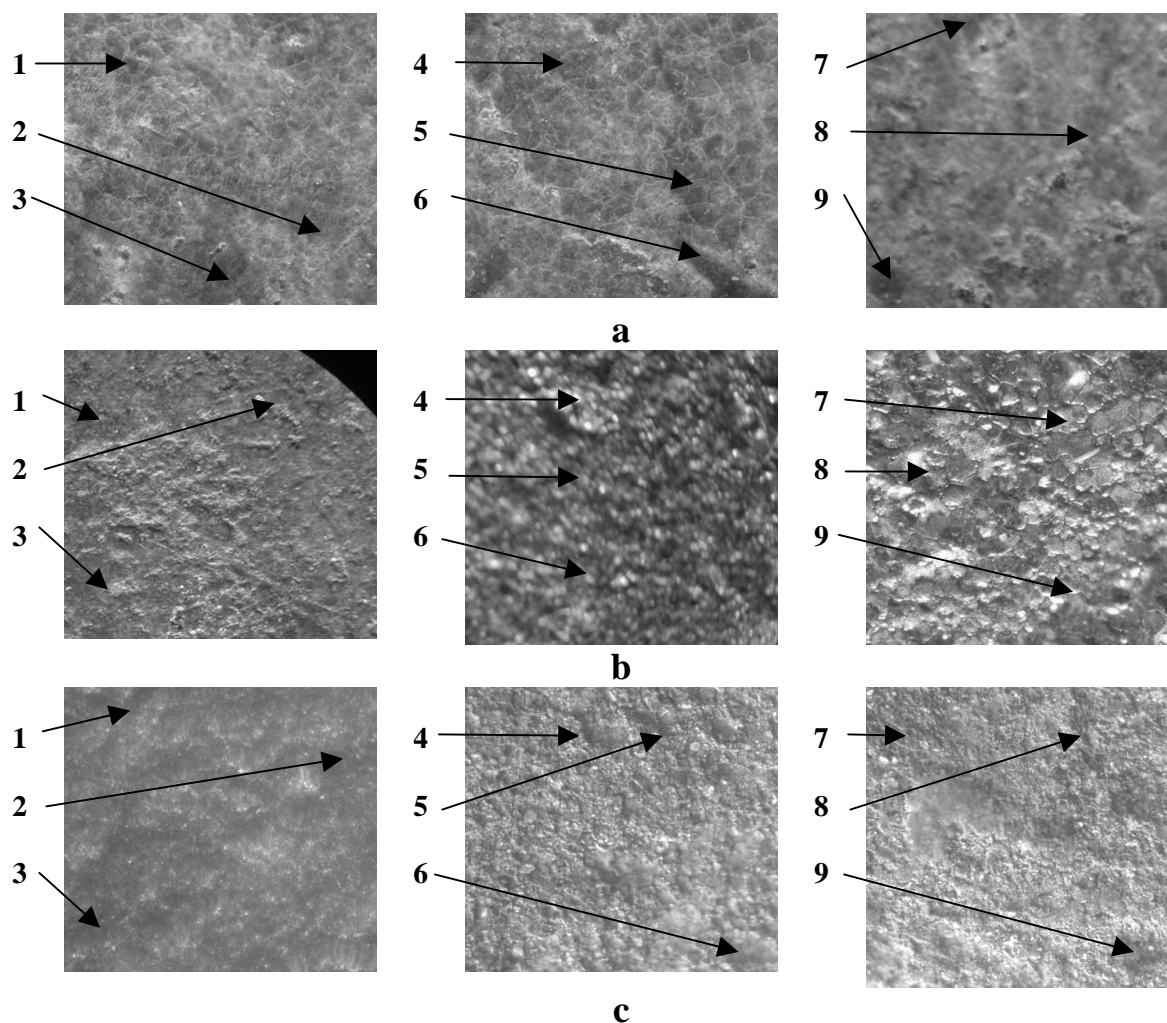


Fig. 6. Images of the surfaces used for colorimetric analysis: a – natural patina; b – cleaned coin; c – artificial patina.

The data obtained from the colorimetric measures for the three types of surfaces: natural patina, cleaned main alloy and artificial patina are reported in the table 1.

Table 1. The colorimetric results (RGB) for the minerals in the structure of the patina analysed by groups of coins

N.	Natural patina			Main alloy			Artificial patina		
	R	G	B	R	G	B	R	G	B
1	121	90	26	223	114	49	114	51	20
2	112	77	11	235	135	75	117	57	29
3	129	93	17	235	119	60	106	64	27
4	124	92	35	229	124	56	105	58	32
5	106	71	5	243	150	81	100	44	17
6	117	86	22	233	110	50	103	45	7
7	122	86	24	244	89	33	121	55	3
8	141	106	25	255	131	75	118	51	25
9	105	49	2	255	145	77	120	55	10

It can be observed that the variation field of the three parameters RGB for each type of material (natural patina, cleaned main alloy or artificial patina) is quite limited and that proves the chromatic homogeneity of the surface structures. Among them the cleaned main alloy and the artificial patina have a certain homogeneity of the tone, while the natural patina has a larger variation of the colours that correspond to a wider number of minerals that are formed in time from the interaction with the exogenous agents.

4. Conclusions

The paper deals with the characteristic of the patina obtained through a patination procedure of ancient bronze coins in the areas restored by chemical, redox and acid-base passivation under the form of an uniform layer as thickness and colour, climatically resistant and adherent to the substrate.

These passivating structures were analysed by scanning electron microscopy (SEM), high force microscopy (AFM), metallography (MM) and colorimetry by reflection (CR), that put in evidence the uniform characteristics of the distribution of microelements in the phases of natural patina, of the area under the natural patina (obtained by its pickling) and of the cleaned and re-varnished area.

References

1. I. Sandu, A. Dima, I.G. Sandu, **Conservarea și restaurarea obiectelor metalice**, Ed. Corson, Iași, 2002;
2. I. Sandu, I.G. Sandu, **Aspecte moderne privind conservarea bunurilor culturale, vol.I, Nomenclatură, tipologii și cazuistici**, Ed. Performantica, Iași, 2005;
3. W. Mourey, **Conservarea antichităților metalice – de la săpătură la muzeu**, Ed. Tehnică, București, 1998;
4. A. Marinescu, Gh. Andonianț, E. Bay, **Tehnologii electrochimice și chimice de protecție a materialelor metalice**, Ed. Tehnică, București, 1984;
5. L. Oniciu, E. Grunwald, **Galvanotehnica**, Ed. Științifică și Enciclopedică, București, 1980;
6. Brevet US 4919787;
7. Brevet EP 0149720;
8. Brevet RO 113660;
9. V.C. Sharma, U. S. Lal. M.V. Nair, „Zinc dust treatment – an effective method for the control of bronze disease on excavated objects”, in **Stud. in Conserv.**, 40, 2, May (1995), p. 110;
10. C.V. Horie, J.A. Vint, „Chalconatronite: a by-product of conservation”, **Stud. in Conserv.**, 27, (1982), p185;
11. W.D. Richey, „The interaction of benzotriazole with copper compounds” in **ICOM Committee for Conservation Triennial Meeting**, Madrid (1972), p. 14;
12. I.G. Sandu, A. Dima, I. Sandu, L. Roibu, A.V. Sandu, “*Procedeu de patinare artistică a pieselor metalice*”, Dosar OSIM nr. A00128/2004
13. I. G. Sandu, A. Dima, I. Sandu, N. Sulițanu, Ș. Stoleriu, I. Neacșu, A.V. Sandu, “*Procedeu de repatinare a pieselor din bronz și alamă*”, Dosar OSIM nr. A00236/2005.

Received May 8, 2005

¹⁾ „Gh. Asachi” Technical University of Iasi, Faculty of Material Science and Engineering

²⁾ „Al.I.Cuza” University of Iasi, Department of Cultural Heritage

³⁾ „Al.I.Cuza” University of Iasi, Department of Solid Physics

⁴⁾ Politechnical University Bucharest, Faculty of Industrial Chemistry

Studiul patinei artificiale obținute pe zonele restaurate a pieselor vechi din bronz

Rezumat – Lucrarea se referă la studiul patinei, obținute prin pasivarea chimică a suprafețelor monedelor vechi, care au suferit intervenții de restaurare. Sunt prezentate comparativ o serie de caracteristici structurale ale patinei obținute conform unui procedeu revendicat de autori în raport cu patina de vechime și aliajul de bază curățat prin decapare. În acest studio se implică o serie de tehnici moderne, cum ar fi: SEM, AFM, analiza metalografică și colorimetria prin reflexie.

STUDY OF THE ARTIFICIAL PATINA OF THE RESTORED ANCIENT BRONZE ARTIFACTS

by

IOAN GABRIEL SANDU¹, ADRIAN DIMA¹, ION SANDU², NICOLAE SULIȚANU³,
STEFANIA STOLERIU⁴, FLORIN DIACONESCU¹

Abstract – The paper deals with the study of the patina obtained by chemical passivation of the ancient coins surfaces that were subject to interventions of restoration. A series of structural characteristics of the patina obtained with a patented procedure are compared with the characteristics of the natural patina and the cleaned basic alloy. Several modern techniques are used in the present study, such as: SEM, AFM, metallographic analysis and colorimetry by reflection.

Keywords: natural and artificial patina, passivation, mineralogical phases, SEM, AFM, metallographic analysis, colorimetry.

1. Introduction

The role and the importance of the natural patina of the ancient cultural goods, especially those made of metal that acquire it in time, either in the archaeological site either during the conservation and exhibition in a museum. This patina gives a noble value to the object and is one of the basic patrimonial elements used in authentication and has also a positive role in protecting the artefact with a passivant layer [1, 2].

Usually, the craftsmen practice of metallic artifacts used as artistic elements made of copper's alloys or with other uses (coins, medals, frames, guard life-lines chandeliers, statues and statuary groups etc.) and the conservation practice of ancient pieces of cultural heritage for obtaining polychrome patinas apply the method of artistic painting with protective layers, by brushing in a thin layer or by immersion or spraying the product. This methods have the great disadvantage of "imitating" the patina, that successively needs a complex elaboration for tones, textures and drawing. On other hand this patina has a limited resistance in time, the product used being easily altered by exfoliation, alveolization, cracking etc., and forming deposits and pellicles that become adherent and monolithic [1, 2, 3].

There are also known the passivation processes for metallic surfaces of bronze and brass, that make use of chemical passivation by oxidation and of electrochemical (anodic oxidation) passivation with aqueous acid or alkaline solutions or with alkaline melting mixtures and oxidizing salts. These procedures can be easily applied on pieces or objects of cultural heritage that have corrossions extended to all the surface, because the technique implies the total immersion in solution or melt and therefore cannot be

applied locally on limited surfaces [6 - 8]. These have also the disadvantage of a very thin, transparent passivant layer that is formed. This layer has a non-uniform unique tone, that is affected chromatically by the oxidized spots formed „in situ” or successively to passivation, in the presence of humid climatic environments.

In the last few years the restoration practice introduced pastes or a wet layer with high porosity that contain oxidizing dispersions of oxides or silver salts [9], calchonatronite, benztriazol and others [10, 11]. These procedures have the disadvantage of giving passivant structures very thin and difficult to be chromatically integrated that in time change their colour due to contamination with sub-products formed in reagents used for treatments.

The present paper deals with a patination procedure by chemical surface passivation patented by the authors [12, 13], that allows the obtaining of an uniform layer as thickness and colour, climatically resistant and adherent to metallic substrata made of copper alloys, using an alcoholic dispersion of ethylic or isopropyl alcohol , that contains Sb penta-sulphide as passivant reagent (with redox and acid-base activity) and two additives, ammonium sulphide and thiourea, structurally characterized by AFM, SEM and colorimetry by reflection. In order to render easier the experiments the samples taken into study are ancient coins, that are the smallest pieces made of copper alloys from, among the objects of cultural heritage. Moreover, their abundance as number, the diversity as alloy composition and casuistic indicate the coins as more appropriate for various studies and researches.

2. Experimental techniques

2.1. Sampling and obtaining the patina of the restored areas

The analyses were done on a group of Romanian bronze coins that circulated between 1867 and 1888 and that presented a very good natural patina.

Half of the front and back sides was treated by immersion in an aqueous solution of nitric acid 40%, in this way being removed the patina and the corrosion products. Afterwards the coins were washed, cleaned and dried. Half of the cleaned area and was re-varnished by brush with a dispersion containing ethylic alcohol and Sb penta-sulphide as passivant reagent (with redox and acid-base activity) and two additives, ammonium sulphide and thiourea. The alcoholic dispersion was obtained by finely grinding the three components and mixing them with gradually added quantities of alcohol. Successively the dispersion was applied on the cleaned surface by brush and friction, at the room temperature for 5 minutes. After the washing with alcohol of the treated area and drying with compressed air device, a protective was applied in a very thin, transparent layer of alcoholic solution of propolis [14].

The so treated coins were analysed by Scanning electron microscopy (SEM), high force microscopy (AFM), metallography (MM) and colorimetry by reflection (CR).

2.2. Scanning Electron Microscopy (SEM)

Scanning Electron Microscopy was done with an electron microscope HITACHI S2600N with EDAX spectrometer, with two functions:

- Image analysis with secondary electron detector (SE): resolution: up to 4.0 nm (at 25 kV in high vacuum mode); magnification range: 15x to 300,000x; accelerating voltage: 0.5 kV to 30kV; 300,000x
- Element mapping with energy dispersive x-ray spectrometer (EDAX): 72 elements from sodium to uranium (up to 8 elements simultaneously) are displayed and automatically overlaid.

2.3. Atomic Force Microscopy (AFM)

An atomically sharp tip is scanned over a surface with feedback mechanisms that enable the piezo-electric scanners to maintain the tip at a constant force (to obtain height information), or height (to obtain force information) above the sample surface. The force between the tip and the sample surface is very small, usually less than 10^{-9} N. AFMs can achieve a resolution of 10 pm, and unlike electron microscopes, can image samples in air. By using AFM can be obtained information on 3-Dimensional topography of surfaces, metrology and analysis of sub-micron phase distribution in metals, thin film mechanical and physical property characterization, defect imaging in metal failure analysis etc.

2.4. Metallographic analysis

For the metallographic analysis a Zeiss – Neophot metallographic microscope was used, and for the nital attack solutions of 25 cm³ HCl (1,19 g/cm³) and 75 cm³ HNO₃ 40% were prepared. The samples were immersed for 5-10 seconds, and successively washed under water jet.

2.5. Colorimetry by reflection

The colorimetric study was done by selecting on the surface of the coins the areas with corrosion products and area with an uniform passivated patina. A digital colorimeter with two types of optical devices (based on optical fibers) with different illumination geometries and observation angles, coupled with a computer with which the values R G B of the CIE colorimetric triangle were established. The analyzed areas were covered with *mylar* (PET), foreseen of small holes that delimit the measuring areas. The number of 3-5 points is corresponding to the comparison areas (basic alloy and patina). In each point the transducer was positioned directly on the material, protecting in this way its colour from the contact.

Because the colorimetric analysis was applied on a non-shining surface, with rough areas, using the same light spot projected in one point, 3-5 determinations were done, in order to eliminate the errors of the measure.

The colorimetric calculation was done on the average spectrum of each point, for which the standard deviation was successively determined. It has to be said that the analysed areas were first cleaned with aqueous and alcohol solutions and for the alloy a side area with active corrosion was chosen for being treated with nitric acid (40%) in order to remove the corrosion layer from the metal. After the nital attack with acid, the coin was attentively cleaned with water and acetone and afterwards desiccated on filter papers.

3. Results and discussions

A group of coins, that circulated on our territory between 1867 and 1888, now in a private collection, was taken into study. The coins have the natural patina very well preserved on the entire surface. The analysts considered also coins with areas affected by active corrosion processes (fig. 1.), that were cleaned, some on half of the surface (for comparison) and others on the entire surface, being removed both the natural patina and the corrosion products and contaminants.

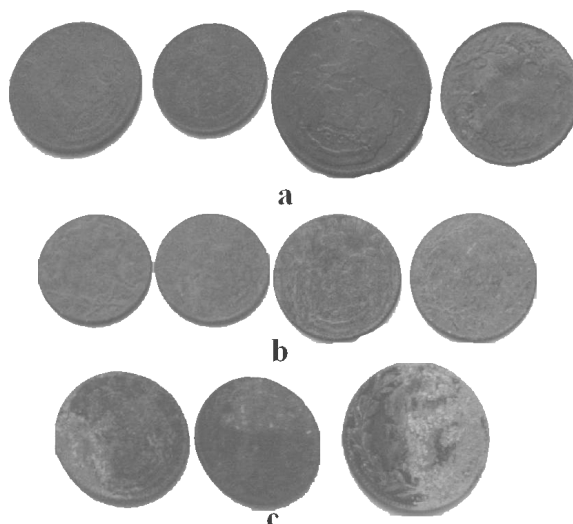


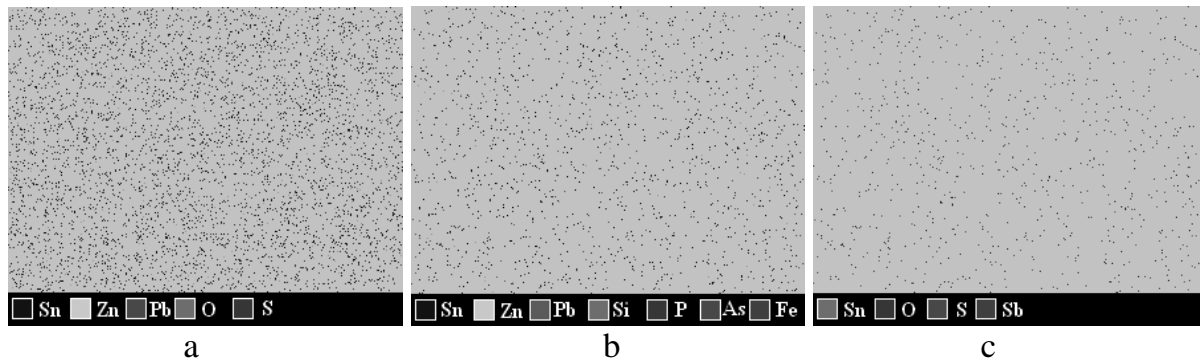
Fig. 1. Coins taken into study: a – with well preserved patina ;
b – with patina and slow extended corrosion ; c – with patina and active corrosion



b**Fig. 2.** Cleaned and varnished coins:

a – on half of the surface for comparison; b – on the entire surface;

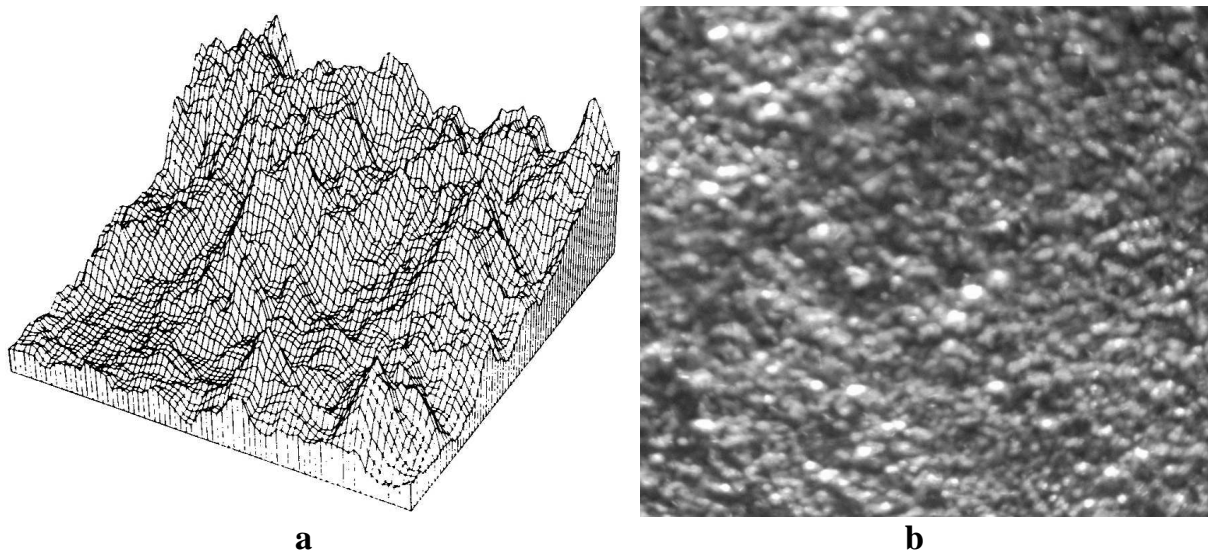
The SEM analysis put in evidence the distribution of the structural components in the natural patina (coin as collection piece), in the basic alloy (cleaned coin) and in the re-varnished structure (Fig. 3).

**Fig. 3.** Distribution of atoms by SEM analysis for:

a – ancient patina; b – basic cleaned alloy; c – re-varnished structure

It can be observed the presence of the oxygen and sulphur atoms both in the ancient patina and in the newly obtained artificial patina, the last having also Sb atoms in composition (a limited number). It can be also observed the uniform distribution of passivant microelements and their crowding in function of the type of patina, natural or artificial.

Figure 4 shows the AFM topography of passivated surface. The AFM images emphasized the uniform distribution of the surface structures after the repatination.

**Fig. 4.** AFM topography of the repatinated surface:

a -3D surface profile image; b – top view surface image.

The figure 5 gives the compared images obtained by metallographic analysis, in which the structures of natural patina under the form of cracked, eroded surface (fig.

5a), the crystalline phases of basic alloy (fig. 5b) and the homogenous structures of the artificial patina (fig. 5c).

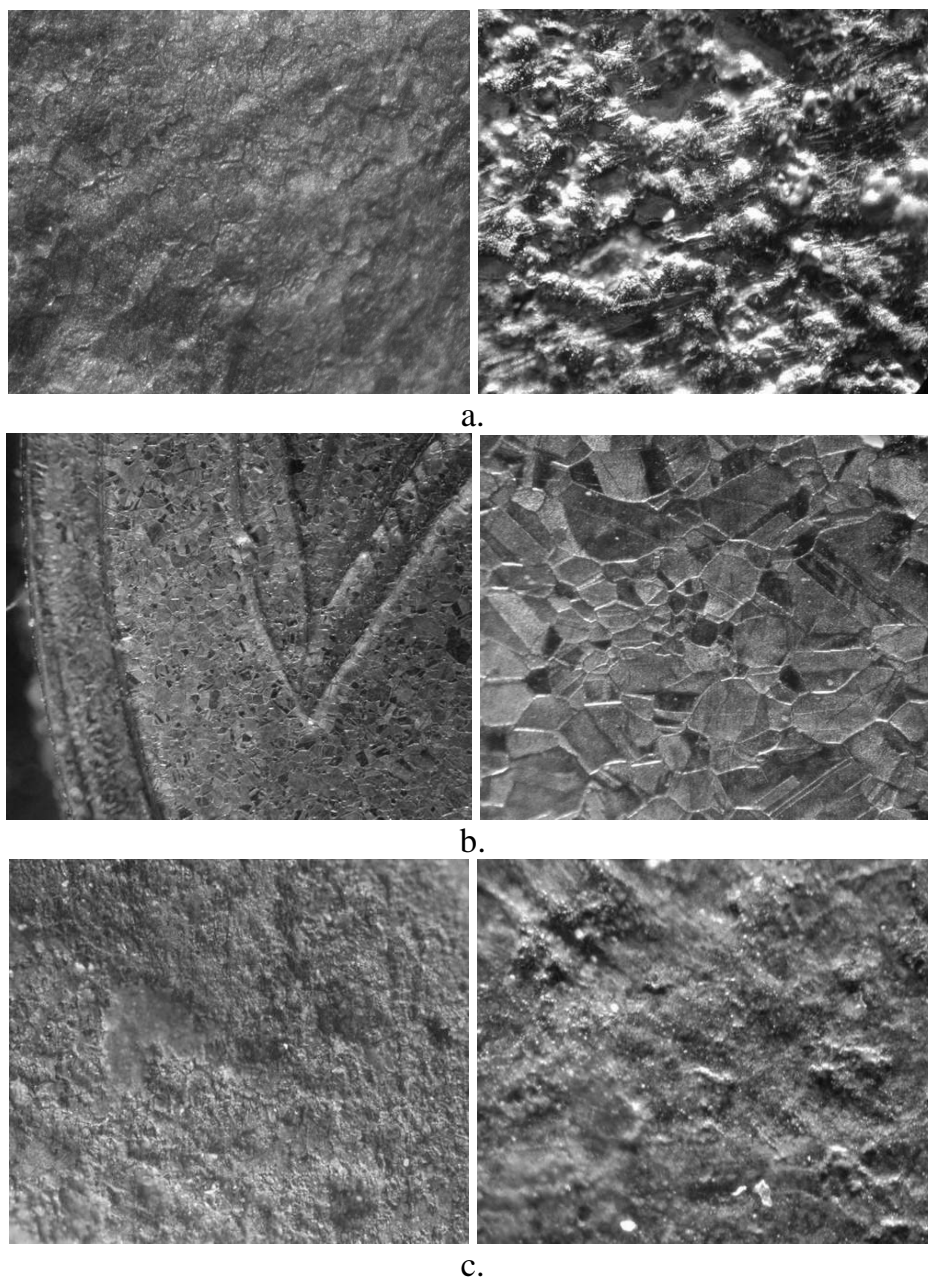


Fig. 5. Metallographic images (40X and 200X):
a – natural patina, b – metal cleaned by nital attack; c – re-varnished surface

The colorimetric analysis took into consideration areas of structures with a homogenous colour. In this respect, for the natural patina (fig. 6a) the measures were done in the points corresponding to some minerals of similar background colour (cuprite, calcocite and tenorite), for the cleaned coin (fig. 6b), in the points with an homogeneous colour corresponding to brass, and for the re-varnished areas (fig. 6c) in the points corresponding to the same minerals as for the natural patina (cuprite, calcocite and tenorite).

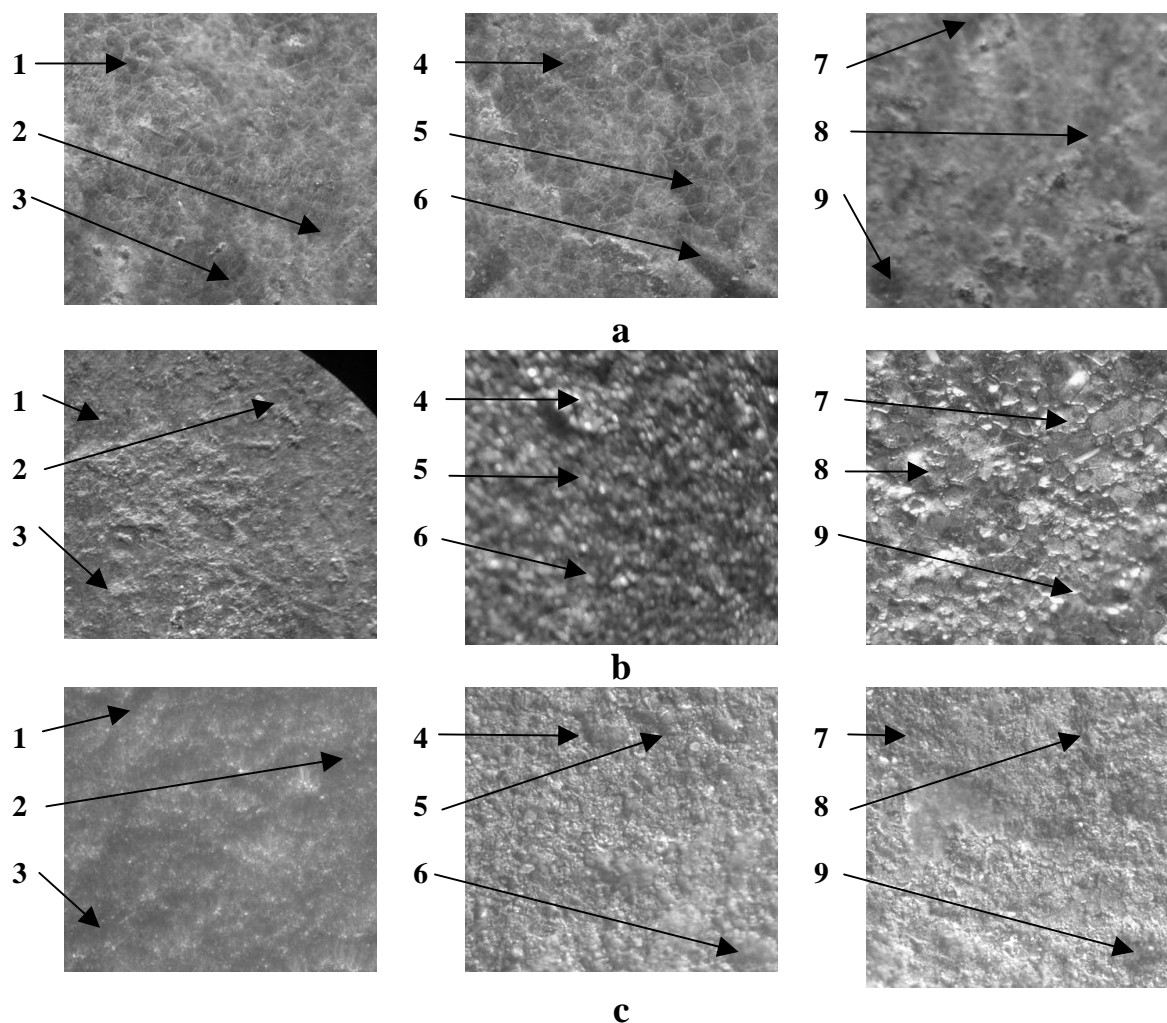


Fig. 6. Images of the surfaces used for colorimetric analysis: a – natural patina; b – cleaned coin; c – artificial patina.

The data obtained from the colorimetric measures for the three types of surfaces: natural patina, cleaned main alloy and artificial patina are reported in the table 1.

Table 1. The colorimetric results (RGB) for the minerals in the structure of the patina analysed by groups of coins

N.	Natural patina			Main alloy			Artificial patina		
	R	G	B	R	G	B	R	G	B
1	121	90	26	223	114	49	114	51	20
2	112	77	11	235	135	75	117	57	29
3	129	93	17	235	119	60	106	64	27
4	124	92	35	229	124	56	105	58	32
5	106	71	5	243	150	81	100	44	17
6	117	86	22	233	110	50	103	45	7
7	122	86	24	244	89	33	121	55	3
8	141	106	25	255	131	75	118	51	25
9	105	49	2	255	145	77	120	55	10

It can be observed that the variation field of the three parameters RGB for each type of material (natural patina, cleaned main alloy or artificial patina) is quite limited and that proves the chromatic homogeneity of the surface structures. Among them the cleaned main alloy and the artificial patina have a certain homogeneity of the tone, while the natural patina has a larger variation of the colours that correspond to a wider number of minerals that are formed in time from the interaction with the exogenous agents.

4. Conclusions

The paper deals with the characteristic of the patina obtained through a patination procedure of ancient bronze coins in the areas restored by chemical, redox and acid-base passivation under the form of an uniform layer as thickness and colour, climatically resistant and adherent to the substrate.

These passivating structures were analysed by scanning electron microscopy (SEM), high force microscopy (AFM), metallography (MM) and colorimetry by reflection (CR), that put in evidence the uniform characteristics of the distribution of microelements in the phases of natural patina, of the area under the natural patina (obtained by its pickling) and of the cleaned and re-varnished area.

References

1. I. Sandu, A. Dima, I.G. Sandu, **Conservarea și restaurarea obiectelor metalice**, Ed. Corson, Iași, 2002;
2. I. Sandu, I.G. Sandu, **Aspecte moderne privind conservarea bunurilor culturale, vol.I, Nomenclatură, tipologii și cazuistici**, Ed. Performantica, Iași, 2005;
3. W. Mourey, **Conservarea antichităților metalice – de la săpătură la muzeu**, Ed. Tehnică, București, 1998;
4. A. Marinescu, Gh. Andonianț, E. Bay, **Tehnologii electrochimice și chimice de protecție a materialelor metalice**, Ed. Tehnică, București, 1984;
5. L. Oniciu, E. Grunwald, **Galvanotehnica**, Ed. Științifică și Enciclopedică, București, 1980;
6. Brevet US 4919787;
7. Brevet EP 0149720;
8. Brevet RO 113660;
9. V.C. Sharma, U. S. Lal. M.V. Nair, „Zinc dust treatment – an effective method for the control of bronze disease on excavated objects”, in **Stud. in Conserv.**, 40, 2, May (1995), p. 110;
10. C.V. Horie, J.A. Vint, „Chalconatronite: a by-product of conservation”, **Stud. in Conserv.**, 27, (1982), p185;
11. W.D. Richey, „The interaction of benzotriazole with copper compounds” in **ICOM Committee for Conservation Triennial Meeting**, Madrid (1972), p. 14;
12. I.G. Sandu, A. Dima, I. Sandu, L. Roibu, A.V. Sandu, “*Procedeu de patinare artistică a pieselor metalice*”, Dosar OSIM nr. A00128/2004
13. I. G. Sandu, A. Dima, I. Sandu, N. Sulițanu, Ș. Stoleriu, I. Neacșu, A.V. Sandu, “*Procedeu de repatinare a pieselor din bronz și alamă*”, Dosar OSIM nr. A00236/2005.

Received May 8, 2005

¹⁾ „Gh. Asachi” Technical University of Iasi, Faculty of Material Science and Engineering

²⁾ „Al.I.Cuza” University of Iasi, Department of Cultural Heritage

³⁾ „Al.I.Cuza” University of Iasi, Department of Solid Physics

⁴⁾ Politechnical University Bucharest, Faculty of Industrial Chemistry

Studiul patinei artificiale obținute pe zonele restaurate a pieselor vechi din bronz

Rezumat – Lucrarea se referă la studiul patinei, obținute prin pasivarea chimică a suprafețelor monedelor vechi, care au suferit intervenții de restaurare. Sunt prezentate comparativ o serie de caracteristici structurale ale patinei obținute conform unui procedeu revendicat de autori în raport cu patina de vechime și aliajul de bază curățat prin decapare. În acest studio se implică o serie de tehnici moderne, cum ar fi: SEM, AFM, analiza metalografică și colorimetria prin reflexie.

THE ENVIRONMENT TECHNOLOGY APPLIED TO THE PURIFYNG STATION "SLOBOZIA"

by

LIDIA CRISTEA*, MARIANA ZSIGMOND* *, IOANA APOSTOLESCU **

***Abstract.** The environment economy consists of the ensemble of specific activities regarding the management of the environment resources for the purpose of satisfying the human community needs by taking into consideration the rational use of natural resources and the preservation of the ecosystems equilibrium. The purification represents an ensemble of works and measures having as a purpose the diminishing of the loading indicators for the residual waters at values which won't modify its quality over certain limits once they got into the emitting a good and friendly technology.*

The waters quality is also affected by an improper purification of the industrial and household waters by the disappearance of the natural areas of water dumping.

The paper presents aspects connected with the structure of the purifying station of water Slobozia .

Keywords: quality, water, purification, technology, environment.

1. INTRODUCTION

The environment quality is connected with the pollution masses and it can affect its functions (fig.1). [1,2]

It is about the used household waters which came from the following sources:

- the household waters of the town of Slobozia,
- the household waters of the village Amara,
- the household waters of the Slaughter House Slobozia,
- the household waters of Dacia Service and the Chemical Laundry.

After being purified, the waters are evacuated in the river Ialomita. In order to be spilled in the river Ialomita, the waters must have the environment index values which should correspond to the quality standards established by the legislation.

The main parameters of quality can be considered:

- $CBO_5 = 35\text{mg/l}$ and
- $\text{imp.} = 30\text{ mg/l}$.

At the moment, the efficiency of the purification of the station is of about 90% with a maximum capacity of 750 l/s.

This efficiency would improve considerably if the tanks for airing would work at a capacity of biological processing of 500-600 l/s, as they were initially calibrated.

This is not possible, because they were built in a wrong way, so they are not hermetically sealed.

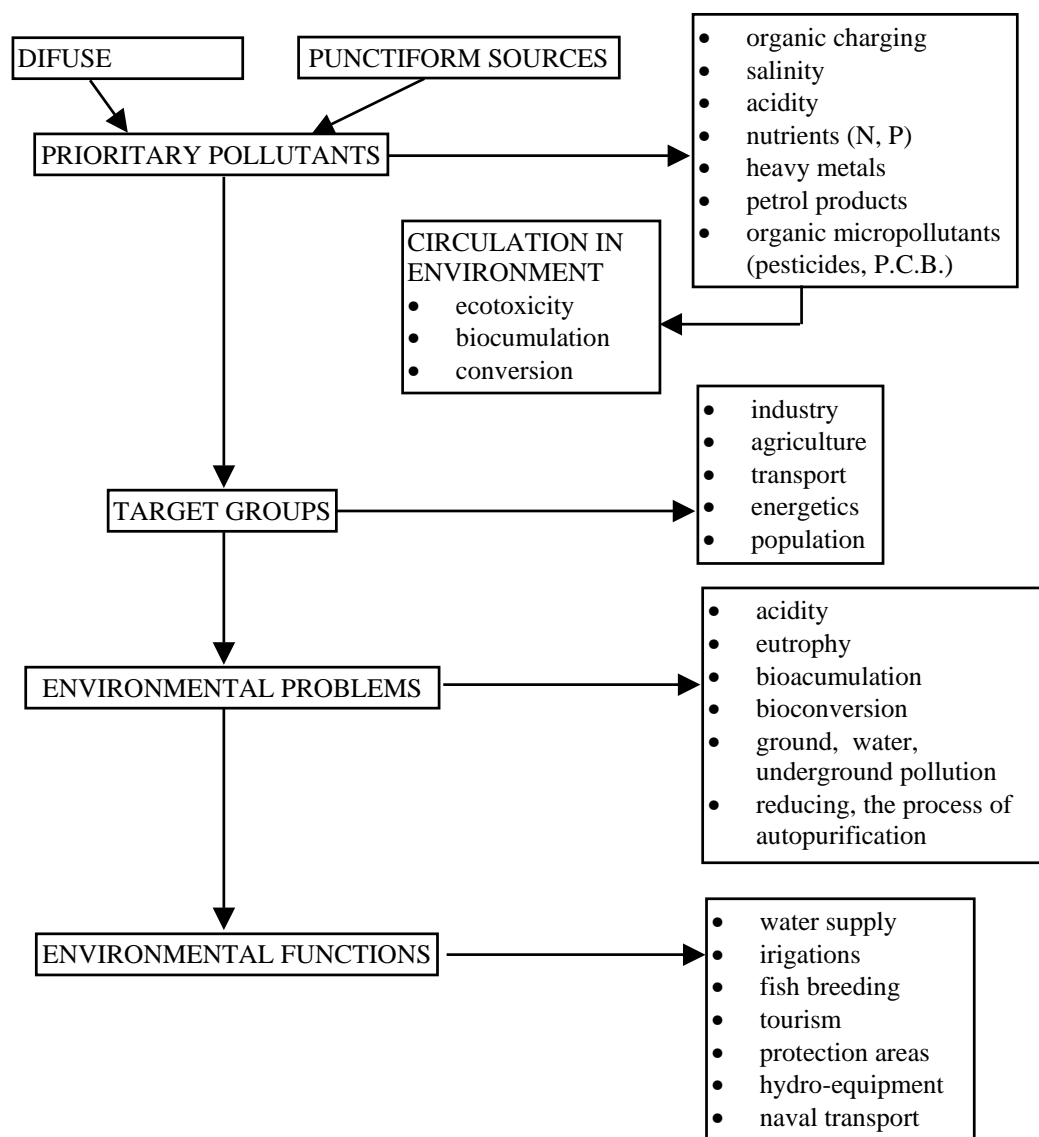


Fig.1 Quality standards for environment

2. THE STRUCTURE OF THE PURIFYING STATION

In order to reduce the concentrations of noxious substances in the residual waters up to the limits admissible by the sanitary rules within the purifying station of Slobozia, there are the following three purifying stages (fig.2):

- the mechanical stage,
- the biological stage,
- the mud processing equipment.

The quantity of oxygen necessary in all parts of the tank for airing must be of 1-3 mg/l. W.W. Eckenfelder shows the existence of a close connection between the purifying efficiency and the necessary oxygen. This relation is shown in the chart from fig.3

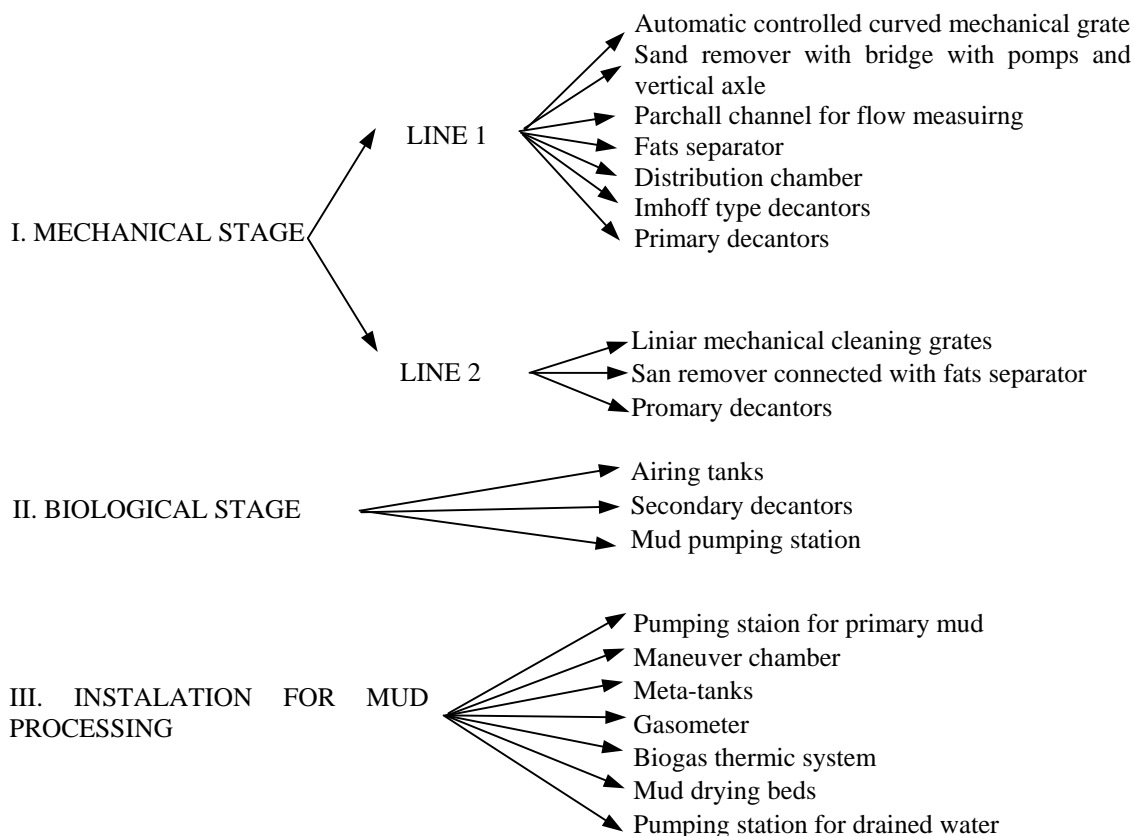


Fig.2 The structure of the purifying station Slobozia

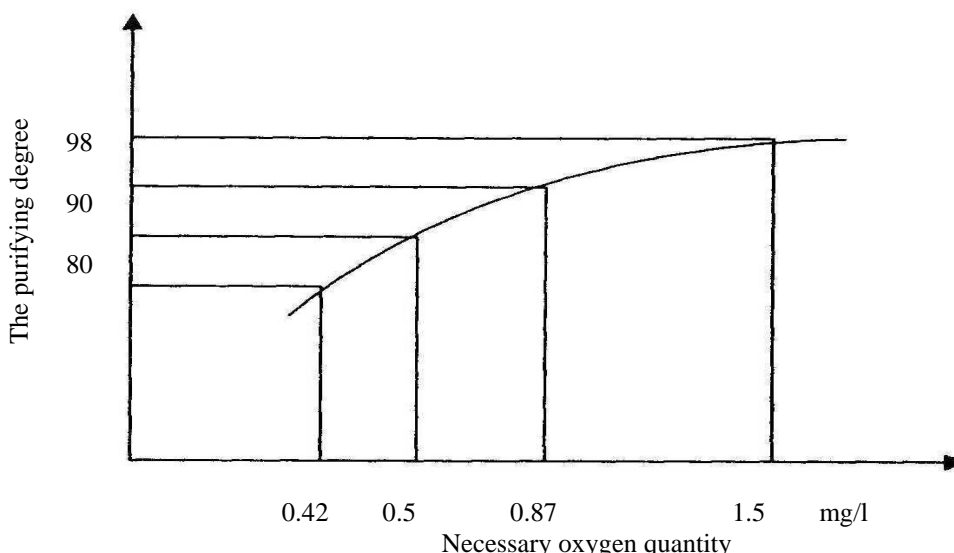


Fig.3 The variation of the necessary oxygen depending on the purifying degree

3. THE WATER STANDARDS OF QUALITY FROM THE POINT OF VIEW OF LAB ANALYSIS

The results presented in this paper were obtained during the period May 5th, 2003 - May 14th, 2003, with the help of the station staff.

The residual water was taken from the sewers at the purifying station ENTRANCE, as well as from the evacuation pipes after the purifying process EVACUATION.

The incoming waters have a fetid smell which partially disappears after the complete purifying process. In the days of the 10th and 11th the water got a faint sulphuric smell which was due to the insufficient O₂, because the airing tanks couldn't be properly used.

The following parameters were analysed:

- pH,
- temperature,
- CCO-Mn,
- CBO₅,
- suspension,
- N total,
- organic substances,
- NH₄.

In table 1 you can see the pH and temperature variation at the ENTRANCE and the EVACUATION of water in the station..

Table 1. pH and temperature variation

ANALYSIS DATE	pH		TEMPERATURE °C	
	ENTRANCE	EVACUATION	ENTRANCE	EVACUATION
May 5	7,28	7,32	23,1	22
May 6	7,19	7,3	23	23,1
May 7	7,25	7,3	17,8	18
May 8	7,36	7,4	19	20
May 9	7,23	7,4	18,5	19
May 10	7,23	7,4	19	19,5
May 11	7,2	7,2	20,5	20,6
May 12	7,24	7,2	19	19,2
May 13	7,31	7,25	21,5	21,6
May 14	7,35	7,1	18	18

Bellow we analyse the pH variation.

Within the 10 days in which the pH values were registered both at the entrance and at the evacuation, there was a slight raise with 0.1-0.3 units in the case of the evacuated water submitted to the purifying process.

The pH index didn't register values which could endanger the activity of organisms from the river Ialomita, because the registered values were within the normal limits of 6.5 - 8.5, which don't affect the life forms .

So, we can perform a good purifying action with the Ph which doesn't go over 8.5.

Any value higher than that would trigger the fungus spreading and would impede the purifying process (fig.4).

The values were registered at 9 o'clock AM.

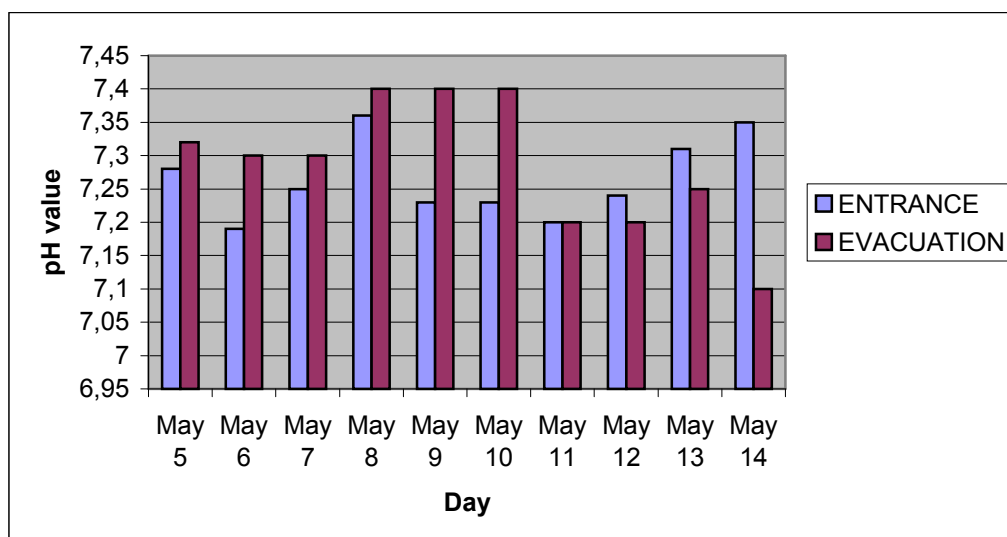


Fig. 4 Registered pH values

4. ECONOMIC ANALYSIS IN THE TECHNOLOGY OF WATER PURIFICATION

The purifying station of household water in Slobozia treats annually 2.962.000 m² of household water which comes from the town population and 91.000 m² which come from economic agents and has a number of 15 people hired for operating the station. The fee requested by S.C. URBAN for purifying the water is 153 lei/m². If we were to estimate the whole amount of money collected by S.C. URBAN for purifying the water, it would be about 3 and half billion lei only for the water which comes from people without taking into consideration the possible changes of price during the year. Detailed lists of expenses for 1 m² of household water are shown in table no.2.

Table 2 The detailed structure of the expenses paid by the population for 1 m² of household water

ELEMENTS OF EXPENSES	ESTIMATED COSTS lei/m ²
1. Variable expenses	171
• technological electrical energy	171
• technological materials	
• expenses for the protection of water quality	
• other specific expenses	
2. Steady expenses, out of which:	927
a) material expenses:	170
• materials	85
• amortization	
• due	30
• repairing within the station	22
• repairing with specialized firms	17
• studies and research	
• other services made by contractors	10
• collaborations	4
• bonus and errands	

<ul style="list-style-type: none"> • protocol, publicity • mail, telecommunications • other material expenses 	6
b) expenses with actual work, out of which:	6
<ul style="list-style-type: none"> • wages 	757
<ul style="list-style-type: none"> • pension 	551
<ul style="list-style-type: none"> • unemployment 	140
<ul style="list-style-type: none"> • heath 	28
c) financial expenses	38
I. Total expenses (1+2)	1098
II. Profit 5%	55
III. Price/fee	1153
IV. The quantity of processed water, including the internal consumption (thousands of m ²)	3000

5. CONCLUSIONS

Out of the total of 1153 lei for one m² of household water:

- 2/3 of its value, namely 757 lei are destined to pay wages for the 15 people working there - so the largest sum goes to the employees;
- an considerable amount - 171 lei is given for the electrical energy necessary to keep the equipment working;
- an small amount is given to the repairing within the purifying station 22+17 =39 lei/m²;
- we can consider that the purifying station registers a little profit 5% out of the value of one m² of household water namely 55 lei;
- the sum which should be paid by a person in Slobozia for the purifying of one m² of water is not very big and if the quality of the purified water is not consistent with the standards in force this thing is due to the bad management of the station.

The repairing of the biological stage would improve the water quality considerably and the expenses for one m² wouldn't be much higher.

The quality of the good technology applied is contributed to increase the standards for water with special em phases for the purification station Slobozia .

Received May 5, 2005

*The Romanian University of Sciences and Arts "Gheorghe Cristea"
**Politehnica University of Bucharest

REFERENCES

1. Baloiu, Liviu, Mihail, Angelescu, Anca, Protecția mediului ambient, Lito A.S.E., București, 1995.
2. Blitz H., Epurarea apelor uzate orășenești, Ed. Tehnica, București, 1966.

THE FOOTWEAR DESIGNING SESSIONS USING CRISPIN DYNAMICS ENGINEER

by

COCEA MARIANA and MARCUS LIVIU

***ABSTRACT** This paper presents how the **CRISPIN Dynamics Engineer** can be used in designing of footwear products. This is a part of application **CRISPIN Dynamics CAD Suite**. This is a range of quality software products to give the shoemaker the advantage of latest technology. With **CRISPIN Dynamics**, one can visualise a range of designs on-screen, work out the costs of a new style and even cut out sample shoe components. Reliance on manual skills is largely eliminated, so the staff can work creatively, but with increased accuracy and productivity. One can even send designs to a distant office or manufacturing centre in a matter of minutes.*

Key word: *footwear, design, computer, part, pattern*

1.INTRODUCTION

By classic methodology, designing footwear is a very complex and laborious activity. This is because classic methodology requires many manual graphic executions, which consume lot of the producer's time. Moreover, the results of this classical methodology may contain many inaccuracies with the most unpleasant consequences for the footwear producer. The decisive step in this way has been made some time ago, with the powerful technical development and massive implementation of electronical calculus systems and informatics, CAD (Computer Assisted Design).

This paper presents the basic functions of **CRISPIN Dynamics CAD Suite Engineer** for footwear design. The software is a 2D application of the **CRISPIN Dynamics CAD Suite**. The **Engineer** program is broken into a series of 'tasks'. Each 'task' has a 'tool tray' that contains a number of separate functions to achieve the task. This are:

- **Drawing**
- **Grade**
- **Assess**

When the Engineering program first starts the Draw task is active and the tool tray is displayed, as shown in the above partial image.

2. THE LAYOUT OF CRISPIN DYNAMICS ENGINEER

The layout of **CRISPIN Dynamics Engineer** follows a pattern established by many PC programs using the 'single document' model as the basis of operation (see figure nr. 1). This means that a single instance of Engineer can only have one pattern file open at a time.

Engineer consists of these main areas:

- A title bar, that shows the program title with the name of the pattern currently loaded.
- A menu bar, at the top, following normal Windows convention.
- A main toolbar, underneath the menu bar (default location).
- A small 3 option task bar, underneath main tool bar.
- A tool tray at the left of the screen, the Draw, tool tray is automatically active at startup (see fig. 1).
- The Parts and layers manager will 'slide out' from the right side of the screen when the mouse pointer 'hits' the side. There is an alternative 'icon browser' view of the parts not shown below.
- A status bar at the base of the screen displays prompts and other information while the program is being used.
- Last but not least is the main workspace area. When a pattern is first loaded the program is in 'selection mode' waiting for a line type or function to be selected.

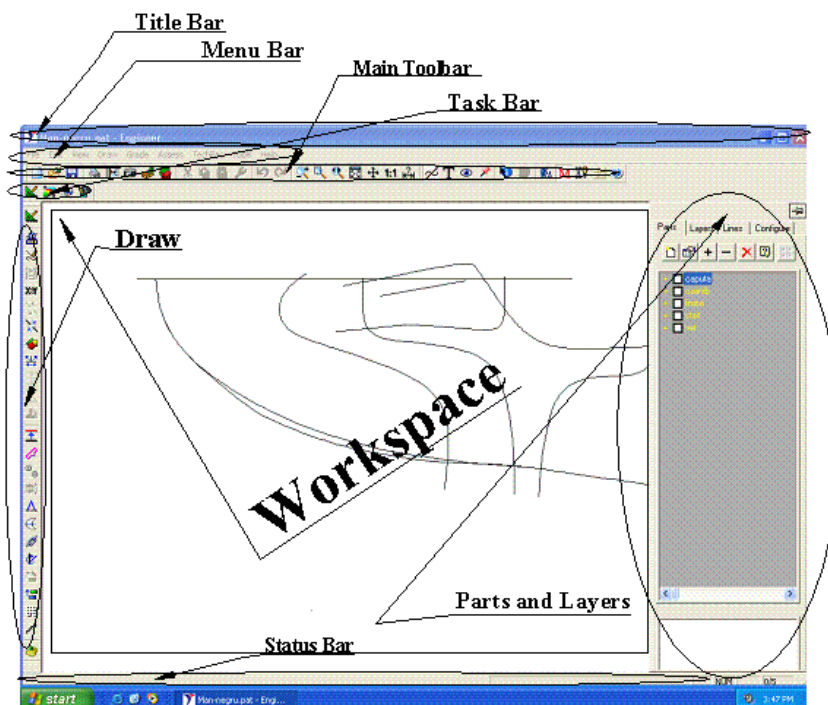


Fig. 1, The layout of CRISPIN Dynamics Engineer

3. THE BASIC FUNCTIONS FOR DRAWING

ICO N	Name of function	Function
	Digitise (a pattern)	The function digitises base lines
	Draw (base line)	The function freehand draws with the mouse
	Duplicate	The function duplicates one or more base line
	Split	Splits a single base line, at any point, to create two more new base lines
	Join	Joins 2 or more base lines together, to create one new base line
	Shape	A function to draw regular geometric base lines shapes
	Construct a base line	A function to draw single straight (two points) base line starting in 'free space', from one base line or two intersecting base lines.
	Mean (Average of two base lines)	Creates an average base line of two approximately parallel lines
	Partial Mean (Average of two base lines)	Creates an average base line of a portion of two approximately parallel lines
	Spring	This function changes existing or creates new base lines by moving and rotating selected lines to a new position
	Margins	A function to create or modify dependant margins
	Markers (Stitch Markers/Slots)	A function to create or modify dependant markers
	Stabs	A function to create or modify dependant stabs (perforations)
	Mirror	A function to create dependant mirrored lines
	Boundary	A Boundary line is just a dependant closed line connecting one or more lines to define the shape of a pattern part

	Chain	A Chain line is connecting two or more lines
	Rotate	A function to create or modify dependant rotated lines
	Translate	A function to create or modify dependant translated lines
	Offset	A function to create or modify dependant offset lines
	Decorative (Feature)	A function to create or modify Decorative features
	Gimp Plus	A function to create or modify Gimp lines

4. RESULTS. THE FOOTWEAR DESIGNING SESSION

4.1. Digitise the flattened half shell or standard

The first step in a footwear design session is to save in the computer's memory the digitized form of 'half shell', or standard. Afterwards, the steps of digitizing are as follows:

- Prepare the flattened half shell or standard for digitising by lightly marking where the key points to record are on the edges and internal lines.
- Align the shell on the digitiser, fix in place with a little low tack tape and digitise all the lines.

The process continues with the input of base line data from a 2D digitising tablet. You can use any 2D digitiser supported by the 'Wintab' standard and as only 3 buttons (and delete) are needed it is easy to learn, quick and accurate.

To begin we will assume that the digitising tablet has been correctly configured and calibrated if necessary. So the first step is to click on the digitise icon, shown above. There is a variation in the process if there is already data on the screen but for the moment let us assume this a new pattern. Align the shell on the digitiser, fix in place with a little low tack tape and digitise all the lines.

For that prepare and mark the shell with a pencil, the points to digitise along the lines.

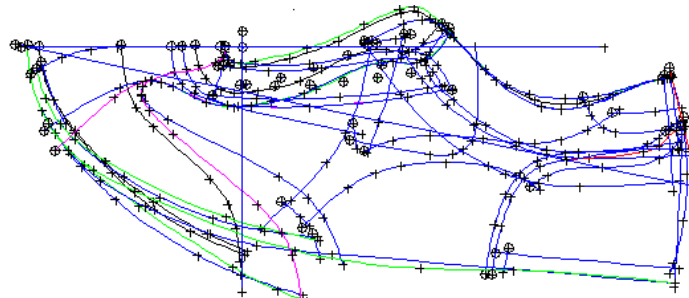


Fig. 2, *Digitise the flattened half shell*

In the process keep the number of data points to a minimum. In picture 2 there is one example of a digitised pattern.

4.2 Develop into a full shell

For define the shape of a pattern part we develop into a full shell using various dependant line types, like margins and boundaries



Fig. 3, *Develop into a full shell*

The system **CRISPIN Dynamics CAD Suite Engineer** offers many functions for the drawing of the footwear pattern. Using the CRISPIN function once can develop into a full shell and create sundries effect for the footwear patterns. Picture 3 presents one example of developing pattern.

4.3 Create the individual parts

The individual parts (see picture 4) will be created using the menu **Parts Manager**.

The selection, creation and management of parts is on the first tab of the dialog that 'slides out' from the right side of the workspace, when the mouse cursor comes within 5 pixels of the edge.

In practice you simply 'bump' the mouse pointer to the edge of the screen and the dialog is displayed. This is easier when the program is 'maximised' as the pointer literally 'hits' the edge of the screen.

This does not happen in all circumstances, for example when 'dragging' an area with a mouse button held down. Also to minimise the accidental selection of this dialog there is a 500 millisecond delay before it activates. This delay can be changed by editing the registry.

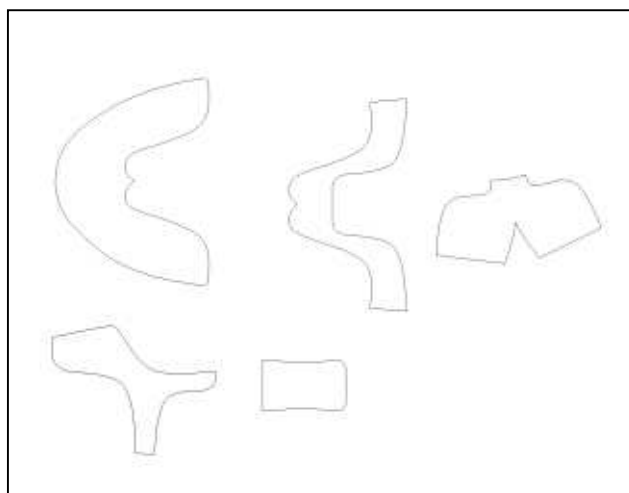


Fig. 4, *Parts of pattern*

The dialog can also be 'pinned' in the 'out' condition. In this mode the dialog will stay visible until a function is started at which point it will be hidden, when the function is complete the dialog will re-appear (see picture 1).

4.4 Grading

The grading a pattern and/or parts can be make using the **Grade Task Tool Tray**. This task is many fuctions wich launches the dialogs providing all the facilities to set up a size range and grading parameters. In picture 6 presents one examples of grade pattern.

The major fuctions for the grade are:

- Choice of **Arithmetic** or **Geometric grade** and whether or not width fittings apply.

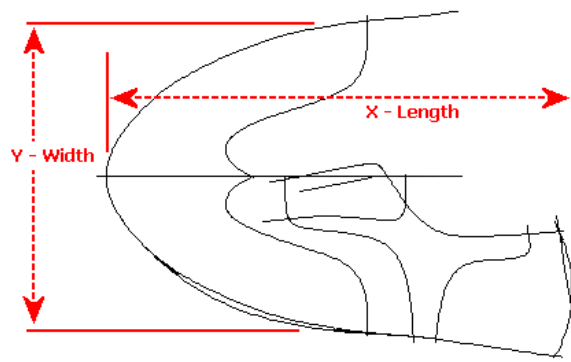


Fig. 5, *Dimension the base pattern*

Using Arithmetic grading basically means that you simply add the size increment value to the previous graded size. If you were to plot the size change on a graph you would find that the resulting line is straight. Geometric grade, where the increment values are applied as a percentage, will produce a curved line.

Using Geometric grading basically means that you apply the size increment value as a percentage of the previous graded size. If you were to plot the size change on a graph you would find that the resulting line is curved.

- The definition of the model size, its length and width measurements. The button at the left will start a special measure function. (see picture 5) The values measured are actually stored within the pattern documentation.

Note:

1. A 'free space' grade centre actually 'sits' on a single point base line. Base line control functions like the context menu option Move can be used to position them.
2. Any subsequent grade centres can be placed on any standard line type or the intersection of any two lines.
3. When a single line is picked you will be able to put the grade centre at either end of the line.
4. A grade centre can be placed on another grade centre's base line point, thus 'stacking' them at a single location.

In picture 6 and 7 will grade the base pattern using two grade centres.

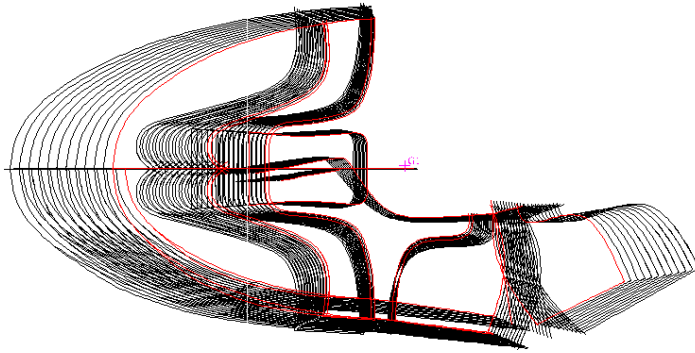


Fig. 6, *Grading the base pattern*

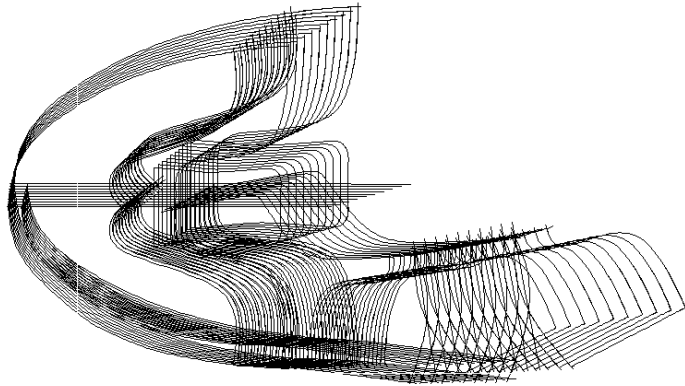


Fig. 6, *Grading the base pattern with moving grade centre*

5. Conclusion

The software produced by *Crispin Dynamics* has remarkable results in footwear design but it is working with an authorisation of the company. A license 'authorises' a computer to run specific **CRISPIN Dynamics** software. Licenses are often also used to specify which options within an application can be run.

The licence for the Faculty of Leather and Textiles, *Crisipin Dynamisc Engineer* was installed thanks to the generosity of *Luca Caironi*, *Sales Manager* for **CRISPIN Systems Limited**. We would like to take this opportunity and express our gratitude to him.

REFERENCES

1. Cocea, M. and Croitoru, D. F., *Proceduri CAD destinate proiectarii încălțămintei*, Editura Gh Asachi, Iasi, 2003
2. Malureanu, G. and Mihai, A. *Bazele proiectării încălțămintei*, Editura Performantica, Iași, 2003
3. *** web site www.crispindynamics.com
4. *** web site www.texon.com

Received May 3, 2005

SESIUNI DE PROIECTARE A INCALTAMINTEI UTILIZIND SISTEMUL CRISPIN DYNAMICS ENGINEER**REZUMAT**

In prezenta lucrare se prezinta principalele secvente de lucru asistate de calculator pentru proiectarea produselor de incaltaminte utilizind aplicatia CRISPIN DYNAMICS ENGINEER. Mentionam ca aceasta aplicatie este un soft profesional elaborat de compania CRISPIN si donat, prin amabilitatea managerului companiei Luca Caironi, Universitatii Tehnice "Gh. Asachi", Iasi, Facultatea de Textile-Pielarie, Catedra Confectii din piele.

A STUDY FOR THE MATHEMATIC MODELING OF 2D IRREGULAR SHAPES FOR FOOTWEAR CAD SYSTEM

by

COCEA MARIANA AND MARCUS LIVIU

***Abstract.** For using a specialized footwear CAD system it's imperative to know the analytical expression of the outlines of the footwear patterns. This brings us to the field of mathematical modeling. Mathematic modeling is based on the equation of the function defining the outline of the model contour. This allows the designer to process or alter the outlines: grading, changing the shape, optimizing the consumption of materials, making economic estimates and so on. This paper presents a study regarding the interpolation of the footwear components and outlines contours and the graphic visualization, using the following methods: Lagrange, B-Spline, Bezier.*

***Key words:** equation, function, footwear, interpolation*

1. Mathematic Modelling of Components. Requierements.

Geometrical shapes commonly used in **Computer Aided Design (CAD)** systems can be defined by several points obtained through the digitizing process. The co-ordinates of the points situated between two nodes can be approximated through both analytic and graphic methods, with interpolation curves. Thus, the analytic expression of the curve that approximates the points will be a interpolation function. The graphical form will be represented by a curve that crosses all the co-ordinates of the digitized points, without bringing any mutations of the initial curve.

Shapes, contours cannot be identified, in designing, by simple function of the form $y=f(x)$, because most of them have irregular forms, with many concavities and convexities, wich explains why their form is intrinsically dependent on the coordinates system. For example, if we want to plot a curve, it is absolutely necessary that we choose the right set of contour points in a system of coordinates, but the important factor in determining the form of the object is the relation between these points, not that between the points and the randomly chosen coordinates system.

Furthe more, the contour forms may have vertical tangents. If the shape were represented by a function $y=f(x)$, the vertical tangents would be an incovenient in designing, wich might be avoided by an aproximation of analytic function (e.g. of

polynomials) For all these reasons, the dominant representation of shapes in CAD is not possible a function $y=f(x)$ but a set of function wich can be obtained on various partions.

The analytic functions, approximating the contour to be designed, may be obtained by extrapolation if and only if there has been made a numeric coding of the geometric body, wich should furnish all necessary data.

As, however, many contours have irregular forms, the mathematic models are aproximative. Taking into account the advantage of computation technigue for these last years, we can asseses that highly performant programmes lead to approximations with minimum of errors.

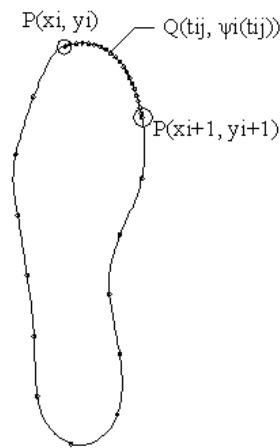


Fig. 1. The points Q between $P(x_i, x_{i+1})$ and $P(x_{i+1}, y_{i+1})$ are defining for the coordinates $(t_{ij}, \psi_j(t_{ij}))$ with $t_{ij} \in (x_i, x_{i+1})$

Mention has to be of the processing centers with numerical command existent in highly developed countries, where, on the basis the coorditates of a set of points, the model to be designed in physically made up with the desired accuracy.

On a local scale, although the description and modelling of bodies, wich is an initial stage of data input, is slow (form keyboard) or very expensive (with specialized equipment) all efforts will be warranted by the spectacular results

obtained.

Therefore, being given a finite number of points describing a curve, an interpolation problem is to be solved.

1.1 Interpolation Methods in Mathematic Modelling. Interpolation is a special case of a more general, approximating problem [3].

A function $f(t)$ will be approximated by interpolation as a finite sum:

of a simple function ψ_i , so as to satisfy a certain set of constraints for function $g(t)$. As the constants c_1, c_2, \dots, c_n have to be determined, it is necessary that the restrictive conditions for function $g(t)$ should be specified.

Usually these conditions are imposed on the function $g(t)$ so as to be a goot aproximation for function $f(t)$.

If function $g(t)$ is continuous over the approximating interval $[a, b]$ then the function $\psi_1(t), \psi_2(t), \dots, \psi_n(t)$, continuous on $[a, b]$, will be chosen. In the approximating theory, the constraints imposed on function $g(t)$ will very often be the following:

- interpolation constraints:

$$g(t_i) = f(t_i) \quad \text{for } i \in [1, n],$$

in other words, the functions curves will have the same number of values within a finite number of points;

- mixture of interpolation and constraints:

$$a) g(t_i) = f(t_i) \quad \text{for } i \in [1, k], k < n,$$

$$b) g'(t_1) = f'(t_1) \text{ and } g'(t_k) = f'(t_k),$$

- c) $g(t)$ - twice differential function;
 - variational constraints:

$$\|f-g\| = \min \{ \|f-h\| / h \in \text{distance}(\psi_1, \psi_2, \dots, \psi_n) \},$$

i. e. constants c_1, c_2, \dots, c_n should be chosen in such a way as to allow that the minimum of a possible functions $\|f-h\|$ should be obtained of the set of all possible linear combinations:

$$h = c_1\psi_1 + c_2\psi_2 + c_3\psi_3 + \dots c_n\psi_n$$

In order to accurately model it is necessary to pay special attention to certain qualities which are characteristic to a set of curves under specific conditions. Some call this quality a shape characteristic.

A whole series of interpolating methods are dealt with in the literature [1]. In this paper we will present methods and results for following interpolation methods:

- L a g r a n g e interpolation;
- B e z i e r interpolation;
- B-S p l i n e interpolation.

2. Lagrange Interpolation

The Lagrange interpolation is a classic method of interpolation. The Lagrange polynomials are among the simplest interpolating polynomials.

Being given $n+1$ discrete points:

$$x_0 < x_1 < x_2 < \dots < x_n$$

and a second set of real numbers:

$$y_1, y_2, y_3, \dots, y_n$$

there may be defined the Lagrange polynomial of n th power, associated to the two sets of number $\{x_i, y_i\}$ as being the polynomial $P(x)$ which solves the interpolation problem:

$$P(x_i) = y_i, \quad i \in [0, n]$$

where x_i are called nodes and the y_i constraints of interpolation function.

The advantage of this way of interpolating is that these polynomials are single. If a function is defined in $x_0, x_1, x_2, \dots, x_n$ and the corresponding $y_0, y_1, y_2, \dots, y_n$ values are known, then:

$$f(x_i) = y_i \quad i \in [0, n],$$

and by Lagrange interpolation of the n th power of the function $f(x)$ in nodes x_i there results polynomial:

$$P_n(x) = \sum_{i=1}^n f(x_i) L_{i,n}(x)$$

with:

$$L_{i,n} = \frac{(x-x_0)(x-x_1)\dots(x-x_{i-1})(x-x_{i+1})\dots(x-x_n)}{(x_i-x_0)(x_i-x_1)\dots(x_i-x_{i-1})(x_i-x_{i+1})\dots(x_i-x_n)}$$

or expressing the classic Lagrange polynomial:

$$P_n(x) = a_0 + a_1x + a_2x^2 + a_3x^3 + \dots + a_{n-1}x^{n-1}$$

It results from the theoretical considerations mentioned above that mathematic modelling by Lagrange method implies solving a system of $n+1$ equations with $n+1$ unknowns of the form:

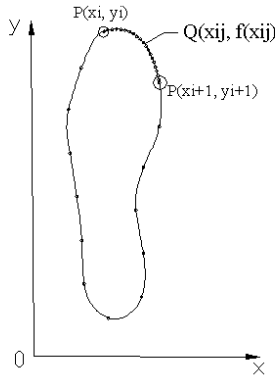


Fig. 2. The points Q between $P(x_i, y_i)$ and $P(x_{i+1}, y_{i+1})$ are defining for the coordinates $(x_{ij}, f(t_{ij}))$ where f is the Lagrange polynomial

$$y_0 = a_0 + a_1x_0 + a_2x_0^2 + a_3x_0^3 + \dots + a_nx_0^n$$

$$y_1 = a_0 + a_1x_1 + a_2x_1^2 + a_3x_1^3 + \dots + a_nx_1^n$$

$$y_2 = a_0 + a_1x_2 + a_2x_2^2 + a_3x_2^3 + \dots + a_nx_2^n$$

$$y_n = a_0 + a_1x_n + a_2x_n^2 + a_3x_n^3 + \dots + a_nx_n^n$$

where (x_i, y_i) with $i \in [0, n]$ are the points describing the forme to be indentified.

Therefore, the problem consists in determining the polynomial coefficients $a_0, a_1, a_2, \dots, a_n$ by solving a system of $n + 1$ equations with $n + 1$ unknowns.

system of XoY coordinates

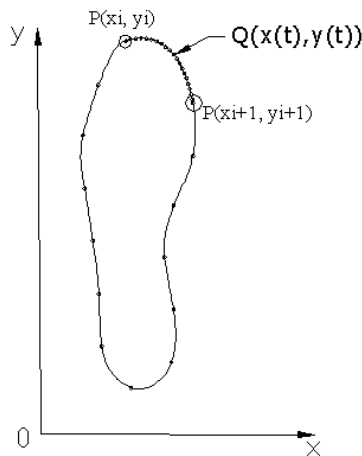


Fig. 3. The points Q between $P(x_i, y_i)$ and $P(x_{i+1}, y_{i+1})$ are defining for the coordinates $(x(t), y(t))$ two interpolating polynoms

2.1 Experimental estimations For mathematical modelling of a contour by Lagrange interpolation will considered a contours of a footwear part to wich a

NOTE

Mention is made to the fact that an accurated modelling of a number of points the n th power of the polynomial does not have to be too big, because is occuring errors and oscillations in displaying the polynomial. For that, we will utilize the parametrically represented.

3. The Parametrically Represented

The shapes of footwear parts cannot be precisely described by a simples function $y=f(x)$. In CAD the shapes are parametrically represented using a set of functions:

$$x = x(t); \quad y = y(t).$$

In order to do that, we will attach two supplementary systems of co-ordinates – tOx and tOy – to the present one – xOy . We select the variation domain of parameter t . Then, we solve the two independent problems of theoretical interpolation for the two variables, x and y using many methods.

The parametric equations used in interpolation are actually polynomial equations, usually bicubic, described as:

$$g(t)=at^3+bt^2+ct+d$$

Thus, we will approximate the set of points $(x_0, y_0), (x_1, y_1) \dots (x_{n-1}, y_{n-1})$ by the aid of two variables $x(t)$ and $y(t)$, defined by two parametric interpolation equations:

$$x(t)=a_x t^3+b_x t^2+c_x t+d_x$$

$$y(t)=a_y t^3+b_y t^2+c_y t+d_y$$

In order to do that, we will attach two supplementary systems of co-ordinates – tOx and tOy – to the present one – xOy . We select the variation domain of parameter t . Then, we solve the two independent problems of theoretical interpolation for the two variables, x and y .

3.1 Defining Bezier interpolating polynoms This will allow the determination of the four coefficients from the following restrictive conditions:

1. The value of the polynom in the nodes must be the same with its numeric value:

$$x(t_i)=x_i, y(t_i)=y_i$$

where $i=0 \dots n$ and x_i and y_i are nodes: $(x_0, y_0), (x_1, y_1) \dots (x_n, y_n)$

2. The vector that is tangent to the curve in a node must be the same as the vector of the initial curve. If the components of the vector tangent to the interpolating curve are:

$$x'(t)=3a_x t^2+2b_x t+c_x$$

$$y'(t)=3a_y t^2+2b_y t+c_y$$

then the restrictive conditions for the limit will be:

$$x'(t_i)=l_i \text{ and } y'(t_i)=m_i$$

where l_i and m_i are the values of the incline of the tangents in the nodes, as determined in the tOx and tOy co-ordinates systems.

0

3.1.2 Theoretically solving the interpolation Bézier curves. Without affecting the general area of an interpolation problem, the interpolating Bézier polynoms derive from the following conditions:

C1. We take the interval $[0,1]$ as a variation domain for parameter t . In this case, the conditions for the limit will be:

$$x(0)=d_x \quad y(0)=d_y$$

$$x(1)=a_x+b_x+c_x+d_x \quad y(1)=a_y+b_y+c_y+d_y$$

C2. The directions of the tangents in the nodes will be defined as the inclination of the tangent led in every node. For example, in the (x_i, y_i) node, they will be calculated with the following relations:

$$l_i=m(x_i-x_{c1}) \quad m_i=m(y_i-y_{c1})$$

$$l_{i+1}=m(x_{i+1}-x_{c2}) \quad m_{i+1}=m(y_{i+1}-y_{c2})$$

where:

- m , known as a **shape factor** in the literature, usually takes the value 3,
- x_i, y_i and x_{i+1}, y_{i+1} are **the co-ordinates of the nodes** (the extreme point of the curves),

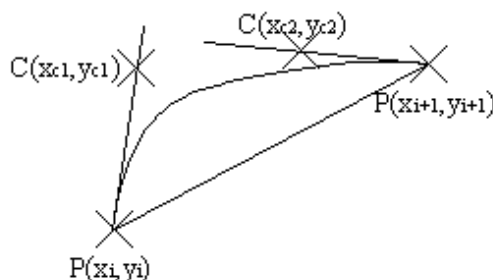


Fig. 4 The Bezier polynom is defined for two nodes and two points of control

- x_{c1}, y_{c1} and x_{c2}, y_{c2} are the co-ordinates of the two points that belong to the tangents to the Bézier curve and they are called **points of control**.

This relations and of the two conditions lead to a system of 8 equations with 8 unknown values, with the following solutions:

$$\begin{aligned} d_x &= x_i & d_y &= y_i \\ c_x &= 3(x_{c1} - x_i) & c_y &= 3(y_{c1} - y_i) \\ b_x &= 3(x_{i+1} - x_i) - c_x & b_y &= 3(y_{i+1} - y_i) - c_y \\ a_x &= x_{c2} - x_i - c_x - b_x & a_y &= y_{c2} - y_i - c_y - b_y \end{aligned}$$

This represents the mathematical expression of the coefficients of the bicubic polynomial Bézier functions.

3.1.3 Discussions

If we analyse the two conditions, the conclusions will be as follows:

1.0000000 A Bézier curve is defined by four points:

- two fixed points on the Bézier curve (nodes), that are fixed;
 - • two other intermediate points, that belong not to the curve, but to its tangents. The two points are called **control points** and are positioned on the tangents of the curve led in the nodes($P(x_i, y_i)$, $P(x_{i+1}, y_{i+1})$, see picture 4).

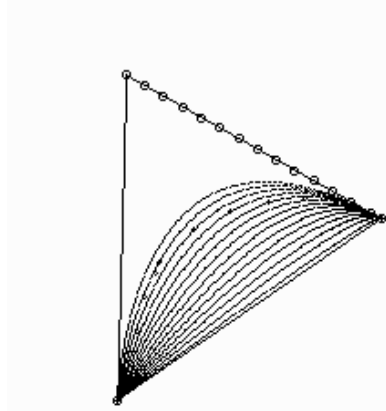


Fig. 5, Between two nodes we can define many Bézier curves

- Between two nodes we can define many Bézier curves, related to the position of the control point on the tangent (see picture 5). This makes it possible, in a CAD work session, to draw several Bézier curves and choose the convenient one – the one that approximates a set of points between the two nodes with the highest precision.

Bézier

3.2 Defining B-Spline interpolating polynoms

Let's take into consideration a network of points called $t_0 < t_1 < \dots < t_n$ whose nodes have known values given by $\{f_i\}$, $i \in [0, n] \rightarrow \mathbb{R}$, where $\{f_i\}$ is an interpolating B-spline function that fulfills the following conditions:

- $g(t)$ is continuous on the (t_0, t_n) interval, together with its first and second rank derivates.
- on each $[t_{i-1}, t_{i+2}]$ interval, the function is a third degree polynom, $i \in [1, n-1]$
- in the nodes of the $\{t_i\}$, $i \in [0, n]$ network, the following conditions are fulfilled:
 $g(t_i) = f_i$, $i \in [0, n]$; g' fulfills the conditions of the limit: $g'(t_{i-1}) = f'(t_{i-1})$
 $g'(t_{i+2}) = f'(t_{i+2})$ g'' fulfills the conditions of the limit: $g''(t_i) = f''(t_i)$

3.2.1 The mathematical expression of the coefficients of the bicubic polynomial B-Spline functions

The B-spline functions are third degree polynoms on portions defined by the pointes $t_{i-1}, t_i, t_{i+1}, t_{i+2}$.

By applying the same methodology as presented in the previous paragraph, the third degree polynomial representing the interpolating B-spline function looks like:

$$\begin{aligned}x(t) &= a_x t^3 + b_x t^2 + c_x t + d_x \\y(t) &= a_y t^3 + b_y t^2 + c_y t + d_y\end{aligned}$$

where:

$$\begin{aligned}a_x &= (-x_{i-1} + 3x_i - 3x_{i+1} + x_{i+2})/6 & a_y &= (-y_{i-1} + 3y_i - 3y_{i+1} + y_{i+2})/6 \\b_x &= (3x_{i-1} - 6x_i + 3x_{i+1})/6 & b_y &= (3y_{i-1} - 6y_i + 3y_{i+1})/6 \\c_x &= (-3x_{i-1} + 3x_{i+1})/6 & c_y &= (-3y_{i-1} + 3y_{i+1})/6 \\d_x &= (x_{i-1} + 4x_i + x_{i+1})/6 & d_y &= (y_{i-1} + 4y_i + y_{i+1})/6\end{aligned}$$

for $i \in [1, n-1]$.

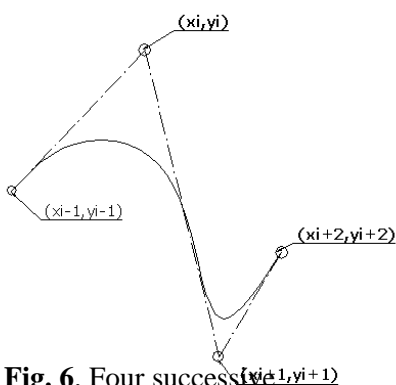


Fig. 6. Four successive coordinates determined a curves B-Spline

The expressions lead to the conclusion that the interpolating B-spline function can be determined only by four successive coordinates of the shape.

3.2.2 Discussion

After those presented, it can be noticed that a point belonging to a B-spline polynomial depends on the coordinates of its neighboring points, but it doesn't depend at all of all the points defining the shape. In the words of specialists, this means that "a B-spline approximation has a local scheme".

The characteristic of being able to decrease the variation and the local character of the approximation when using a B-spline function can be explained by looking at the

geometrical behavior of the B-spline curves.

- a point on such a curve is a convex combination of K neighboring nodes of the polygon and thus the curve can very well "fit" with the polygon.
- if one node of the polygon is moved, the curve will only be modified locally, in the neighborhood of the node. This characteristic is essential in design, because it allows the creator to modify a curve he is not satisfied with, without having to re-make the whole outline.

References

1. Dogaru D., *Elemente de grafica 3D*. Editura Stiintifica si Enciclopedica, Bucuresti, 1989
2. Eric J. Stollnitz, Anthony D DeRose, *Wavelets for Computer Graphic, Theory and Application*, The Morgan Kufman Publishers, 1996
3. Cocea Mariana, *Utilizarea tehnicii de calcul in industria confecțiilor din pile si înlocutori*, Ed. Tehnica Chișinău, Iași, 2002

Rezumat

Prezenta lucrare cuprinde un studiu teoretic cu mici aprecieri experimentale privind utilitatea metodelor de modelare matematică în sisteme CAD pentru proiectarea încălțămintei.

SELF AND THERMO ADHESIVE TEXTILE MATERIALS USED IN FOOTWEAR MANUFACTURING

FLORENTINA HARNAGEA and AURA MIHAI

***Abstract:** Self and thermo adhesives woven or knitted fabrics are used for strengthening uppers in footwear modern making technologies. These materials have to be resistant on stress conditions from lasting process, as well on wear period, to maintain the shape and to ensure dimensional stability of the product. The experiments have been designed from footwear producer point of view regarding the product shape stability, reason for that the materials were presented into the codified manner. Not a specific commercially named textile material is the subject of this study, but the percentage of plastic deformation from total deformation of the doubled uppers structures, characteristic that predict how the shoe will preserve shape and dimensions in wearing.*

***Key words:** fabrics, leather, footwear, lasting, deformation*

1. Introduction

Self and thermo-adhesive textile fabrics (woven fabrics and knit fabrics) for strengthening stitches and leather uppers are increasingly used in modern technologies of ready-made shoe products. The use of self and thermo-adhesive textile fabrics in the process of shoe manufacturing is justified by the reducing of toxicity at the place of work, the insurance of the process accuracy and, implicitly, the increment of the work productivity. The characteristic trait of self-adhesive textile fabrics is the permanently gluey state due to the pressing-sensitive contact adhesives and the modality of application by simply pressing with the hand. The thermo-adhesive materials join with leather or leather substitute with special pressing machine at 60-70°C because a bigger temperature could influence the upper surface and its mechanical properties.

The self and thermo-adhesive textile fabrics, along with the uppers, have to be stress proof during the shape forming process (named lasting process) and during utilisation; they have to insure the product shape and the dimensional stability preservation in time [1]. Usually, for the uppers there are used leather and leather substitutes, which are characterised by their elastic and mouldable (plastic) behaviour. During the shape forming process, the uppers are subject to tension stress occurring while they are being pulled on the last. The uppers are tensioned so that they are shaped according to the complex spatial shape of the last and the form reliability is provided after the extraction of the last out of the finished product and especially during its use [2].

Taking into consideration that, the total deformation achieved by the tension stress when pulling the uppers on the last is the sum of elastic and plastic deformations, the mouldable component has to provide the conferred spatial shape after the cessation of the tension, by the annullment of the elastic component of the deformation. In order to stabilise the behaviour of the spatial shape, which is conferred to the half-finished good during the forming process, it is necessary to cause a remnant deformation in the structure of the material, a ratio as high as possible of the total deformation to be transformed in plastic deformation [3]. The weight of the plastic deformation within the total deformation underlines the materials shaping capacity and it is appreciated that the higher the weight the higher the spatial reliability which resulted from the spatial shaping proces

The size of the deformation during the tension stress is influenced by the materials assembly composition and structure and by the duration of the tensioned state as well. If after the deformation of the material it preserves its tensioned state, there takes place a relaxation of the tension (stress relaxation) within the material after a while and at the same time an increment of the remnant (plastic) deformation (creep) [4,5].

It is known the fact that during tension stress of the elastic and plastic materials, the increment of the deformation is not linear with the load, as the Hooke' s law is described. The loading curve does not correspond with the unload curve. This phenomenon has been called "elastic after-effect", being related to deviation from the Hooke law, i.e. stress relaxation, creep, contraction, histeresis loops, etc.

The strengthening of the uppers is in correspondance with the shoe model chosen. Thus it is shown the strengthening patterns for vamp, quarter and heel, figure 1

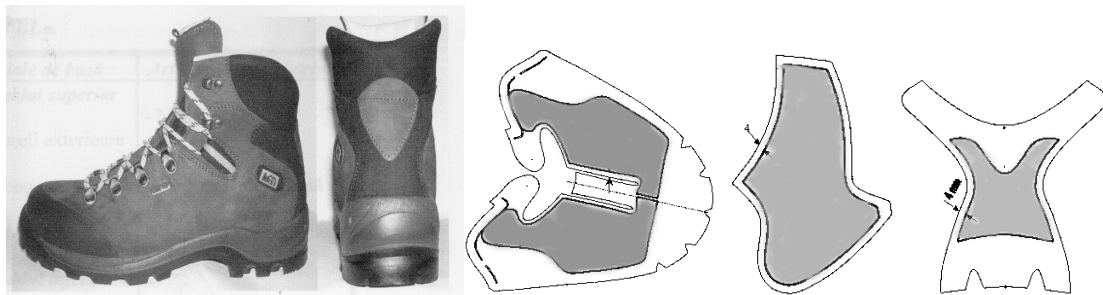


Figure 1

Starting from these general considerations, the present study intends to establish the modality by which the self and thermo-adhesive textile fabrics used in strengthening uppers determine the size of the plastic deformation, which is decisive in preserving the shape of the shoe.

2. Method and experiments

In order to highlight the influence of the self and thermo-adhesive textile fabrics used for strengthening leather uppers over the size of the total deformation and, implicitly, over the plastic deformation when tension stress, there were carried out experiments both with simple test samples and with reinforced test samples (coated). For reinforcing the leather or leather substitutes references there were used self and

thermo-adhesive woven fabrics and thermo-adhesive knit fabrics. Materials used in this study were commercial grade products, being tested from footwear manufacture point of view.

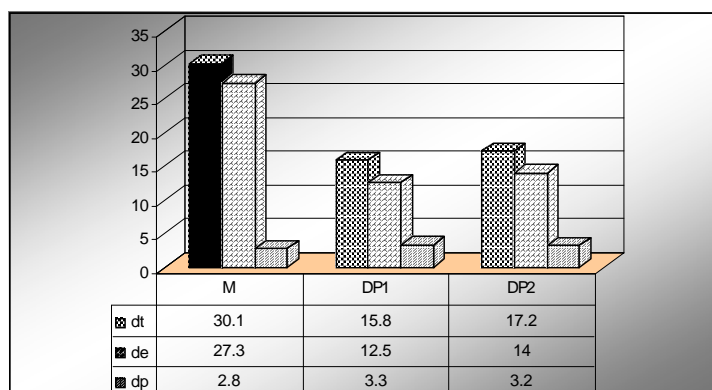
The test samples were subject to tension stress on universal tensile testing machine in the following conditions: stress under 10 N/mm^2 , of 7 N/mm^2 , respectively, the initial length of the test sample of 100 mm, the deformation speed of 100 ± 10 mm/minute, in accordance with ISO 3376/76, adopted in Romania in 1997. The samples were cut in the shape of dumb-bell and the dimensions in accordance with described standard. All samples have been conditioned for 48h at standard atmosphere (temperature $T=20 \pm 2^\circ \text{ C}$, humidity $65 \pm 5\%$). For the imposed stress value there was registered the total deformation. When ceasing the stress, part of this deformation is annulled, remaining the plastic deformation. In all cases 10 samples were tested and average value reported.

The total deformation (d_t), the instantaneous elastic deformation (d_{ei}), the delayed elastic deformation (d_{ed}) and the plastic or remnant deformation (d_p) were calculated according to the initial length of the test sample, the length of the test sample between the trappers, when the load reached the imposed value of 7 N/mm^2 ; the length of the test sample measured immediately after the cessation of the tensioned state, the length of the test sample measured at 30 minutes after the cessation of the tensioned state.

3. Results and discussions

During the spatial shaping process, while acting the tension unidirectional stress with an imposed value of the stress, the deformability of genuine leather which is reinforced with self adhesive and thermo-adhesive textile fabrics is radically different from the deformability of the non-strengthen materials.

Therefore, with the non- strengthen materials the plastic (remnant) deformation represents a small percentage of the total deformation. By their coating with self and thermo-adhesive textile fabrics it is highlighted the increment of the remnant deformation (plastic deformation).



Legend:

M - Leather (witness sample)

DP1 - Leather + Woven fabric 1 self-adhesive

DP2 - Leather + Woven fabric 2 self-adhesive

dt - total deformation

de - elastic deformation

dp - plastic deformation

Figure 2

It is presented the variation of plastic and elastic deformation comparatively to total deformation in the

case of using self-adhesive textile materials, Fig.2 and for thermo-adhesive textile materials, Fig.3.

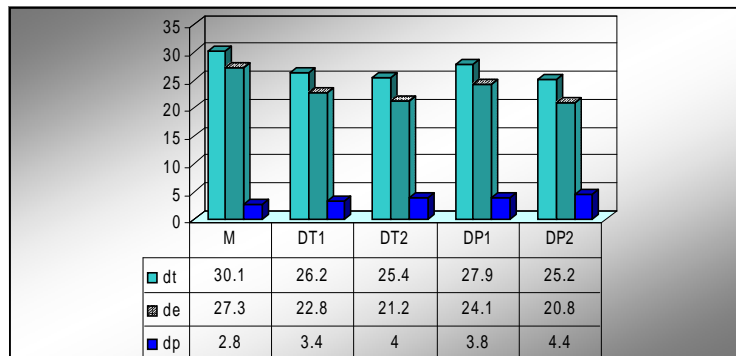


Figure 3

Legend:

M - Leather (witness sample)

DT1 - Leather + Knitted fabric 1 thermo adhesive

DT2 - Leather+Knitted fabric 2 thermo adhesive

DP1 - Leather+Woven fabric 1 thermo adhesive

DP2 - Leather+Woven fabric 2 thermo adhesive

dt - total deformation

de -elastic deformation

dp -plastic deformation

This increment is even more obvious by the maintenance in a tensioned state for 5 minutes and 30 minutes, respectively, Fig.4

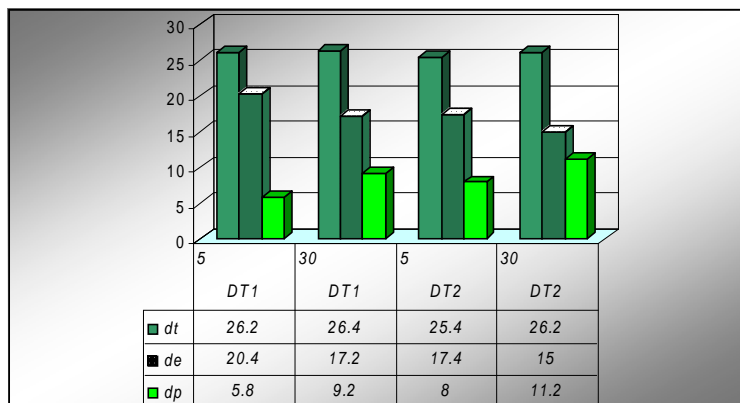


Figure 4

Legend:

DT1 - Leather + Knitted fabric 1 thermo adhesive

DT2 - Leather+Knitted fabric 2 thermo adhesive

dt - total deformation

de - elastic deformation

dp - plastic deformation

The capacity of preserving the shape after the load that caused the deformation is being removed will be even more marked by the maintenance of the spliced vamps with self and thermo-adhesive textile fabrics in tensioned state. By their coating with self and thermo adhesive textile materials, it is highlighted the increment of the plastic deformation of the total deformation by the ratio dp/dt , fig.5 and fig.6.

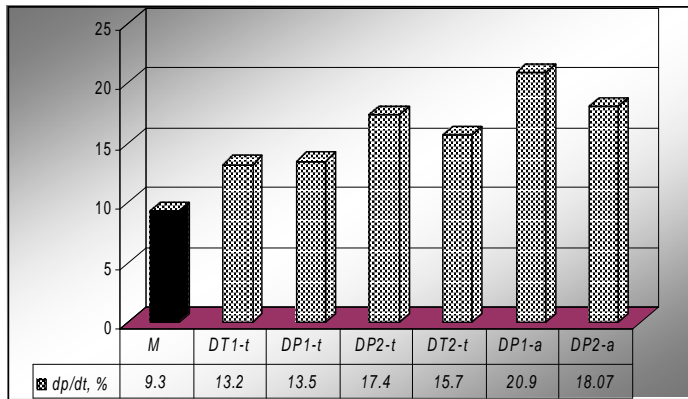


Figure 5

Legend:

- M- Leather (witness sample)
- DT1-t: Leather + Knitted fabric 1 thermo adhesive
- DT2-t: Leather+Knitted fabric 2 thermo adhesive
- DP1-t: Leather+Woven fabric 1 thermo adhesive
- DP2-t: Leather+Woven fabric 2 thermo adhesive
- DP1-a: Leather+Woven fabric 1 self-adhesive
- DP2-a: Leather+Woven fabric 1 thermo adhesive

Out of the two types of tested materials (woven fabrics and knit fabrics), the highest value of the ratio d_p/d_t was achieved for the leather coated with woven fabric 1-article 375 (with cloth weave).

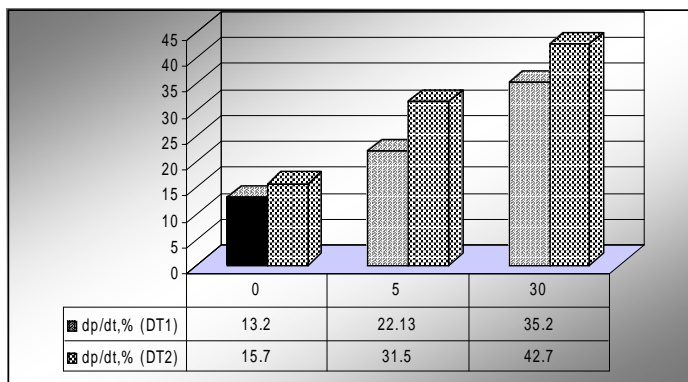


Figure 6

Legend:

- DT1- Leather + Knitted fabric 1 thermo adhesive
- DT2-Leather+Knitted fabric 2 thermo adhesive

By preserving the tension stress, an increment of the ratio d_p/d_t results; the highest value is registered in the case of the leather coated with thermo-adhesive knit fabric 2 (42.7% respectively in comparison with 15.7%).

4. Conclusions

1. In order to provide reliability to the ready-made shoe products, it is recommended the use of the self and thermo-adhesive textile fabrics that, by the ratio of the plastic deformation within the total deformation, are to influence the capacity of preserving the spatial shape after the vamps are removed from the lasts.
2. The size of the remnant (plastic) deformation achieved in the case of the materials used during the experiments highlights their different behaviour in the same working conditions.
3. The values of the duration of tension state maintenance had as a main purpose the increment of the plastic deformation within the total deformation. This increment of the plastic deformation within the total deformation is evidenced by the ratio d_p/d_t , being even more marked by keeping the test samples in tensioned state for 30 minute.

4. In practical conditions, there are used the materials which allow a satisfactory dimensional stabilisation by reducing the elastic elongation for the plastic elongation (necessary in preserving the shape of the shoe and the commercial appearance), taking into account the possibilities of these materials application, too.

References

- [1]. Vidru M., Aspecte privind extinderea chimizarii procesului de confecție a incaltamintei, Vol. "A X-a conferinta de textile pielarie", Iasi, 1992, p.201-208
- [2] Harnagea F. Mălureanu G., Studiu privind influenta unor parametri tehnologici asupra proprietatilor fizico-mecanice ale materialelor în vederea asigurarii fiabilitatii formelor spatiale, Vol. "A X-a conferinta de textile pielarie", Iasi, 1992, p.15-19
- [3] Harnagea F., Ionescu C., *L'influence du régime de thermofixation sur les propriétés physico-mécaniques du cuir synthétique en vue de l'assurance de la fiabilité des formes spatiales*, Buletinul I.P.Iasi, tomul XLI (XLV), fasc. 3-4, 1995
- [4] Mihai A., Harnagea F., Metoda de apreciere a deformatiei remanente a materialelor flexibile folosite la confectionarea incaltamintei-, "Creativitate. Tehnologie. Marketing", ISBN 9975 -910 -06-8, Ed. Tehnica, Chisinau, 1996, p.138-142
- [5] Harnagea F., Mihai, A., *Modelarea matematica a comportarii la solicitarea de tractiune a inlocuitorilor de piele*, Lucrările celei de-a XII-a Conferinta româna de Textile-pielarie, Iasi, 2002, Ed.Performantica

Received May 4, 2005

Gh. Asachi Technical University of Iasi, Faculty of Leather and Textiles Engineering, Footwear Department

MATERIALE TEXTILE AUTO SI TERMOADEZIVE FOLOSITE LA CONFECTIONAREA INCĂLĂMINTEI

Rezumat

Materialele textile auto și termoadezive pe bază de țesături sau tricot sunt folosite tot mai mult în tehnologiile actuale de confecționare a încălțămintei pentru întărirea fețelor. Aceste materiale trebuie să fie rezistente la solicitările din procesul de formare spațială și din timpul purtării produselor, să asigure menținerea formei și a stabilității dimensionale în timp. În acest sens, pentru menținerea formei spațiale conferite în procesul de tragere pe calapod, este importantă componenta plastică a deformației totale. Prin întărirea fețelor încălțămintei cu materiale textile auto și termoadezive, respectiv prin menținerea în stare tensionată, este posibilă creșterea ponderii deformației plastice în total deformație.

ASPECTS REGARDING THE USE OF ADHESIVE DISPERSIONS IN FOOTWEAR INDUSTRY

FLORENTINA HARNAGEA, and AURA MIHAI

***Abstract.** The paper presents the results of the research concerning the use of water based adhesive dispersions in modern technologies of soles bonding in shoe manufacturing. Thus there have been established mathematical models of bond strength function of the open time for adhesive dispersions and solvents. These allow estimating the best time corresponding to the maximal bond strength.*

***Keywords:** adhesive, dispersion, bonding, open time, footwear.*

1.Introduction

Solvent-based adhesive has been traditionally used in shoemaking for their excellent performance in service. When looking at footwear production processes from an environmental viewpoint, an important issue is restricting the emissions of solvents and other toxic vapours.

Solvent-free adhesives are, however, becoming more common worldwide as manufacturers have to be more environmentally conscious and seek ways to meet increasingly stringent environment protection legislation.

The product classes „Dispersions”(so called „water based products”) represent surely the most matured replacement for solvent adhesives. A large amount of quantities of uppers-soles bonding are carried out successfully with these products already.

This paper illustrates the results obtained through the research of the bonding adhesive strength, case of adhesive dispersions in comparison with solvent-based adhesive, using mathematical models of dependence.

2.Method and experiments

There had been used identical substrates made from standard rubber and also different substrates: leather or standard rubber.

The bonding of substrates has been done with:

- ✓ PUR adhesive dispersion ECO248 in 40% concentration
- ✓ PUR solvent based adhesive POLIGRIP 325 in 20±1% concentration.

Samples from leather and rubber have been cut at dimensions of 20x120mm and were conditioned in standard parametres; they have been bonded as in the classical bonding technology.

Samples have been joined in order to result a perpendicular application effort on the bonding layer; after that there has been applied a tensile effort at 72 hours from the pressing

The peel strength after 72hours has been established with the relation:

$$Rd = \frac{F_{med}}{b}$$

Where:

F_{med} -the medium force, in N

b - width of the bonding, in mm

The medium force at which the bonding peel takes place is:

$$F_{med} = \sum_{i=1}^n F_i / n$$

where:

F_i –the force in every measuring point or at reading time intervals, in N,

n – number of measuring or reading points

In the case of using Eco PU 248 in free atmosphere, the open time varies from 20, 25,.....,45, being done 5 determinations for each value.

3. Results and discussions

The variation of peel strength depending on the open time it is shown in figure nr.1. In this case the bonds have been done with nonhalogen rubber substrates. From figure nr.1 it results a maximum peel strength established at an open time of 35min. The same maximum value for peel strength is also reached for bonds with adhesive emulsion using halogen rubber substrates, figures nr.2.

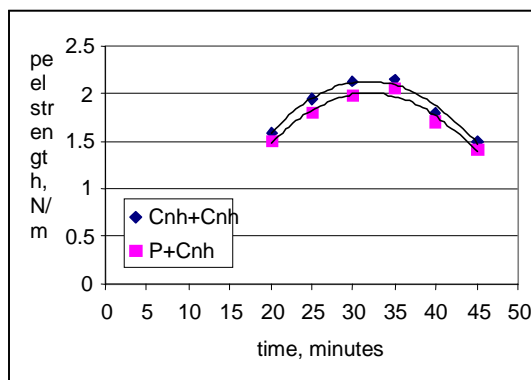


Figure 1

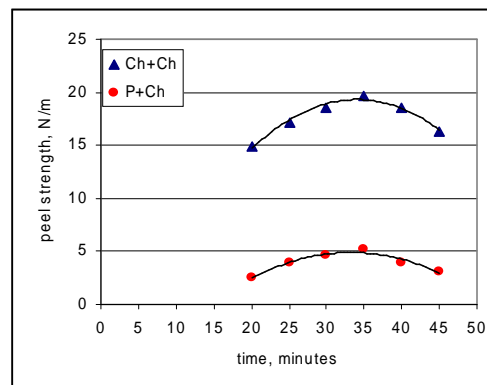


Figure 2

There can be noticed that the bond strength for rubber+ nonhalogen rubber has a value of 20N/mm.

Figure nr.3 shows the peel strength of the bonds with rubber substrates using adhesive emulsion and also of the bonds with PUR solvent based adhesive. For a value of the open time of 35 minutes it results the maximum peel strength using leather+halogen rubber.

The variation of the peel strength in the case of using PUR solution Poligrip 325 it is illustrated in figure nr.4 + figure nr.5.

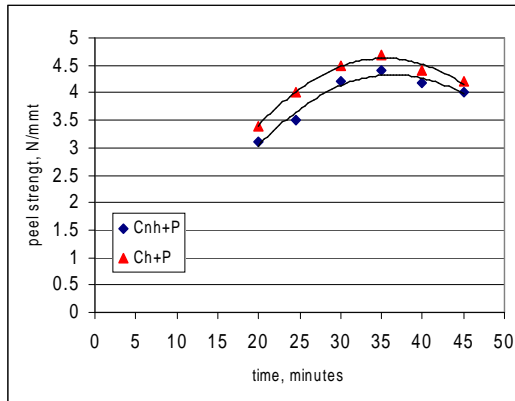


Figure 3

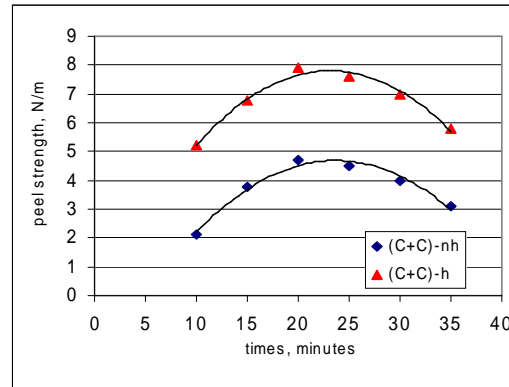


Figure 4

There can be observed that the best time corresponding to the maximal peel strength has a value of 20minutes.

The regression models are of polynomial type and have the following relation:

$$R = -at^2 + bt + c$$

Where: R – the peel strength, in N/mm or daN/cm

t-open time, in minutes

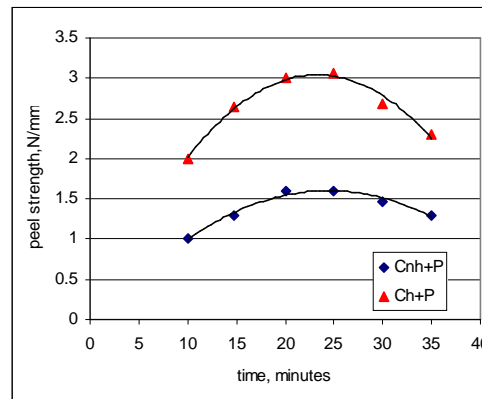


Figure 5

From regression curves of the final peel strength there can be established the best time corresponding to the maximum bond strength.

The maximum value of the bond strength it is reached for $\frac{\partial R}{\partial t} = 0$.

Table nr.1 presents the mathematical models of peel strength in connection to the open time.

Table 1

The nature of the adhesive	Code	The nature of the substrates from bonding	Mathematical model	Coef.
PUR dispersion ECO248	P+Cnh	Leather+ nonhalogen rubber	$-0.0037t^2 + 0.2335t - 1.7223$	0.9627
	Cnh+Cnh	(Rubber+ rubber) nonhalogen	$-0.0038t^2 + 0.2437t - 1.7443$	0.9716
	P+Ch	Leather+ halogen rubber	$-0.0139t^2 + 0.9207t - 10.393$	0.9466
	Ch+Ch	(Rubber+rubber)-halogen	$-0.0236t^2 + 1.6024t - 7.9129$	0.9736
Solution for leather Dispersion for rubber	P+Cnh	Leather+nonhalogen rubber	$-0,0052t^2 + 0.367 t - 1.8646$	0.9789
	P+Ch	Leather+halogen rubber	$-0,0048t^2 + 0.349t - 2.029$	0.9631
PUR solution Poligrip 325	(C+C)nh	(Rubber+rubber)- nonhalogen	$-0,0133t^2 + 0.6299 t - 2.7609$	0.9725
	(C+C) h	(Rubber+rubber) halogen	$-0,0149t^2 + 0.6674 t - 0.1457$	0.9811
PUR solution – Poligrip 325	P+Cnh	Leather+nonhalogen rubber	$-0,0029t^2 + 0.1422t - 0.134$	0.972
	P+Ch	Leather+halogen rubber	$-0,0058t^2 + 0.2702t - 0.1037$	0.9809

Figure nr.6 presents comparatively the variation of the bond strength for halogen rubber substrates using emulsion (Eco Pu 248) and adhesive solution (Poligrip 325).

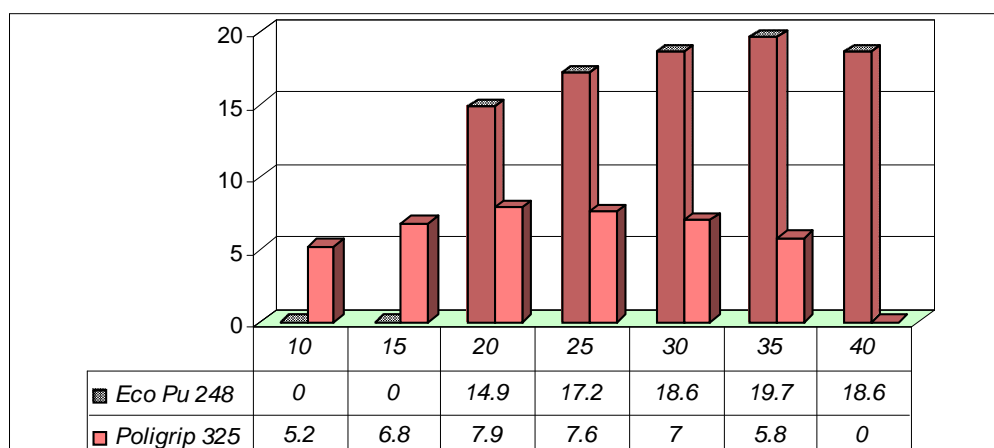


Figure 6

Graphics show that for PUR adhesive emulsion, the bond strength has a higher value than for PUR adhesive solutions.

Conclusions

1. The non-linear regression models are of polynomial type and have the following relation:

$$R = -at^2 + bt + c$$

Where: R – the peel strength, in N/mm or daN/cm

t - open time, in minutes.

2. The bond strength with adhesive PUR emulsion is superior to the bond strength with PUR solvent based adhesive.

3. The best time for obtaining maximum bond strength can be established using the regression curves.

4. The water based adhesives represent the best realizable alternative compared to usual solvent based adhesive.

References

- 1.F. Harnagea, A. Mihai, Cociu V., *Contribuții la stabilirea regimului optim de formare a peliculei solide în procesele de îmbinare prin lipire*, Analele Universității Oradea, 2001, Ed.Univerității din Oradea, 2001, ISSN 1582-5590
- 2.Harnagea F ., Cociu V., Roșculeț V., Modelarea matematică a comportării la solicitarea de tracțiune a îmbinărilor prin lipire, Rev. de Pielărie-Incălțăminte, nr.1, ISSN 1583-4433, 2003
3. Roșculeț V., Harnagea F.- Aspecte privind utilizarea adezivilor pe bază de apă în industria de încălțăminte-Rev. de Pielărie-Incălțăminte, nr.1, 2003, ISSN 1583-4433

Received May 4, 2005

Gh. Asachi Technical University of Iasi, Faculty of Leather and Textiles Engineering, Footwear Department

ASPECTE CU PRIVIRE LA UTILIZAREA DISPERSIILOR ADEZIVE IN INDUSTRIA DE ÎNCĂLȚĂMINTE

Rezumat

Lucrarea prezintă rezultatele cercetării cu privire la utilizarea dispersiilor apoase de adezivi poliuretani în tehnologiile moderne de lipire a tălpilor în industria de încălțăminte. În acest sens, au fost stabilite pe baza datelor experimentale, modele matematice de dependență a rezistenței în funcție de timpul deschis. Acestea au permis estimarea timpului optim de formare a peliculei solide, corespunzător rezistenței maxime a îmbinărilor adezive în cazul utilizării dispersiilor adezive, comparativ cu soluțiile adezive pe bază de solvenți organici.

THE COMBUSTION FURNACES OPTIMISATION ASSISTED BY COMPUTER

by

PETRICĂ VIZUREANU

***Abstract.** The purpose of the heating operation is the metallic materials preparation for the forging processes in the technological flow. The heating technologies play an important part in the future quality of the product. For satisfying the production needs it is necessary to achieve a sharp control of heating processes' parameters. In such a context the development of the computer control system has a vital importance for obtaining the functional optimisation of the furnace through the mathematical model, by processing a big volume of data. The using of computer in the equipment designing and operation beside the using of new refractory materials and the burning equipment optimisation can lead at optimum heating furnaces from the constructive and operational point of view.*

***Keywords:** furnace, combustion, heating, optimisation*

I. Heating regimes design for semi - products in view of forging

The heating process of metallic materials in view of forging has to ensure the achieving of the required temperature as more possible uniform distributed upon the entire section of semi - product, in a time as short as possible and without producing the fracturing or cracking of the material. The decreasing of heating time leads to the fuel consumption reducing and at the decreasing of oxidation and of decarburation of the heated material. The exaggerate decreasing of the heating time leads to a big temperature difference between the core and the semi - product surface and at stresses that lead to fractures and cracking in the material.

Taking into account the previous presented it results that, for achieving an optimum heating regime in the shortest time and without semi - product cracking danger, there is necessary such a leading of the furnace so the temperature difference between the core and the ingot surface be close to maximum acceptable value during heating. For the correct setting of the heating regime the values of the physical – mechanical parameters have to be those of the current material temperature during heating or at least average values for small temperature intervals.

For this it is necessary a computer programme with the help of which one can plot heating diagrams for the rang of polygonal ingots or round and prismatic semi-products. The programme starts from the heat transfer relations presented in the literature [4].

The initial data of this programme are:

- semi - product sizes;
- heating temperature;
- physical and mechanical feature of the steel that will be heated (λ , c , β , γ , E).

The programme is applicable for every kind of steel for which one know the physical - mechanical features values as function of temperature and the breaking limit function of material state (the cast reminded strains).

II. The combustion process optimisation by using of new burning equipment

There exists two trends in this direction:

- heat recovery from hot gases using regenerative burners;
- the using of gas analysers for burning control in heating furnaces.

II.1 Heat recovery from hot gases using regenerative burners

In the forge sections, important energy consumers, a special place was be represented by the heating furnaces for plastical deformation, which use as combustibile the methane gas and at which during the technological processes there is a low degree of energy utilisation. The most part of the energy loss will be done by the gases vented from the working space and as it was be known, the most efficient recovery is that by which the energy was used in the charge heating process: primary recovery. Thus one can make appeal to the regenerative method by which the from the burned gases will be used to intensively preheat the combustion air using regenerative burners.

By this method the temperature of burned gases became 100-200°C by comparison with the previous situation when the gases vented from the working space can have temperatures sensible equal with those of the furnace. One recommands the using of regenerative burners on heating furnaces with maximum working temperatures about 1250°C with continuous or discontinuous operation. The regenerative method wasn't recommended to other gases due to its impurities.

II.2. The using of combustion gases analysers for burning control in heating furnaces

The advantages of the last burned gas analysers' generation were identified by the following features:

- they are made from a block of sensors placed on the pipes of burned gases of the boiler and from an electronic block placed in the furnace command desk zone, the link between them being achieved by a protective cable;
- the burned gases are being vented from the block of pipes passed through a floppy filter (which is permanently being cleaned from solid particles by reverse blowing of its inactive zone), or they filter themselves in the case of thermo-diffusive extraction and then they are being passed through the sensors and after that are sent back in the pipes (figure 1);
- the block of sensors has a ZrO_2 sensor for oxygen concentration measurement and the catalytic combustion sensor with platinum cataliser for combustibile gases measurement;
- the block of sensors works at the high temperature making possible its location closer possible by the burner.

The electronic block is being endowed with a microprocessor that has several entrances and exits analogues and digital, playing the part of a general controller of burning. It fulfils the following functions:

- it displays oxygen and combustibles gases concentration values given by the block of sensors;
- it calculates and displays the values of optimum necessary and effective air excess;
- it accomplishes the adjustment through various adjustment laws and commands the execution elements (operation) for the getting of the required flow rates for combustible and air;

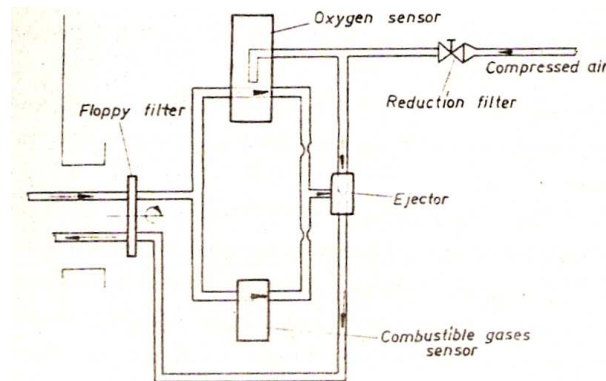


Figure 1.

- it facilitates an active dialogue with the operator which by means of a functional keyboard and of a display block can set the adjustment and advertising parameters and commands directly at the execution elements;
- it watches and commands the burners operation;
- in case of some disfunctionalities it brings the parameters at previous settled values.

This burning adjustment system optimises the efficiency of burning process by minimising the losses due to the air excess in the furnace or to unburned evacuate combustible. At the same time it helps at the maintaining of a proper fraction air/combustible despite the variation of caloric power, pressure, temperature or combustible density.

III. The computer assisted design of heating equipment

As a result of the experience there follows that the designing of heating furnaces implies laborious calculation for the thermal regime as well as for the effective dimensioning. With the PC aid and with an advanced software one could elaborate sets of programmes for analytical designing of heating furnaces.

The designing methodology supposes the elaboration of a mathematic algorithm by which starting with a calculation of the combustible burning one pass to the designing of the thermal regime for the required heating technology and the proper heat recovery system.

An important chapter in the designing stages is the establishment of the thermal balance of the heating equipment that has to have optimum balance features [3].

Each section of the thermal balance of the furnace is being calculated using analytical relations that model the heat transfer. After the calculation of each type of heat flow rate one makes with the computer aid a feed-back cycle as in the case of the heat loss through to the walls. After the average temperature calculation of the middle layer of the furnace brickwork by means of feed-back cycle, these are being approximate such as the difference does not exceed 10 %. If this difference exists one makes the calculation again taking into account the average temperatures of the middle layers previously settled.

In this way one accomplish the calculation for the other chapters of the balance too, having in view the specificity of each.

References

1. Chelu, Gh. - Optimizarea regimurilor de încălzire a lingourilor și semifabricatelor în vederea forjării, Revista Metalurgia nr. 1, 1993, p. 5-11.
2. Grancea, V., Dima, A., Vizureanu P. - Necesitatea introducerii dimensionării asistate de calculator a cuptoarelor de încălzire în procesul didactic - Sesiunea tiințifică "45 ani de învățământ superior", Galați, oct. 1993, vol.2, p.170-174.
3. Dima, A., Grancea, V., Vizureanu P. - Computer Assisted Mathematic Modelling of Heating Processes in the Solidus Field of Fe-C Alloys - Heat Treatment Conference - Dunayvaros - Ungaria, 1993, p.85-90.
4. Grancea, V., Vizureanu, P., Alexandru, M. - New Trends in the Forging Furnaces Constructive and Operational Optimisation, Buletinul I.P. Iași, tomul XL (XLIV), secția IX, Știința și Ingineria Materialelor, vol. II, 1994, pp.613-618.

Received May 4, 2005

Technical University Iași

OPTIMIZAREA CUPTOARELOR CU COMBUSTIE CU AJUTORUL COMPUTERULUI

Rezumat. Încălzirea materialelor metalice în vederea deformării plastice la cald se face cu ajutorul cuptoarelor cu combustie. În acest sens este necesară optimizarea regimurilor termice din aceste utilaje mari consumatoare de energie. Optimizarea se referă la posibilități de recuperare a energiei termice furnizate prin intermediul elementelor încălzitoare.

INDUSTRIAL INCINERATION SYSTEMS

by

PETRICĂ VIZUREANU

Abstract. *Refractory performance is a key factor in the economics in large scale incinerator operations since repair and relining of incinerators involves costly downtime or lost production. The search for more durable refractories has been particularly intense in the early 1990's leading to rapid adaptation of new products with improved spalling resistance.*

Refractories wear by thermal shock in the extreme thermal environment in secondary combustion chambers of large incinerators and by corrosion processes involving lime iron aluminosilicate liquids. In other incinerator components, abrasion, acid gas and liquid attack, alkali attack, and physical damage on slag removal influence refractory life.

Further improvements in refractory life can be expected with improvements in incinerator design to limit thermal loading on the hot face of refractories. In this respect, incinerator practices can evolve as have practices in slagging utility boilers.

Keywords: *refractory, incinerator, corrosion, slag, waste, hazardous waste, biological waste, sewage sludge, volatile organic compound (VOC), thermal shock.*

I. INCINERATION PROCESS

Incineration of waste materials is becoming a growing necessity in developed countries with increasing industrial growth and as societies become acutely aware that traditional means of disposal such as landfill will either be unavailable in the future or that the environmental risk of landfill or ocean disposal are unacceptable. Developing countries have the option to avoid the same problems on waste disposal that the developed countries have already experienced.

There is a great diversity of waste material that is currently being incinerated. Generally wastes are considered as „hazardous” or “non-hazardous” with respect to human health. In the United States, the Federal Resource Recovery and Conservation Act of 1976 (known as “RRCA”) requires that hazardous wastes must be properly recycled, treated, or sent for disposal. Also in the USA, the Federal Comprehensive Environmental Remediation, Compensation, and Liability Act of 1980 (known as “CERCLA” or “Superfund”) places ultimate responsibility on the generator of any waste with respect to handling, treatment, storage, and disposal. This makes it possible for any waste considered as “non-hazardous” today to be classified as “hazardous” tomorrow. Incineration thus becomes a means of permanently disposing of waste while managing future liability under CERCLA since all incinerator residuals are sent to hazardous waste landfills.

Another key piece of US legislation affecting incineration is the Federal Hazardous and Solid Waste Amendments of 1984 (HSWA) which mandates incineration of certain classes of hazardous wastes unless the US Environmental Protection Agency can set standards for treatment of these wastes prior to disposal or rule that land disposal is the only viable option. Efforts by the EPA to set the requisite standards have continued into the early 1990's. There are many literature citations on social and legislative issues regarding waste disposal and incineration [1,2,3].

Waste materials that can be incinerated include organic and inorganic solids, organic liquids, organic vapors, and inorganic solids mixed with organic liquids. Waste streams from manufacturing include solvents and materials used to filter and clean solvents. Volatile organics from manufacturing are now "incinerated" or oxidized in large quantities. Agricultural wastes that can be incinerated including residuals from seeds and grains. Military ordinance such as chemical weapons may be incinerated as the only means of destroying toxic materials [4].

Incineration is being considered as one of the safe means of treating soils contaminated with polychlorinated biphenyls or PCB's [5]. Town wastes incinerated can include garbage and sanitary sewage.

Under US regulations, hazardous waste incinerators are required to destroy or remove at least 99.99% of the principal organic constituents in the waste and meet standards on inorganic emissions. These inorganic emissions include acid gases, trace heavy metals, and particulates. A common acid gas which must be removed from the incinerator gas stream is hydrogen chloride (HCl) generated on combustion of chlorinated hydrocarbons. Due to its high solubility in water, equipment for HCl removal typically consists of wet scrubbers with neutralization by lime (CaO) or another basic substance like sodium hydroxide. Incinerator operators may try to trap trace metals in a slag or vitreous phase formed in the oxidation section or secondary

II. INCINERATION. DESIGN AND OPERATION

There are many types of incinerators in use with the most popular including rotary furnaces types, fixed or movable (non-rotating) hearth types, liquid or vapor injection types, and box or boiler types, the latter of which are typical of smaller units [6, 7, 8, 9]. The key components of the incineration systems are discussed below.

II.1. Waste Stream Delivery System

Liquids are typically injected into the primary combustion chamber using pumping and storage systems after delivery in drums or from bulk trucks. The typical hazardous waste incinerator will log liquid identity, fuel value (heat release on combustion), and composition. Attempts are made to control heat release by mixing liquids, although refractory performance results often suggest very high temperatures are achieved and injection may be sporadic causing problems in thermal shock of refractories.

Solids are typically injected into incinerators using pusher or ram mechanisms. Solids may be bulk solids as in the case of municipal incinerators or "tab packs" in the case of hazardous waste incinerators. Solids include glass and metal containers which influence slag chemistries within the incinerator components.

Gas streams laden with volatile organic compounds (VOC's) are injected into incinerators either directly from their source or after gas cleanup operations such as solids removal.

II.2. Primary Combustion Chamber

The primary combustion chamber (PCC) has the function of the initial incineration or burning of the waste material. The chamber is typically refractory lined in thick wall (brick or monolithic) conventional designs or thin wall (monolithic or tile) boiler-type designs. Waste solids ignite within a few feet of the injection port where local temperatures are maintained in excess of 1150°C through burning of hazardous waste liquids or auxiliary fuels. Temperatures measured by the incinerator operator by thermocouple measurement may range up to 1300-1400°C although practical observations of primary combustion chamber walls suggest localized temperatures may be higher.

In incinerators designed for continuous use, there is a means to force the burning solid process burden to progress along the hearth. This is why rotary kilns are popular designs. Smaller incinerators may use movable multiple hearths which intermittently push the process burden along the step wise inclined hearth. Some new designs propose fluid beds to achieve the same purpose.

There is a residual or "ash" or "slag" produced by the primary combustion process. This ash may exit into a water sealed quench tank, and it is conveyed to storage. It is important to note that any residual from a hazardous waste incinerator is also considered as hazardous waste requiring disposal in a hazardous waste permitted landfill.

In some incinerators, such as municipal incinerators, oxidation of combustibles may be sufficient in the PCC so that a second step, called secondary combustion or secondary oxidation, may be unnecessary. If secondary combustion is unnecessary, the gases are next neutralized and cleaned of particulates.

II.3. Secondary Combustion Chamber

The secondary combustion chamber (SCC) is typically a refractory lined chamber, either rectangular or cylindrical, with an auxiliary burner system and a sufficient volume to allow for oxidation of organic volatiles which were a product of incomplete combustion in the primary combustion chamber. To achieve the required oxidation, the SCC must operate above 'red heat' or above about 1100°C, but operating temperatures may reach 1375°C or greater in hazardous waste incinerator SCC's.

Another important function of the SCC in hazardous waste incinerators is the creation of a slag or vitreous phase to capture particulates laden with heavy metals. Slag removal by gravity flow is favored by higher temperatures.

While incinerator operators might question the magnitude of these local temperatures, many speak of a "fireball" in the entrance section of the SCC where auxiliary burners, air injection, and even oxygen injection are used. Since the "control thermocouple" can be downstream from the fireball zone, there may be poor comprehension by the operators of the extremes of temperature reached in these zones. Another important point is that the operator is controlling oxidation efficiency by monitoring carbon monoxide (CO) gas emissions at the stack suggesting that complete

oxidation is a first priority despite the generation of high refractory surface temperatures which result from these efforts to achieve complete oxidation.

If stack emissions of CO increase, a primary control response is to increase the auxiliary combustion or oxidant rate into the SCC which obviously results in higher local temperatures and possibly sporadic thermal conditions in the SSC.

Slag is removed from the SCC in slagging units through a slag tap involving a water quench. Slag accumulation may reach a depth of up to as much as two meters during an incinerator campaign in those incinerators where slag is not continuously tapped. Like slag from the PCC, SCC slag from hazardous waste incinerators must be sent to a permitted landfill.

II.4. Gas treatment

Gas treatment may involve quench by water spray, or use of a “wetted bottom” furnace chamber, followed by neutralization, demisting, or particulate removal in a conventional baghouse prior to atmospheric release. Exhaust monitoring equipment includes gas analysis monitors and opacity measuring equipment. Gas treatment may produce a filtercake residual which is sent to a permitted landfill.

III. Refractory Materials Used in Incinerators

Literature on refractory materials for incinerator applications is usually of a very general nature [8] or is produced as commercial literature by refractory suppliers [10, 11, 15]. A more specific reference is available giving incinerator designs [13]. Technical meetings have been held in the United States and in Europe with sessions on incinerator refractories [12, 14].

A problem exists in the lack of engineering information on refractories for incinerators in the United States. Incinerator operators tend to hold refractory performance results in-house as if any public perception of a “problem” with incinerator operation would add to negative sentiment on incinerators. Refractory suppliers may hold performance information in-house due to negative publicity from “failures” during the evolution of incinerator operations and because of potential liabilities.

Another problem exists in that incinerator operation is highly developed in terms of emissions (due to regulation), but the operation of incinerators has not evolved in a similar fashion as with other industrial furnaces such as utility boilers. For example, more complete information on surface temperature distribution in incinerators and knowledge of the effects of varying fuel rates on the life of refractories would help improve the life of refractories in incinerators.

CONCLUSION

Designers of incinerators should include surface temperature calculations in various zones to limit corrosion processes. Control of temperatures is particularly important in secondary combustor or oxidizer sections. Operators using incinerators retrofitted for hazardous waste incineration should realize how equipment limitations and operating conditions can adversely affect refractory life.

Progress in obtaining better refractory life in incinerators can come with application of engineering analysis to refractory performance with discussion in public scientific circles. Collective action by those involved in incineration to develop

methods and procedures with respect to refractories should be a priority of the industry so that incineration quickly becomes as well developed as are slagging utility boilers with respect to refractory performance. Society as a whole will benefit from such collective action.

References:

1. Thomas J. Overcamp, Issues In Hazardous Waste Incineration, White Paper Report Prepared For The South Carolina Research and Education Foundation, Clemson University, September, 1990.
2. E.T. Oppelt, "Incineration of Hazardous Waste ... A Critical Review," JAFCA, 37 (5), 558-586 (1987).
3. 'Hazardous Waste Incineration: A Resource Document,' American Society of Mechanical Engineers, New York, 166 pp, 1988.
4. "Burning Chemical Weapons," USA Today, May 14, 1991, p. 11
5. "AOSTRA-SoilTech Anaerobic Thermal Processor Treats PCBs in Soils at Wide Beach Superfund Site In Brant, New York," EPA Information Update, May, 1991.
6. "Permit Writer's Guide To Test Burn Data," EPA/625/6-86/01 2, Environmental Protection Agency, 1986.
7. L. Theodore and J.P Reynolds, Introduction To Hazardous Waste Incineration John Wiley and Sons, New York, 1987.
8. T. Banner et. al., Hazardous Waste Incineration Engineering, Noyes Data Corporation, Park Ridge, NJ, 1981.
9. Wafter R Niessen Combustion and Incineration Processes Application In Environmental Engineering Marcel Dekker New York 1998.
10. „Refractories To Tame The Hottest Incinerators Under The Sun”, Carborundum Company 1998.
11. "Incinerators" in Modern Refractory Practice Harbison-Walker Refractories Company, 1991.
12. St Louis Section, The American Ceramic Society, May 24, 1991.
13. Technology of Monolithic Refractories, Plibrico Japan Company Limited, Tokyo, 1994.
14. XXXIV International Colloquium on Refractories, Aachen, Federal Republic of Germany, September 23-26, 1991.
15. Brosnan, D.A., „Refractories for incinerators”, Key Engineering Materials, vol. 88, 1993, pp. 71-102, Trans Tech Publications, Switzerland.

Received May 4, 2005

Technical University Iasi

SISTEME INDUSTRIALE DE INCINERARE

Rezumat. Performanțele materialelor refractare utilizate pe scară largă în construcția sistemelor industriale de incinerare reprezintă un factor cheie atât în timpul exploatării, cât și în timpul reparării sau refacerii izolațiilor termice ale acestora. Factorii agresivi la care trebuie să reziste aceste materiale refractare în exploatare sunt de ordin mecanic (abraziune), termic (până la 1400°C) și chimic (coroziune, mediu alcalin, acizi etc.)

THE HETEROGENEOUS NUCLEATION AND HYDROGEN ROLE ON THE PRIMARY MICROPOROSITY IN ALUMINUM ALLOYS

BY

PETRU MOLDOVAN, LUCIA FIRESCU, IOANA APOSTOLESCU,
GABRIELA POPESCU, MIHAI BUTU

Abstract: This paper presents the formation procedure and increase of the primary microporosities in aluminum alloys and some scientifically consideration on the heterogeneous nucleation role and the hydrogen concentration evolution during solidification.

Keywords: microporosity, heterogeneous nucleation, pores, hydrogen concentration

1. Introduction

Porosity is one of the most encountered defects in aluminum alloys and it is responsible for the significant decreasing of the parts qualities and especially the physical – mechanical properties and the surface quality of the cast products.

The porosity formation process is controlled by a lot of factors which simultaneously appear, thus is very difficult to distinct their separate influence.

Porosity appears in one of this ways:

- Pores formation by hydrogen atoms diffusing from the solution (primary gaseous porosity);
- Solidification contraction;
- Combining these two effects.

Gaseous porosity of the aluminum alloys is determined especially by the hydrogen.

For the bubble formation in the melt or in the solidified material it should be passed the condition:

$$p_B \geq p_A + p_M + p_k$$

where: $p_k = \frac{2\sigma}{r}$

p_B – is the pressure inside a hydrogen bubble in the melt;

p_A – atmospheric pressure (in open furnaces);

p_M – metalostatic pressure;

p_k – capillary pressure;

σ – melt surface tension;

r – formed bubble radius.

During aluminum alloys solidification, the internal pressure of the hydrogen bubble increases constantly due to the decrease of the solubility of the hydrogen in the melt. In actual cases, p_A and p_M are usually constant. If the internal pressure of the hydrogen

p_B is equal or over the sum between p_A+p_M formation and increasing of the bubble depend only on p_K .

2. Theoretical consideration

Probability of the gas bubble formation capable to grow in the melt, in case of the homogeneous germination can be determined by the germination theory in heterogeneous environment. Starting from the differences between the specific superficial and volumetric energies, the critical radius of the germ capable to increase can be determined.

Number of the germs with critical radius is determined with the aid of the relationship:

$$N = \sqrt{\frac{2\sigma}{\pi m}} n_G \exp\left[-\frac{16\pi\sigma^3}{3kT(p - p_0)}\right]$$

where: N is the number of the gas nuclei with critical dimension;

k - Boltzman constant, J/K;

m - molecule mass, g;

n_G - gas concentration, ppm;

p - gas bubble pressure (nucleus), barr;

p_0 - pressure over the melt, barr;

T - temperature, °C or K;

σ - superficial tension, dyn.cm⁻¹.

To the heterogeneous nucleation, the bubbles formation energy decrease function of the wetting angle θ . This energy decreasing to the plane interface solid / liquid can be expressed by Volmer (fig. 1)[1]:

$$f(\theta) = \frac{A(\theta)}{A_0} = \frac{1}{4}(2 - \cos\theta)(1 + \cos\theta)^2$$

where: $A(\theta)$ is the heterogeneous nucleation energy; A_0 - homogeneous nucleation energy; θ - wetting angle.

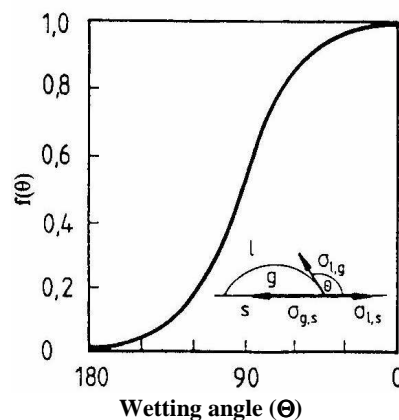


Fig. 1. Function $f(\theta)$ for the bubble formation case.

The nucleation energy is proportional with the square of the saturation pressure (p_h) of the dissolved hydrogen, necessary for the gaseous bubble formation:

$$\frac{p_h}{p_0} = \sqrt{f(\theta)}$$

where: p_0 "fracture pressure of the liquid by homogeneous nucleation.

Mechanism formation of the bubbles on the fractures and voids is presented in fig 2 and 3[1].

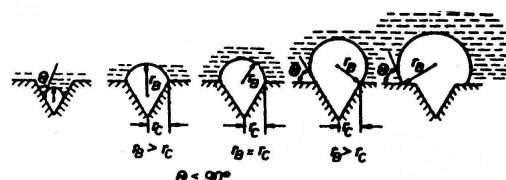
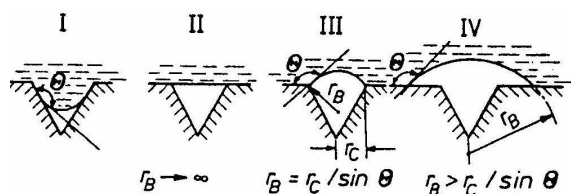


Fig. 2. Heterogeneous nucleation of the bubbles on the fractures and voids for wetting angle $\theta > 90^\circ$

Fig 3.. Heterogeneous nucleation of the bubbles on the fractures and voids for wetting angle $\theta < 90^\circ$

For $\theta > 90^\circ$ the nucleation can easily take place on the base of the depth. Before the bubble to be capable to grow, the process is inhibited due tot the fact that the radius of the bubble should pass over a critical values to fulfill the growing criteria.

To reduce the energy of the heterogeneous nucleation Chalmers presented another geometrical model for the gas bubble formation. As it can be seen in the fig 4 [1], the nucleus capable to grow can be formed at the concave interface with the atoms less than convex interface of the other atoms, thus the appearance of the nuclei capable to grow needs a smaller nucleation energy and realize a reduce undercooling.

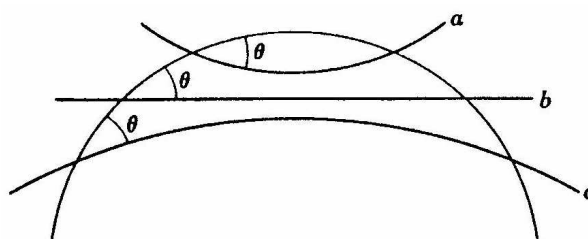
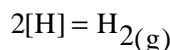
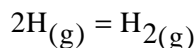
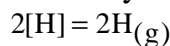


Fig. 4. The influence of the geometry on the heterogeneous nucleation at the same angle θ :
1 – convex surface; 2 – plane surface; 3 – concave surface

In the vacuum degassing process, when the equilibrium in the system gas phase / metal is destroyed, in the melt the following reactions take place:



We can consider that hydrogen is eliminated by the separation surface, by convective diffusion and formation, growing and ascension of the gaseous bubble. The mechanism of the H_2 induced porosity can be analyzed considering separation of the dissolved hydrogen on the solid/liquid interface.

During solidification, the interdendritic liquid is easily enriched with H_2 as the solid fraction grows, due to the fact that that most the H_2 quantity is rejected to the solid / liquid

The heterogeneous nucleation to the gas bubble formation in the melt is realized on the solid particles suspended in the metallic bath and on the crucible walls or of the mould. The heterogeneous nucleation energy is reduced to the solid / liquid limit by decreasing the wetting of the solid due to the melt.

In the specialty literature there are some recent information that clearly shown that excepting the free hydrogen in liquid alloys there always a certain oxide quantity and other nonmetallic inclusions which are responsible on the contraction porosity appearance.

Contraction microporosity is dispersed in the interstitial of the solidification dendrite regions, underlining especially in alloys with a wide range of solidification.

The inadequate or limited feeding with liquid metal in interdendritic areas is an important cause of this porosity type formation.

The growing process of the pores to the porosity formation is described by Pehkle schematically in fig. 5[1].

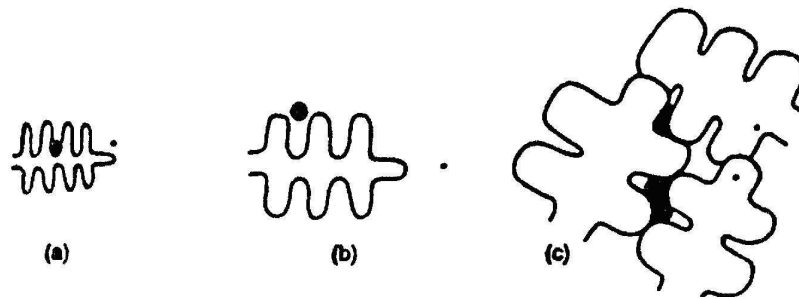


Fig. 5. Growing of pores process

The gaseous pores can nucleate on the base of dendrite arms (fig 5). Synergy between contraction and gaseous porosity pass the negative free energy to form the gas metal surface, facilitate the nucleation process (fig.5a). Ongoing the solidification, the pores grow due to the intense degassing of the gas in liquid alloy. The pores radii become large enough to decrease the contribution of the inter phase energy and the pores are detaching the dendrite (fig. 5b). Next the neighbors dendrite are joining together making difficult the liquid feeding among the dendrites and the porosity increases to compensate the solidification contraction (fig. 5c).

The pores can be formed during solidification of aluminum alloys. Pores that are formed before solidification are spherical and relatively large and the pores formed after solidification has irregular shape and are caused by the contraction porosity.

3. Methods used to determine the porosity in aluminum alloys

The principal methods used for determine the porosity in aluminum alloys are:

- Quantitative microstructure analyzes;
- Computerized tomography;
- VAC – TEST procedure to determine the primary porosity of the aluminum alloys;

Quantitative microstructure analyzes

In cast aluminum alloys porosity is reduced but the pores dimensions are quite large and as a result, pores density is small. To the microscopic enlargement, where the resolution is satisfactory, we can observe one or two pores in the visual area and some microscopic fields do not contain pores.

This fact causes serious problems of determination the porosity in alloys samples. There is large variation form one field to another due to the fact that the pores are randomly spread. So the errors in measuring the micro pores are large enough. Thus the measuring of some fields are inefficient due tot the fact that is not possible for large enough areas to be observed on a microstructure. The creating of some montage with a large number of microstructure for example 100 or more is not viable from the practical point of view. Also the micro pores measures are not quite exact.

Recently a method based on image analyzes software which ensures a montage with a high number of microstructure associated parts in the memory of the image analyzer [2].

This procedure allows the automatic measurement of the area, perimeter, dimension and coordinates (X, Y) of each micro pore in the montage which covers the entire area of the sample. All the microstructure parameters can be calculated from these data with the aid of the computer.

Using the montage allows the measuring of the distances between the micro pores which aren't in the same field ensuring that the measuring is realized on each field in metallographic plane and each field is observed and analyze only once.

The volumetric fraction of the micro pores V_V is correlated with the mean value of the micro porosity fraction area $\overline{A_A}$, observed in metallographic plan by the general relationship:

$$V_V = \overline{A_A}$$

The area fraction $\overline{A_A}$ is equal to the sum of the all pores area observed on the montage divided to the montage area.

The total surface area of the micro pores on the unit volume, S_V , can be estimated by using the relationship:

$$S_V = \left(\frac{4}{\pi}\right)L_A$$

where L_A is the sum of the perimeters of all micro pores from the montage divided to the montage area.

The mean curvature of the pores, H, can be estimated from the next relationship:

$$H = \left[\pi^2 N_A\right] / [2L_A]$$

where: N_A is the density of the pores in the montage (number of pores on the surface unit of the montage)

Using a special transformation technique (Saltykov), in certain conditions, can be calculated the three-dimensional distribution of the micro pores from the two dimensional distribution observed in metallographic plane.

The computerized tomography method

The computerized tomography method borrowed from medicine can be applied in the aluminum alloys industry but due to the elevated cost is limited to the parts used in aerospace industry.

In the last years, two new techniques for facilitating of the industrial use of the computerized tomography (TC):

- Using a TC volumetric scanner, capable to produce hundreds of inspection plans from one single scanning;
- Incorporating of the mathematic – morphological techniques for facilitating automatic data interpretation and quantitative information in actual time.

Traditional computerized tomography consists in inspection of a section of 1.5 mm thickness and needs 3 seconds.

The volumetric scanner TC, recently realized, is capable to reconstruct over the 500 sections by one single scanning which needs 180 seconds.

The automatic image analyses to auto detect the porosity consists in detection, quantification and display.

The computerized with X rays tomography is based on the penetration of the radiation for a large number of angles for reconstructing of the image of the transversal section of some object.

The X ray flux attenuation which passes through an object measured by a detection system placed on the other part of the object. The object is rotated with 180 degrees during measuring. The measured projections are reconstructed by the computer in a two dimensional image of the attenuation coefficients of the transversal section irradiation.

The computerized technology quantitatively determines, point by point, the density values in the thin sections of some object. Each point in TC images is defined as a volume element (voxel) which represents finite dimensions X, Y and Z of the scanned object [3].

The data base of the computerized tomography has a contrast resolution very high (ability of measuring the differences very small of the density) and the large spatial resolution (ability of solving fine structural details).

For processing is necessary a ultra good computer, thus the method is very expensive.

VAC-TEST procedure

This method is based on the calculus of the density index of two samples: one solidified in vacuum (80 mbarr) and the second one solidified under atmospheric pressure. The aluminum alloy is melted in an electric furnace and melted at 750°C. At this temperature the alloy is maintained for few minutes. The samples are taken with the aid of a special spoon and are cast in two crucibles. One of the crucible is placed on the working bank and the melt is solidifying at atmospheric pressure and the other one is placed in the vacuum room (80 mbarr) (fig. 6a.). After the samples were solidified, they were extracted from the crucibles and subjected to the process of measuring of the density index on the density terminal (fig 6b).

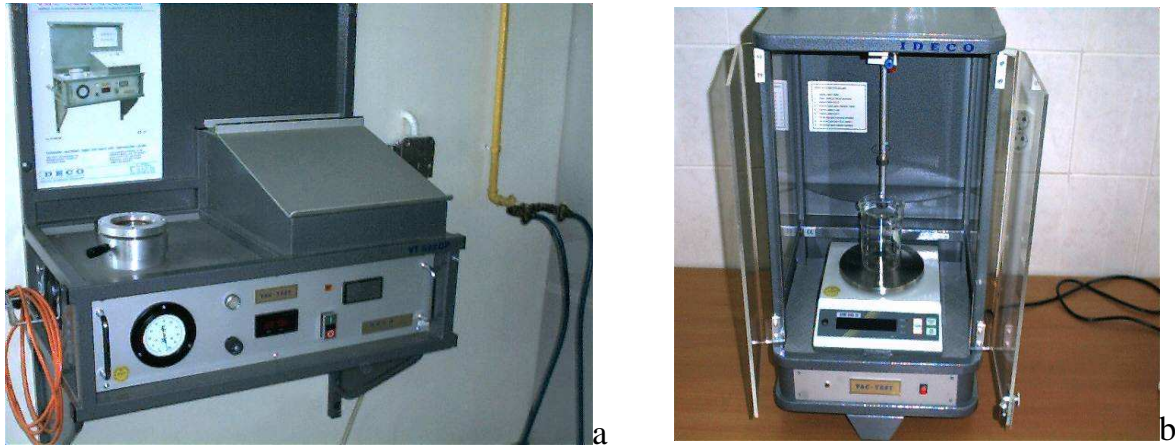


Fig. 6. VAC-TEST device

The density index (D.I.) which is automatic displayed evaluates the primary porosity of the alloy. The calculus of the density index is realized with the aid of the relationship:

$$ID = \frac{D_{aer} - D_{vid}}{D_{aer}}$$

where: D.I. – density index (primary porosity);
 D_{aer} – air density;
 D_{vid} – vacuum density.

VAC – TEST procedure ensures a rapid and efficient evaluation of the aluminum alloys porosity by measuring the density index and has the main advantage that could separate the gaseous porosity [4]. In fig 7 is shown the analyze of the porosity type underlining in samples of AlSi7Mg0.3.



AlSi7Mg0.3 solidified a. in air, b in vacuum (80 mbarr) $0.5\text{cm}^3\text{H}_2/100\text{g}$, ID 6.5, gaseous porosity



AlSi7Mg0.3 solidified a. in air, b in vacuum (80 mbarr) $0.008\text{cm}^3\text{H}_2/100\text{g}$, ID 5.7, contraction porosity



AlSi7Mg0.3 solidified a. in air, b in vacuum (80 mbarr) 0.3 cm³ H₂/100g, ID 6, combined (gaseous and contraction) porosity

Fig. 7. Examples of porosity types on a AlSi7Mg0,3 alloy

4. Conclusions

The realized analyze was for the pores nucleation at the aluminum alloys solidification.

Some methods for determination of the primary porosity of aluminum alloys were analyzed and compared.

REFERENCES

1. P. Moldovan – *Treatment of Molten Metals*, V.I.S. PRINT, Bucharest, 2001, ISSN 973-99924-5-5, **293-332**.
2. A. M. Samuel, F. H. Samuel – *Porosity factor in aluminium castings*, **AFS Transactions**, vol. 92, 1989, **657 – 665**;
3. V. Lauren, C. Rigaut – *Experimental and numerical study of criteria functions for predicting microporosity in cast aluminium alloys* , **AFS Transactions**, vol. 92, 1989, **647 – 654**;
4. VAC TEST, *Technical Documentation*, **IDECO**, Bochold, Germany, 2002

Received May 9, 2005

POLITEHNICA University Bucarest

NUCLEEREA HETEROGENA SI ROLUL HIDROGENULUI ASUPRA POROZITATII PRIMARE IN ALIAJELE DE ALUMINIU

Rezumat: In aceasta lucrare sunt prezentate procesele de formare si de crestere a microporozitatilor primare si cateva consideratii stiintifice privind rolul nucleerii heterogene si a evolutiei concentratiei hidrogenului in timpul solidificarii.

PARAMETRIC MODELING OF ELECTROMAGNETIC SHEET METAL FORMING DEVICES

BY

GEORGETA CIOBANASU^a and DORIN LUCA^b

Abstract: This paper focuses on a new approach of computer modeling technology, known as the feature-based parametric modeling technique, applied in the electromagnetic sheet metal forming device design. The main advantage of this new design technique is the capability to produce very flexible designs and evaluate them with minimum effort.

Keywords: electromagnetic forming devices, sheet metal forming, parametric modeling, CAD design, solid modeling, assembly modeling.

1. Introduction

The electromagnetic forming process is one of the more common high rate techniques. The source of energy used to deform the metal is an electrical discharge. This process is primarily used for three forming operations, namely sheet metal forming, tube expansion and tube compression.

Electromagnetic forming is the only high velocity forming technique to gain significant acceptance in commercial metal working. The electromagnetic forming technique has been in use commercially for the last 30 years. It has been mostly used for joining and assembly of concentric parts. The minimal springback inherent in all high velocity forming processes makes for high quality joints. One of the most common applications is the compression crimp sealing and assembly of axisymmetric components such as automotive oil filter canisters. As the name implies, electromagnetic forces are used in this technique to form the material. A current pulse from a capacitor bank is passed through a coil which is placed in proximity to a workpiece. The current pulse causes a high magnetic field around the coil. This field introduces an eddy current in the workpiece and an associated secondary magnetic field. The two fields are repulsive and the force of magnetic repulsion causes the deformation of the workpiece. Depending upon the forming operation [1], three types of coils are used:

- a) a flat coil which consists of a metal strip wound spirally in a plane – coils of this type are used for forming of sheet metal [2];
- b) a helical coil used for tube expansion – for an expansion operation, the coil is placed inside the tube to be expanded;
- c) a coil used for ring compression – this coil is similar in geometry to an expansion coil – however, during the forming operation, the coil is placed surrounding the tube to be compressed.

This work approach types a) for electromagnetic sheet metal forming.

2. Computer Modeling process of the Proposed Device

The experimental device has been designed using a parametric, feature-based modeling (FBM) approach, with SolidWorks software. Using parametric modeling, has several advantages for engineering design. One of these is that models can be updated by changing the sizes and relationships that define the model as the design changes.

Another advantage is that FBM make the modeling process more efficient by creating and modifying geometric features of a solid model in a way that represents how geometries are created using common manufacturing processes. A last aspect is that parametric modeling stores information about each feature and its relationship to its parent feature. This is known as parent-child relationship and is critical to maintaining design intent of a part.

To reduce the complications of the product design SolidWorks software, as other 3D parametric modelers, provides different design environments, as follows:

- **Part mode**, to create solid models of individual parts. Using SolidWorks, the virtual part on the screen will look very similar to the actual part once it has been manufactured.
- **Assembly mode**, to create assemblies by assembling the components created as individual part files. Two types of assemblies, regarding the direction and the time order in which the components are elaborated, can be used here: top-down assemblies and bottom-up assemblies.
- **Drawing mode** is used for the documentation of the parts or the assemblies in the form of the two-dimensional engineering drawing representations.

The part mode is the driving mode for all other modules. The modeling procedure begins with part mode. Subsequent assemblies and drawings are based on the original part files. The advantage of SolidWorks environments is their dynamic links (fig. 1). Any change to a part model will automatically be updated to any corresponding assembly or drawing files. Again, the assembly or drawing can be edited and the change will reflect back to the part.

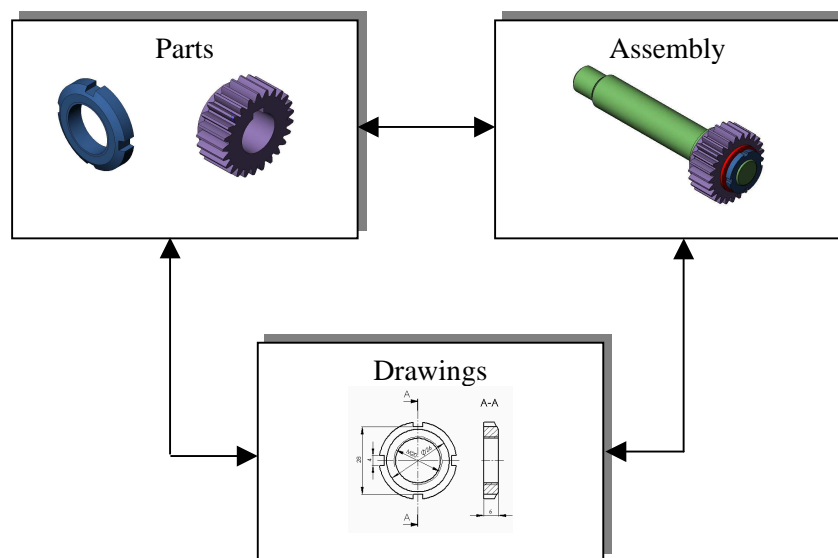


Fig.1. Bidirectional associativity among SolidWorks design modules.

The design process of the virtual device starts by designing the individual components, created as separate part files (*. Sldprt). For example, in fig. 2 is illustrated how the flat coil component from body coil subassembly (fig. 3) was generated. The modeling process begins by creating a 3D sketch profile (a composite curve formed by a spiral, lines and arcs) for the path and a 2D sketch (a circle) as profile curve (fig. 2a).

The next step is sweeping the profile along the path curve (fig. 2b). Because all of the parts are parametrically defined, one or more of the parametric features can be easily modified [4]. So, due to there many types of forming coil used for the present device with a parametric model this can be easily generated (see fig. 2c).

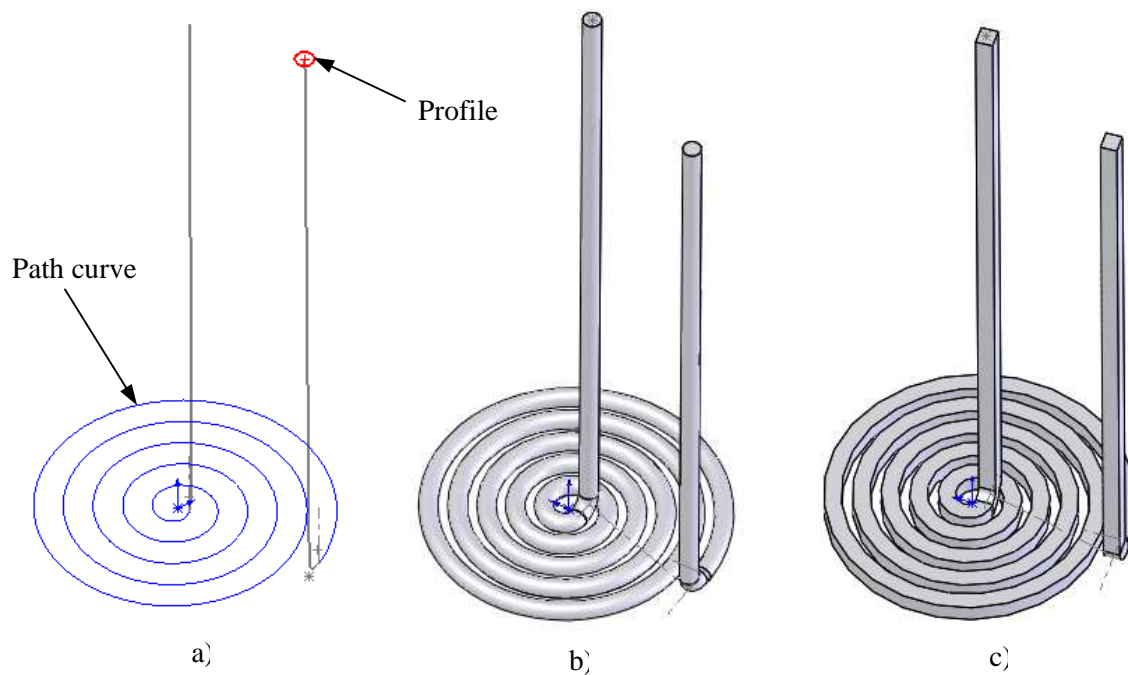


Fig. 2. Creating the flat coil using a sweep operation a) sketch profiles b, c) different profile models.

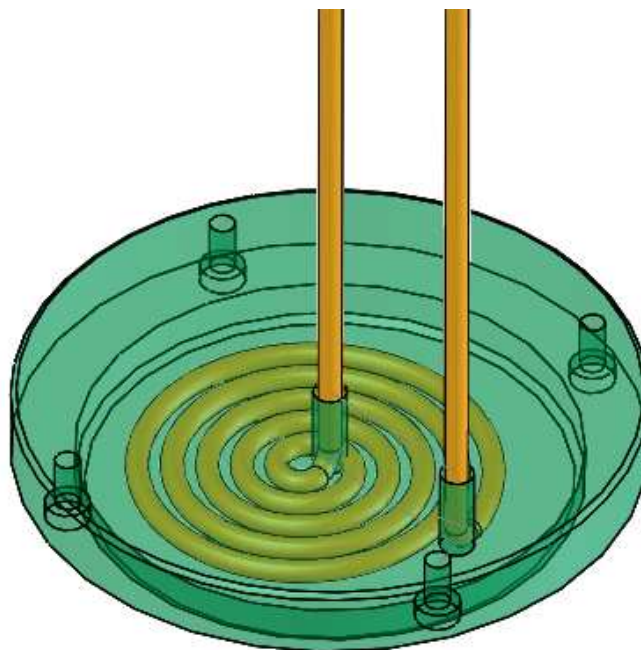


Fig.3. The body coil subassembly [5], [6], [8].

Another component modeling example is given next. Because most of the device components are turned parts, these are typically very well suited for manipulation with the Revolve command (fig. 4). The other features of these parts are then directly applied to the base feature using the Hole wizard tool.

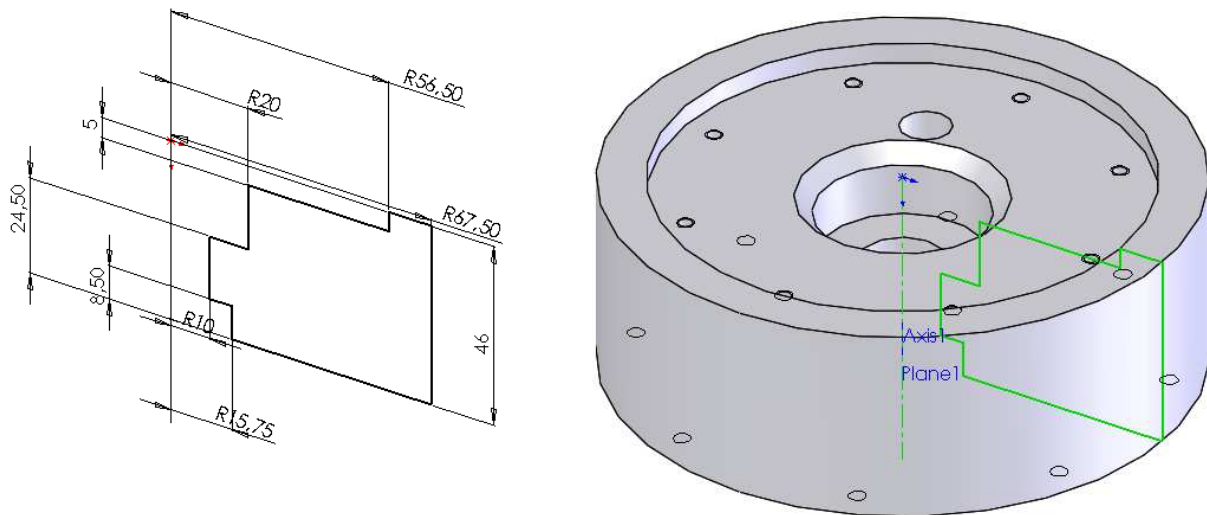


Fig. 4. Sketch geometry for the revolved base feature and the complete part after adding all features.

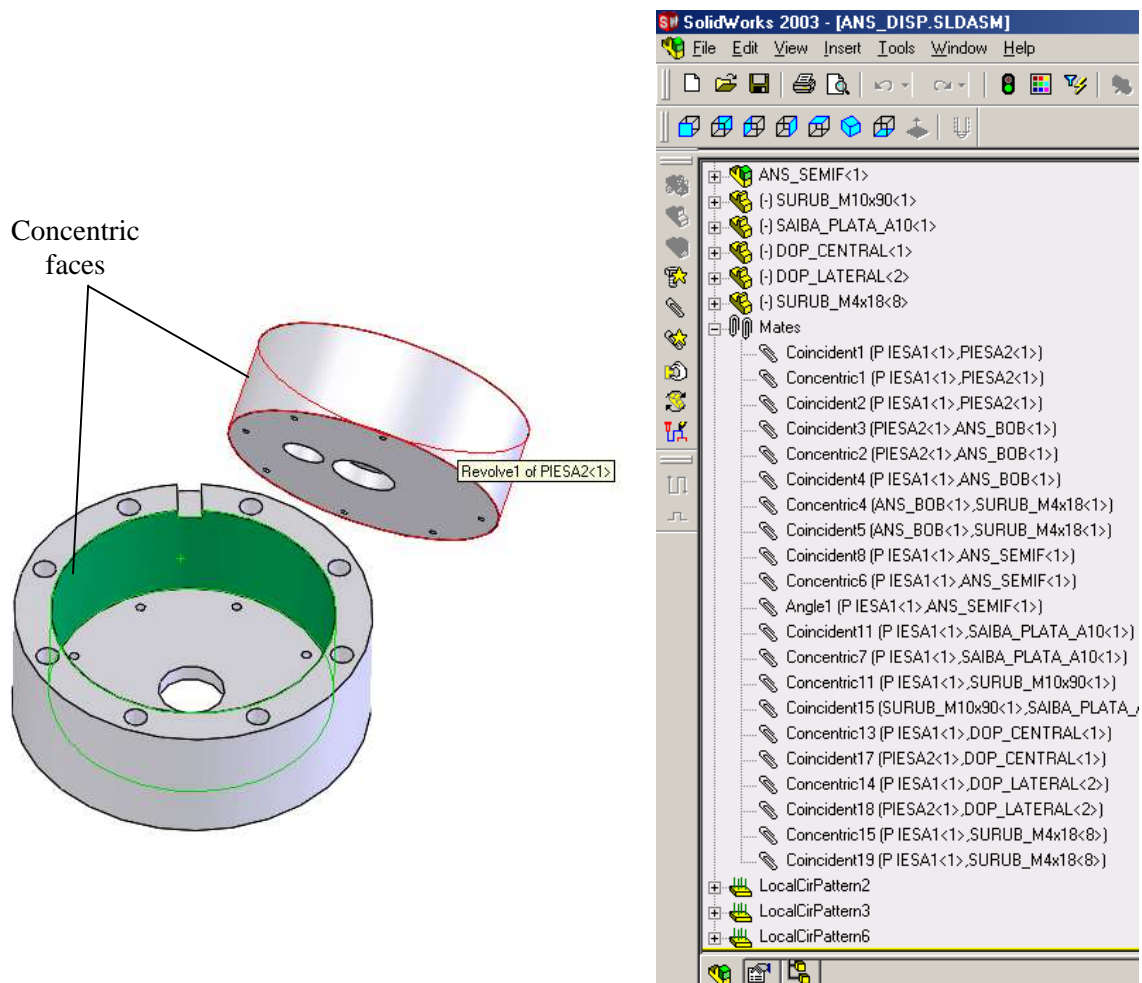


Fig.5. Concentric mate between two components and the assembly mate structure for full assembly.

Once all components of the device have been created they are inserted into an assembly document (*.Sldasm) and then attached to one another using assembly constraints (or mates). Mates help restrict degrees of freedom for an assembly component. In SolidWorks, the components are assembled using seven basic mate types.

In our case, only concentric and coincident mates have been used for assembling the components.

For example, in fig. 5 is illustrating a concentric mate applied to adding a cylindrical component into another component.

The FeatureManager design tree has a mates area that lists mates defined within an assembly. Fig. 5 shows this structure for our assembly.

Fig. 6 presents the finished virtual model of the device, with a short presentation of the components. In order to assure a good resemblance with the real assembly, the components received color and texture properties to make them as natural as possible.

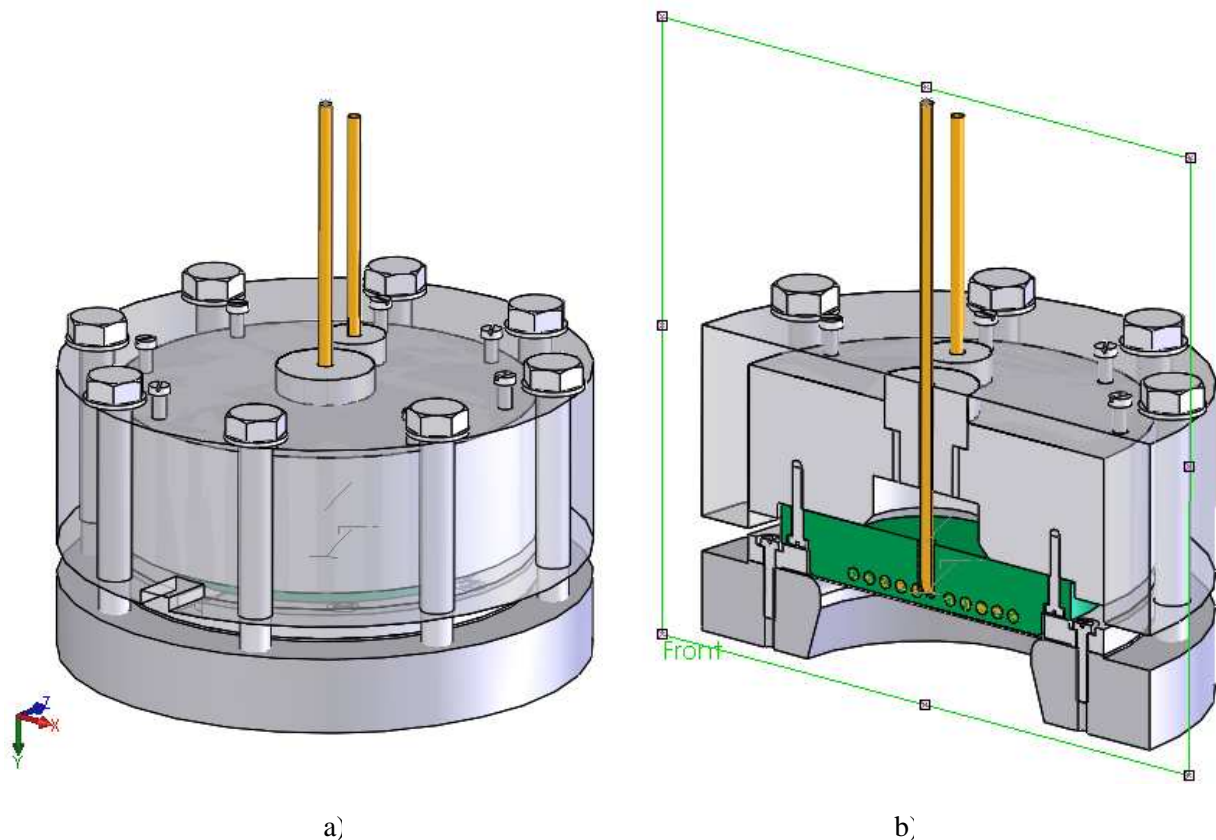


Fig.6 The finished virtual assembly in shaded mode a) and as section view b) [6], [7], [8].

For a better understanding of the device, fig. 7 presents an exploded view of the assembly. This view has the advantage that allows a more precise illustration of the reciprocal positions between components and to visualize the assembly procedure. Each component is separated from the components with which it mates, usually along the assembly axis.

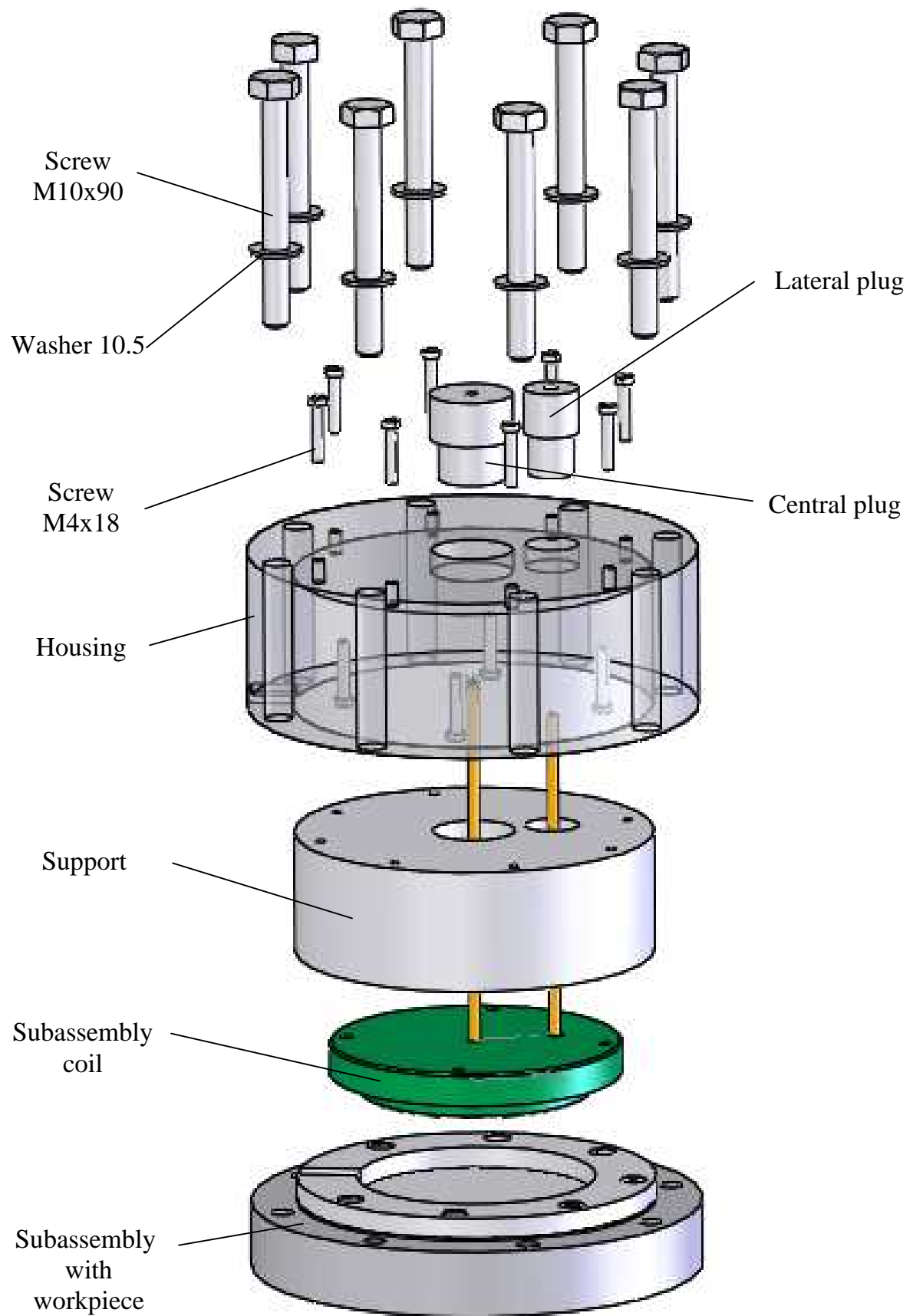


Fig.7. The exploded view of device assembly [3], [8].

Once all of the components have been assembled, the assembly can be checked for the interference and clearances between parts.

The last step of device design was to generate the two-dimensional drawings based on existing parts and device assembly. The automated process used to create drawings with SolidWorks is very user friendly and eliminates many of the tedious aspects normally associated with drafting.

The finished assembly drawing for our device is shown in fig. 8.

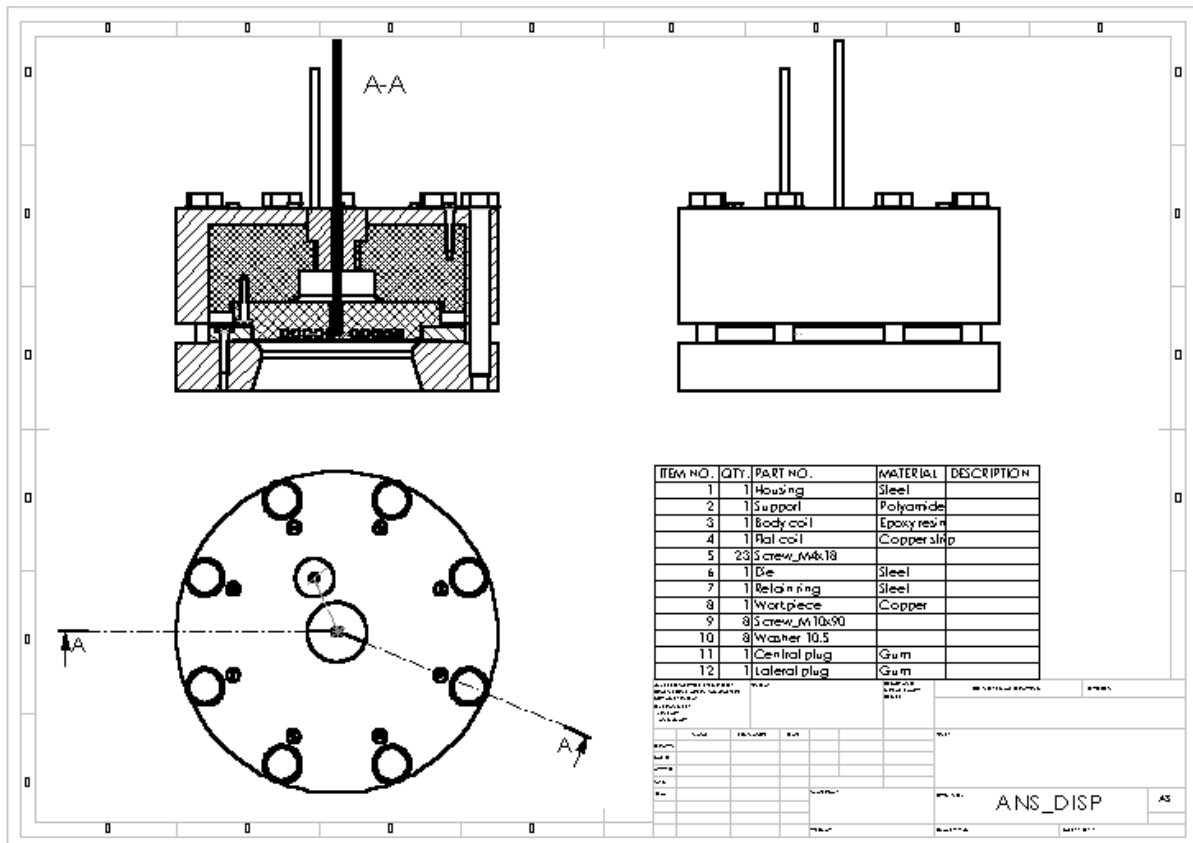


Fig.8. The device partial assembly drawing.

3. Conclusions

Parametric assembly creation, which is a relatively new addition to the world of product modeling is an important tool in the hands of design engineers. Parametric models are easier to interpret and can be easily altered. Parametric models can be applied to the models and the results graphically displayed.

Therefore, it is important that assembly modeling be included in the engineering design graphics curriculum.

Acknowledgements

The authors wish to express their thanks to Professor Dr. Petre Dusa for his support; this material has been used for academic purposes.

SolidWorks is a trademark of SolidWorks Corporation.

Remark

This paper presents some results of researches achieved by the authors within the framework of the Grant CNCSIS type A, cod 529/2005.

Received, April 20, 2005

The "Gh.Asachi" Technical University Iași

^{a)} Department of Descriptive Geometry and Technical Drawing

^{b)} Faculty of Materials Science and Engineering

REFERENCES

1. Luca, D. – *Research and contributions regarding plastic processing by the electromagnetic forming proceeding*. PhD Thesis (in Romanian). Iasi: Technical University, 2000.
2. Luca, D.; Zaharia, L.; Gheorghiu, Diana; Mihordea, T. – *Researches Regarding the Flat Coils for Electromagnetic Forming, Metal '98. 7th International Metallurgical Symposium*, Ostrava, 1998, vol. 4, pp. 252-255. ISBN 80-86122-14-X.
3. Luca, D. – *Device for sheets formability testing* (in Romanian), Romanian Patent no. 114.877, 1997.
4. Ciobanasu, Georgeta, Segal, L. – *Parametric modeling and design of robot grippers mechanism Bulletin of the Politechnic Institute of Jassy*, 2004, Tom L (LIV) - Fascicula 6A, Secția Construcției De Mașini, pp. 339-344.
5. Racoccea, Cristina; Ciobanasu, Georgeta; Segal, L. – *3D Modeling and the design process, Bulletin of the Politechnic Institute of Jassy*, 2001, Tom XLVII (LI)-supliment – Mașini Unelte și Scule , Secția Construcției De Mașini, pp. 51-56.
6. Ungureanu, G. – **Computer Aided Design**, Editura Tehnopress, Iași, 2005.
7. Bertoline, G., Wiebe, E. and Miller, C. – **Fundamentals of Graphics Comunication** – second Edition, McGraw-Hill Companies, 1998, ISBN 0-07-289201-3.
8. * * * – *User's Guide SolidWorks*, 2003.

MODELAREA PARAMETRIZATĂ A DISPOZITIVELOR DE DEFORMARE ELECTROMAGNETICĂ A TABLELOR

Rezumat: Această lucrare prezintă una dintre cele mai noi concepții privind proiectarea asistată (CAD) și anume proiectarea parametrizată bazată pe caracteristici, cu aplicație la proiectarea dispozitivelor de procesare a tablelor prin magneformare. Principalul avantaj al acestei noi tehnici de proiectare îl reprezintă posibilitatea de a realiza desene flexibile, ușor de modificat.

HIGH RESIDUAL STRESS MEASUREMENTS

BY

OCTAVIAN CIOBANU, GHEORGHE POP and DORU CANTEMIR

Abstract: The study was conducted with reference to the case of semi-infinite body carrying a blind hole. A uniform stress distribution was assumed at large distance from the hole and the material was considered to exhibit a bilinear stress-strain behavior. In hole drilling method, strains produced by stress relaxation are relatively small and as a consequence, the material plastic behavior can be linearly approximated without significant errors, provided that this relationship is specifically selected in order to reproduce the near stress-strain curve. Using a corrective procedure and analytic relations, the measurement of residual stress is improved, permitting measurements up to 90% of the material yield strength.

Keywords: high residual stress, tensometry, hole drilling method, corrective procedure

1. Introduction

Residual stresses are the stresses present in a body which is free from external load. Processes involved in the manufacture of structures and components often result in the formation of residual stresses.

The effects of residual stresses are often not evident until the components or the structures are subjected to external loads or exposed to an adverse environment. Residual stresses are superposed upon loading stresses, thus resulting in a change of the load capacity of a structure.

Industry has been searching for methods capable of measuring residual stresses accurately, quickly and easily without damaging the material to be tested.

Several methods have been developed; the most important are:

1. Conventional methods: cutting (destructive method), sectioning (destructive method), hole drilling (partially destructive method).
2. Nondestructive methods: X ray diffraction technique, ultrasonics, electromagnetics

The effects of residual stresses can be either beneficial or detrimental and depend upon its sign, magnitude and distribution. Surface compressive stresses, produced in metal components by peening operations are known to extend fatigue life.

Detrimental residual stresses are particularly insidious because their existence is generally not recognized or even considered until structure performance falls short of design and service requirements. Detrimental residual stresses lead to early warpage and corrosion of the metal and reduce its tensile strength.

The hole drilling-strain gage method was formalized in the U.S. standard ASTM, Standard Method E 837 [1] and it is probably the most cost-effective and least destructive of all conventional methods. A hole-drilling strain gage consists of two, three or four tensometric elements forming a rosette. The strain gage is placed in the

area of measurements and a hole is drilled at the geometric center of the strain gage rosette to a depth of about 0.4 of the main diameter of the strain gage circle (D). Residual stresses relax in the surrounding recording instrument. Within close vicinity of the hole, the stress relief is nearly complete.

The surface strain relief is related to the relieved principal stresses by relations of following type:

$$\varepsilon = (A + B \cos 2\alpha) \sigma_1 + (A - B \cos 2\alpha) \sigma_2 \quad (1)$$

where ε it is the relieve strain measured by a radially aligned strain gage centered at a point P;

A and B are calibration constants according to ASTM E 837;

α it is the angle position of P point;

σ_1 and σ_2 are the main stresses; σ_1 it is the maximum principal stress and σ_2 it is the minimum principal stress in the hole location before drilling.

Rendler N.J. [2] and Whitney T.J. [5] showed that this kind of strain gage rosettes is usually limited to relatively low stress levels (up to 50% of yield stress).

Other studies [3, 4, 6] show that the blind hole drilling method it is the unique standardized stress measuring method and the most cost-effective of all conventional methods. Accurate results are obtained when two or three methods are used for the same measurements [4].

One of the most significant limits in the application of the ASTM standard is the maximum stress that can be measured. Residual stress in components should not exceed one-half of the material yield strength. Another limitation is connected with the requirement of through-thickness uniformity of residual stress; significant variations of residual stress with depth are often observed in practical applications.

The classical approach to the problem is based on the hypothesis of a linear elastic isotropic material which allows to apply the superposition principle for relating residual stress to relaxed measured strain.

Recently, the effect of plasticity on the measurement was systematically investigated in order to increase the range of measurable residual stress [1].

A general procedure for evaluating residual stresses when plasticity is present was proposed which accounts for the influence of stress biaxiality and material strain-hardening properties.

2. Experimental procedure

The study was performed in the laboratories of Mechanic Engineering Department of Pisa University, during an international research grant, with reference to the case of semi-infinite body carrying a blind hole. A uniform stress distribution was assumed at large distance from the hole and the material was considered to exhibit a bilinear stress-strain behavior.

In order to obtain results with less errors at high stress, a new original method developed at University of Pisa [2,3,4,5] was applied containing a corrective calculus in some steps:

1. Computation of the principal residual stresses σ_x and σ_y according to ASTM standard:

$$\sigma_x, \sigma_y = (\varepsilon_1 + \varepsilon_2)/4A \pm ((\varepsilon_1 - \varepsilon_2)^2 + (\varepsilon_1 + \varepsilon_2 - 2\varepsilon_3)^2)^{1/2}/4B \quad (2)$$

where ε_1 , ε_2 and ε_3 are deformations measured by transducers and A and B are the calibration constants of rosette [7].

$$2. \text{ Computation of the biaxiality factor: } \Omega = \sigma_{ASTM} / \sigma_{xASTM} \quad (3)$$

$$3. \text{ Computation of } \sigma_{eqi} : \quad \sigma_{eqi} = \sigma_{yi}(1 - \Omega + \Omega^2)^{1/2}/(3 - \Omega) \quad (4)$$

$$4. \text{ Computation of a loading factor: } f_{ASTM} = (\sigma_{eq} - \sigma_{eqi}) / (\sigma_y - \sigma_{eqi}) \quad (5)$$

$$\text{where } \sigma_{eq} \text{ is: } \quad \sigma_{eq} = (\sigma_{max}^2 + \sigma_{min}^2 - \sigma_{max} \sigma_{min})^{1/2} \quad (6)$$

5. Computation of the effective loading factor:

$$f = (-1 + (4 * C * f_{ASTM})^{1/2}) / 2 * C \quad (7)$$

$$\text{where } C \text{ is a parameter: } C = (0,167 - 0,28 * r) \sin 2\gamma + (0,299 - 0,390 * r) \quad (8)$$

$$\text{with } \gamma = \arctg \Omega \quad (9)$$

$$\text{and } r = 0,01 \text{ (hardening coefficient)} \quad (10)$$

$$6. \text{ Computation of } \sigma_{correction} = \sigma_{yi} (f (1 / (\Omega^2 - \Omega + 1)^{1/2} - 1 / (3 - \Omega)) + 1 / (3 - \Omega)) \quad (11)$$

In hole drilling method, strains produced by stress relaxation are relatively small. As a consequence, the material plastic behavior can be linearly approximated without significant errors, provided that this relationship is specifically selected in order to reproduce the near stress-strain curve.

A stress-strain curve of an elastic-perfectly plastic steel is presented below in figure 1.

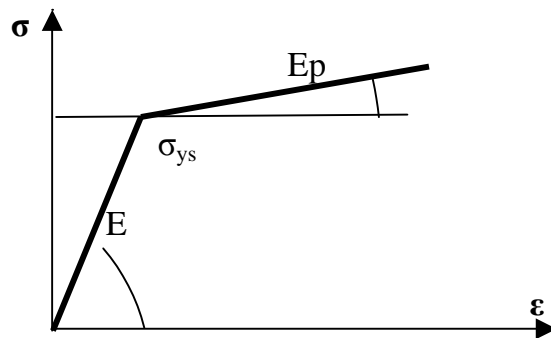


Fig. 1 Stress-strain curve of an elastic-perfectly plastic steel

In this figure, E =Young`s modulus, E_p = Young`s modulus in plastic condition and σ_{ys} = yield strength.

In order to get a residual stress free steel, two treatments were performed on samples:

- stress relief treatment by heating;
- normalization treatment

Stress relief treatment was accomplished by heating the material up to 600° and cooling it smoothly inside furnace.

Normalization treatment was accomplished by heating the material up to 900° and cooling it outside furnace.

Following these treatments, the material of samples was closer to an elastic-perfectly plastic behavior like the figure 2. Its characteristics were: $E = 210000 \text{ N/mm}^2$, Poisson coefficient = 0.27 and Yield strength = 280 N/mm^2

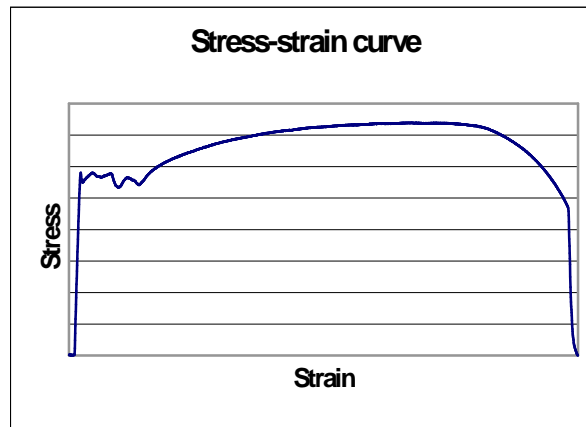


Fig.2 Stress strain curve of steel samples used in experiments

Shape of samples and positions and orientation of four gage rosettes are presented in figure 3. Figure 4 presents a picture of connections to gages.

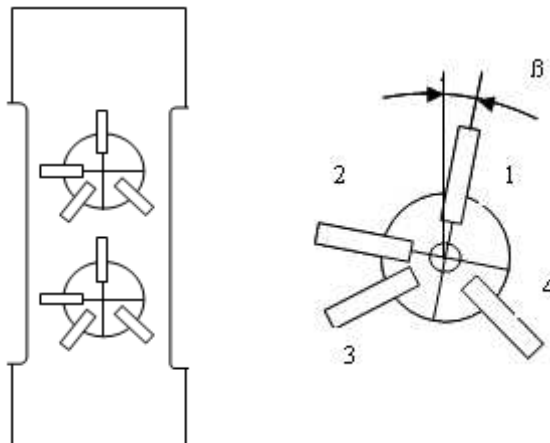


Fig.3 Shape of samples and position and orientation of rosettes

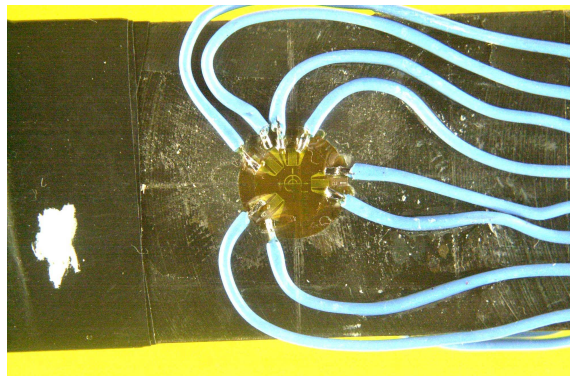


Fig 4 A photo of connections to the gages

Loading machine and position of sample and of tensometric rosettes are presented in figure 4



Fig.4 Loading machine used in stressing samples

3. Experimental results and discussion

In this research, residual stress was simulated using external loads. In order to simplify the procedure of determining high residual stresses, there were 3 steps:

- samples were subjected to external load in elastic domain, registering signals produced by rosettes (ϵ^0);
- samples were drilled (blind hole method);
- drilled samples were subjected to high external load, registering rosette signals (ϵ^+).

All samples used in this study were drilled using a special device produced by SINT Technology S.a.- Calenzano, FI, Italy. The drilling and control system consists of a high speed air turbine (300000 rpm), a carbide cutter electronic device for air pressure control and signals adapter, a PC unit with a Labview software and a data acquisition card (PC-LPM-16).

Position of cutter is controlled along 3 orthogonal axes: x, y and z. Vertical movement of cutter is controlled using a precise step by step electric motor. The electronic device assures electric power stabilization, control of air pressure and connexion with PC.

Precise initial position of cutter of device is furnished by a microscope having the same axis as the cutter.

All holes were drilled in successive increments of depth in order to minimize production of residual stress. Drilling operation was controlled on line (speed, number of increments and depth of drilling) using Labview soft: drilling speed: 300000 rpm; vertical speed of cutter: 0,08 mm/min, depth of holes: 2 mm; number of increments (steps in depth): 20, increment depth: 0,1 mm, cutter diameter: 1,5 mm, medium diameter of rosette: 5,04 mm.

If ϵ^0 and ϵ^+ are the signals produced by a gage before drilling and after drilling, the counting of simulated high residual stress can be done using the difference:

$$\epsilon = \epsilon^+ - \epsilon^0 \quad (12)$$

After calibration of rosettes (k, A and B constants), undrilled samples were gradually stressed under an increasing and then decreasing traction load as in figure 5.

Signals produced by the four gage rosette are similar to the example from figure 5. The highest signals (upper graph) are produced by the transducer 1 (oriented as in Fig.3), parallel to direction of applied force.

Signals produced by transducers 3 and 4 (middle signals) are almost equals. If the β angle (Fig.3) is 0, theoretically signals produced by 3 and 4 transducers must be equal. Signals produced by transducer 2 have a negative sign.

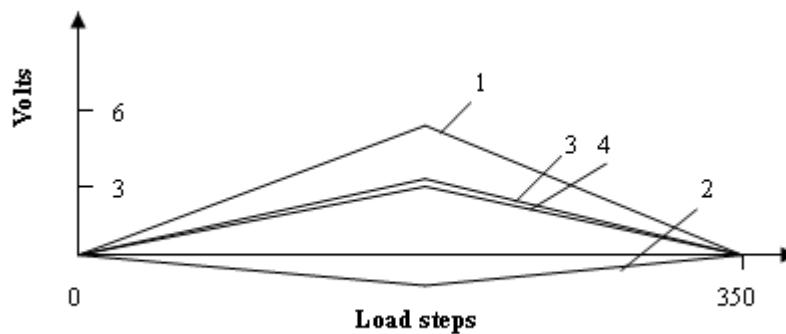


Fig.5 Signals produced by the four gages under stress

Following the steps described before, the principal stresses in the sample can be computed using the method presented in ASTM standard:

$$\sigma_x, \sigma_y = (\epsilon_1 + \epsilon_2)/4A \pm ((\epsilon_1 - \epsilon_2)^2 + (\epsilon_1 + \epsilon_2 - 2\epsilon_3)^2)^{1/2} / 4B \quad (2)$$

where $\epsilon_1, \epsilon_2, \epsilon_3$ are deformations measured by transducers 1, 2 and 3 (Fig. 4) and A and B are the calibration constants of rosette [6].

Stresses calculated with ASTM method has large errors in the domain of high stress (at 0.9 of stress yield) as can be seen in Fig. 6, where stress curve computed after ASTM method is the upper curve with greatest errors at high load.

Stresses computed using the new method described in this paper (6 steps of corrective calculus) and in the same samples, have less errors as can be seen in Fig.6 (middle curve) and comparing with the real stress.

In elastic conditions, the errors can be considered as negligible.

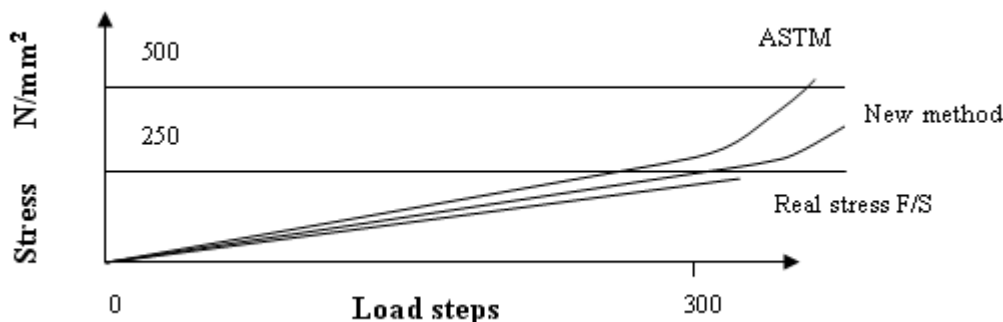


Fig.6. Stresses in a sample (ASTM procedure, new method and computing F/S –force/surface).

4. Conclusions

One of the most significant limits in the application of the classic stress measurement ASTM standard is the maximum stress that can be measured. This means that residual stress in metallic components should not exceed 50% of the material yield strength. Another limitation is connected with requirement of through-thickness uniformity of residual stress; significant variations of residual stress with depth are often observed in practical applications.

It can be observed in one of the charts obtained from experimental results (Fig.6) that residual stresses computed after ASTM procedure may be overestimated. Using the new method with corrective calculus the errors at high stress had diminished and show a better approximation of real stress level.

This research and other studies confirm that corrective procedure (and blind hole method), permit residual stress measurements up to 90% of the material yield strength with acceptable errors.

Acknowledgements

Prof. O. Ciobanu wishes to thank Prof. Leonardo Bertini and Prof. Marco Beghini from University of Pisa for their valuable expertise and support in the experimental works for testing the high residual stress measurement method.

REFERENCES

1. M. Beghini, L. Bertini, P. Raffaelli *Numerical Analysis of Plasticity Effects in the Hole –Drilling Residual Stress Measurement* Journal of Testing and Evaluation, Nov. 1994
2. M. Beghini and L. Bertini *Recent Advances in the Hole Drilling Method for Residual Stress Measurement* Journal of Materials Engineering and Performance 1998, 7, pp 163-172

3. M. Beghini, L. Bertini *Analytical expressions of the influence functions for accuracy and versatility improvement of hole drilling method* Journal of Strain Analysis vol 35, 2000, pp 125-135
4. M. Beghini, L. Bertini *Efetto delle deformazioni plastiche nella misura delle tensioni residue* Gruppo di lavoro AIAS. Studi per una proposta di raccomandazione sulla Analisi Sperimentale delle tensioni residue, 2001
5. M. Beghini, L. Bertini *An analytical expression of the influence functions for hole drilling residual stress measurement* The International conference on material engineering, Gallipoli-Lecce 4-7 september 1996
6. E 837-99 Standard Test Method for Determining Residual stresses by Hole-Drilling Strain-Gage Method

The "Gr.T.Popa" University

MĂSURAREA TENSIUNILOR REMANENTE MARI

Rezumat: Una dintre principalele deficiențe ale metodei de măsurare a tensiunilor remanente din oțeluri cu ajutorul mărcilor tensometrice este mărimea domeniului de măsurare. Tensiunile remanente măsurate cu ajutorul mărcilor tensometrice nu pot depăși 50% din rezistența admisibilă a oțelului încercat. Utilizând o metodă nouă, dezvoltată la Universitatea din Pisa, se poate ajunge cu domeniul de măsurare al mărcilor tensometrice până la 90% din rezistența admisibilă în anumite condiții. Lucrarea prezintă o serie de încercări mecanice care au permis testarea și aplicarea acestei metode.

STRATEGIES FOR REASONING CONTROL IN EXPERT SYSTEMS BASED ON PRODUCTION RULES

By

GHEORGHE BADARAU, MIHAI STEFAN and IULIAN IONITA

Abstract: The paper presents the main strategies in reasoning control that are being used in the expert systems based on production rules.

Keywords: expert system, production rule, strategy of control

1. Introduction

The expert system represents the concretisation in the structure of a computer of a component based on knowledge and high capacity of specialized processing so this system can offer an intelligent advise or to provide an intelligent decision regarding a processing activity.

In fact the experts systems are particular cases of production systems that address to some domains with a very narrow specialization.

Figure 1 shows the type of structure the most often seen of an expert system.

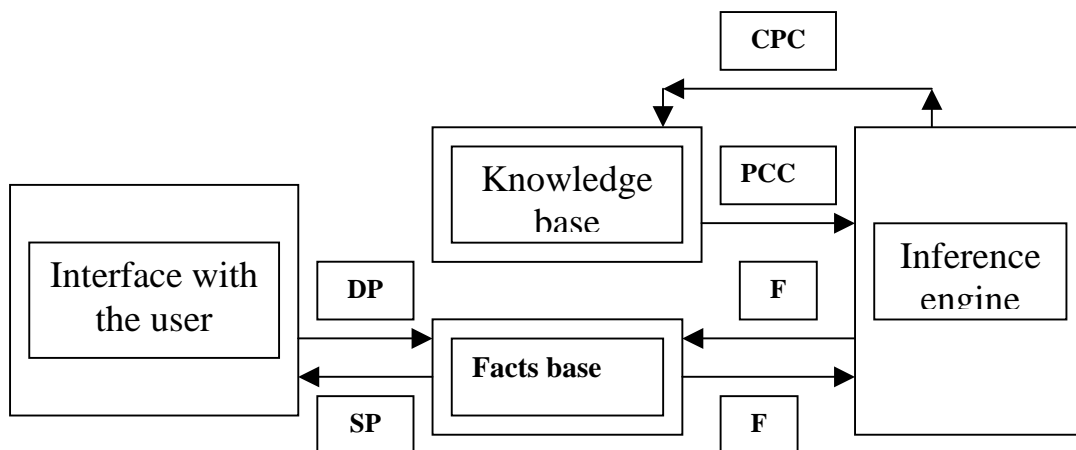


Fig 1 Principle scheme of an expert system

DP input; SP output; PCC conceptual knowledge pieces; CPC request of knowledge pieces; F facts

As in the case of a human expert, the expert system has a limited competence sphere, generally very restricted and it functions having as a base the human reasoning.

Starting from certain knowledge or facts the expert system develops a series of inferences (by means of an inference engine) and reaches a certain conclusion.

Being a component of the production systems the expert system is one of the most frequently used model for the representation and manipulation of knowledge.

The signification of the word production can be interpreted rather as production of new facts, that add in the knowledge base following a set of rules and must not be taken by mistake as what happens in factories and enterprises.

The functioning of an expert system having the structure like in figure 1 consists in the following: the user, by means of an interface formulates the problem naming the dates that constitute the initial context of it.

The dates are disposed in the basis of facts. Starting from the initial context and from the type of problem to solve the inference engine request from the knowledge basis the pieces of necessary knowledge (CPC).

With the help of the knowledge contained in the basis (PCC), the inference engine ensures the developing of the reasoning by modifying or not (by deposition of intermediary results) the content of the basis of facts (the problem context) and furnishes, in the end the solution of the problem (SP).

In the case of expert systems, the inference engine ensures the functions of the resolutive system and even a part of the functions of the cognitive system. This is why this mechanism of control or rules interpreter, frequently named as inference engine ensures the establishment of the order of application of the rules for the existing data base, the selection of rule which must be applied and the solving of the conflicts.

2. The functioning of an inference engine

The functioning of an inference engine consists in the cycling derulement of four phases:

- the selection phase – all the parts of knowledge are selected (rules) that satisfy certain criteria. The set of all rules selected make the “set of applicable rules”;
- the filtering phase – enables the reduction of the cardinal of the set of applicable rules by the retaining among these only of those for what there were found pieces of knowledge that satisfy the conditions from the premise: the set obtained constitutes “the conflictual set”;
- the phase of solving of the conflicts – if the conflictual set contains more than one element, then one eliminates first the one which produce replies of those symbols in the context, then the remaining rules are sorted according to the strategy of solving the conflicts of priority applicable ti the respective domain of use;
- the execution phase – it is executed the part of action of the rule with the higher priority; if there are no applicable rules nothing is executed; one of the direct effects of these phase is the modification of the context of the problem (the modification of the base of facts).

If at the end of the resolutive cycle the objective of the problem was reached (the solution was found) then the event is signaled to the user.

If the problem solution was not found but the context of the problem was modified by applying the rules in the phase of execution, a new resolutive cycle is initiated.

In the remaining case the problem has no solution in the context and on the basis of the available knowledge from the base of knowledge.

3. Strategies for the control of reasoning

The reasoning is defining a process of building of inferential network between the premises and the conclusions of a problem. This process is fundamented on data furnished by the problem text and knowledge about the respective type of problem.

Having represented the problem to be solved, its solving supposes the performing of a reasoning so, starting from the premises to reach the results (conclusions) of the problem. How, a reasoning contains a network of inferences more or less complex, its correct development must ensure on the basis of a strategy that ensures the correct succession of inferences.

The main strategies for reasoning control are:

- control forward;
- control backward;
- control forward – backward;
- circumstantial control.

3.1. The strategy of control forward

The strategy of control forward starts from the initial state (dates of the problem) and by applying some rules or of some operators generates successively “conditions” at the solutions until one obtains an answer corresponding to the objective of the problem.

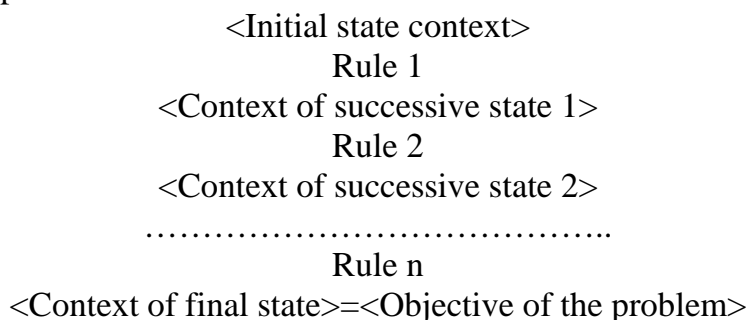


Fig. 2 The strategy of control forward

Starting from the facts contained at a certain moment in the data base (initial context) by successive applying of various rules (selected upon certain criteria) one passes successively from a state to another testing each time the concordance between the current state and the objective of the problem until they become equivalent, moment in which the process stops.

By applying the strategy of control one obtains a tree of knots forming a space of problem states.

The methods based on the strategy of control forward are called also productive methods and about the strategy one can say that is directed by the problems dates (from bottom to top) and leads to searching in the space of states.

3.2. The strategy of control backward

The strategy of control backward starts from the objective of the problem and tries, by means of applying of certain rules to obtain the decomposition of it in smaller complexity problems or refrasing the problem in terms derived on the basis of the rule used.

Figure 3 shows a scheme of the control backward strategy.

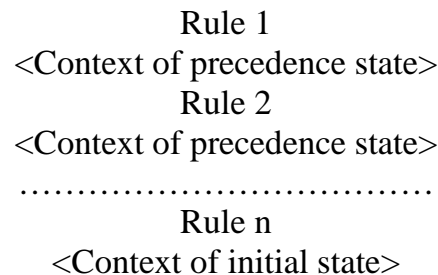


Fig. 3 Strategy of control backward

The strategy of control backward is driven by the objective of the problem from top downwards.

Each context becomes sub-objectives of the given problem.

The methods based on this strategy of control are named also reductive methods.

3.3 The strategy of combined control

The strategy of combined control backward –forward applies reductive methods for obtaining sub-problems and solves these problems by productive or reductive methods.

One must remark the fact that excepting the case when meta-problems are being approached (when the primitive symbols identify, themselves, problems), once the solving started by a productive control method, this must be kept through the obtaining of the final solution (of the problem or of the sub-problem). This condition is necessary because the productive methods generate even from the first step candidates for the solution in terms of primitive objectives of the problem as it is not possible to quit the productive method for continuing solving with other methods.

3.4. The circumstantial strategy of control

The circumstantial strategy of control is characterised by the fact that the validity of the rules depends on the circumstances of their applying. This supposes, beside the evaluation of the condition of truth, as a function of the current state of the problem also the analysis of the relational characteristics resulted from the current situation of the objectives of the problem.

The use of circumstantial strategies of control can lead to the enhancement of the performances of resolute systems.

4. Perspectives of the expert systems

Even if at the beginning the expert systems promoters hoped to reach at the developing of certain systems that overcome by their performances the human experts, this desire did not fulfil yet. This is because the data acquisition in an expert system is a more complicated thing that it appears. The difference, the most important of them, is that the human expert gains not only knowledge but experience. Simple knowledge enable the developing of reasoning based on rules (as in an expert system). Experience, on the other hand enables more subtle reasoning, what we can call inspiration or instinct; for the moment this kind of behaviour is not accessible to computer programs.

References

1. Ignizio, J.P., Introduction to expert systems: The Development and Implementation of Rule-Based Expert Systems, Mc.graw hill, 1991
2. Jeffery, K., Expert database Systems, Academic Press Ltd., London, 1992
3. Turban, E., aroson, J., decision support systems an dIntelligent Systems, Prentice – hall, NJ, 1998
4. Zaharia, M., Hospodar, A., Sisteme expert, Editura Lux Libris, Brasov, 1999
4. Zaharie, D. s.a., Sisteme expert. Teorie si aplicatii, Editura Dual Tech Bucuresti, 2002

Gheorghe Badarau
Mihai Stefan
Iulian Ionita

Faculty of Materials Science and Engineering
Technical University “Gh. Asachi” Iasi

STRATEGII DE CONTROL A RATIONAMENTELOR IN SISTEME EXPERT BAZATE PE REGULI DE PRODUCTIE

Rezumat: Lucrarea face o trecere in revista a strategiilor de control a rationamentelor in sistemele expert bazate pe reguli de productie. Sunt prezentate succint cele mai cunoscute metode de strategii de control.

INTERIOR POINT METHODS OF IN THE CONVEX OPTIMISATION OF THE PREHENSION FORCE OF A ROBOT USED IN THE TECHNOLOGICAL PROCESS OF CASTING

By

IULIAN IONITA, MIHAI STEFAN and GHEORGHE BADARAU

Abstract: The paper deals with some methods of optimisation of the prehension force of a robot used in foundries. The mathematical model is described together with a preliminary discussion about the role and place of the robots in this branch of metallurgy.

Keywords: optimisation, interior point methods, prehension force of a robot

1. Introduction

the producing of castings in little and medium series imposes in the present, all over the world the flexible automation of the technological flow of casting. For this purpose there are used manipulators and robots, placed in various flexible cells inside the main flow. For every operation of the casting technological flow (preparing of moulds, core mounting, closing and ensuring of the casting assembly, casting itself, extraction of piece from the mould, cleaning and selecting of castings etc.) there is a specialised flexible cell, working in interdependency with other cell of the flow.

The robotiation of the operations inside a foundry have at least the following advantages:

- the shortening and the simplification of the fabrication cycle in the conditions of the essential diminishing of slow work (physical work) and substantial increasing of work productivity;
- the improving the castings quality and of the drawing coefficient of the liquid alloy by the precise observing of the sequences of the technological flow;
- the diminishing of human accident risk and of the volume on Nox inhaled by people through a complete protection of workers (protection against heat, noise, vibrations, gases, toxic substances etc.);
- the diminishing of working spaces by the use of rigid and durable moulds (metallic casting dies) easy to manipulate by the robot;
- the elimination of some classic operations in the foundry shops and of the spaces necessary by using of metallic moulds recommended for automate flows (deposits and spaces for preparation of the moulding sands and core mixtures, moulding itself on special moulding machines, zones and equipment for moulds and core drying, zones and installations for regeneration of the sands etc.).

The introduction of robots in the technological process of casting transforms the inexactities of human operator and human errors into precision and higher quality. It appears in this way a new connection in the production system, namely, human-robot-machine, different from the human – machine connection.

An important step in the industrial implementation in foundries is the designing of the robots. At the industrial robot designing one takes into account the complexity and autonomy degree of them in the environment in which they work, these two elements being a function of the number of levels of command and programming.

Also in the designing (dimensioning) of a robot it is necessary to have in view the optimization of the prehension force.

In a general presentation the optimization of the prehension force of a robot has at the base the convex optimization which consists in the determination of a point that achieves the minimum of a convex function observing some restrictions expressed with convex or affine functions.

The interior point methods in the convex optimization are ones of the most powerful resources in sense of algorithm definitions with superior properties, complexity and convergence.

The interior point methods in the mathematical programming constitute one of the most fascinating adventures in the field of optimization and, in the applied mathematics and computer science in general.

Moreover, we can not speak about the optimization of the prehension force of a robot without having in view the interior point methods for the second order conical programming.

The second order conical programming consists in the minimising of a linear function by rapport with the intersection of an affine set with the product of some second order (square) cones.

The second order conical programming can be expressed by the following mathematical program:

$\min f^T x$ referring at:

(1)

$$\|A_i x + b_i\| \leq c_i^T x + d_i, i = 1, \dots, N$$

where: $x \in R^n$ is the vector of the optimising variables, $f \in R^n$, $A_i \in R^{(n_i-1) \times n}$, $b_i \in R^{n_i-1}$, $c_i \in R^n$ and $d_i \in R$. The norme that appears in the problem (1) is the standard euclidian norme, i.e. $\|u\| = (u^T u)^{1/2}$.

Lets remark that the problem has the objective function a linear one. This is not an impediment because any problem of mathematical programming can be reduced in one having the objective function a linear one.

$$\text{The restriction: } \|A_i x + b_i\| \leq c_i^T x + d_i \quad (2)$$

Is called second order cone (square) of size n_i . The motive we use this name is that the standard unit cone (convex) of size k is defined as:

$$C_k = \left\{ \begin{bmatrix} u \\ t \end{bmatrix} : u \in R, \|u\| \leq t \right\} \quad (3)$$

frequently refered as the cone of Lorentz or square cone. For $k=1$ one redefines the second order cone as:

$$C_1 = \{t : t \in R, 0 \leq t\} \quad (4).$$

The set of points that satisfy a conical restriction of second order is the inverse image of the unit second order cone of an affine transformation, i.e.:

$$\|A_i x + b_i\| \leq c_i^T x + d_i \Leftrightarrow \begin{bmatrix} A_i \\ c_i^T \end{bmatrix} x + \begin{bmatrix} b_i \\ d_i \end{bmatrix} \in C_{n_i} \quad (5).$$

So this set is convex. The problem (1) is a convex program because the objective function is convex and the restrictions define a convex set.

2. The optimization of the prehension force of a robot

Let us consider a rigid (but fragile) body which is hold by the hand of a robot having N fingers. Let suppose that the mass centre of the body is the origin on the axis system. The fingers action with various forces of contact in the points $p_1, p_2, \dots, p_n \in R^3$ the unit vector normal to the surface of the body directed toward its interior, in the i^{th} point of contact and $F^i \in R^3$ the force applied in that particular point.

Each force of contact F_i can be decomposed in two components:

- one normal to the surface of the body,

$$(v_i)^T F^i v^i;$$

- one tangential at the surface,

$$(I - v^i (v^i)^T) F^i.$$

We suppose that the tangential component is due to friction and its amplitude can not overcome a certain fraction of the normal component given by the friction coefficient $\mu > 0$, i.e.:

$$\|(I - v^i (v^i)^T) F^i\| \leq \mu (v^i)^T F^i, i = 1, \dots, N \quad (6)$$

Obviously these conical restrictions of friction are of second order but in the variables F^i .

Finally, we suppose that that the forces and external momentum that acts on the body are equivalent with a single external force F^e with the point of application in the origin (the mass centre of the piece) and an external momentum M^e . With these, the static equilibrium of the body is characterised by six linear equations:

$$\sum_{i=1}^N F^i + F^e = 0, \sum_{i=1}^N p^i F^i + M^e = 0 \quad (7)$$

The problem is to find the contact forces F^i that satisfy the friction conical conditions (6), the static equilibrium conditions (7) and certain superior limitations imposed to the normal component of the contact force:

$$(v^i)^T F^i \leq f_{\max}.$$

This is a matter of feasibility of a conical second order problem.

When the problem is admitted then we can select a particular set of forces by optimising of a certain criterion. For instance we can calculate the finest prehension force i.e. the set of forces F^i for which the prehension is stable and minimises the normal maximum force in the contact points. This means solving the following problem of second order conical programming:

min t

Referring at:

$$\begin{aligned}
(v^i)^T F^i &\leq t, i = 1, \dots, N, \\
\|(I - v^i(v^i)^T F^i)\| &\leq \mu(v^i)^T F^i, i = 1, \dots, N, \\
\sum_{i=1}^N F^i + F^e &= 0, \\
\sum_{i=1}^N p^i F^i + M^e &= 0
\end{aligned} \tag{8}$$

3. Conclusions

Even if the mathematics of the model seems to be a little difficult, the implementation of the appropriate numerical methods will solve the problem.

More over, in the stage of testing of the robot hand, some particular corrections can be stored in the computer program and made the adjustments if they are necessary.

Nevertheless, it is obvious that this method is very productive by shortening the periods of regulation and give to the designer and builder of the robot hand a solid point for starting the tests.

References

1. Andrei, N., Metode de puinct interior in optimizarea convexa, Matrix Rom, Bucuresti, 2000
2. Buss, M., Faybusovich, L., Moore, J.B., Recursive algorithm for real time grasping force optimization, Proceedings of International Conference on Robots and Automation, 1997
3. Iunius, ray, Fl., Chioreanu, S., Proiectarea turnatoriilor, UT Brasov, Facultatea de Utilaj Tehnologic, 1990
4. Lobo, M.,S., Vanderberghe, L., Boyd, S., Lebret, H., Applications of second order cone programing. Linear algegra and its applications, vol 284, pp193-228, nov.1998

Iulian Ionita
Mihai Stefan
Gheorghe Badarau

Faculty of Materials Science and Engineering,
Technical University "Gh.Asachi" Iasi

METODE DE PUCT INTERIOR IN OPTIMIZAREA CONVEXA A FORTEI DE PREHENSIVNE A UNUI ROBOT UTILIZAT IN PROCESUL TEHNOLOGIC DE TURNARE

Rezumat Lucrarea trateaza o metoda de optimizare a fortei de prehensiune a unui robot utilizat in turnatorii. Este descris modelul matematic alaturi de o investigare preliminara a rolului si locului robotilor in procesele tehnologice din turnatorii.

METHODS OF INTERIOR POINT FOR THE CONVEX OPTIMIZATION OF THE LINEAR REGULATORS FOR THE PREDICTIVE CONDUCTION OF THE HEAT TREATING FURNACE, THE LABORATORY TYPE

By

MIHAI STEFAN, IULIAN IONITA and GHEORGHE BADARAU

***Abstract:** The paper deals with some aspects concerning the mathematical model of optimization of the linear regulators used at the heat treatment furnaces, the laboratory type.*

***Keywords:** optimisation, linear regulator, predictive control, interior point methods*

1. Introduction

In the present the technology of predictive control can be met in a very wide variety of applications that include processes in the chemical, food, automotive, air-space, metallurgical, paper industries.

Everybody knows that a process functions, as a rule at a point of operation obtained at the intersectin of the restrictions. The regulator must, in this case to maintain the system as close as possible from the restrictions without braking them. Moreover, the industrial processes are complex, nonlinear, multivariable having a dynamic behavior that modifies in time because of the changes in the operation points

Because of these reasons advanced techniques of conducting this kind of systems were developed and constructed, based on the regulation of a model of the process itself.

In the industries a general methodology of control based on models developed, for which the problem of dynamic optimization is being solved on-line at each moment of application of the command to the process.

The commands are calculated to optimise the future behavior of the process through a period of time named prediction horizon.

The regulator is designed by the minimisation of a square objective function. The dynamics of the fixed part is described by an explicit model of the process, that may take, as a principle any mathematical shape.

The restrictions imposed for the input dates and exits of the process are directly included in the formulation of the control problem and so, future violations of the restrictions are anticipate and prevented. The first element from the optimal command sequence is applied to the process and the problem is being solved again in the moment of application of the command using the new sizes of the measured parameters of the process.

2. Elements of optimisation predictive control

In the predictive conducting of a heat treatment furnace, the laboratory type, the linear regulators with closed loop, of a single variable (time) have as a function to optimised the temperature. According the temperature difference (between the prescribed temperature and the real temperature from the furnace) a regulation measurement is being extracted (the difference of temperature itself) that can be amplified as a function of the regulation precision and transmitted to the linear regulator. In this sense the problem is to optimise this temperature difference that must be minimum.

This kind of problem can be inscribed in the interior point convex optimisation and represents an interesting application of second order conical programming (a set very efficient methods).

We will consider the case of static systems, the extension of the dynamic case being made directly.

The close loop system we will consider is shown in figure 1.

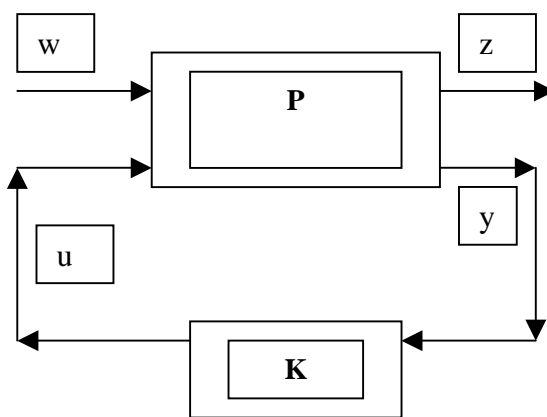


Fig. 1 Close loop system

The signals have the following meaning:

- w exogene input $w \in R^{n_w}$, that can be perturbation or noise;
- z is the output $z \in R^{n_z}$, the measure to control;
- u is the command measure $u \in R^{n_u}$, we can manipulate it by means of the regulator K in the sense of satisfying the needs of regulating z ;
- y – is the output measured $y \in R^{n_y}$, input measure for the regulator K .

In all the cases R^n is the real n dimensional space;

We suppose that the installation P is known. The problem is to design the regulator K .

We consider P and K as linear, represented by a matrix of corresponding sizes, the signals being linked by the relations:

$$\begin{bmatrix} z \\ y \end{bmatrix} = \begin{bmatrix} P_{zu} & P_{zw} \\ P_{yu} & P_{yw} \end{bmatrix} \begin{bmatrix} u \\ w \end{bmatrix}, \dots u = Ky \quad (1)$$

for formulating the problem of designing of the regulator we must describe the set of possible perturbations w , how we measure the critical values z we want to regulate and what are the limit of evolution of the input values u . for this a lot of scenarios can be imagined. A simple case supposes that the vector of perturbations w is included in the given elipsoide:

$$W = \{\bar{w} + Fp : \|p\| \leq 1\}.$$

The system performance in closed loop is appreciated after the worst functioning given on the pick of the critical measure z :

$$Z = \max_{w \in W} \max_{i=1, n_z} |z_i| \quad (2)$$

Because we work with signals of finite values we will impose a limit of the maximum pick of u that can be determined by w :

$$U = \max_{w \in W} \max_{i=1, n_u} |u_i| \quad (3)$$

in such conditions, the problem of the designing of the regulator K can be rephrased as:

$$\begin{aligned} & \min z \\ & \text{referring to:} \\ & U \leq U_{\max} \end{aligned} \quad (4)$$

what is the same like saying: lets chose the matrix of the regulator $K \in R^{n_u \times n_y}$ that determines U and Z according the relations (3) and (2) so the picks Z and U to be small.

In the following we will show how this problem can also be rephrased as a second order conical program. For the beginning lets express the signals z and u in terms of the matrix K . Eliminating y from (1) we get $z = Hw$, where:

$$H = P_{zw} + P_{zu} K (I - P_{yu})^{-1} P_{yw} \quad (5)$$

I – the unit matrix of n order.

We remark that H , that defines the transfer between perturbations and the critical measures to regulate depends in a very complicated manner of the K matrix.

We suppose that the matrix $I - P_{yu}K$ can be reversed. Similar, we express u like $u = Gw$, where:

$$G = K (I - P_{yu}K)^{-1} P_{yw} \quad (6)$$

From the relations from above, on the components we can write:

$$\begin{aligned} z_i &= h_i^T (\bar{w} + Fp), \\ u_i &= g_i^T (\bar{w} + Fp) \end{aligned} \quad \text{where, } \|p\| \leq 1 \text{ parametrises } w \text{ and } h_i^T \text{ and } g_i^T \text{ represent the line } I$$

from the matrix H and respectively G .

With these taking into account the relations (2) and (3) we can write the expressions of Z and U in terms of the lines of matrixes H and G . Indeed from (3), taking into account that for $\|p\| \leq 1$, $p^T c$ is in the domain given by $\pm \|c\|$ we obtain:

$$U = \max_{i=1, \dots, n_u} \max_{\|p\| \leq 1} |g_i^T (\bar{w} + Fp)| = \max_{i=1, \dots, n_u} (|g_i^T \bar{w}| + \|F^T g_i\|)$$

In a similar way from (2) we get:

$$Z = \max_{i=1, \dots, n_z} (|h_i^T \bar{w}| + \|F^T h_i\|)$$

Then the problem of designing (4) can be expressed as:

$$\begin{aligned} & \min \gamma \\ & \text{referring to:} \\ & \left| h_i^T \bar{w} \right| + \left\| F^T h_i \right\| \leq \gamma, i = 1, \dots, n_z \\ & \left| g_i^T \bar{w} \right| + \left\| F^T g_i \right\| \leq U_{\max}, i = 1, \dots, n_u \end{aligned} \quad (7)$$

in which the variables of the problem are the matrix K and the scalar γ .

As it can be seen the problem (7) is a very complicated one, nonlinear and nonconvex optimization. For making it treatable we must execute a changing of the variables in (7), in view of transforming it into an equivalent problem but a convex one. We define the matrix:

$$Q = K(I - P_{yu}K)^{-1} \in R^{n_u \times n_y} \quad (8)$$

as the matrixes H and G from (5) and (6) become:

$$H = P_{zw} + P_{zu}QP_{yw}, G = QP_{yw}.$$

It is important to note that this algebra artifice make G a linear function of Q and H an affine function, i.e. a linear function plus a constant, what contrast powerful with the very complicated matrix dependency of matrixes H and G upon K .

Now, being sure that the matrix $I + QP_{yu}$ is reversible we can reverse the transformation from above for getting K as a function of Q :

$$K = (I + QP_{yu})^{-1}Q \quad (9)$$

With these we see that (8) and (9) are inverse relations that link each K by a matrix Q very particular and vice versa.

Considering now Q as a designing variable, once determined the optimum matrix Q , than from (9) one can calculate immediately the matrix of the regulator K .

3. Conclusions

So, as an expression of Q the problem of the regulator becomes:

$$\begin{aligned} & \min \gamma \\ & \text{referring to:} \\ & \left| h_i(Q)^T \bar{w} \right| + \left\| F^T h_i(Q) \right\| \leq \gamma, i = 1, \dots, n_z \\ & \left| g_i(Q)^T \bar{w} \right| + \left\| F^T g_i(Q) \right\| \leq U_{\max}, i = 1, \dots, n_u \end{aligned} \quad (10)$$

in which the designing variables are the matrix Q and the scalar γ .

Because h_i and g_i are functions affine of Q it results that the problem (10) is a conic second order program.

A very interesting extension of the optimisation of linear regulators consists in the considering of the problem of the optimisation of affine regulators. In essence the problem has the same formulation in the conditions in which one supposes that the installation P and the regulator K are described by affine relations, i.e. linear relations plus a constant.

An affine regulator corresponds to a linear regulator having a reference given value. The extension, in the case of this type of regulators is immediate. A new

component of the vector w is added fixed at a value equal with 1. In the same time this unit signal is introduced in the regulator as a new component of y .

So the expanding of the optimisation of the regulator follows the same procedure described above, fact that shows the idea that the techniques of conical programming of second order can be used for optimising both the reference and the matrix of the regulator.

References

1. Andrei, N., Programarea matematica. Metode de punct interior, Ed. Tehnica, Bucuresti, 1999
2. Boyd, S.P., Barratt, C., Linear controller design. Limits and performance, Prentice hall, 1991
3. Lazar, C., Conducerea predictiva a proceselor cu model cunoscut, Matrix Rom, Bucuresti, 1999
4. Salcudean, S., Algorithms for optimal design of feedback compensators, Ph.D. Thesis, University of California, Berkeley, 1986

Mihai Stefan, Faculty of Materials Science and Engineering
Iulian Ionita The Technical University "Gh.Asachi" from Iasi
Gheorghe Badarau

METODE DE PUNCT INTERIOR IN OPTIMIZAREA CONVEXA A REGULATOARELOR LINIARE PENTRU CONDUCEREA PREDICTIVA A CUPTOARELOR DE TRATAMENT TERMIC TIP LABORATOR

Rezumat: Lucrarea prezinta tehnica optimizarii prin metode de punct interior cu exemplificare pe un regulator cu bucla inchisa specific cuptoarelor de trament termic tip laborator.

OPTIMIZATION AND COMPUTATIONAL METHODS IN MATERIAL SCIENCE AND ENGINEERING

by

MIHAI STEFAN, GHEORGHE BADARAU AND IULIAN IONITA

Abstract: The paper shows the link between mathematical optimization and computational methods and their place in the materials' science

Keywords: optimization, mathematical model, computer science, rolling mill

The theory and practice of the optimization is based on the development of computer sciences. In a wider sense the computational sciences consists in the use of computers for analyzing of scientific problems.

All the intellectual structure humanity dispose of is based on a small number of fundamental principles. The first principle is that of the simplicity in the sense the nature seems to enable descriptions starting from a surprisingly small number of hypotheses. This does not mean that these representations, even expressed with mathematical symbols, (i.e. using mathematical models) are simple but there is a simplicity in the concepts they express. It is important to note the facts that the natural phenomena are not powerful nonlinear. It seems that nature, in its entire splendor and complexity can be represented very well by second order non-linearities. There are lots of examples in mechanics or in the electromagnetic field – actually all the mathematical equations are differentials of second degree.

The second principle that seems to govern the nature laws is that often they can be expressions of an equilibrium implying a minimum or a maximum. We can call this principle the principle of the economy. The third principle is that of the simetricity and the fourth refers to the fact that the mathematics as we know enable the modelling of the technico-engineering phenomena.

The essence is the fact that the way of approaching is the localist one, based on small variations in the neighborhood of a functioning point

So, the first sciences that “awakes thinking” are the sciences of the number and of measurement (calculus and mathematics), actually the computer sciences. The entire technical progress, the elaboration and development of the theories in various field of the finest refinement and abstraction are due entirely to mathematical sciences, in fact to computational sciences.

The effort of seeing and understanding nature functioning requests a special intellectual concentration, meaning the representation of nature in terms of mathematical models. In this sense the model maker builds a path from the real world

of physical processes and phenomena to the world of mathematical symbols. The purpose of computational sciences is to obtain an understanding of the functioning of a part of the creation, by analyzing the associated mathematical models. Thus, the mathematical modeling stands in a central place in the frame of computational sciences. The idea is that by modeling to get information carrying added value, non-hypothetical, about the evolution of a given phenomenon. From this it results that for a given part of the creation one can build a diversity of models, all of them having the same nucleus, the analyzed phenomenon. The process of solving of a problem can be shown as in figure 1.

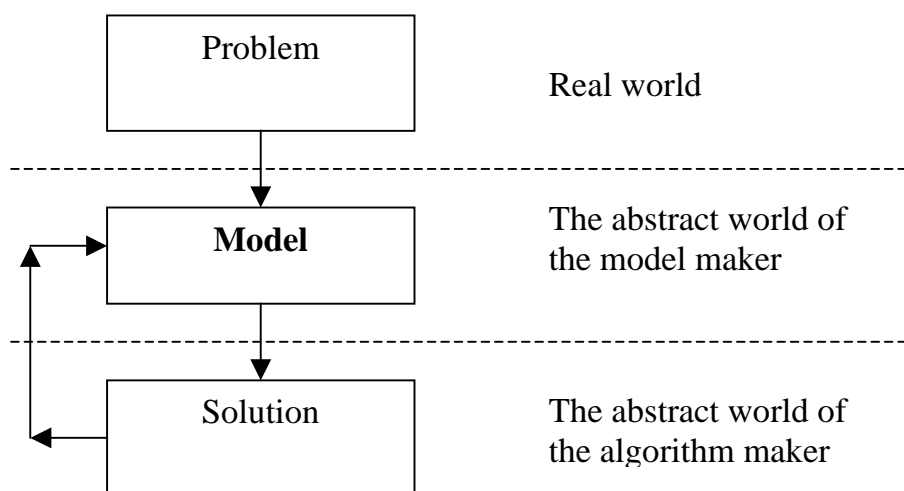


Fig. 1 The process of solving a problem

We can see that from the real world one can build the mathematical model of the problem in which we are interested in, placing us in an abstract world in which the mathematics rule. Using theories non related with the physical signification of the elements of the problem the model is solved and one gets a solution. The interpretation of the solution can lead to a modification of the model by re-addressing to the real world.

In the abstract world of the model maker, one operates with a series of concepts and laws, specific for the field in which the model is done, the phenomenology that characterizes the field. Also at this level one operates with concepts from the theory of compilers, languages theory that contribute to the definition of some software instruments that conceive, elaborate, modify and maintain the models – the elaboration of the languages of mathematical programming oriented on the algebra or on icons.

On the other hand the algorithm maker operates in his world with mathematical concepts from the linear algebra, differential calculus, convex analysis etc. that contribute to the definition of the algorithms of solving the problem (model) and study of its properties of convergence and complexity. This is the place where the software is made too.

It is clear that for a large number of problems their model must be simplified for being able to solve it with the available mathematics. So the following question arise: what is more desirable – to use an approximate model and determine an exact

solution on this base or, to get an exact as possible model and to obtain an approximate solution? Experience shows that the last approach gives better results.

The optimization problems, known also as mathematical programming can be framed in this kind of solving. Characteristic for these problems is that now one has a well done theory, naming the conditions for getting a solution, doubled by a body of techniques, methods, algorithms and software materializing and implementing this theory.

What ever the domain of application, the materials science make no exception the computational sciences problems have the following characteristics:

1. They have a precise mathematical description (mathematical model);
2. They can non be treated by traditional methods;
3. They request very detailed knowledge in the field of the problem as well as knowledge in the field of mathematical and computational techniques involved in solving the problem.

The language of communication of ideas in the computer sciences is mathematics and programming languages. Now the effort of developing of a programming language that offers flexibility and structure seams to give results in Fortran 90, Matlab and also in some packages written in C or C++.

Matlab is a high performance package of programs, in fact a working environment to solve a large diversity of problems, dedicated to numeric calculus and graphic representation. By using the package TOMLAB, specialized for solving large sized problems of optimization, Matlab becomes a very respectable tool.

The discussion can continue in this respect very much, but we must emphasize that the community of computer sciences is very divers and includes researches with many terms and development methodologies, placing it in the zone of multidisciplinary research.

For instance in the materials science there are a lot of domains where computers take more and more charge in designing of technologies and control of process.

More over, in the conditions of the high quality requested for the materials by the down flow manufactures the optimization of the control becomes a necessary tool in the efforts of obtaining economic results.

Some of the domains in what the optimization of the quality of the products using computers is now the cold rolling of profiles.

It is well known that making sheets of steel is not a problem, but at the quality required by the appliance industry the problem becomes very serious for engineers and designers. Because of the surface quality requested and also of the small tolerances at the main size, thickness constancy, making steel sheet is not so easy at it can seam. For solving it the great manufacturers made efforts in implementing complex programs of mill control. The software must transpose an optimization problem "the surface quality of the product" in the conditions of obtaining of the thickness requested.

By controlling the parameters of the equipment, online regulations, adding new equipment requested "by the mathematical model" (for example cooling zones for stabilizing the structure and the shape) one can solve these kind of high complexity problems.

References

1. Andrei, N., Sisteme si pachete de programe pentru programarea matematica, Ed. Tehnica Bucuresti, 2002
2. Grace, A., Optimization Toolbox for use with Matlab. Users' guide. The Math Works Inc., 1995
3. Holmstrom, K., Bjorkman, M., The TOMLAB NLPLIB toolbox for non linear programming, Advanced Modelling and Optimization, Vol.1, no. 1, 1999, pp. 70-86
4. Holmstrom, K., Bjorkman, M., Dotzauer, E., The TOMLAB OPERA toolbox for linear and discrete optimization, Advanced Modelling and Optimization, Vol.1, no. 2, 1999, pp. 1-8

Mihai Stefan, Gheorghe Badarau, Iulian Ionita – Technical University of Iasi
Faculty of Materials Science and Engineering

OPTIMIZARE SI METODE COMPUTATIONALE IN STIINTA MATERIALELOR

Rezumat: Lucrarea prezinta foarte pe scurt circuitul de legatura dintre optimizarea matematica si metodele computationale si locul lor in stiinta materialelor.

MATHEMATICAL MODELING AND OPTIMISATION IN MATERIALS SCIENCE AND ENGINEERING

BY

MIHAI STEFAN, IULIAN IONITA and GHEORGHE BADARAU

Abstract: The paper presents some considerations about the place and importance of the mathematical modeling and optimization in the materials science and engineering.

Keywords: optimization, mathematical modeling

1. Introduction

The world trend in the economy development, especially the globalization require more and more flexibility and performance in each sector of activity. Performance and economic efficiency, this is the goal of each manager in every enterprise no matter the size.

The technological level of our days has as a support the material in its various structures, shapes and designs. The progress in materials can and must be the engine of the new economic growing.

This is why, the materials science field is one of the most dynamic in the economy. The possibility of progress in this field is, like in many others the introducing of information technology, together with the better modeling and optimization of the processing technologies. Particular in the metallurgy, in the conditions of materials reduction and environment protection the optimisation is needed more then ever.

2. Modeling and optimisation

The possibility of solving more and more complicated technical problems stays in solving bigger and mare complex mathematical problems fact that requests the elaboration of mathematical modeling and optimization instruments more and more sophisticated. Among these, the modeling languages for mathematical programming imposed themselves as being the ones able to formulate and solve, in an industrial context the real optimization problems.

The algebra's languages have as a characteristic a structure based on the declarations, expressing more "what we calculate" than "how we calculate". But the most important characteristic of them is their extensive use in the domains of variations for the variable indexes or of the parameters of the problem. The most important algebra languages and for mathematical modeling, very much used in the conceptualization, formulation and communication of optimization models are: GAMS, AMPL, ALLO, MPL, described in the literature /1/. The use of mathematical programming languages lead at the possibility of construction of large sizes

mathematical models for optimization which, beside the fact they offer the possibility of a better representation (more precise) of the reality, so of practical use, they were one of the most challenges in what concerns the development of techniques, methods and algorithms of non-linear optimization.

The mathematical modeling for optimization is a powerfully iterative process that implies a series of steps for: identifying the parameters and variables that characterize the analyzed phenomenon; the definition of the sets of evolution of the indexes of these elements; the pointing of the definition domains of variables (the boundaries); the elaboration of the objective function; writing the relations that link the variables and the parameters and collecting the dates associated with the model.

The next step, consists in solving the model, the analyzing of the solution and, on this base to start a new modeling process. Figure 1 shows the main steps of the modeling process an model solving.

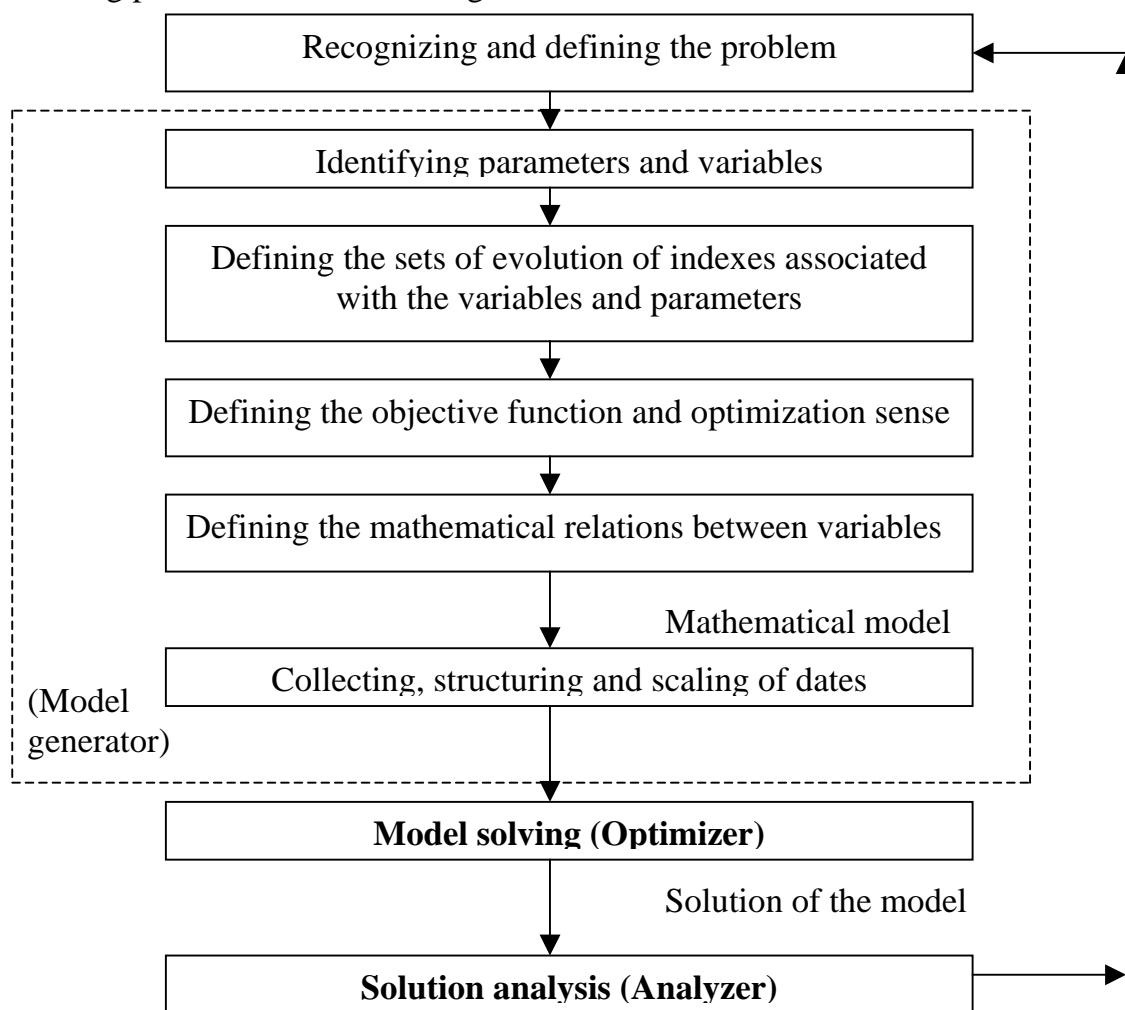


Fig 1 The modeling process

The model maker passes through these steps many time, repeating some steps until the model is completely defined.

Nevertheless the recognizing and defining the problem is the most difficult part, stage in which one insulate a part of the univers and imposes the conditions and requests from it.

The analyzing of the solution that implies before the solving of the model determines the restarting of the modeling process.

The first four steps of the modeling finish with the mathematical model. At this moment one must send the model to an optimizer that will give a solution or establish the impossibility of solving the model.

The information technology, enabling this transmission, is given by the mathematical programming languages. The purpose of the modeling languages is to achieve a link between the natural formulation of the model, as it is made by the model maker, and the scheme of input dates accepted by the optimizer. Real problems imply thousands or tenth of thousands of variables and restrictions that can not be generated manually. A modeling language enables the model imaging in which the model maker describes in a clear, concise and efficient shape the relations between variables and parameters. In any mathematical programming language, it is important, if not, fundamental to have the ability of grouping entities in similar sets that can be followed by indexes.

As a difference from the programming languages, in which the procedures are in a dominant position by rapport to declarative instructions, the mathematical programming languages use the last ones more. Nevertheless, the complexity of models imposed the use of structures as: if-then-else or loops, beside the simple read/write or solve.

An important feature of some modeling languages (AMPL, GAMS) is that of treating non-linear models. In this case, after setting the domains of variation of indexes of variable and parameters the model maker writes the non-linear expression of the model in the usual algebra notations. The translator associated has the role of evaluation for the non-linear expression and elaboration of the differentials automatic or/and symbolic needed for the optimizers. The most interpreters included in the programming languages are based on automatic differentials. The interfaces between the mathematical programming and optimizers can be enough complicated to define so it appeared an another trend.

This trend consists in the elaboration of the systems of modeling and optimization. In these systems the modeling language is placed in a central place. What characterizes a modeling and optimization system is the presence of the problem analyzers and solution analyzers. The most known instruments of analyzing the mathematical programming problems are ANALIZE and MPROBE. ANALIZE is dedicated to the analyze of linear programming and MPROBE is better in non-linear problems.

In the same time these systems can be coupled with a data base that enable the correct generation of large size models.

A model in a mathematical programming language is a ASCII file containing the declarations of defining of the elements of the model. It may have also a filter enabling the translation of data toward and from a data base. The interfacing between an user and the mathematical programming language can be done by developing of the links between the system of management of the data base, model and files associated with the model. Having in view that for the most part of the real model the structure is more stable then the data that instance the model, often, the mathematical programming languages enable the elaboration of models prototypes.

In the case of the icon oriented programming languages, the models are been achieved by combining certain reusable blocks, characterized by well stated mathematical relations, interconnected according the structure modeled. For a given domain, i.e. materials science and engineering, some representative entities must be identified , illustrated by icons representing the functioning of a certain part of the reality. These entities, as elements of the icon modeling have inputs and outputs and internal variables between which certain mathematical relations act. The model maker calls these entities in a scheme of the analyzed process by introducing the links between the icons, defining names for these links, evolution ranges, values for parameters, variables etc. that will participate to the model generation. LPFORM is a representative system for generating models in the linear programming. Using analogies with objects from the real world, the icon representation is relatively real. From the point of view of the cognitive complexity the model maker is somehow limited in maintaining a simple structure but this kind of systems enable a more rapid building of very complex models of optimization.

3. The link between the model and optimization

In a modeling system, once the model generated, the optimization can be called in two ways. The first consists in the initiating of an independent process. The other method is calling a subroutine linked with the modeling system directly or by a construction DLL (dynamic link library).

Both situations need the construction of an internal representation of the model understandable by the optimization package. This implies the use of special routines specific for each modeling-optimization coupling construction.

The advantages of using systems for modeling and optimization is the easy way of executing of numerical experiments, being possible to implement various models in various algebra configurations leading to a better understanding and more efficient solving of the problem.

References

1. Andrei, N., Pachete de programe, modele si probleme de test pentru programarea matematica, Ed. Matrix Rom, Bucuresti, 2001
2. Chinneck, J.W., Analyzing Mathematical Programs using Mprobe, Annals of Operations Research Special Issue on Modeling Languages, Technical Report, Systems and Computer Engineering, Carleton University, 1999
3. Hurlimann, T., Modeling and optimization, Kluwer Academic Publishers, 1999
4. Murphy, F.H., Stohr, E.A., Asthana, A., Representation scheme for linear programming models, Management Sciences, vol 38, 1992, pp. 964-991.

MIHAI STEFAN, IULIAN IONITA, GHEORGHE BADARAU

Faculty of materials Science and Engineering

Technical University "Gh.Asachi" Iasi

MODELARE MATEMATICA SI OPTIMIZARE IN STIINTA SI INGINERIA MATERIALELOR

Rezumat: Lucrarea prezinta unele consideratii despre locul si importanta modelarii matematice si a oprimizarii in stiinta si ingineria materialelor, si implicatiile noilor tehnologii informatonale in aceste domenii.

HARDWARE AND SOFTWARE FOR ULTRASONIC FLOW METER TRANSDUCERS

BY

Claudiu ISARIE and Alexandru MARIN

Abstract: *The paper is focused on analyzing, respectively on hardware - software implementation of a case-study for a transit-time working principle flow meter. This new-technology type flow meters take the advantage of modern microprocessor-based technology and they generally outperform their precursors, particularly in their accuracy levels of $\pm 1\%$ or better.*

The device uses two transducers, which function as both ultrasonic transmitters and receivers, clamped to the outside of a closed pipe at a specific distance from each other. After a thorough examination of the working principles, the authors described the hardware - analogue/numerical converter for 8 bits, with 4 multiplexed inputs - and software implementation of the ultrasonic device on a PC, which realizes the change of information with the flow measurement system using the parallel port LPT 1; for graphic interface the program language Borland C++ was used.

For the application and the case-study of the transient-time working principle, it was concluded, by comparison with Doppler effect procedure, the selection criteria for choosing a specific technological implementation. Also, it were made considerations on the multi-path ultrasonic flow meters, using multiple pairs of transducers that alternate in their functions as senders and receivers over the same path length.

Keywords: *ultrasonic flow meter, Doppler flow meter principle, transit-time principle, hardware-software implementation*

1. Introduction

I.1. Electronic flow meters

While the flow measurement technologies named as *electronic* are neither exclusively electronic in nature, they do represent a logical grouping of flow measurement technologies. All have no moving parts - excepting maybe some vibrations, are relatively non-intrusive and are feasible by today's sophisticated electronics technology. Magnetic flow meters, for example, are the most directly electrical in nature, deriving their first principles of operation from Faraday's law. Vortex meters depend on piezoelectric sensors to detect vortices shed from a stationary shedder bar. Today's ultrasonic flow meters owe their successful application to sophisticated digital signal processing.

I.2. Ultrasonic flow meters - Measuring Principle

The flow measurements with ultrasound signals are physically grounded on penetrating the pipe. Time differences, frequency variations or phase shifts of the

ultrasonic signals, caused by the flowing liquid, are subsequently evaluated.

The measurement of flow is based on the principle that sound waves traveling in the direction of flow of the fluid require less time than when traveling in the opposite direction. The difference in transit times of the ultrasonic signals is an indication for the flow rate of the fluid.

Since ultrasonic signals can also penetrate solid materials, the transducers can be mounted onto the outside of the pipe.

Fast digital signal processors and sophisticated signal analysis guarantee reliable measuring results, even under difficult conditions, where previously ultrasonic flow meters had failed.

I.3. Principle of Doppler flow meter

For cases, where the liquid is not sonically conductive, i.e. for liquids with a very high solid or gaseous content ($> 10\%$ of volume), another measuring principle, similar to the Doppler principle has been developed for ultrasonic flow meters. This principle actually relies on particles or gas bubbles flowing with the liquid in order to give a flow rate reading. The Doppler flow meter measures the velocity of particles moving with the flowing fluid. Acoustic signals of known frequency are transmitted, reflected from particles and are picked up by a receiver. The received signals are analyzed for frequency shifts and the resulting mean value of the frequency shifts can be directly related to the mean velocity of the particles moving with the fluid. Software can be used to reject stray signals and correct for frequency changes caused by the pipe wall or transducer protective material. No special transducers are required for the ultrasonic flow meters to operate in Doppler mode. Both the reflection and diagonal transducer mounting method are suitable (see Figure 1).

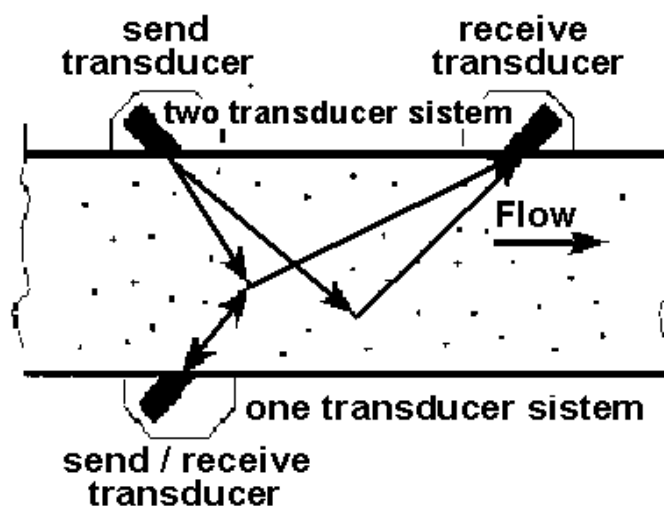


Fig. 1 Reflection and diagonal transducer mounting method

The accuracy of the flow meter operating in Doppler mode is less than when

working in transit-time mode. Doppler flow meter performance is highly dependent on physical properties such as the liquid's sonic conductivity, particle density, and flow profile. Likewise, non uniformity of particle distribution in the pipe cross section leads in a computed mean velocity that is incorrectly weighted. Therefore, the meter accuracy is sensitive to velocity profile variations and to distribution of acoustic reflectors in the measurement section. Unlike other acoustic flow meters, Doppler meters are affected by changes in the liquid's sonic velocity. As a result, the meter is sensitive to changes in density and temperature. These problems make Doppler flow meters unsuitable for highly accurate measurements in some applications. Doppler meters play a very important role where other meters will not work. These might be liquid slurries, aerated liquids or liquids with some small or large amount on suspended solids.

Doppler flow meter transducers operate at 0.640 MHz (in clamp-on designs) and at 1.2 MHz in wetted sensor designs. The transducer sends an ultrasonic pulse or beam into the flowing stream. The sound waves are reflected back by such acoustical discontinuities as particles, entrained gas bubbles, or even by turbulence vortices (see Figure 2).

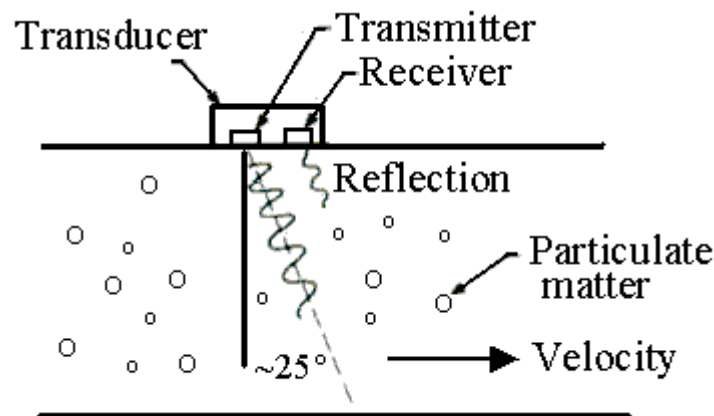


Fig. 2 Working scheme of an Doppler flow meter transducers

For clamp-on designs, measurement inaccuracy ranges from $\pm 1\%$ to $\pm 5\%$ full scale (FS). The meter detects the velocity of the discontinuities, rather than the velocity of the fluid, in calculating the flow rate. The flow velocity (v) can be determined by:

$$v = (f_0 - f_1)C_t / 2f_0 \cos(a) \quad (1)$$

where C_t is the velocity of sound inside the transducer, f_0 is the transmission frequency, f_1 is the reflected frequency, and a is the angle of the transmitter and receiver crystals with respect to the pipe axis. Because $C_t / 2f_0 \cos(a)$ is a constant (K), the relationship can be simplified to:

$$v = (f_0 - f_1)K \quad (2)$$

Thus, flow velocity v (ft/sec) is directly proportional to the change in frequency. The flow (Q in gpm) in a pipe having a certain inside diameter (ID in inches) can be obtained by:

$$Q = 2,45 \cdot v \cdot (ID)^2 = 2,45[(f_0 - f_1)K](ID)^2 \quad (3)$$

The presence of acoustical discontinuities is essential for the proper operation of the Doppler flow meter. The generally accepted rule of thumb is that for proper signal reflection there be a minimum of 80-100 mg/l of solids with a particle size of +200 mesh (+75 micron). In the case of bubbles, 100-200 mg/l with diameters between +75 and +150 microns is desirable. If either the size or the concentration of the discontinuities changes, the amplitude of the reflected signal will shift, introducing errors.

2. Application and case-study on the transit-time principle

The present paper is focused on analyzing, respectively on hardware - software implementation of a case-study for a transit-time working principle flow meter. This device uses two transducers, which function as both ultrasonic transmitters and receivers. The transducers are clamped to the outside of a closed pipe at a specific distance from each other. This distance is calculated by the flow meter after all pipe and medium parameters have been entered into the instrument.

The transducers can be mounted in reflection (see Figure 3) or in diagonal mode (see Figure 4). This selection is based on pipe and liquid characteristics.

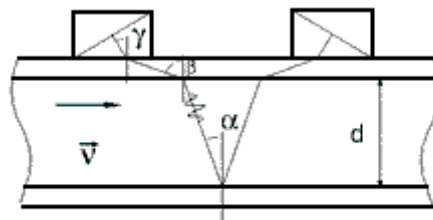


Fig. 3 Transducers mounted in reflection mode

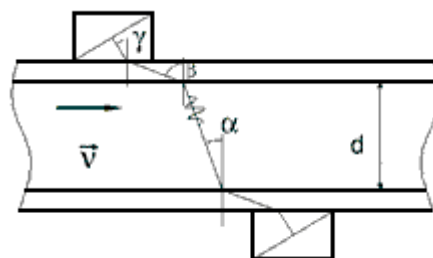


Fig. 4 Transducers mounted mode

The flow meter operates by alternatively transmitting and receiving ultrasonic signal pulses between the two transducers. The ultrasonic signals are first transmitted in the direction of the fluid (fd) and then against fluid flow (afd). Since sound energy in a moving liquid is carried faster when it travels in the direction of flow than against it, a time difference (td) between the signals' time-of-flight will occur (see Figure 5).

When the flow is zero, the time for the signal T_1 to get to T_2 is the same as that required to get from T_2 to T_1 . When there is flow, the effect is to boost the speed of the signal in the downstream direction, while decreasing it in the upstream direction. The flowing velocity (V_f) can be determined by the following equation:

$$v_f = Kdt / T_L \quad (4)$$

where K is a calibration factor for the volume and time units used, dt is the time differential between upstream and downstream transit times, and T_L is the zero-flow transit time.

The time difference of the ultrasonic signals is proportional to the flow velocity in the pipe. The measured flow velocity is multiplied with the cross-sectional area of the pipe; hence the flow rate of the fluid can be calculated.

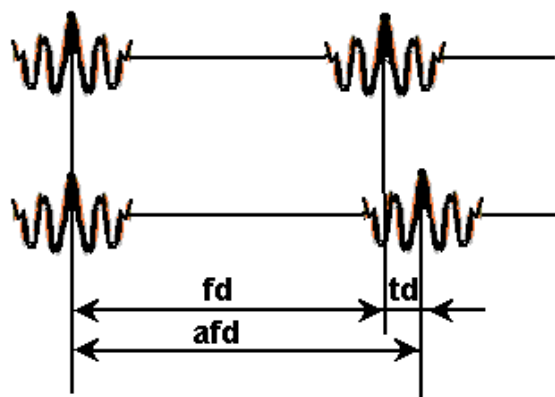


Fig. 5 Time difference between the signals' time-of-flight occurring

Using the transit-time technique, accuracies of 1 % of measured value can be achieved without process calibration. Measurement accuracy can be in the range 1 to 3 percent of measured value of 0.5 percent with process calibration depending on the application. The portable microprocessor-based electronics unit provides a local display and has a keypad for setting up and diagnostics. The flow meter can read flow units in common imperial or metric units, measures flow in both directions, can store data points internally, give analogue or serial outputs and has optional inputs for thickness gauges. The electronics unit can log data for measuring sites. It can also provide a PC interface via RS-232 serial communication, and an output of 4-20 mA DC for operating a digital controller.

Block sketch of flow measuring system is presented in Figure 6.

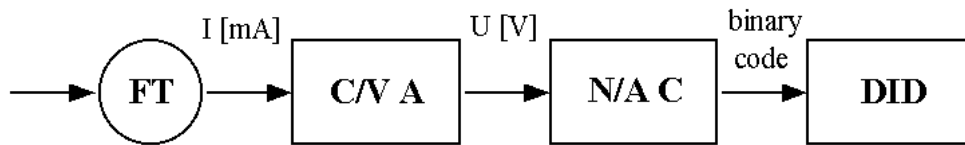


Fig. 6 Block sketch of flow measuring system

The measuring system contains (see Figure 6):

- flow transducer (FT);
- current/voltage adapter (C/V A);
- numerical/analogical converter (N/A C);
- decimal index display (DID).

The flow rate Q is converted by the transducer (FT) in an electric signal I . In Figure 7 is presented the characteristic $I = f(Q)$, between I and Q existing a linear dependence described by the following relationship:

$$I = 0,8 \cdot Q + 2 \quad (5)$$

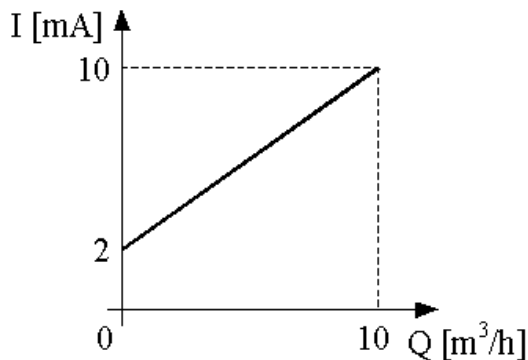


Fig. 7 Characteristic $I = f(Q)$

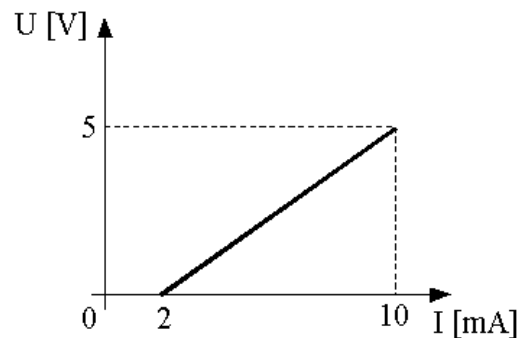


Fig. 8 Characteristic $U = f(I)$

The current/voltage adapter (C/V A) has the roll to convert the current I into a voltage. The linear dependence between these two signals is done by the following relationship:

$$U = 0,625 \cdot I - 1,25 \quad (6)$$

This could be observed also in the graphics representation (see Figure 8) of the characteristic $U = f(I)$.

This kind of transducers has a satisfying precision only for stationary flows, which pass a limit depending of the transducer used in the application.

The numeric/analog converter (N/A C), realizes the voltage conversion V in a binary code on 8 bit. This conversion is described by the relationship:

$$n = \frac{2^8 - 1}{U_{\max}} \cdot U = \frac{255}{U_{\max}} \cdot U = 51 \cdot U \quad (7)$$

The decimal number N corresponds to the read binary code. It is the integer of the number n. As example, in the Table 1 the corresponding values n and N for certain values of V are given.

Table 1

Nr.	U [V]	n	binary code	N
1	0	0	0000 0000	0
2	0.5	25.5	0001 1001	25
3	1	51	0011 0011	51
4	1.5	76.5	0100 1100	76
5	2	102	0110 0110	102
6	2.5	127.5	0111 1111	127
7	3	153	1001 1001	153
8	3.5	178.5	1011 0010	178
9	4	204	1100 1100	204
10	4.5	229.5	1110 0101	229
11	5	255	1111 1111	255

The decimal index display (DID) has the role to convert the binary code in decimal and to display the value of the flow rate. The relationship is:

$$Q_m = \frac{Q_{\max}}{2^8 - 1} \cdot N \quad (8)$$

In Table 2 results of 11 measured points (Q_m) are given.

Table 2

Nr.	Q [m ³ /h]	I [mA]	U [V]	N	Q _m [m ³ /h]
1	0	2	0	0	0.0000
2	1	2.8	0.5	25	0.9804
3	2	3.6	1	51	1.9608
4	3	4.4	1.5	76	2.9804
5	4	5.2	2	102	3.9608
6	5	6	2.5	127	4.9804
7	6	6.8	3	153	6.0000
8	7	7.6	3.5	178	6.9804
9	8	8.4	4	204	7.9608
10	9	9.2	4.5	229	8.9804
11	10	10	5	255	10.0000

For estimate the range of error we use the equation:

$$a_m = \frac{1}{\text{exp.}} \cdot \left(\sum Q - \sum Q_m \right) = 0,0196 \text{ [m}^3\text{/h]} \quad (9)$$

An analogue/numerical converter for 8 bits, with 4 multiplexed inputs was used. The inputs may be configured for the following operation modes:

- with the reading of a single input, measuring the voltage between the input and null;
- with differential reading, measuring the voltage between the two entrances.

The converter realizes the entrance voltage conversion, corresponding to one of the two operating modes, in a binary number of 8 bits.

We implemented the procedure on a PC, which realizes the change of information with the flow measurement system using the parallel port LPT 1. For graphic interface the program language Borland C++ was used.

The information received from the measuring system is read at the following entrances of the parallel port: Busy, ACK, Paper Empty and Select. The selection signals are on the outputs: Data1 and Data2.

The program contains also a graphic module that indicates the variation of flow. A sequence from the "Flow rate calculation software" is presented here below:

```

.....
/* Graph mode init. */
detectgraph (&gdriver, &gmode);
initgraph (&gdriver, &gmode, 'C:\BC45\BGI ');
maxx = getmaxx ( ); maxy = getmaxy ( );
plansa (maxx,maxy);
do
{
rate=0;
/* Binary code reading - first group */
outportb(DATA, 0x04); input=inportb(STATUS);
input=input^XORINPUT;
if((input&0x80)==0x80)
rate=rate+128;
if((input&0x40)==0x40)
rate=rate+64;
if((input&0x20)==0x20)
rate=rate+32;
if((input&0x10)==0x10)
rate=rate+16;

/* Binary code reading - second group */
outportb(DATA, 0x02); input=inportb(STATUS);
input=input^XORINPUT;
if((input&0x80)==0x80)
rate=rate+8;
if((input&0x40)==0x40)
rate=rate+4;
if((input&0x20)==0x20)
rate=rate+2;

```

```
if((input&0x10)==0x10)
    rate=rate+1;

/* Flow compute display and graph */
rate=rate*10/255; write_rate(rate)
x_o=x_i; y_o=y_i;
x_i++;y_i=460-ceil(flow*30);
setlinestyle(0,0,3); setcolor(RED);
line(x_o, x_i, y_o, y_i);
setlinestyle(0,0,3); delay(100);
.....
```

3. Conclusions

Pipe size and the ability to resolve time differences are the main practical limits for the time transit flow meter. An advantage is that a determination of velocity can be made every transmit cycle, which allows rapid response in large pipe. Therefore, it is an ideal choice for pipe diameter above 1 meter.

Measuring in ultrasonic Doppler mode is not the preferred mode for most of the applications, but there are some cases, which fit this method.

Multipath ultrasonic flow meters use multiple pairs of transducers that alternate in their functions as senders and receivers over the same path length. By averaging the values given by the different paths, the flow rate is determined with greater accuracy than single-path meters can provide. Multipath instruments are used in large-diameter conduits, such as utility stacks, and in other applications where non-uniform flow velocity profiles exist.

Selection criteria will necessarily include:

- the characteristics of the fluid to be measured;
- the level of measurement accuracy required;
- the extent to which the fluid can be confined, touched, or altered;
- accessibility for maintenance requirements;
- price.

Received May 9, 2005

REFERENCES

1. Miller R.W., *Flow Measurement Engineering Handbook*, McGraw Hill, 1996;
2. Ginesi D., *Flow Sensing: The Next Generation*, Control Engineering, November 1997;
3. Espina P., *Ultrasonic Clamp-On Flowmeters: Have They Finally Arrived?*, Flow Control, January 1997.

Tipar Digital realizat la **Tipografia pim**

Șoseaua Ștefan cel Mare nr. 11

Iași - 700498

Tel. / fax: **0232-212740**

e-mail: editurapim@pimcopy.ro

www.pimcopy.ro